

SYNTHESIS AND PHOTOPHYSICS OF LIGHT-CONVERTING LANTHANIDE COMPLEXES

PROEFSCHRIFT

ter verkrijging van
de graad van doctor aan de Universiteit Twente,
op gezag van de rector magnificus,
prof. dr. F. A. van Vught,
volgens besluit van het College voor Promoties
in het openbaar te verdedigen
op vrijdag 19 mei 2000 te 15.00 uur.

door

Stephen Isadore Klink

geboren op 16 mei 1971
te Alkmaar

Dit proefschrift is goedgekeurd door:

Promotor	Prof. dr. ir. D. N. Reinhoudt
Assistent promotor	Dr. ir. F. C. J. M. van Veggel

Aan mijn grootouders

This research has been financially supported by the Council for Chemical Sciences of the Netherlands Organization for Scientific Research (CW-NWO), in the framework of the Young Scientist program, 1995.

ISBN 90-3651436-3

Contents

Chapter 1

General Introduction

1.1 General Introduction	1
1.2 References and Notes	6

Chapter 2

Photoluminescent Materials: the Trivalent Lanthanides

2.1 Introduction	7
2.2 Electronic Configuration	8
2.3 The Optical Transitions of Lanthanide Ions	9
2.3.1 Introduction	9
2.3.2 The 4f energy levels	9
2.3.3 The luminescence properties of lanthanide complexes in solution	12
2.4 Sensitized Lanthanide Emission	14
2.4.1 The sensitization pathway	14
2.4.2 The external heavy atom effect	16

2.4.3 The role of the antenna triplet state	17
2.4.4 External triplet quenchers	18
2.4.5 The role of the antenna singlet state	18
2.4.6 The electron-exchange energy transfer mechanism	19
2.4.7 Energy back-transfer	20
2.4.8 Ligand-to-metal charge transfer	21
2.5 Quenching by High Frequency Oscillators	23
2.5.1 The energy gap law	23
2.5.2 The Franck-Condon factor	24
2.5.3 The Förster energy transfer mechanism	26
2.6 Lanthanide Luminescence Characteristics	27
2.6.1 Eu ³⁺ luminescence	27
2.6.2 Tb ³⁺ luminescence	28
2.6.3 Nd ³⁺ , Er ³⁺ , and Yb ³⁺ luminescence	28
2.7 Luminescent Lanthanide Complexes	29
2.7.1 Introduction	29
2.7.2 β-diketonate chelates	30
2.7.3 Cyclen derivatives	31
2.7.4 Cryptates	32
2.7.5 EDTA and DTPA derivatives	33
2.7.6 Calix[4]arenes	34
2.7.7 <i>m</i> -Terphenyl-based ligand systems	36
2.8 Applications	37
2.8.1 Fluoroimmunoassays	37
2.8.2 Optical amplification	38
2.9 Outlook	39
2.10 References and Notes	39
Appendix	44

Chapter 3

Near-Infrared and Visible Luminescence of Terphenyl-based Lanthanide Complexes Modified with Amide and Sulfonamide Pendant Arms

3.1 Introduction	47
3.2 Results and Discussion	50
3.2.1 Synthesis	50
3.2.2 Structure of the (Y) 1a , (Y) 1c , and (Y) 2 complexes	51
3.2.3 ^{17}O NMR of the (Dy) 1a complex in methanol	55
3.2.4 Luminescence properties of the Eu^{3+} and Tb^{3+} complexes	56
3.2.5 Luminescence properties of the Dy^{3+} and Sm^{3+} complexes	60
3.2.6 Luminescence properties of the Er^{3+} , Nd^{3+} , and Yb^{3+} complexes	61
3.3 Conclusion	64
3.4 Experimental Section	65
3.4.1 Synthesis	65
3.4.2 Photophysical studies	70
3.4.3 Molecular dynamics and molecular modeling calculations	71
3.5 References and Notes	72

Chapter 4

A Systematic Study of the Photophysical Processes in *m*-Terphenyl-Based Lanthanide Complexes Functionalized with a Triphenylene Sensitizer

4.1 Introduction	77
4.2 Results and Discussion	80
4.2.1 Synthesis	80
4.2.2 Molecular dynamics studies	81
4.2.3 Sensitized emission of (Eu) 1 and (Tb) 1	82
4.2.4 Sensitized emission of (Nd) 1 , (Er) 1 , and (Yb) 1	86
4.2.5 Antenna fluorescence and phosphorescence	88

4.2.6 The intramolecular energy transfer process in (Eu) 1 and (Tb) 1	91
4.2.7 The intramolecular energy transfer processes in (Nd) 1 , (Er) 1 , and (Yb) 1	97
4.3 Conclusion	99
4.4 Experimental Section	99
4.4.1 Synthesis	99
4.4.2 Photophysical studies	101
4.4.3 Electrochemical measurements	102
4.4.4 Molecular dynamics and molecular modeling calculations	102
4.5 References and Notes	103

Chapter 5

Sensitized Luminescence of Ternary Eu^{3+} and Nd^{3+} Complexes

5.1 Introduction	107
5.2 Results and Discussion	110
5.2.1 Synthesis	110
5.2.2 Molecular mechanics studies	111
5.2.3 Monitoring the formation of the ternary complex	112
5.2.4 Photophysical properties of the <i>m</i> -terphenyl-based ternary Eu^{3+} complexes	113
5.2.5 Luminescence of the calix[4]arene-based ternary complexes	119
5.3 Conclusion	120
5.4 Experimental Section	121
5.4.1 Synthesis	121
5.4.2 Photophysical studies	123
5.4.3 Molecular mechanics calculations	124
5.5 References and Notes	124

Chapter 6

Fluorescent Dyes as Sensitizers for Near-Infrared Nd³⁺ Emission

6.1 Introduction	127
6.2 Results and Discussion	131
6.2.1 Synthesis	131
6.2.2 Molecular dynamics studies	134
6.2.3 Photophysical properties of the mono-dye-functionalized complexes	134
6.2.4 Photophysical properties of the bis-dye-functionalized complexes	140
6.3 Conclusion	142
6.4 Experimental Section	143
6.4.1 Synthesis	143
6.4.2 Photophysical studies	149
6.4.3 Molecular dynamics and molecular mechanics calculations	149
6.5 References and Notes	149

Chapter 7

Ferrocene and Ru-tris(bipyridine) as a New Class of Photosensitizers for Near-Infrared Yb³⁺ and Nd³⁺ Luminescence

7.1 Introduction	151
7.2 Results and Discussion	153
7.2.1 Synthesis	153
7.2.2 Photophysical properties of the [(Ln ₂ -Ru)1] ²⁺ complexes	155
7.2.3 Photophysical properties of the (Ln)2 complexes	160
7.3 Conclusion	163
7.4 Experimental Section	164
7.4.1 Synthesis	164
7.4.2 Photophysical measurements	168
7.4.3 Electrochemical measurements	168
7.5 References and Notes	168

Appendix

Towards Polymer Optical Amplifiers Based on Lissamine-Functionalized Nd³⁺ Complexes

A1. Introduction	171
A2. Recently Reported Organic Systems Based on Nd ³⁺	173
A3. Choice of the Polymer Matrix and the Nd ³⁺ Complex	174
A4. Results and Discussion	175
A5. Conclusion	177
A6. Experimental Section	177
A7. References and Notes	178
Summary	179
Samenvatting	183
Nawoord	187
Curriculum Vitae	191

Chapter 1

General Introduction

1.1 General Introduction

The luminescence properties of the trivalent rare earth or lanthanide cations in solution and in the solid state are characterized by narrow emission bands and relatively long luminescence lifetimes of up to milliseconds.¹ Except for lanthanum (La^{3+}) and lutetium (Lu^{3+}), each lanthanide ion has its specific emission bands: for example, the lanthanide ion europium (Eu^{3+}) emits red light, terbium (Tb^{3+}) green light, and neodymium (Nd^{3+}), ytterbium (Yb^{3+}), and erbium (Er^{3+}) near-infrared light. These characteristics have led to the application of lanthanide ions as probes in fluoroimmunoassays (Eu^{3+} and Tb^{3+}),^{2,3} laser systems (e.g. Nd^{3+}),⁴ and optical amplifiers (Er^{3+} and Pr^{3+}).⁵ The host material of the lanthanide ions can be organic (an organic ligand with lanthanide complexing moieties)⁶ or inorganic (a glass or a crystal),⁷ which can have a profound influence on the luminescence properties. The work described in this thesis is part of the ongoing research in this group that is concerned with the development of an optical amplifier based on organic lanthanide complexes.^{8,9}

Optical signal amplifiers play a crucial role in long range optical data transport, where data is transported as light pulses through silica fibers. The fibers have been fabricated in such a way that the optical signals are confined and guided in the fiber by the phenomenon of total internal reflection. Since silica fibers are transparent in the near-infrared region of the electromagnetic spectrum, two specific telecommunication windows in this region are being used for (long distance) data transport: a window around 1330 nm and a window around 1550 nm. The transport of light is inevitably accompanied by signal losses, for example due to local imperfections in the silica fibers, signal splitting, reflection by impurities, or some residual absorption. As a result, the optical signals have to be amplified periodically to prevent a total loss of the signal (approximately after every 80 km of fiber). In the beginning, electronic amplifiers were used, but their mode of operation is relatively slow, due to the fact that the optical signal has to be transformed into an electronic signal, followed by the amplification of the electronic signal, and finally, the electronic signal has to be transformed back into an optical signal. Optical signal amplifiers operate much faster since they amplify the signal directly via the mechanism of stimulated emission (see Figure 1.1).

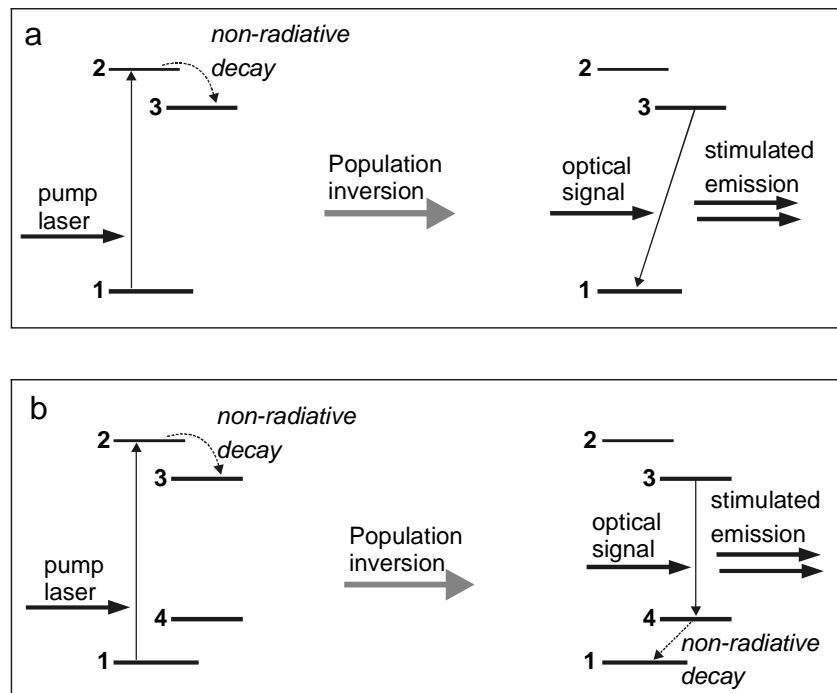


Figure 1.1: Schematic representation of a 3-level (a) and a 4-level laser (b) (laser = Light Amplification by Stimulated Emission of Radiation). In a 3-level laser there has to be a population inversion between level 3 and the ground state level 1, whereas in a 4-level laser there has to be a population inversion between the levels 3 and 4.

Current optical amplifiers are based on the lanthanide ions Er^{3+} (1550 nm) or Pr^{3+} (1330 nm), that are doped in an inorganic matrix such as silica. In these optical amplifiers, emission is stimulated from a specific excited (luminescent) state of the lanthanide ion corresponding to the frequency of the optical signal (see Figure 1.1). A requirement is that there should be a population inversion, *i.e.* that more lanthanide ions are in the excited state than in the ground state. The population inversion is achieved by using an external pump laser.

Despite the frequent use of erbium-doped silica fiber amplifiers (EDFAs), these amplifiers have some drawbacks. The dopant concentration of lanthanide ions has to be very low (< 5 ppm) in order to prevent ion clustering. The reason for this is that if the lanthanide ions are in close proximity to each other (< 10 Å), energy transfer processes may occur that ultimately lead to energy losses. This means that the length of the optical amplifier has to be sufficiently long (10-50 m) in order to achieve a significant amplification (gain) of the signals. For example, a typical EDFA that contains 10^{17} Er^{3+} ions/ cm^3 must be 20-50 m long to achieve a signal gain of 25 dB (300x).

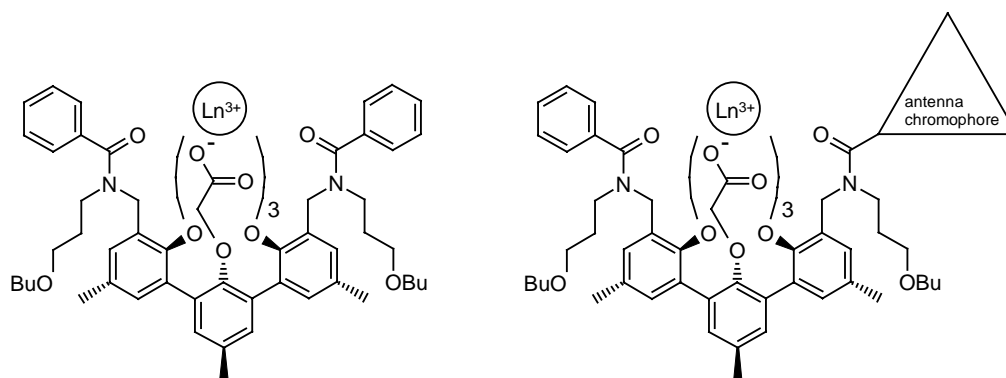
Silica fibers are excellently suited for the transport of optical data. However, once the data have arrived at their destination, the data have to be processed, for example the optical signals must be separated. Such manipulations require integrated optics, *i.e.* planar waveguide structures in which splitters, switches, and (de)multiplexers are combined. For this reason there is an interest in the development of a polymeric planar optical amplifier on a silicon substrate that can be integrated with other (existing) polymeric optical components such as splitters, resulting in polymer-based integrated optics. Polymers are attractive because they are easy to process and complex waveguide structures can be fabricated relatively easily using standard lithography. Due to their small dimensions, planar amplifiers require high lanthanide doping concentrations. However, lanthanide ions are usually not soluble in polymers. For this reason the lanthanide ions have to be encapsulated by an organic ligand resulting in a (preferably neutral) complex that is compatible with the polymer matrix.

The goal of the research described in this thesis is the design and synthesis of organic ligands that form stable complexes with lanthanide ions and that effectively shield the lanthanide ion from its environment. This is necessary because the environment may quench the excited state of the lanthanide ion. The resulting lanthanide complexes should be soluble in organic solvents and in the polymer matrix, and must enable an efficient excitation of the complexed lanthanide ion via an antenna chromophore. An important part of this thesis is devoted to the excitation of lanthanide ions by energy transfer from suitable antenna

chromophores. A thorough understanding of the photophysical pathways that are involved in this sensitization process is crucial and provides a feedback for design rules and optimization.

The complexation of the trivalent lanthanide ions is based on electrostatic interactions. The lanthanide ions prefer hard donor atoms such as neutral (amide carbonyl) or negatively charged (carboxylate) oxygen atoms.⁶ As a result, lanthanide ions have a strong tendency to bind water. Unfortunately, the lanthanide luminescence is very sensitive to quenching by OH groups.¹⁰ Since the hydration number of lanthanide ions varies from 8 to 9, the ligand of interest should have eight or nine donor atoms to obtain a water-free complex. Ligands in which these coordinating groups are preorganized are likely to form stable complexes with lanthanide ions. This principle of preorganization has first been formulated by Cram.¹¹ The ligands described in this thesis are based on the *m*-terphenyl building block,¹² and they have been functionalized with eight hard oxygen donor atoms for the encapsulation of the lanthanide ion (see Chart 1.1).

Chart 1.1



This ligand allows the incorporation of an organic antenna chromophore (the *sensitizer*) which is usually a conjugated π -system that can absorb the excitation light, and can subsequently donate the excitation energy to the lanthanide ion. Provided that the energy transfer process is efficient, this way of indirect excitation is more efficient than direct excitation, because the absorption coefficients of lanthanide ions are very low (typically less than $10 \text{ M}^{-1}\text{cm}^{-1}$),¹ whereas the absorption coefficients of the organic antenna chromophores can be as high as 10^5 - $10^6 \text{ M}^{-1}\text{cm}^{-1}$.¹³ Furthermore, the excitation wavelength can be tuned by incorporating appropriate antenna chromophores, allowing visible light excitation with green or red diode lasers. These excitation sources are compact and available at relatively low cost.

In chapter 2 the general photophysical properties of the trivalent lanthanide ions are discussed, including the mechanism to excite lanthanide ions indirectly via an antenna chromophore (the sensitizer). Some examples of the specific energetic and structural requirements are given that are necessary to obtain an efficient sensitizer-functionalized lanthanide complex, as well as a short overview of recently reported luminescent lanthanide complexes and their specific photophysical properties.

Chapter 3 is focused on the design and synthesis of the novel *m*-terphenyl ligand on which the antenna-functionalized complexes described in chapters 4-7 are based. The *m*-terphenyl ligand bears two amido or two sulfonamido coordinating moieties and three bidentate oxyacetate moieties. The structure of the corresponding lanthanide complexes has been studied using (temperature dependent) ^1H NMR, ^{19}F NMR, and ^{17}O NMR spectroscopy, as well as luminescence spectroscopy of the visible light emitting Eu^{3+} and Tb^{3+} complexes. The sensitized luminescence of the near-infrared light emitting Er^{3+} , Yb^{3+} , and Nd^{3+} complexes is described and evaluated.

Chapter 4 describes the synthesis and photophysics of the *m*-terphenyl ligand that has been covalently functionalized with a triphenylene antenna chromophore. The sensitized visible and near-infrared luminescence is described in terms of the luminescence lifetimes and quantum yields. The different steps in the sensitization process, *i.e.* the excitation of the complexed lanthanide ion via the triphenylene antenna, have been studied systematically in order to get insight into where the system can be improved.

Instead of *m*-terphenyl-based lanthanide complexes covalently functionalized with an antenna chromophore, the lanthanide complexes and the antennae described in chapter 5 are held together by electrostatic interactions. In these ternary complexes, the antenna chromophore is directly coordinated to the lanthanide ion. The investigated antenna chromophores are β -diketonates, 1,10-phenanthroline, and tetraazatriphenylene, and contain (bidentate) lanthanide coordinating groups. This chapter mainly focuses on the photophysical properties of the ternary Eu^{3+} complexes. Furthermore, it is demonstrated that this concept can also be extended to ternary Nd^{3+} complexes.

In chapter 6 four different dyes (dansyl, coumaryl, and the Rhodamine-B derivatives Lissamine and Texas Red) are described for the sensitization of the near-infrared emitting lanthanide ion Nd^{3+} . The incorporated fluorescent dyes allow visible light excitation of up to 600 nm. It is shown that the complexed Nd^{3+} ion influences the photophysical properties of the dye antenna chromophores in such a way that the sensitization process is enhanced.

In chapter 7 a new class of sensitizers for the sensitization of near-infrared Nd³⁺ and Yb³⁺ emission is reported: the organo-*d*-metal complexes Ru-tris(bipyridine) and ferrocene. The feasibility of sensitized lanthanide emission in these new type of complexes is demonstrated.

Finally, a dye-functionalized Nd³⁺ complex has been incorporated in a planar polymer waveguide, and the sensitized luminescence is presented in the appendix.¹⁴

1.2 References and Notes

1. Gschneider Jr., K.A.; Eyring, L. *Handbook on the Physics and Chemistry of Rare Earths*, North Holland Publishing Company, Amsterdam, **1979**.
2. Hemmilä, I. K. *Applications of Fluorescence in Immunoassays*, Wiley and Sons, New York, **1991**.
3. (a) Steemers, F. J.; Verboom, W.; Reinhoudt, D. N.; van der Tol, E. B.; Verhoeven, J. *W. J. Am. Chem. Soc.* **1995**, *117*, 9408. (b) Steemers, F. J.; Meuris, H. G.; Verboom, W.; Reinhoudt, D. N. *J. Org. Chem.* **1997**, *62*, 4229.
4. Moncorge, R.; Merkle, L. D.; Zandi, B. *MRS Bull.* **1999**, *24*, 21, and references cited therein.
5. Desurvire, E. *Phys. Today* **1994**, *97*, 20.
6. (a) Sabbatini, N.; Guardigli, M.; Lehn, J.-M. *Coord. Chem. Rev.* **1993**, *123*, 201. (b) Parker, D.; Williams, J. A. G. *J. Chem. Soc., Dalton Trans.* **1996**, 3613.
7. Blasse, G.; Grabmaier, B. C., *Luminescent Materials*, Springer Verlag, Berlin, **1994**.
8. Oude Wolbers, M. P.; van Veggel, F. C. J. M.; Peters, F. G. A.; van Beelen, E. S. E.; Hofstraat, J. W.; Geurts, F. A. J.; Reinhoudt, D. N. *Chem. Eur. J.*, **1998**, *4*, 772.
9. Slooff, L. H.; Polman, A.; Oude Wolbers, M. P.; van Veggel, F. C. J. M.; Reinhoudt, D. N.; Hofstraat, J. W. *J. Appl. Phys.* **1998**, *83*, 497.
10. (a) Haas, Y.; Stein, G. *J. Phys. Chem.* **1971**, *75*, 3668. (b) Haas, Y.; Stein, G. *J. Phys. Chem.* **1971**, *75*, 3677.
11. Cram, D. J. *Angew. Chem.* **1988**, *100*, 1041.
12. Oude Wolbers, M. P.; van Veggel, F. C. J. M.; Snellink-Ruël, B. H. M.; Hofstraat, J. W.; Geurts, F. A. J.; Reinhoudt, D. N. *J. Am. Chem. Soc.* **1997**, *119*, 138.
13. Murov, S. L.; Carmichael, I.; Hug, G. L. *Handbook of Photochemistry, 2nd Ed.*, Marcel Dekker, New York, **1993**.
14. In collaboration with Akzo Nobel and the FOM Institute in Amsterdam.

Chapter 2

Photoluminescent Materials: the Trivalent Lanthanides

2.1 Introduction

The trivalent lanthanide or rare earth ions are characterized by their partially filled 4f shells, except for lanthanum (La^{3+}), which has a completely empty, and lutetium (Lu^{3+}), which has a completely filled 4f shell. Some of these lanthanide ions and their organic complexes are known to exhibit photoluminescence in solution and in the solid state, which is characterized by line-like emission bands, relatively long luminescence lifetimes, and a strong sensitivity towards quenching by high frequency vibrations such as the O-H vibration.^{1,2} An important feature of luminescent lanthanide ions is that their luminescence can easily be photosensitized by an appropriate antenna chromophore (the sensitizer).^{1,2} In this process, which can be very efficient, the sensitizer donates its excitation energy to the lanthanide ion, which results in the population of the lanthanide luminescent state and subsequent emission. In this chapter the characteristics of lanthanide ions and their complexes will be discussed, and in particular the process of sensitized lanthanide luminescence.

2.2 Electronic Configuration

The trivalent lanthanide ions or rare earth ions from cerium to lutetium are the fourteen elements that follow lanthanum in the Periodic Table, in which the fourteen 4f electrons are successively added to the lanthanum (La^{3+}) configuration $[\text{Xe}]4f^0$ (see Table 2.1).³ The most stable and therefore predominant oxidation state of the lanthanide ions is 3+.⁴ Exceptions are Eu^{3+} and Yb^{3+} , ions that are relatively easily reduced to their 2+ state with standard electrode potentials of -0.35 and -1.05 V in water (vs. NHE), respectively.⁴ The 4f electrons are shielded from the environment by an outer shell of completely filled 5s and 5p orbitals, and this has a profound effect on the coordination properties of lanthanide ions: the ions are essentially spherical and the 4f orbitals are in general not available for chemical bonding. Furthermore, in contrast to transition metals, the stabilization due to crystal-field effects is small (*vide infra*).⁵

Table 2.1: Electronic configuration of lanthanide atoms and trivalent ions as well as the radii of the trivalent ions.⁶

Z	Element	Symbol	Atom	M^{3+}	M^{3+} radius (Å)
57	Lanthanum	La	$[\text{Xe}]5d^16s^2$	$[\text{Xe}]$	1.061
58	Cerium	Ce	$[\text{Xe}]4f^15d^16s^2$	$[\text{Xe}]4f^1$	1.034
59	Praseodymium	Pr	$[\text{Xe}]4f^36s^2$	$[\text{Xe}]4f^2$	1.013
60	Neodymium	Nd	$[\text{Xe}]4f^46s^2$	$[\text{Xe}]4f^3$	0.995
61	Promethium	Pm	$[\text{Xe}]4f^56s^2$	$[\text{Xe}]4f^4$	0.979
62	Samarium	Sm	$[\text{Xe}]4f^66s^2$	$[\text{Xe}]4f^5$	0.964
63	Europium	Eu	$[\text{Xe}]4f^76s^2$	$[\text{Xe}]4f^6$	0.950
64	Gadolinium	Gd	$[\text{Xe}]4f^75d^16s^2$	$[\text{Xe}]4f^7$	0.938
65	Terbium	Tb	$[\text{Xe}]4f^96s^2$	$[\text{Xe}]4f^8$	0.923
66	Dysprosium	Dy	$[\text{Xe}]4f^{10}6s^2$	$[\text{Xe}]4f^9$	0.908
67	Holmium	Ho	$[\text{Xe}]4f^{11}6s^2$	$[\text{Xe}]4f^{10}$	0.899
68	Erbium	Er	$[\text{Xe}]4f^{12}6s^2$	$[\text{Xe}]4f^{11}$	0.881
69	Thulium	Tm	$[\text{Xe}]4f^{13}6s^2$	$[\text{Xe}]4f^{12}$	0.869
70	Ytterbium	Yb	$[\text{Xe}]4f^{14}6s^2$	$[\text{Xe}]4f^{13}$	0.858
71	Lutetium	Lu	$[\text{Xe}]4f^{14}5d^16s^2$	$[\text{Xe}]4f^{14}$	0.848

The decrease in ionic radius along the series to the heavier lanthanide ions with an increased nuclear charge arises from the increase in effective nuclear charge (the outer 5s and

5p orbitals penetrate the 4f subshells, and are thus not shielded from the increasing nuclear charge). This effect is called the lanthanide contraction. The lanthanide ions belong to the hard acid class in the Pearson designation.⁷ Ions in this class bind to hard bases, primarily those that contain oxygen and nitrogen as donor atoms. As a result, the rare earth trivalent cations have a strong tendency to bind water. The hydration number of the bare lanthanide ions in water changes along the lanthanide series from nine to eight around Gd^{3+} because of the decrease in ionic radius.

2.3 The Optical Transitions of Lanthanide Ions

2.3.1 Introduction

The trivalent lanthanide ions and their complexes are known to luminesce, giving rise to line-like atomic bands corresponding to intra-4f transitions. The characteristic shape of the bands is explained by the fact that the ground and excited states of these transitions have the same equilibrium geometry, since excitation only involves rearrangement of the electrons within f-orbitals. Moreover, since the 4f orbitals are shielded from the environment by an outer shell of 5s and 5p orbitals, the emission bands remain narrow, even at room temperature in solution or in an organic matrix.

Judd⁸ and Ofelt⁹ independently derived expressions for the intensities of induced electric dipole transitions within the $4f^n$ configuration. Since their results are similar, and were published simultaneously, the basic theory has become known as the Judd-Ofelt theory. This theory provided the possibility to interpret the absorption spectra of the lanthanide ions in terms of the intra $4f^n$ transitions.

2.3.2 The 4f energy levels

The energy levels of the 4f orbitals are not degenerate because of electronic repulsion, spin-orbit coupling, and (in a coordination environment) the ligand field (see Figure 2.1). The strongest interaction, the electronic repulsion between the electrons, disrupts the degeneracy of the 4f energy levels and yields terms with separations in the order of 10^4 cm^{-1} . Spin-orbit coupling is the interaction between the magnetic moments of the electrons due to their spin (spin angular momentum) and the magnetic moments due to their movement around the nucleus (orbital angular momentum). This causes further splitting of the energy levels into so-

called J-states. The splitting of these energy levels is in the order of 10^3 cm^{-1} . The J-degeneracy is partially removed in a coordination environment by the ligand field. These splittings being in the order of 10^2 cm^{-1} , are not very pronounced since the 4f electrons are shielded effectively by the filled 5s and 5p orbitals.

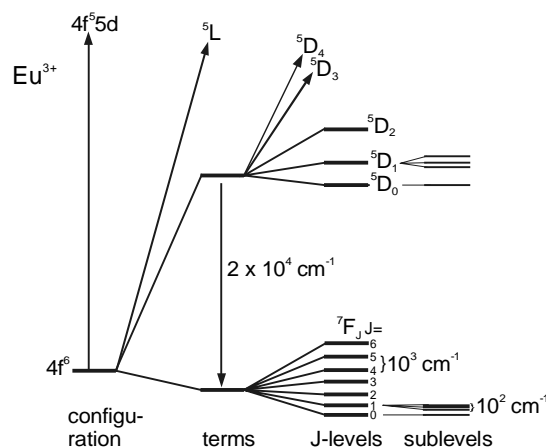


Figure 2.1: Splitting of the 4f energy levels of Eu^{3+} as a result of electronic repulsion, spin-orbit coupling, and the ligand field.

The term symbol of the J-states is written as $^{2S+1}L_J$ according to the Russel-Saunders coupling scheme.¹⁰ The spin multiplicity $2S+1$, where S is the total spin-impulse momentum of the system, gives the maximum of possible spin orientations, and denotes the degeneracy of the J-states. The value of the total orbital angular momentum L is represented by the symbols S ($L=0$), P ($L=1$), D ($L=2$), F ($L=3$), G ($L=4$), etc. The value of L is obtained by coupling the individual orbital angular momenta l_i : $L = (l_1+l_2+\dots+l_i), (l_1+l_2+\dots+l_i-1), \dots, |(l_1-l_2-\dots-l_i)|$. The total angular momentum J indicates the relative orientation of the spin and the orbital momenta: $J = L+S, L+S-1, L+S-2, \dots, |L-S|$.

The energy levels that are depicted in Figure 2.2 were published by Stein and Würzberg,¹¹ and are based on the absorption spectra of hydrated lanthanide ions in dilute acid solutions.¹² In general the atomic spectra have to obey the following selection rules:

- $\Delta S = 0$, the overall spin is not allowed to change, because light does not affect the spin.
- $\Delta L = 0, \pm 1$, with $\Delta l = \pm 1$, the orbital angular momentum of an individual electron must change.

- $\Delta J = 0, \pm 1$, but $J = 0$ to $J = 0$ is forbidden.
- The parity selection rule, which forbids electric dipole transitions between levels with the same parity, examples are electronic transitions within the d-shell, within the f-shell, and between d and s shells.

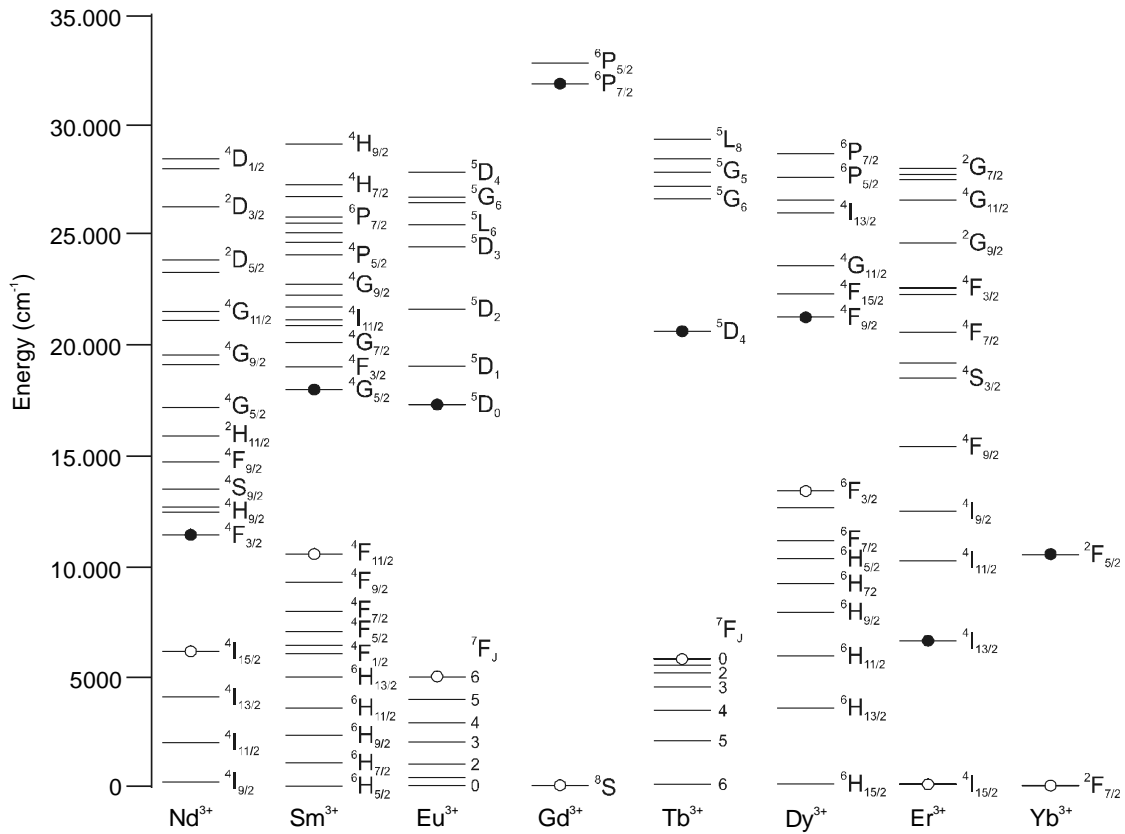


Figure 2.2: Energy diagram of the 4f levels responsible for the lanthanide luminescence. A filled circle denotes the lowest luminescent state, and an open circle denotes the highest non-luminescent state.¹¹

Magnetic dipole transitions within the $4f^n$ configuration, which obey the selection rule $\Delta J = 0, \pm 1$ are allowed (except for $J = 0$ to $J = 0$), but have low oscillator strengths. The electric dipole intra-4f transitions are in principle parity forbidden, and those transitions that do not occur within the ground multiplet may also be spin-forbidden ($\Delta S \neq 0$). However, in an asymmetric environment, the electric dipole f-f transitions become weakly allowed (with an oscillator strength of 10^{-6}) by mixing of opposite parity wave functions (primarily the 5d wave functions) into the 4f wave functions. In other words the parity forbidden intra-4f transitions ‘steal’ some intensity from the allowed 4f-5d transitions.

The spin selection rule is relaxed by the fact that heavy atoms have large spin-orbit couplings. Because the oscillator strengths of these induced electric dipole transitions are in the same order of magnitude as those of magnetic dipole transitions, both transitions can be observed in lanthanide absorption and emission spectra. The forbidden character of intra-4f transitions causes them to have low absorptivities, with absorption coefficients in the visible spectral range of less than $10 \text{ M}^{-1}\text{cm}^{-1}$, and relatively long luminescence lifetimes (in the range of μs to ms).

For certain induced electric dipole transitions that have $|\Delta J| < 2$, $|\Delta L| < 2$, and $\Delta S = 0$, the intensities are much more sensitive to complexation than other transitions, and have been termed *hypersensitive transitions*. The intensities of these transitions may be up to 200 times larger than the corresponding transition in the hydrated ion whereas the intensities of the other transitions are generally approximately the same.

2.3.3 The luminescence properties of lanthanide complexes in solution

When the emission spectrum of a complexed lanthanide ion is compared to that of the hydrated ion, three effects are observed: firstly, usually there are small shifts of the bands towards longer wavelengths, secondly the bands undergo additional splitting of the J-levels (or at least show a different splitting), and finally, there is a significant change in the molar absorptivity of the individual bands (typically less than an order of magnitude). Each of these effects can be readily related to the changes in the strength and symmetry of the crystal field produced by the ligands. Except for the hypersensitive transitions, complexation does not profoundly alter the spectrum of a trivalent lanthanide ion.

The typical emission bands of the Eu^{3+} , Tb^{3+} , Nd^{3+} , Er^{3+} , and Yb^{3+} complexes in solution are summarized in Table 2.2. In most cases, the decay of the lanthanide luminescent level is not controlled by the radiative rate constant, which is the rate constant of spontaneous emission, but by non-radiative processes. For lanthanide ions, the most important non-radiative processes are those that emerge from interaction of the lanthanide 4f electronic states with suitable vibrational modes of the environment. The *luminescent* trivalent rare earth cations can be classified into two groups:

The first group of lanthanides consists of praseodymium, neodymium, holmium, erbium, thulium, and ytterbium, and this group exhibits only weak luminescence in the visible and/or the near-infrared region. The main reason for this is that the energy difference between the lowest luminescent state and the highest non-luminescent state is relatively small. This small

energy gap makes the competing radiationless decay more likely to occur, *i.e.* vibronic quenching by high frequency oscillators.

Table 2.2: The typical emission bands of the lanthanide ion Eu^{3+} , Tb^{3+} , Nd^{3+} , Er^{3+} , and Yb^{3+} in solution. The hypersensitive transitions are bold-faced.

Ion	Transition	Emission	Ion	Transition	Emission	
Eu³⁺	$^5\text{D}_0 \rightarrow ^7\text{F}_0$	580 nm	Nd³⁺	$^4\text{F}_{3/2} \rightarrow ^4\text{F}_{9/2}$	880 nm	
	$^7\text{F}_1$	590 nm		$^4\text{F}_{11/2}$	1060 nm	
	$^7\text{F}_2$	613 nm		$^4\text{F}_{13/2}$	1330 nm	
	$^7\text{F}_3$	650 nm	Er³⁺	$^4\text{I}_{13/2} \rightarrow ^4\text{I}_{15/2}$	1550 nm	
	$^7\text{F}_4$	690 nm		Yb³⁺	$^2\text{F}_{5/2} \rightarrow ^2\text{F}_{7/2}$	980 nm
	$^7\text{F}_5$	710 nm				
Tb³⁺	$^5\text{D}_4 \rightarrow ^7\text{F}_6$	490 nm				
	$^7\text{F}_5$	545 nm				
	$^7\text{F}_4$	590 nm				
	$^7\text{F}_3$	620 nm				
	$^7\text{F}_2$	650 nm				

The second group of lanthanides consists of samarium, europium, terbium, and dysprosium, and exhibits strong luminescence. These lanthanide ions have large energy gaps between the lowest luminescent state and the highest non-luminescent state, and are therefore less sensitive towards vibronic quenching by high frequency oscillators. These energy gap considerations are known as the energy gap law theory, which will be discussed in paragraph 2.5.

The lanthanide ions lanthanum, lutetium and gadolinium do not exhibit any, or hardly any luminescence. Because the 4f subshells are completely empty or completely filled in La^{3+} and Lu^{3+} , respectively, no intra-4f transitions are possible. Luminescence is seldomly observed for Gd^{3+} , because of the large energy gap between the ground and the first excited state.

2.4 Sensitized Lanthanide Emission

2.4.1 The sensitization pathway

In the previous paragraph, we have seen that the lanthanide ions have unique luminescence properties, but that they possess low absorption coefficients which is a major drawback for efficient excitation. In order to overcome this disadvantage, lanthanide ions are usually excited via an organic antenna chromophore (the sensitizer), that has a much higher absorption coefficient. Upon excitation of the antenna chromophore, the excitation energy is transferred to the lanthanide ion, effecting the population of the lanthanide luminescent state. It has been established that this process in general takes place via the antenna triplet state with an electron exchange (Dexter) mechanism.¹³ Such a mechanism requires a physical overlap between the orbitals of donor and acceptor, and is therefore strongly distance dependent. In fact, the energy transfer rate diminishes rapidly at distances larger than 5 Å.

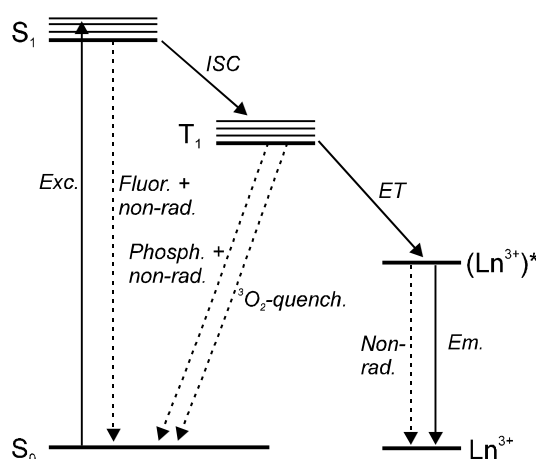


Figure 2.3: Photophysical model describing the main processes in the sensitization pathway.

The sensitization pathway in luminescent lanthanide complexes consists of excitation of the antenna chromophore into its singlet excited state, subsequent intersystem crossing of the antenna to its triplet state, and energy transfer from the triplet state to the lanthanide ion.^{14,15,16,17} These processes together with the competing processes are depicted in Figure 2.3. Examples of competing processes are fluorescence of the antenna, which is competing with intersystem crossing, and quenching of the triplet state by dissolved molecular oxygen, which is competing with the energy transfer to the lanthanide ion. The overall quantum yield of sensitized emission (Φ_{SE}) is therefore the product of the intersystem crossing quantum yield

(ϕ_{ISC}), the energy transfer quantum yield (ϕ_{ET}), and the lanthanide luminescence quantum yield (ϕ_{lum}):

$$\phi_{SE} = \phi_{ISC} \cdot \phi_{ET} \cdot \phi_{lum} \quad (1)$$

The lanthanide luminescence quantum yield indicates the efficiency of the lanthanide luminescence once the energy has been *transferred* to the lanthanide ion, and is defined as

$$\phi_{lum} = k_0 / (k_0 + \Sigma k_{non-rad}) \quad (2)$$

where k_0 is the rate constant of spontaneous emission, and $\Sigma k_{non-rad}$ the sum of the non-radiative rate constants.

It can be seen from equation (1) that sensitization of the lanthanide luminescence, instead of direct excitation, cannot increase the luminescence quantum yield ($\phi_{SE} \leq \phi_{lum}$). However, the effectiveness of the sensitization process can be demonstrated if we consider the luminescence intensity, which is the product of the absorption coefficient at the excitation wavelength and the quantum yield ($\epsilon \times \phi_{SE}$). Since organic chromophores usually have absorption coefficients that are 10^3 - 10^6 $M^{-1}cm^{-1}$ compared to 1-10 $M^{-1}cm^{-1}$ for lanthanide ions, sensitization can increase the luminescence intensities up to a 10^6 -fold, if the energy transfer process is efficient, *i.e.* $\phi_{ISC} = 1$, and $\phi_{ET} = 1$.

For an efficient sensitization process in sensitizer-functionalized lanthanide complexes the following conditions have to be considered:

- The intersystem crossing yield of the antenna chromophore should be high, although the lanthanide ion can enhance the intersystem crossing via an external heavy atom effect.¹⁸ This effect can be very large: the intersystem crossing yield can increase from values as low as 0.01 to unity.
- The antenna should have matching triplet state energy levels for energy transfer to the lanthanide luminescent states. If the energy difference between donor and acceptor is too small a thermally activated energy back-transfer can occur, whereas large energy differences may lead to slower energy transfer rates.

- The antenna should have a high absorption coefficient, in order to obtain high luminescence intensities ($\epsilon \times \phi_{SE}$).
- The antenna chromophore should be in close proximity to the lanthanide ion, because the energy transfer process is strongly distance dependent.

2.4.2 The external heavy atom effect

The enhancement of electronic transitions of (antenna) chromophores by lanthanide ions is called the external heavy atom effect.¹⁹ The external heavy atom effect is not precluded to heavy metal ions, but also solvents containing heavy atom nuclei can enhance the electronic transitions of the dissolved chromophores. In particular, the spin-forbidden singlet-triplet transitions (intersystem crossing) and the triplet-singlet transitions (phosphorescence and/or non-radiative transitions) of the antenna chromophore are increased, which generally results in a reduction of the fluorescence intensity. The presence of a lanthanide ion in close proximity to the antenna chromophore causes mixing of the antenna singlet and triplet state wavefunctions, thereby giving the singlet state a little triplet character and vice versa. As a result, the transitions that originally were spin-forbidden, become weakly allowed. The mixing of the antenna singlet and triplet states has been ascribed to an enhanced spin-orbit coupling of the system, and to an exchange interaction of metal-unpaired 4f electrons with the π -electrons of the organic chromophore.¹⁸

Table 2.3: The fluorescence quantum yields (ϕ_f), intersystem crossing quantum yields (ϕ_{ISC}), and phosphorescence lifetimes of two series of lanthanide chelates ($\tau_{phos,77K}$).¹⁸

Chelate	ϕ_f	ϕ_{ISC}	$\tau_{phos,77K}$ (ms)
La(BFA) ₃	0.002	0.15 ^a	130
Gd(BFA) ₃	0.006	0.84 ^a	2.4
Lu(BFA) ₃	0.012	0.76 ^a	120
La(MS) ₃	0.24	0.12	30.2
Gd(MS) ₃	0.01	0.18	1.1
Tb(MS) ₃	<0.01	--	--
Lu(MS) ₃	0.21	0.19	25.3

BFA = benzoyltrifluoroacetate; MS = methylsalicylate; ^a $\phi_{phos,77K}$

A decrease of the antenna fluorescence upon complexation of the lanthanide ion is often observed.²⁰ Tobita and coworkers¹⁸ have studied the influence of different lanthanide ions on

the photophysical properties of the ligand (the antenna) in a series of lanthanide-tris(methylsalicylate) ($\text{Ln}(\text{MS})_3$) and lanthanide-tris(benzoyltrifluoroacetate) ($\text{Ln}(\text{BFA})_3$) complexes. Some of their results are summarized in Table 2.3. They found that in the paramagnetic Gd^{3+} and Tb^{3+} chelates the antenna fluorescence intensity was significantly reduced compared to the diamagnetic Lu^{3+} and La^{3+} chelates. Furthermore, the paramagnetic Gd^{3+} ion was found to lower the antenna triplet state lifetime more than the diamagnetic Lu^{3+} and La^{3+} ions. A similar paramagnetic effect has been observed for the influence of complexed Cu^{2+} and Zn^{2+} ions on the intersystem crossing rates of porphyrins. The paramagnetic Cu^{2+} ion strongly enhances the intersystem crossing rate, whereas the diamagnetic Zn^{2+} ion, which has approximately the same mass as Cu^{2+} , has a much smaller effect.²¹

2.4.3 The role of the antenna triplet state

Already in 1942 Weisman found that upon near-UV excitation of Eu -tris(β -diketonate) chelates in solution, the typical Eu^{3+} luminescence can be observed.²² Since then many studies have been devoted to these type of chelates to elucidate the sensitization pathway that involves the intramolecular energy transfer from the ligand to the lanthanide ion. These studies, *e.g.* variation of the ligand triplet state relative to the lanthanide luminescent state¹⁴ and time-resolved luminescence studies,¹⁶ have established that in general the energy transfer takes place through the ligand triplet state. Sato and Wada studied a series of Eu -tris(β -diketonato) complexes in several solvents and found that there is an optimum in the overall luminescence quantum yield when the energy difference between the triplet state of the ligand and the Eu^{3+} luminescent level is varied.¹⁴ In Eu^{3+} complexes energy transfer usually takes place to the $^5\text{D}_1$ state ($19,000\text{ cm}^{-1}$) and the $^5\text{D}_0$ state ($17,500\text{ cm}^{-1}$). They concluded that for a fast and irreversible energy transfer, the energy difference between the antenna triplet state and the $\text{Eu}^{3+} ^5\text{D}_1$ state should be approximately $1,500\text{ cm}^{-1}$.¹⁴ If this energy difference is too small a thermally activated energy back-transfer process becomes possible, which makes the overall process less efficient. (see paragraph 2.4.7). Similar results were obtained by Hayes and Drickamer who used a high pressure luminescence technique.²³ This technique is based on the fact that the ligand triplet states are extremely sensitive to pressure, which results in large energy shifts (up to $2,000\text{ cm}^{-1}$). However, owing to the shielding by an outer shell of 5s and 5p electrons, the lanthanide 4f energy levels are not sensitive to pressure. Thus an

increase in pressure can tune in a continuous way the ligand singlet and triplet excited states relative to the lanthanide levels.

2.4.4 External triplet quenchers

Since the triplet state is the donating energy level in the energy transfer process, quenching of the antenna triplet state by dissolved molecular oxygen is a competing process. If the energy transfer process is not fast compared to the oxygen quenching rate, the triplet state is deactivated by oxygen instead of contributing to the population of the lanthanide luminescent state. Studying the oxygen sensitivity of the sensitized lanthanide luminescence intensity by deoxygenation of the samples is in fact a practical tool to estimate the energy transfer rate. The competing oxygen quenching rate k_{ox} can be estimated as the product of the diffusion controlled quenching rate constant k_{diff} (which is generally in the order of $10^{10} \text{ M}^{-1} \text{ s}^{-1}$)²⁴ and the oxygen concentration in the solvent $[\text{O}_2]$:

$$k_{\text{ox}} = k_{\text{diff}}[\text{O}_2] \quad (8)$$

Parker and coworkers have exploited the oxygen sensitivity of their (sensitizer-functionalized) luminescent lanthanide complex to make an oxygen sensor.²⁵ Also other external triplet quenchers with appropriate triplet state energies, *e.g.* piperylene, can quench the triplet state of the ligand in Eu-tris(β -diketonate) complexes, and thus the sensitized luminescence intensity.²⁶

2.4.5 The role of the antenna singlet state

The efficient population of the antenna triplet state requires not only a high intersystem crossing yield, but also an efficient population of the antenna singlet excited state, *i.e.* high absorption coefficients. Furthermore, the energy of the singlet excited state determines the excitation wavelength. If it is assumed that the antenna chromophore displays a singlet-triplet energy gap of at least $5,000 \text{ cm}^{-1}$, which appears to be a lower limit for π -systems,²⁴ and that its triplet state energy must be at least $1,500 \text{ cm}^{-1}$ above the main receiving state of the lanthanide ion, the long wavelength absorption edge of the antenna (the $0-0$ transition in the absorption spectrum) will be around 370 nm for Tb^{3+} , and around 390 nm for Eu^{3+} complexes. The near-infrared luminescent lanthanide ions Nd^{3+} , Yb^{3+} , and Er^{3+} , have much lower lying luminescent states, and by applying the same energetic considerations it can be

calculated that these lanthanide ions can be excited via antenna chromophores that have absorption bands in the 500 - 600 nm region.

2.4.6 The electron-exchange energy transfer mechanism

It has been established that in general the energy transfer from the antenna triplet state to the lanthanide ion proceeds via an electron-exchange mechanism (Dexter), and is not likely to proceed via a resonance dipole-dipole mechanism (Förster). This can be illustrated with simple energy transfer treatments: the induced electric dipole transitions of lanthanide ions are very weak, leading to small spectral overlap integrals in Förster's theory. Furthermore, the energy transfer process involves a spin-forbidden transition of the donor (antenna triplet-singlet transition), which is forbidden in Förster's theory of energy transfer.

In Dexter's theory of short-range energy transfer an electron-exchange mechanism is involved, therefore a physical contact between the orbitals of donor and acceptor, *i.e.* the sensitizer and lanthanide ion, is required. This process can be visualized as a simultaneous exchange of electrons from the excited antenna to the lanthanide ion and from the lanthanide ion to the antenna. Dexter has demonstrated that the transfer of energy also occurs over distances larger than those of van der Waals contact.

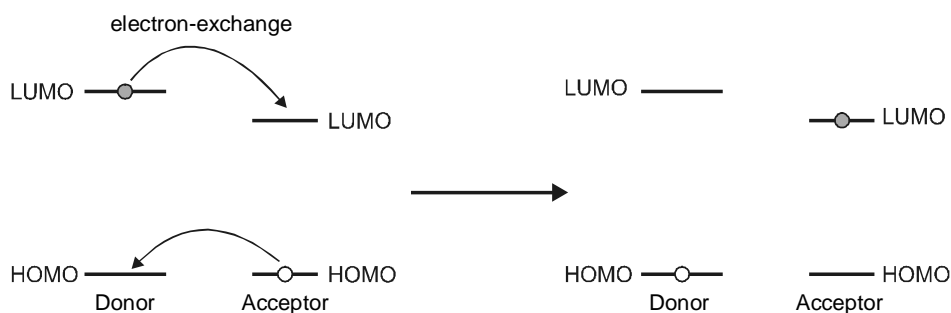


Figure 2.4: Schematic representation of the energy transfer from a donor to an acceptor due to an electron-exchange mechanism

The electron-exchange mechanism further requires a spectral overlap between the donor and acceptor. This means that the phosphorescence spectrum of the sensitizer should have a spectral overlap with the absorption bands of the lanthanide ion. According to Dexter the rate constant for energy transfer (k_{ET}) is given by the following equation:

$$k_{\text{ET}} = (2\pi/\hbar)Z^2 \cdot \int F_d(\nu)\epsilon_a(\nu)d\nu \quad (3)$$

The first term $(2\pi/\hbar)Z^2$ is related to the specific orbital interactions, and is therefore strongly dependent on the distance between donor and acceptor. Dexter derived that

$$Z^2 \sim e^{-2R/L} \quad (4)$$

where R is the distance between donor and acceptor, and L is the sum of the van der Waals radii of the donor and acceptor. The second term $\int F_d(\nu)\epsilon_a(\nu)d\nu$ is the spectral overlap integral, where $F_d(\nu)$ in this case is the phosphorescence spectrum of the sensitizer and $\epsilon_a(\nu)$ is the absorption spectrum of the lanthanide ion. The integrals of the phosphorescence and the absorption spectra are normalized, so that $\int F_d(\nu)d\nu = 1$ and $\int \epsilon_a(\nu)d\nu = 1$. This means that the overlap integral does not depend on the optical properties of the lanthanide transitions, *i.e.* the absorption coefficient ϵ .

2.4.7 Energy back-transfer

One of the factors that can limit the energy transfer efficiency in sensitizer-functionalized lanthanide complexes, is the thermally activated energy back-transfer from the lanthanide ion to the triplet state of the antenna. This process occurs when the energy difference between the triplet state and the main receiving lanthanide state is less than $1,500 \text{ cm}^{-1}$, and can be recognized if the lanthanide luminescence lifetimes are oxygen and/or temperature dependent.

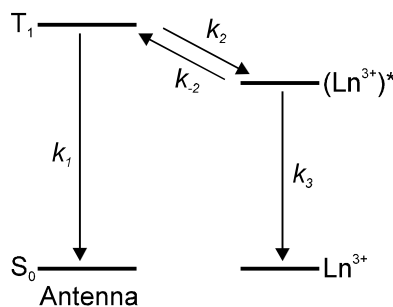


Figure 2.5: Schematic representation of the equilibrium between the lanthanide luminescent state and the antenna triplet state, where k_1 and k_3 represent the sum of deactivation via radiative and non-radiative processes, k_2 represents the energy transfer rate, and k_{-2} represents the energy back-transfer rate.

Oxygen does not quench the luminescent states of lanthanide ions, but quenches the antenna triplet state. As a result the energy back-transfer rate is increased relative to the forward transfer, which leads to an increased deactivation of the lanthanide luminescent state. Raising of the temperature also increases the (endothermic) energy back-transfer rate relative to the forward transfer. Due to the fact that practical applications require near UV-Vis excitation of the sensitizer,³¹ energy back-transfer occurs to a greater extent for Tb³⁺ complexes (luminescent state at 20,400 cm⁻¹) than for Eu³⁺ complexes (luminescent state at 17,500 cm⁻¹).

2.4.8 Ligand-to-metal charge transfer

One of the problems that has frequently been encountered in the search of efficient sensitizers for Eu³⁺ is photo-induced electron transfer.^{27,28,29} Upon excitation of the antenna into its singlet excited state an electron is transferred to the Eu³⁺ ion, resulting in an antenna radical cation and Eu²⁺, instead of intersystem crossing to the triplet state and subsequent energy transfer. One of the reasons for the occurrence of this competing process is the low reduction potential of Eu³⁺ in comparison with other trivalent lanthanide ions: -0.35 V in water (vs. SHE). In general, the rate of any photo-induced electron transfer process is strongly distance dependent. If the distance is small, the electron transfer rate may be comparable with the absorption of a photon. In this limit the process is better described as a ligand-to-metal charge transfer (LMCT), and gives rise to additional bands in the UV-Vis absorption spectrum. Although these LMCT transitions are generally centered at wavelengths below 286 nm, their absorption bands are broad with tails extending to 400 nm.³⁰ For most systems studied in aqueous solutions, the non-radiative relaxation pathways of these LMCT states do not pass through the ⁵D_J excited state manifold, and therefore, do not lead to sensitized Eu³⁺ emission.

Recently, it was found that 2-methylnaphthalene is a surprisingly inefficient sensitizer for Eu³⁺.^{31,32} Since the antenna fluorescence intensity of the Eu³⁺ complex was only 10% of that measured for the corresponding Tb³⁺ and Gd³⁺ complexes, an additional deactivation of the singlet state by a photo-induced electron transfer was suspected. The driving force $-\Delta G$ of a photo-induced electron transfer (PET) can be estimated with the equation:

$$\Delta G_{\text{PET}} = E(\text{Ant}^{\bullet+}/\text{Ant}) - E_{\text{Ant}^*} - E(\text{Eu}^{3+}/\text{Eu}^{2+}) \quad (5)$$

The application of equation (5) with $E(\text{Napht}^{\bullet+}/\text{Napht}) = 1.45 \text{ eV}$ and $E_{\text{napht}^*} = 3.9 \text{ eV}$, leads to an estimated ΔG of -2.1 eV for the photo-induced electron transfer from the singlet state of naphthalene to Eu^{3+} . In view of this highly exothermic free energy change, it is not surprising that electron transfer is significant in this system. An intermolecular quenching study has shown that k_Q for electron-transfer quenching of naphthalene by Eu^{3+} has a value of $7.2 \times 10^9 \text{ M}^{-1}\text{s}^{-1}$ in acetonitrile.³³

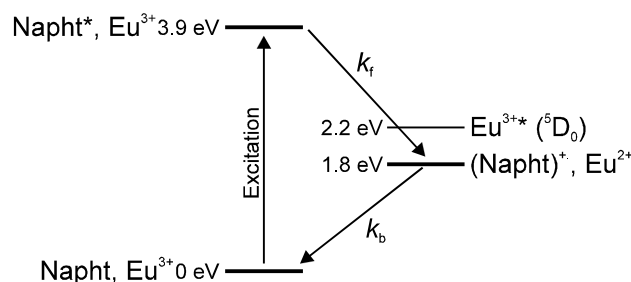


Figure 2.6: Possible electron transfer scheme between naphthalene* and Eu^{3+} where k_f and k_b are the forward and backward electron transfer rates.

Using this system as an example, it can be illustrated why the $^5\text{D}_J$ manifold cannot be populated via the LMCT state. Upon excitation of the naphthalene antenna an electron is transferred and Eu^{2+} and (naphthalene)⁺ are formed. The former is a strong reducing reagent and the latter a strong oxidant, causing the electron to return to produce Eu^{3+} and ground state naphthalene. However, since $E(\text{Napht}^{\bullet+}/\text{Napht}) - E(\text{Eu}^{3+}/\text{Eu}^{2+})$ is 1.8 eV, which is lower than the $^5\text{D}_0$ state of Eu (2.2 eV), the Eu^{3+} ion thus formed will not be in its excited state.

Recently, there has been some discussion about the sensitization process of Yb^{3+} . It has been reported that Yb^{3+} , which has only one excited state at $10,200 \text{ cm}^{-1}$ ($^2\text{F}_{5/2}$), can be sensitized via antenna chromophores that have triplet states far higher in energy. It has been argued that the sensitization process does not proceed via the triplet, because the spectral overlap is negligible. Horrocks and coworkers studied the tryptophane-sensitized Yb^{3+} luminescence of parvalbumin loaded with Yb^{3+} .³⁴ Based on the fact that like Eu^{3+} , Yb^{3+} is relatively easily reduced to Yb^{2+} , they proposed a photo-induced electron transfer mechanism for the tryptophane-sensitized Yb^{3+} luminescence. In this case the $E(\text{Trp}^{\bullet+}/\text{Trp}) - E(\text{Yb}^{3+}/\text{Yb}^{2+})$ is 2.36 eV, which is higher in energy than the $^2\text{F}_{5/2}$ luminescent state of Yb^{3+} (1.27 eV), thus the return of the electron can lead to a Yb^{3+} ion in its excited state.

This photo-induced redox energy transfer mechanism does not appear to be a general mechanism, because other systems have been reported in which the energy transfer proceeds via the antenna triplet state. For example, the recently reported fluorescein and eosin sensitized Yb^{3+} emission exhibited an oxygen dependence, which indicated that the energy transfer proceeds via the triplet state.³⁵

2.5 Quenching by High Frequency Oscillators

2.5.1 The energy gap law

The measured lifetimes of luminescent species are generally shorter than the natural lifetimes, because non-radiative processes compete with the radiative decay. High frequency O-H and C-H vibrations in the local environment and the size of the energy gap between the excited and the ground state of the lanthanide ion, play an important role in removing energy non-radiatively from the lanthanide excited state.^{36,37} The deactivation arises from a weak vibronic coupling between the f-electronic states of the lanthanide ions and the vibrational states of O-H and C-H. To provide an efficient deactivation route, the energy gap between the excited and the ground state of an excited lanthanide ion must be bridged by these vibrational states. According to the theory of the energy gap law¹¹ the smaller the harmonic number of vibrational quanta that is required to match the energy gap between the lowest luminescent state and the highest non-luminescent state of the lanthanide ion, the more effective the vibronic quenching will be. The harmonic number of vibrational quanta (ν) of several vibrations that is required to match the energy gap in Tb^{3+} , Eu^{3+} , Yb^{3+} , Er^{3+} , and Nd^{3+} are indicated in Figure 2.7.

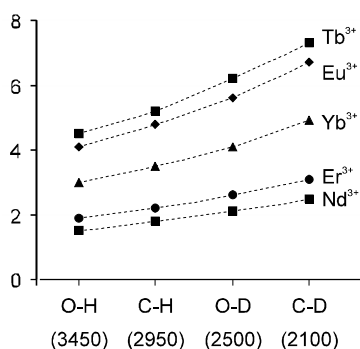


Figure 2.7: Graphical representation of the number of vibrational quanta of four high frequency oscillators that is required to match the energy gap between the lowest luminescent state and the highest non-luminescent state of the lanthanide ion (the dashed line is merely a guide to the eye).

The Tb^{3+} ion, which has a large energy gap, is the least sensitive towards quenching by high frequency oscillators, and as a result has a higher luminescence quantum yield than for example Eu^{3+} . It can furthermore easily be seen from Figure 2.7 that the near-infrared luminescent lanthanide ions are more prone to quenching by vibrations in their environment than the visible emitting lanthanide ions. Indeed, the observed lifetimes of Eu^{3+} and Tb^{3+} complexes in solution are in the ms range, whereas the observed lifetimes of the near-infrared luminescent lanthanide complexes are in the μs range. It has been shown that by replacing the C-H bonds in the ligands by C-D bonds the luminescence lifetimes of the complexed lanthanide ions are increased.^{38,39}

The sensitivity of Eu^{3+} and Tb^{3+} luminescence towards quenching by solvent OH groups has been studied in detail, and it was experimentally found that the luminescence lifetimes vary linearly with the number of coordinated water molecules in the first coordination sphere. The following expression was derived empirically:^{40,41}

$$n = q \times (1/\tau_{\text{H}_2\text{O}} - 1/\tau_{\text{D}_2\text{O}}) \quad (6)$$

where n is the total number of OH groups in the first coordination sphere, and $\tau_{\text{H}_2\text{O}}$ and $\tau_{\text{D}_2\text{O}}$ are the luminescence lifetimes in H_2O and D_2O , respectively. The constant q depends on the lanthanide ion, and is empirically derived: q is 1.05 for a Eu^{3+} complex, and 4.2 for a Tb^{3+} complex. Recently, this equation has been extended with a term that corrects for closely diffusing second-sphere water molecules:⁴²

$$n = q \times (1/\tau_{\text{H}_2\text{O}} - 1/\tau_{\text{D}_2\text{O}} - k_{\text{corr}}) \quad (7)$$

where k_{corr} is 0.25 ms^{-1} for Eu^{3+} and 0.05 ms^{-1} for Tb^{3+} . Based on the assumption that methanol behaves like half a water molecule, a similar equation can be written when methanol is the solvent. In this case, q is 2.1 and k_{corr} is 0.125 ms^{-1} for Eu^{3+} , whereas q is 8.4 and k_{corr} is 0.025 ms^{-1} for Tb^{3+} .

2.5.2 The Franck-Condon factor

The energy gap law is a practical result of the Franck-Condon factor of vibronic transitions,⁴³ which is in this case a measure for the amount of vibronic coupling between the

f-electronic states of the lanthanide ions and the vibrational states of high frequency oscillators. The harmonic matching number ν of the energy gap law for the energy gap of a lanthanide ion and a high frequency oscillator denotes the overtone of the vibration to which the energy is transferred. For example, the 5D_0 luminescent state of Eu^{3+} is non-radiatively deactivated by energy transfer to the 4th overtone of the O-H vibration.

The intensity of the vibronic transition depends on the square of the overlap integral between the initial ($\nu=0$) and final ($\nu=4$) vibrational state wavefunctions of the O-H oscillator. The square of this overlap integral is known as the Frank-Condon factor F . As the vibrational quanta increase, the Frank-Condon factor decreases. Using the undistorted oscillator model for the vibration the factor F can be estimated quantitatively.⁴⁴ In this model, F is given by

$$F(E) = (\exp(-\gamma)\gamma^\nu) / \nu! \quad (8)$$

where γ is the displacement factor defined by $\gamma = \frac{1}{2}k (q - q^0)^2 / \hbar\omega$ (q and q^0 are equilibrium positions in vibration states). If γ is assumed to be 1, F is obtained as 0.18, 0.061, 0.015, and 0.0031 at $\nu = 2, 3, 4,$ and $5,$ respectively. The vibronic coupling becomes rapidly weaker with the increasing overtone of a vibration. If the O-H oscillator is replaced by the O-D oscillator, the energy of the $\text{Eu}^{3+} {}^5D_0$ level must be transferred to the 5th overtone, the factor F decreases from 0.015 to 0.0031, hence the quenching is much less efficient.

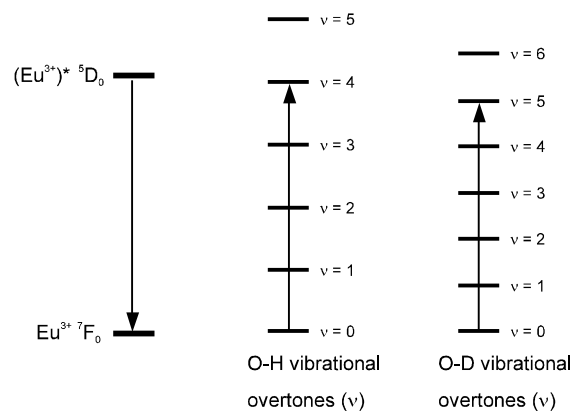


Figure 2.8: Schematic representation of the vibronic quenching of the $\text{Eu}^{3+} {}^5D_0$ luminescent state by the 4th overtone of the O-H vibration or the 5th overtone of the O-D vibration.

2.5.3 The Förster energy transfer mechanism

The quenching of the luminescent state of a particular lanthanide ion does not only depend on the energy gap, but also on the distance between the lanthanide ion and the high frequency oscillator. The transfer of excitation energy takes place via the Förster dipole-dipole mechanism,^{5,45} which depends on the distance between the lanthanide ion and the high frequency oscillator with the inverse of the sixth power. The dipole-dipole interaction is in fact only the first in a multipole-multipole expression, but it is the most important term. Förster computed that the rate of energy transfer is:

$$k_{\tau} = (1/\tau_D)(R_0/r)^6 \quad (9)$$

where τ_D is the lifetime of the donor (the lanthanide ion) in the absence of the acceptor (the high frequency oscillator), r is the distance between donor and acceptor, and R_0 is the critical distance for energy transfer. The donor has two ways to decay to the ground state: energy transfer to the acceptor, and radiative decay (the non-radiative decay is neglected, but can be included in the rate of radiative decay). The critical distance for energy transfer is defined as the distance for which the energy transfer rate is equal to the radiative rate, *i.e.* R_0 is the distance at which 50% of the excitation energy is transferred to the acceptor. This distance can be calculated from the following equation

$$R_0 = 8.78 \times 10^{-25} \kappa^2 \phi_D n^{-4} J \quad (10)$$

where κ is an orientation factor, ϕ_D is the quantum yield of the donor in the absence of the acceptor, n is the refractive index of the medium intervening between the donor and acceptor, and finally J is the spectral overlap and is defined by

$$J = (\int F(\nu) \epsilon(\nu) \nu^4 d\nu) / (\int F(\nu) d\nu) \quad (11)$$

where $F(\nu)$ is the luminescence intensity of the donor, $\epsilon(\nu)$ is the molar extinction coefficient of the acceptor (in $M^{-1}cm^{-1}$), and ν is the frequency in cm^{-1} . The orientation factor κ accounts for the directional nature of the dipole-dipole interaction. For a solution containing randomly

oriented donor and acceptor transition dipole moments (*i.e.* randomly oriented molecules), κ^2 has the value $2/3$.

2.6 Lanthanide Luminescence Characteristics

2.6.1 Eu^{3+} luminescence

The luminescence originating from the Eu^{3+} ion can be used as a probe for the coordination environment, not only to estimate the number of coordinated water or methanol molecules (*vide supra*), but also to obtain information concerning the symmetry of the first coordination sphere. The optical transitions of Eu^{3+} are a special case in the theory of induced electric dipole transitions. The induced electric dipole transitions have an additional selection rule if the initial level has $J = 0$, as is the case for Eu^{3+} ($^5\text{D}_0$): transitions to odd J are forbidden. This generally results in the following emission spectrum:

- $^5\text{D}_0 \rightarrow ^7\text{F}_0$ (580 nm): extremely weak, induced electric dipole ($J = 0$ to $J = 0$ is forbidden).
- $^5\text{D}_0 \rightarrow ^7\text{F}_1$ (590 nm): magnetic dipole emission.
- $^5\text{D}_0 \rightarrow ^7\text{F}_2$ (613 nm): hypersensitive induced electric dipole emission, which is usually dominating.
- $^5\text{D}_0 \rightarrow ^7\text{F}_3$ (650 nm): extremely weak, induced electric dipole emission.
- $^5\text{D}_0 \rightarrow ^7\text{F}_4$ (~700 nm): weak, induced electric dipole emission.

Experimental data on a variety of Eu^{3+} complexes have established that the emission band centered around 590 nm, corresponding to the $^5\text{D}_0 \rightarrow ^7\text{F}_1$ transition that is magnetic dipole in character, is relatively strong and largely independent of the coordination sphere, *i.e.* the ligand field. The electric dipole $^5\text{D}_0 \rightarrow ^7\text{F}_2$ transition centered around 613 nm is hypersensitive and extremely sensitive to the symmetry of the coordination sphere. Kirby and Richardson established that the relative intensity of the $^5\text{D}_0 \rightarrow ^7\text{F}_2$ and the $^5\text{D}_0 \rightarrow ^7\text{F}_1$ emission is a good measure of the symmetry of the first coordination sphere.⁴⁶ In a centrosymmetric environment the magnetic dipole $^5\text{D}_0 \rightarrow ^7\text{F}_1$ transition of Eu^{3+} is dominating, whereas distortion of the symmetry around the ion causes an intensity enhancement of electric dipole transitions such as the hypersensitive $^5\text{D}_0 \rightarrow ^7\text{F}_2$ transition. They have determined that this ratio is 8.0 for a

single crystal $\text{Eu}(\text{DBM})_3 \cdot \text{H}_2\text{O}$ (DBM = 1,3-diphenyl-1,3-propanedionate) in which the Eu^{3+} ion has an asymmetric coordination sphere, whereas they found an intensity ratio of 0.67 for the centrosymmetric $[\text{Eu}(\text{ODA})_3]$ complex (ODA = oxydiacetate).

Another probe is the ${}^5\text{D}_0 \rightarrow {}^7\text{F}_0$ emission line around 580 nm. Since the ${}^7\text{F}_0$ and ${}^5\text{D}_0$ states are non-degenerate, the number of emission bands observed in the emission spectrum is related to the number of chemically distinct environments of the Eu^{3+} ion.

2.6.2 Tb^{3+} luminescence

The luminescence of Tb^{3+} complexes is characterized by emission from the ${}^5\text{D}_4$ state resulting in green luminescence. The ${}^5\text{D}_4 \rightarrow {}^7\text{F}_5$ emission band at 545 nm is hypersensitive, but is not as sensitive to the changes in the environment as the ${}^5\text{D}_0 \rightarrow {}^7\text{F}_2$ emission of Eu^{3+} . The spectra show some structuring within the emission bands, but do not provide the basis for a reliable diagnostic probe of the symmetry of the complex, as is the case for the Eu^{3+} spectra.⁴⁷ This is caused by the fact that the J-values of the levels involved in the transitions are high, resulting in splitting of the J-levels into many sublevels.⁵

2.6.3 Nd^{3+} , Er^{3+} , and Yb^{3+} luminescence

Most of the luminescence spectra of Nd^{3+} , Er^{3+} , and Yb^{3+} reported in literature are of these ions in inorganic solid state materials. These materials have found their applications in solid state lasers and optical amplification. However, an increasing number of emission spectra of these lanthanide ions and their organic complexes is becoming available, due to a recent interest in their near-infrared luminescence in solution.

Although one of the first emission spectra of an organic $\text{Nd}(\text{PFP})_3\text{Phen}$ (PFP = pentafluoropropionate; Phen = 1,10-phenanthroline) complex in $\text{DMSO}-d_6$ has already been reported in 1967 by Heller,⁴⁸ more emission spectra of Nd^{3+} complexed by different organic host molecules have only been reported recently. In general, three emission lines at 880, 1060, and 1330 nm are observed for Nd^{3+} , that correspond to the ${}^4\text{F}_{3/2} \rightarrow {}^4\text{I}_{9/2}$, ${}^4\text{I}_{11/2}$, and ${}^4\text{I}_{13/2}$ transitions, respectively. In organic matrices, the 1060 nm emission of Nd^{3+} is the strongest and the 1330 nm emission the weakest, as is the case for the emission spectra of Nd^{3+} in inorganic matrices.

Sensitized emission from Er^{3+} in organic matrices, for example encapsulated by a calix[4]arene-based ligand,⁴⁹ is only observed at 1540 nm (${}^4\text{I}_{13/2} \rightarrow {}^4\text{I}_{15/2}$ transition). In

principle Er^{3+} could also show emission at 980 nm (${}^4\text{I}_{11/2} \rightarrow {}^4\text{I}_{15/2}$ transition) or at 820 nm (${}^4\text{I}_{9/2} \rightarrow {}^4\text{I}_{15/2}$ transition), but obviously these states are non-radiatively deactivated to the ${}^4\text{I}_{13/2}$ state or to the ground state (${}^4\text{I}_{15/2}$).

In 1958, the first sensitized emission spectrum of an $\text{Yb}(\text{DBM})_3$ chelate at 77 K was reported by Crosby and Kasha.⁵⁰ Emission from Yb^{3+} in solution is observed at 980 nm, with a shoulder at 1030 nm, corresponding to the ${}^2\text{F}_{5/2} \rightarrow {}^2\text{F}_{7/2}$ transition.

The main difference in optical properties between the near-infrared luminescent lanthanide ions in inorganic matrices and organic matrices, is that the luminescence lifetimes in the former are much longer, with typical lifetimes of 0.250 ms for Nd^{3+} ,⁵¹ 11 ms for Er^{3+} ,⁵² and 1 ms for Yb^{3+} .⁵³ In organic matrices the luminescence lifetimes are much shorter due to the vibronic quenching of for example O-H and C-H vibrations of the solvent and ligand. The luminescence lifetimes of, for example, a deuterated $\text{Nd}(\text{HFA})_3$ (HFA = hexafluoroacetylacetonate) chelate in methanol- d_4 is 0.70 μs , and 6.30 μs in DMSO- d_6 .⁵⁴ The luminescence lifetime of Er^{3+} in a calix[4]arene-based ligand in DMSO is 1.71 μs .⁴⁹ Compared to the Nd^{3+} and Er^{3+} complexes, the Yb^{3+} complexes typically have relatively long luminescence lifetimes ranging from 20 to 40 μs ,⁵⁵ owing to the large energy gap between the Yb^{3+} luminescent state and the ground state (see paragraph 2.5.1).

2.7 Luminescent Lanthanide Complexes

2.7.1 Introduction

The trivalent lanthanide ions are spherical, triply charged cations, that preferably bind to hard bases such as oxygen and nitrogen. Since the hydration number of lanthanide ions varies from eight to nine, the ligand of interest should have at least eight or nine donor atoms to obtain a solvent free complex. Examples of strongly coordinating groups are charged oxygen atoms such as carboxylates, phosphonates, and phosphinates, and neutral donors that possess large ground state dipole moments such as amide carbonyl oxygens. Ligands in which these coordinating groups are preorganized form stable complexes with lanthanide ions. Cram has formulated this principle of preorganization as follows: *the more highly hosts and guests are organized for binding and low solvation prior to their complexation, the more stable will be their complexes.*⁵⁶ Ligand coordination occurs predominantly via ionic bonding interactions,

and the geometrical arrangements of the ligands will be mainly controlled by steric factors and electronic repulsion between charges on the ligands. Obviously, also the conformational properties of the ligand play an important role.

2.7.2 β -Diketonate chelates

The first reported luminescent lanthanide complexes are the lanthanide β -diketonate complexes. The two substituents at the propanedione skeleton of β -diketonate ligands can vary from simple methyl groups to CF_3 groups, (substituted) phenyl groups, or polyaromatic moieties (see Figure 2.9). The complexes can be formed as negatively charged lanthanide-tetra(β -diketonate) complexes or as neutral lanthanide-tris(β -diketonate) complexes, depending on the preparation procedure.⁵⁷

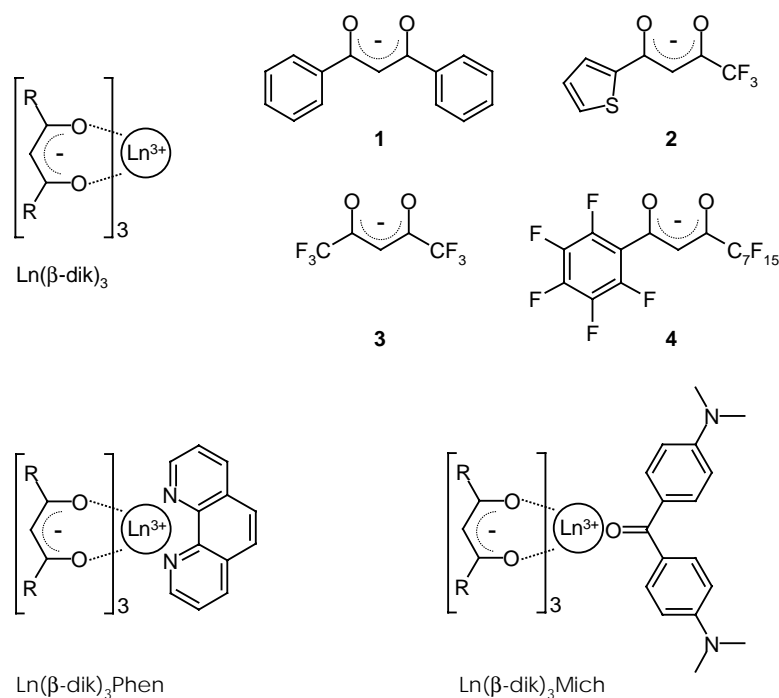


Figure 2.9: Examples of lanthanide- β -diketonate complexes and ligands.

The stability of the complexes in organic solvents depends on the amount of steric hindrance between the substituents, and on the pK_a of the β -diketonate ligand. The corresponding lanthanide complexes are less stable with increasing acidity of the β -diketonate ligand. The chelates are not stable in water, because of hydrolysis of the complexes. The excitation wavelength and the energy transfer efficiency (thus the sensitized luminescence intensity) is strongly influenced by the substituents.^{14,58} For the Eu^{3+} complexes the influence

of the various substituents is mainly found in the stability and the thermally activated quenching of the 5D_0 state by the ligand triplet state¹⁴ or by LMCT states.^{30,59} A typical feature of the emission spectra of the Eu-tris(β -diketonate) complexes is the extreme domination of the hypersensitive $^5D_0 \rightarrow ^7F_2$ transition.

Some attention has been paid to the synergistic coordination of Eu^{3+} and Tb^{3+} by 1,10-phenantroline (Phen) and β -diketonates. The complexes show a significant increase in the sensitized lanthanide emission.^{57,60} Another example of such a synergistic complex is the complex of $\text{Eu}(\text{fod})_3$ and Michler's ketone⁶¹ in benzene. Upon coordination to the Eu^{3+} ion, the absorption band of Michler's ketone shifts to 450 nm, allowing visible light excitation with high overall luminescence quantum yields (0.17).⁶²

2.7.3 Cyclen derivatives

A large family of water soluble ligands and complexes are based on the 1,4,7,10-tetraazacyclododecane skeleton (cyclen).^{63,64} Functionalized with four pendant arms containing additional donors, the resulting ligands play an important role in the applications of lanthanide complexes in aqueous solutions, such as MRI contrast reagents (Gd^{3+} complex)⁶⁵ and as luminescent probes in fluoroimmunoassays (Eu^{3+} and Tb^{3+} complexes). Cyclen can be functionalized with amide, carboxylate, phosphate, or phosphinate groups. Depending on the charge of the donor groups, the resulting complexes may be cationic, neutral, or anionic.

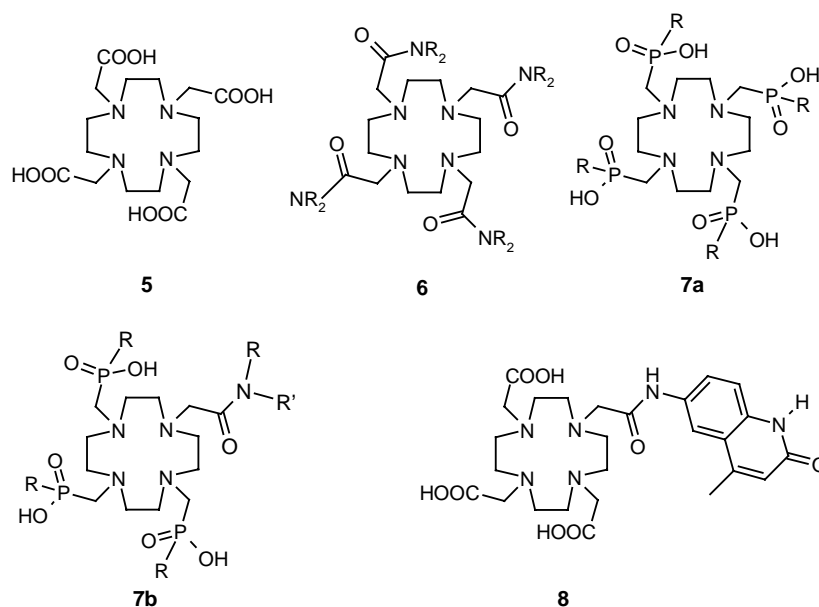


Figure 2.10: Examples of cyclen-based ligands.

Of the anionic complexes, the complexes of 1,4,7,10-tetra-azacyclododecane-1,4,7,10-tetraacetate (DOTA) and 1,4,7,10-tetraazacyclododecane-1,4,7,10-tetraphosphinate are the most important. These type of ligands provide an excellent shielding of the lanthanide ion, together with a high stability of the complexes. Parker and coworkers recently investigated the influence of different coordinating pendant arms of the ligands **5**, **7a**, and **7b** on the luminescence properties of the complexed Eu^{3+} ion. The changes in the relative intensities of the ${}^5\text{D}_0 \rightarrow {}^7\text{F}_2$ and the ${}^5\text{D}_0 \rightarrow {}^7\text{F}_1$ emissions demonstrate the varying symmetry around the Eu^{3+} ion in the different complexes: the ${}^5\text{D}_0 \rightarrow {}^7\text{F}_2 / {}^5\text{D}_0 \rightarrow {}^7\text{F}_1$ ratio varies from 0.6 to 1.4.⁶⁶

The tetraamine skeleton can be monofunctionalized with a pendant arm that may contain a sensitizer. The photophysical properties of carbostyryl-124-functionalized complexes of Eu^{3+} and Tb^{3+} have been studied. The sensitization of Tb^{3+} was clearly more efficient than the sensitization of Eu^{3+} , with overall luminescence quantum yields of 0.15 and 0.014, respectively. In the Eu^{3+} complex the singlet state of the antenna is deactivated by a photo-induced electron transfer to the lanthanide ion, whereas the moderate Tb^{3+} quantum yield was explained by a thermally activated energy back-transfer.⁶⁷

2.7.4 Cryptates

The Eu^{3+} complex of cage-type ligand **9** is the first lanthanide complex in which the donor atoms of the ligand are preorganized for complexation.^{27,68} Although the ligand itself has no absorption bands in the 300 nm region, the Eu^{3+} complex has a weak LMCT band at 298 nm, corresponding to a charge transfer transition involving the amine nitrogens and Eu^{3+} .

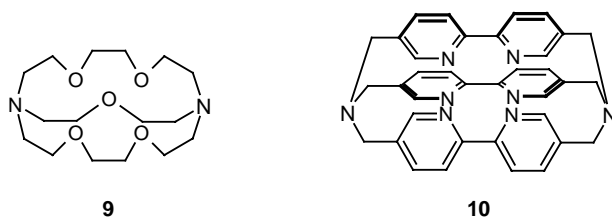


Figure 2.11: The 2.2.1 cryptand and the tris(2,2'-bipyridine) cryptand.

A moderate solvent shielding in water was observed: approximately 3 water molecules were still coordinated to the lanthanide ion. The Eu^{3+} luminescence lifetime was temperature dependent, indicating a thermally activated decay process that involved the low-lying LMCT state. The luminescence lifetime was enhanced by the addition of fluoride ions to the

solutions, which shift the LMCT states to higher energy and can replace solvent molecules in the coordination sphere of the lanthanide ion.²⁷

Lehn and coworkers synthesized the tris(2,2'-bipyridine) cryptand **10**,⁶⁹ which possesses absorption bands in the 300 nm region due to the $\pi \rightarrow \pi^*$ transitions in the bipyridine units. Complexation of Eu^{3+} and Tb^{3+} leads to charged complexes that are kinetically stable in water. Three water molecules are coordinated to the lanthanide ion in the complex. The overall luminescence quantum yields of these cryptates were only a few percent. For the $[\text{Tb} \subset \mathbf{10}]^{3+}$ cryptate the luminescent lifetime is strongly temperature dependent, indicating thermally activated energy back-transfer from the excited lanthanide level ($20,400 \text{ cm}^{-1}$) to the triplet state of the ligand ($21,600 \text{ cm}^{-1}$). For the $[\text{Eu} \subset \mathbf{10}]^{3+}$ cryptate no temperature dependence of the lifetime was observed, but the deactivation of the lanthanide ion via LMCT states still plays a role here.

2.7.5 EDTA and DTPA derivatives

Hemmilä and coworkers combined the chelating properties of EDTA (ethylenediaminetetraacetic acid) with that of the sensitizer capability of the (extended) pyridine moiety.⁷⁰ In this way the sensitizer is positioned in close proximity to the lanthanide ion in order to achieve strong lanthanide luminescence. Incorporation of more than one sensitizer in a ligand system improves the luminescence characteristics as was demonstrated for complexes of **12**.⁷⁰

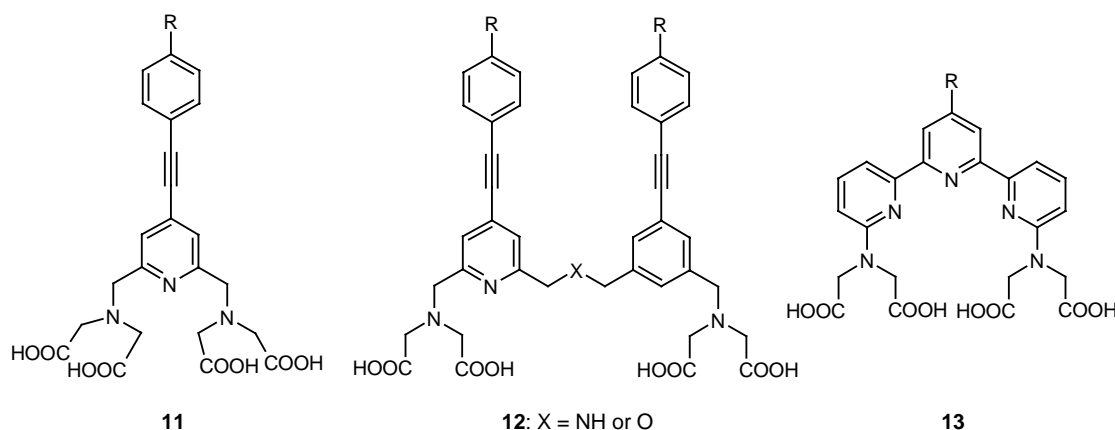


Figure 2.12: Schematic representation of the pyridine-based ligands functionalized with aminodiacetate moieties.

Hemmilä and coworkers extended their work to the terpyridine antenna resulting in highly luminescent Tb^{3+} complexes.⁷¹ Further utilization of these complexes for coupling to

bioactive molecules was achieved by introduction of functional groups in the sensitizer part or at one of the pendant arms of the complexing moieties (R in Figure 2.12).

The ligands based on DTPA (diethylenetriaminepentaacetic acid) provide good shielding for the lanthanide ion leaving only room for approximately 1 water molecule, and the complexes are stable in water. The DTPA ligand allows the easy incorporation of sensitizers like carbostyryl-124 for Eu^{3+} and Tb^{3+} ,⁷² and fluorescein for the near-infrared luminescent lanthanide ions Nd^{3+} , Er^{3+} , and Yb^{3+} .³⁵

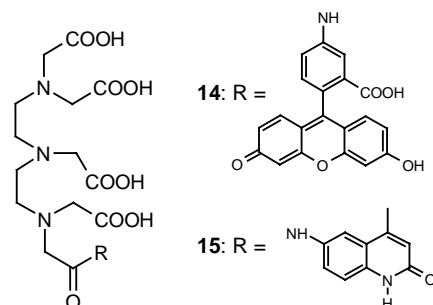


Figure 2.13: DTPA ligands functionalized with fluorescein (**14**) or carbostyryl-124 (**15**) as sensitizers.

2.7.6 Calix[4]arenes

Calix[4]arenes are versatile building blocks that allow upper and lower rim functionalization.⁷³ The calix[4]arene-based ligands that have been reported in the literature for lanthanide complexation have coordinating groups attached to the lower rim. This can readily be achieved by functionalization of the phenolic OH groups. Examples of these lower rim substituted calix[4]arenes are the tetracarboxylate and tetraamide derivatives.

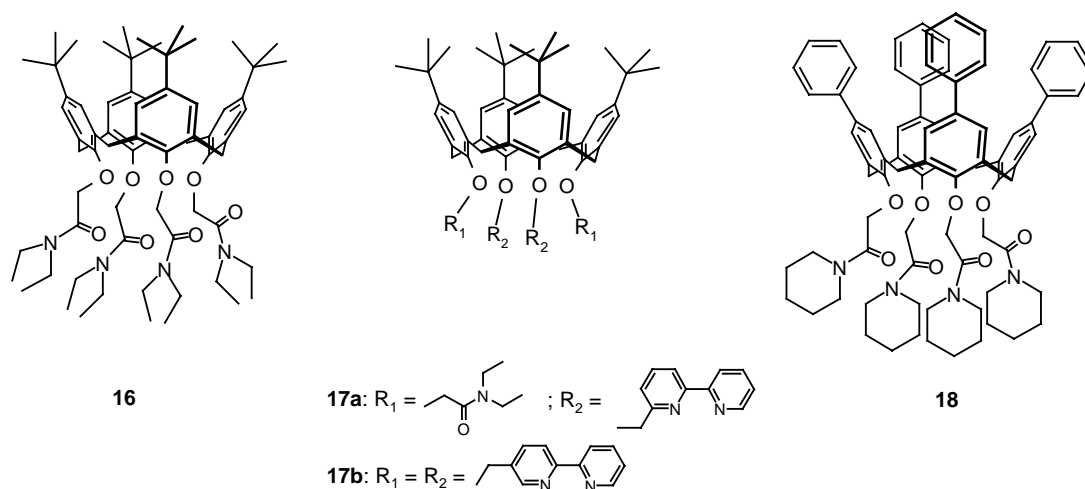


Figure 2.14: Calix[4]arene-based ligands for lanthanide complexation.

Sabbatini *et al.* have reported the photophysical properties of the Eu^{3+} and Tb^{3+} complexes of tetraamide **16**, in which the calix[4]arene aromatic groups act as the sensitizer.⁷⁴ The overall luminescence quantum yield in water is promising for Tb^{3+} (0.1), but very low for Eu^{3+} (2×10^{-4}), due to a deactivation of the ligand singlet state by an MLCT transition.

Table 2.4: Photophysical properties of the calix[4]arene-based lanthanide complexes in acetonitrile by Sabbatini *et al.*

Complex	λ_{max} (nm)	Lifetime τ (ms)	Quantum yield (ϕ_{SE})
$[(\text{Eu})\mathbf{16}]^{3+}$	273	0.65	2×10^{-4}
$[(\text{Tb})\mathbf{16}]^{3+}$	273	1.5	0.20
$[(\text{Eu})\mathbf{17a}]^{3+}$	305	0.65	0.04
$[(\text{Tb})\mathbf{17a}]^{3+}$	306	1.9	0.12
$[(\text{Eu})\mathbf{17b}]^{3+}$	309	1.6	0.15

Sabbatini *et al.* have extended their work to bipyridyl-functionalized calix[4]arenes (ligands **17a-b** in Figure 2.14).⁷⁵ These bipyridine moieties combine coordinating properties and sensitizing capabilities. The best results were obtained for $[(\text{Eu})\mathbf{17b}]^{3+}$ with a luminescence quantum yield of 0.15 in acetonitrile.

Shinkai and coworkers have synthesized similar tetraamide calix[4]arenes with sensitizers appended to the lower rim or to the upper rim (for example ligand **18** in Figure 2.14).⁷⁶

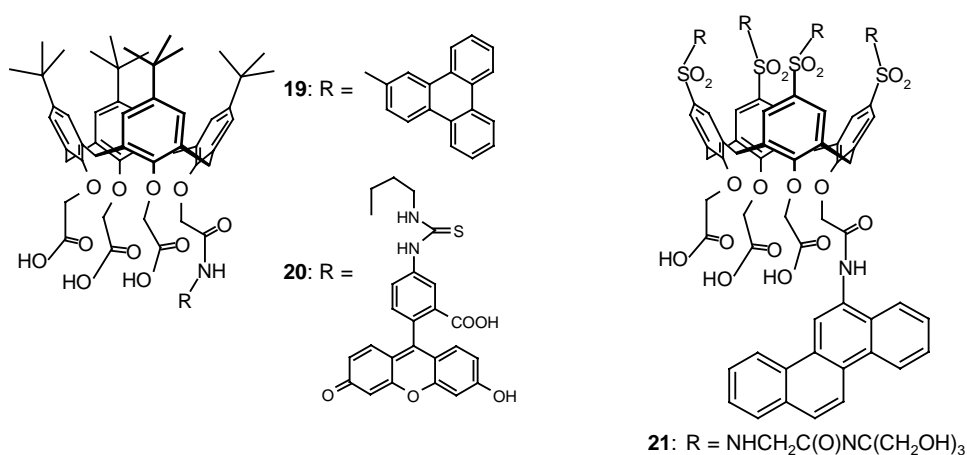


Figure 2.15: Triacid monoamide calix[4]arene ligands for lanthanide complexation.

Rudkevich *et al.* have reported the synthesis and photophysical properties of tricarboxylate monoamide derivatives that form overall neutral complexes with lanthanide ions.⁷⁷ Comparison of the luminescence lifetimes of the Eu^{3+} complexes in methanol (typically 0.65 ms) and methanol- d_4 (typically 1.3 ms) indicate that the lanthanide ion is shielded from the solvent with only one to two remaining methanol molecules coordinated to the lanthanide ion. These results were supported by data obtained from molecular dynamics simulations.⁷⁸

The incorporation of a sensitizer such as triphenylene³¹ for Eu^{3+} and Tb^{3+} or fluorescein⁴⁹ for Nd^{3+} , Er^{3+} , and Yb^{3+} at the amide position does not alter the complexation properties of the ligand. Further functionalization of the upper rim of the calix[4]arene with water-soluble groups, resulted in water-soluble lanthanide complexes, that could be linked to bioactive molecules.²⁹

2.7.7 *m*-Terphenyl-based ligand systems

In 1997 Oude Wolbers *et al.* reported hemispherand **22** for the complexation of lanthanide ions.³⁸ The ligand provides nine donor atoms: five ether oxygens, three carboxylate oxygens, and one nitrogen atom.

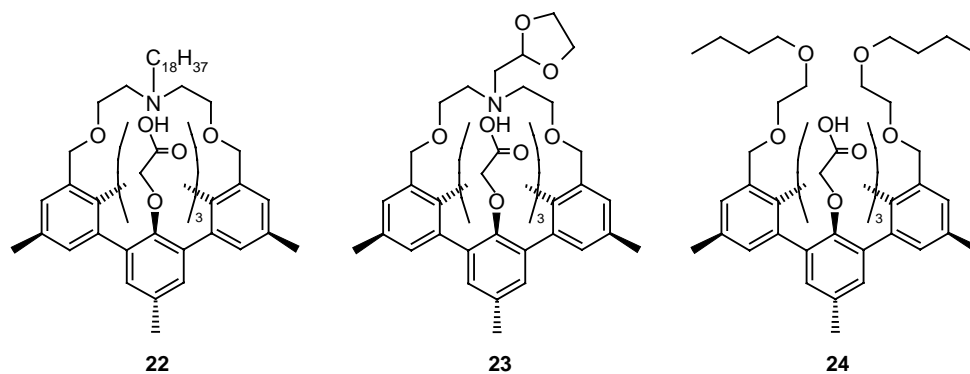


Figure 2.16: *m*-Terphenyl-based ligands for lanthanide complexation.

The lanthanide ion was excellently shielded from the solvent, with only one remaining methanol molecule in the first coordination sphere. The terphenyl moiety is a sensitizer for different luminescent lanthanide ions ranging from the visible light emitting to the near-infrared light emitting lanthanide ions. The rate constants for quenching by several high energy vibrational modes surrounding the Eu^{3+} ion have been determined by systematic deuteration of ligand **22**. Deuteration of the crown ether bridge and the oxyacetate groups also increased the luminescence lifetimes of other complexed lanthanide ions.

Table 2.5: Luminescence lifetimes of the Eu^{3+} complexes in methanol and methanol- d_1 (10^{-4} M), as well as the number of solvent molecules (n).

Complex	$\tau_{\text{CH}_3\text{OH}}$	$\tau_{\text{CH}_3\text{OD}}$	n
(Eu) 22	0.75	1.17	1.0
(Eu) 23	1.42	1.53	0.1
(Eu) 24	0.72	2.05	1.9

In derivatives of this ligand system the *m*-terphenyl methyl groups were substituted by *t*-butyl moieties to improve the solubility of the complexes, and the tertiary amine of the crown-ether bridge was functionalized with a dioxolane group, which further improved the shielding of the complexed lanthanide ion. In order to study the effect of the flexibility of the encapsulating ligand, an acyclic *m*-terphenyl based ligand system was synthesized.⁷⁹ The shielding of the lanthanide ion in the acyclic ligand was decreased compared to the cyclic ligand; two methanol molecules remained in the first coordination sphere of Eu^{3+} .

2.8 Applications

2.8.1 Fluoroimmunoassays

The use of Eu^{3+} and Tb^{3+} complexes as luminescent labels has been studied extensively, because their luminescence properties make them unique labels for fluoroimmunoassays.⁸⁰ The long luminescent lifetimes allow time-resolved separation of the lanthanide signal from the biological and instrumental interferences which have luminescent lifetimes of <100 ns. The lanthanide luminescence is not oxygen sensitive unlike most other long-lived luminophores. In sensitized emission there is a large difference between the wavelength of excitation and emission (typically 300 nm).

The near infrared luminescent Nd^{3+} and Yb^{3+} complexes are also promising probes for fluoroimmunoassays and *in vivo* applications, because human tissue is relatively transparent for near-infrared light around 1000 nm. The main problem with these complexes seems to be the low luminescence quantum yields of these lanthanides, because the narrow energy gaps between the luminescent state and the highest ground state make them very sensitive to quenching by O-H and C-H vibrations.

2.8.2 Optical amplification

The enormous increase in optical data transport, among others due to an increased internet traffic, has led to a substantial expansion in new fiber-optic networks. An increased capacity of the fiber-optic networks has also been achieved by utilizing more of the available bandwidth present in the currently installed fiber. Erbium-doped fiber amplifiers (EDFA) play an important role by providing efficient broad band optical signal amplification of 1530-1560 nm, the so-called third telecommunication window.

In optical telecommunication networks data is transported as optical pulses through silica fibers. Compared to coaxial cable or copper wire, data transport with fiber-optics is much faster, has a higher information capacity and allows transport over longer distances. Since silica is transparent to near-infrared light, two wavelength regions are used for the optical pulses: around 1330 nm (second communication window) and around 1550 nm (third communication window). To prevent a total loss of the optical signal, the signal has to be amplified after every ~80 km of fiber. In the 1980s, amplification was done with electronic devices called repeaters. These repeaters detected the light, converted it to an electronic signal, which was subsequently amplified and retimed, and then retransmitted as an optical pulse. Optical amplifiers based on Er^{3+} are currently used for amplification of optical pulses with a wavelength of about 1550 nm,⁸¹ which corresponds to an optical transition of Er^{3+} . This technology, which meant a real breakthrough for optical data transport, is relatively new: EDFAs were first fabricated in 1986 by Mears.⁸²

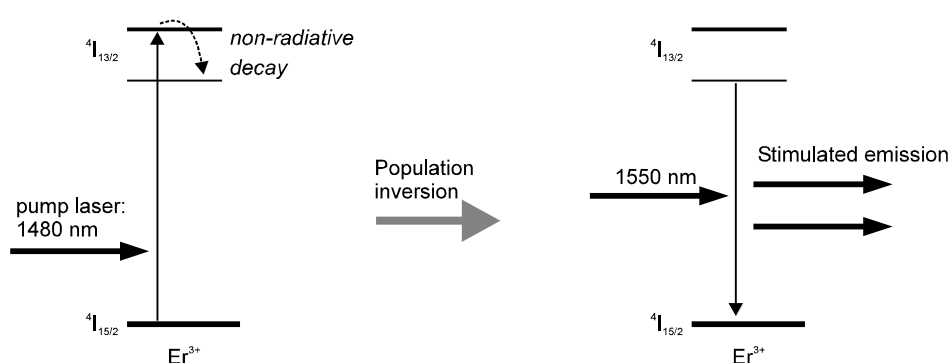


Figure 2.17: Schematic representation of the amplification of light of 1550 nm by Er^{3+} .

The mechanism of an optical amplifier is based on the principle of stimulated emission (see Figure 2.17). Using a pump laser of 1480 nm, Er^{3+} is excited into the first excited manifold ($^4\text{I}_{13/2}$) which is followed by a rapid non-radiative decay to the lowest level of that

manifold. When sufficient pump power is applied, *i.e.* if the pump rate is faster than the rate of spontaneous emission, more Er^{3+} ions will be in the excited state than in the ground state. This is called a population inversion between the first excited state and the ground state. A 1550 nm signal travelling through the Er^{3+} -doped amplifier will then stimulate the excited Er^{3+} ion (before it has time to luminesce) to emit a photon of the same wavelength that will be in phase and propagating in the same direction as the stimulating photon, resulting in signal amplification.

2.9 Outlook

The work described in this thesis is part of our research that is concerned with the development of a polymer-based optical amplifier in which lanthanide complexes bearing antenna chromophores are incorporated in planar polymeric waveguides.⁸³ By varying the lanthanide ion in the complex, various emission wavelengths become accessible, and hence optical signals of a range of wavelengths can be amplified. The polymer-based amplifiers can be integrated in existing polymeric optical components such as splitters, switches, and multiplexers.⁵² The main advantage of polymer-based components lies in their ease of processing, which enables low-cost manufacturing technologies to be applied. Polymer-based amplifiers can be monolithically integrated with other polymer-based functionalities. Recently, a polymeric waveguide doped with neodymium chloride has been shown to amplify light of 1060 nm.⁸⁴

2.10 References and Notes

1. Sabbatini, N.; Guardigli, M.; Lehn, J.-M. *Coord. Chem. Rev.* **1993**, *123*, 201.
2. Parker, D.; Williams, J. A. G. *J. Chem. Soc., Dalton Trans.* **1996**, 3613.
3. Gschneider Jr., K.A.; Eyring, L. *Handbook on the Physics and Chemistry of Rare Earths*, North Holland Publishing Company, Amsterdam, **1979**.
4. Bard, A. J.; Parsons, R.; Jordan, J. *Standard Potentials in Aqueous Solution*, Marcel Dekker Inc., New York, **1985**.
5. Blasse, G.; Grabmaier, B.C., *Luminescent Materials*, Springer Verlag, Berlin, **1994**.

6. Buono-Core, G. E.; Li, H. *Coord. Chem. Rev.* **1990**, *99*, 55.
7. Pearson, R. G.; Songstad, J. *J. Am. Chem. Soc.* **1967**, *89*, 1827.
8. Judd, B. R. *Phys. Rev.* **1962**, *127*, 750.
9. Ofelt, G. S. *J. Chem. Phys.* **1962**, *37*, 511.
10. Karplus, M.; Porter, R. N. *Atoms and Molecules*, The Benjamin-Cummings Publishing Company, Amsterdam, **1970**.
11. Stein, G.; Würzberg, E. *J. Chem. Phys.*, **1975**, *62*, 208.
12. Carnall, W. T.; Fields, P. R.; Rajnak, K. *J. Chem. Phys.* **1968**, *49*, 4424.
13. Dexter, D. L. *J. Chem. Phys.* **1953**, *21*, 836.
14. Sato, S.; Wada, M. *Bull. Chem. Soc. Jpn.* **1970**, *43*, 1955.
15. Crosby, G. A.; Whan, R. E.; Alire, R. M. *J. Chem. Phys.* **1961**, *34*, 743.
16. Tanaka, M.; Yamaguchi, G.; Shiokawa, J.; Yamanaka, C. *Bull. Chem. Soc. Jpn.* **1970**, *43*, 549.
17. Haynes, A. V.; Drickamer, H. G. *J. Chem. Phys.* **1982**, *76*, 114.
18. (a) Tobita, S.; Arakawa, M.; Tanaka, I. *J. Phys. Chem.* **1984**, *88*, 2697. (b) Tobita, S.; Arakawa, M.; Tanaka, I. *J. Phys. Chem.* **1985**, *89*, 5649.
19. Streck, W.; Wierzchaczewski, M. *Chem. Phys.* **1981**, *58*, 185.
20. Parker, D.; Williams, J. A. G. *J. Chem. Soc., Perkin Trans. 2* **1996**, 1581.
21. Asano-Someda, M.; Kaizu, Y. *Inorg. Chem.* **1999**, *38*, 2303, and references cited therein.
22. Weissman, S. I. *J. Chem. Phys.* **1942**, *10*, 214.
23. Hayes, A. V.; Drickamer, H. G. *J. Chem. Phys.* **1982**, *76*, 114.
24. Murov, S. L.; Carmichael, I.; Hug, G. L. *Handbook of Photochemistry, 2nd Ed.*, Marcel Dekker, New York, **1993**.
25. Parker, D.; Williams, J. A. G. *Chem. Commun.* **1998**, 245.
26. Bhaumik, M. L.; El-Sayed, M. A. *J. Chem. Phys.* **1965**, *42*, 787.
27. Sabbatini, N.; Perathoner, S.; Lattanzi, G.; Dellonte, S.; Balzani, V. *J. Phys. Chem.* **1987**, *91*, 6136.
28. Prodi, L.; Maestri, M.; Zissel, R.; Balzani, V. *Inorg. Chem.* **1991**, *30*, 3798.
29. Steemers, F. J.; Meuris, H. G.; Verboom, W.; Reinhoudt, D. N. *J. Org. Chem.* **1997**, *62*, 4229.
30. Napier, G. D. R.; Neilson, J. D.; Shepherd, T. M. *Chem. Phys. Lett.* **1975**, *31*, 328.

31. Steemers, F. J.; Verboom, W.; Reinhoudt, D. N.; van der Tol, E. B.; Verhoeven, J. W. *J. Am. Chem. Soc.* **1995**, *117*, 9408.
32. Parker, D.; Williams, J. A. G. *J. Chem. Soc., Perkin Trans. 2*, **1995**, 1305.
33. Sabbatini, N.; Indelli, M. T.; Gandolphi, M. T.; Balzani, V. *J. Phys. Chem.* **1982**, *36*, 3585.
34. Horrocks Jr., W. D.; Bolender, J. P.; Smith, W. D.; Supkowski, R. M. *J. Am. Chem. Soc.* **1997**, *119*, 5972, and references cited therein.
35. Werts, M. H. V.; Hofstraat, J. W.; Geurts, F. A. J.; Verhoeven, J. W. *Chem. Phys. Lett.* **1997**, *276*, 196.
36. (a). Haas, Y.; Stein, G. *J. Phys. Chem.* **1971**, *75*, 3668. (a). Haas, Y.; Stein, G. *J. Phys. Chem.* **1971**, *75*, 3677.
37. Ermolaev, V. L.; Sveshnikova, E. B. *Russ. Chem. Rev.* **1994**, *63*, 905.
38. Oude Wolbers, M. P.; van Veggel, F. C. J. M.; Snellink-Ruël, B. H. M.; Hofstraat, J. W.; Geurts, F. A. J.; Reinhoudt, D. N. *J. Am. Chem. Soc.* **1997**, *119*, 138.
39. Hemmilä, I.; Mikkala, V.-M.; Takalo, H. *J. Fluorescence* **1995**, *5*, 159.
40. Kropp, J. L.; Windsor, M. W. *J. Chem. Phys.* **1965**, *42*, 1599.
41. (a) Horrocks, W. DeW. Jr.; Sudnick, D. R. *Acc. Chem. Res.* **1981**, *14*, 384. (b) Holz, R. C.; Chang, C. A.; Horrocks, W. DeW. Jr. *Inorg. Chem.* **1991**, *30*, 3270.
42. Beeby, A.; Clarkson, J. M.; Dickins, R. S.; Faulkner, S.; Parker, D.; Royle, L.; de Sousa, A. S.; Williams, J. A. G.; Woods, M. *J. Chem. Soc., Perkin Trans. 2* **1999**, 493.
43. Gilbert, A.; Baggot, J. *Essentials of Molecular Photochemistry*, Blackwell Scientific Publications, London, **1991**.
44. Hasegawa, Y.; Murakoshi, K.; Wada, Y.; Yanagida, S.; Kim, J.-H.; Nakashima, N.; Yamanaka, T. *Chem. Phys. Lett.* **1996**, *248*, 8, and references cited therein.
45. Förster, T. *Discuss. Faraday Soc.* **1959**, *27*, 7.
46. (a) Kirby, A. F.; Foster, D.; Richardson, F. S. *Chem. Phys. Lett.* **1983**, *95*, 507. (b) Kirby, A. F.; Richardson, F. S. *J. Phys. Chem.* **1983**, *87*, 2544.
47. Richardson, F. S. *Chem. Rev.* **1982**, *82*, 541.
48. Heller, A. *J. Am. Chem. Soc.* **1967**, *89*, 167.
49. Oude Wolbers, M. P.; van Veggel, F. C. J. M.; Peters, F. G. A.; van Beelen, E. S. E.; Hofstraat, J. W.; Geurts, F. A. J.; Reinhoudt, D. N. *Chem. Eur. J.* **1998**, *4*, 772.
50. Crosby, G. A.; Kasha, M. *Spectrochim. Acta* **1958**, *10*, 377.

51. Weber, M. J. *Phys. Rev.* **1968**, *171*, 283.
52. Miniscalco, W. J. *J. Lightwave Technol.* **1991**, *9*, 234.
53. Schaffers, K. I.; Deloach, L. D.; Payne, S. A. *IEEE J. Quantum Electron.* **1996**, *32*, 741.
54. Hasegawa, Y.; Kimura, Y.; Murakoshi, K.; Wada, Y.; Kim, J.-H.; Nakashima, N.; Yamanaka, T.; Yanagida, S. *J. Phys. Chem.* **1996**, *100*, 10201.
55. Pavier, M. A.; Richardson, T.; Searle, T. M.; Huang, C. H.; Li, H.; Zhou, D. *Supramol. Sci.* **1997**, *4*, 437.
56. Cram, D. J.; Cram, J. M. *Container Molecules and Their Guests, Monographs in Supramolecular Chemistry*, Stoddart, J. F., Ed., The Royal Society of Chemistry, London, **1994**.
57. Melby, L. R.; Rose, N. J.; Abramson, E.; Caris, J. C. *J. Am. Chem. Soc.* **1964**, *86*, 5125.
58. Filipescu, N.; Sager, W. F.; Serafin, F. A. *J. Phys. Chem.* **1964**, *68*, 3324.
59. Berry, M. T.; May, P. S.; Xu, H. *J. Phys. Chem.* **1996**, *100*, 9216.
60. Frey, S. T.; Gong, M. L.; Horrocks, Jr., W. DeW. *Inorg. Chem.* **1994**, *33*, 3229.
61. fod = 6,6,7,7,8,8,8-heptafluoro-2,2-dimethyloctane-3,5-dione; Michler's ketone = 4,4'-bis(*N,N*-dimethylamino)benzophenone.
62. Werts, M. H. V.; Duin, M. A.; Hofstraat, J. W.; Verhoeven, J. W. *Chem. Commun.* **1999**, 799.
63. Parker, D.; Williams, J. A. G. *J. Chem. Soc., Dalton Trans.* **1996**, 3613.
64. Arneud-Neu, F. *Chem. Soc. Rev.* **1994**, 235.
65. Aime, S.; Botta, M.; Fasano, M.; Terreno, E. *Chem. Soc. Rev.* **1998**, *27*, 19.
66. Aime, S.; Botta, M.; Parker, D.; Williams, J. A. G. *J. Chem. Soc., Dalton Trans.* **1996**, 17.
67. Parker, D.; Williams, J. A. G. *J. Chem. Soc., Perkin Trans. 2*, **1996**, 1581.
68. Lehn, J.-M. *Acc. Chem. Res.* **1978**, *11*, 49.
69. Alpha, B.; Lehn, J.-M.; Mathis, G. *Angew. Chem. Int. Ed. Engl.* **1987**, *26*, 266.
70. Takalo, H.; Hemmilä, I.; Sutela, T.; Latva, M. *Helv. Chim. Acta* **1996**, *79*, 789.
71. Mukkala, V.-M.; Helenius, M.; Hemmilä, I.; Kankare, J.; Takalo, H. *Helv. Chim. Acta* **1993**, *76*, 1361.
72. (a) Selvin, P. R.; Rana, T. M.; Hearst, J. E. *J. Am. Chem. Soc.* **1994**, *116*, 6029. (b) Li, M.; Selvin, P. R. *Proc. Natl. Acad. Sci. USA* **1994**, *91*, 10024.
73. (a) Gutsche, C. D. *Calixarenes, Monographs in Supramolecular Chemistry*, Stoddart, J.

- F., Ed., The Royal Society of Chemistry, London, Vol.1, **1989**. (b) Vicens, J.; Böhmer, V. *Calixarenes: A versatile Class of Macrocyclic Compounds, Topics in Inclusion Science*, Kluwer Academic Press, Dordrecht, Vol. 3, **1991**.
74. Sabbatini, N.; Guardigli, M.; Mecati, A.; Balzani, V.; Ungaro, R.; Ghidini, E.; Casnati, A.; Pochini, A. *J. Chem. Soc., Chem. Commun.* **1990**, 87.
75. Sabbatini, N.; Guardigli, M.; Manet, I.; Ungaro, R.; Casnati, A.; Fischer, C.; Ziessel, R.; Ulrich, G. *New J. Chem.* **1995**, 19, 137.
76. (a) Sato, N.; Shinkai, S. *J. Chem. Soc., Perkin Trans. 2* **1993**, 621. (b) Matsumoto, H.; Shinkai, S. *Chem. Lett.* **1994**, 901.
77. Rudkevich, D. M.; Verboom, van der Tol, E.; van Staveren, C. J.; Kaspersen, F. M.; Verhoeven, J. W.; Reinhoudt, D. N. *J. Chem. Soc., Perkin Trans. 2* **1995**, 131.
78. van Veggel, F. C. J. M.; Reinhoudt, D. N. *Recl. Trav. Chim. Pays-Bas*, **1995**, 114, 387.
79. (a) Oude Wolbers, M. P.; van Veggel, F. C. J. M.; Hofstraat, J. W.; Geurts, F. A. J.; Reinhoudt, D. N. *J. Chem. Soc., Perkin Trans. 2* **1997**, 2275. (b) Oude Wolbers, M. P.; van Veggel, F. C. J. M.; Snellink-Ruël, B. H. M.; Hofstraat, J. W.; Geurts, F. A. J.; Reinhoudt, D. N. *J. Chem. Soc., Perkin Trans. 2* **1998**, 2141.
80. Hemmilä, I. K. *Applications of Fluorescence in Immunoassays*, Wiley and Sons, New York, **1991**.
81. Desurvire, E. *Phys. Today* **1994**, 97, 20.
82. Mears, R. J.; Reekie, L.; Jauncy, I. M.; Payne, D. N. *Electron. Lett.* **1987**, 23, 1026.
83. Lin, S.; Feuerstein, R. J.; Mickelson, A. R. *J. Appl. Phys.* **1996**, 79, 2868.
84. An, D.; Yue, Z.; Chen, R. T. *Appl. Phys. Lett.*, **1998**, 72, 2806.

Appendix

Absorption

The experimentally determined absorption spectrum consists of a number of spectral features exhibiting different wavelengths of maximum absorption, and different intensities. An experimental measurement of absorption intensity is provided by the Beer-Lambert law, which states that the intensity of the light (I) that has passed through a layer of thickness (l) containing an absorbing species at a molar concentration (c) is proportional to the thickness of the layer, the concentration, and the incident intensity (I_0), or in formula:

$$\log(I/I_0) = -\epsilon cl \quad (12)$$

where ϵ is the molar absorption coefficient belonging to the transition that causes the absorption (at constant wavelength or frequency). Absorption bands generally spread out over a range of frequencies, and so quoting the absorption coefficient at a single frequency might therefore not give a true indication of the intensity of a transition. The integrated absorption coefficient (A) is the total sum of the absorptions and is a measure of the total strength of a specific transition.

$$A = \int \epsilon(\nu) d\nu \quad (13)$$

The integrated absorption coefficient is sometimes expressed in terms of the dimensionless oscillator strength (f), and is a measure of the strength (intensity) of an electric dipole transition compared to that of a free electron oscillating in three dimensions. The oscillator strength is defined as

$$f = A \cdot (4m_e c \epsilon_0 \ln 10 / N_a e^2) \quad (14)$$

where ϵ_0 is the vacuum permittivity. The oscillator strength has a direct connection with the wave functions of the initial and final states involved in the transition. The transition dipole ($\mu_{f,i}$) between these states is a measure of the dipole moment associated with the shift of

charge that occurs when the electron redistribution takes place and is defined in the usual way as

$$\mu_{f,i} = \int \phi_f^* \mu \phi_i \, d\tau \quad (15)$$

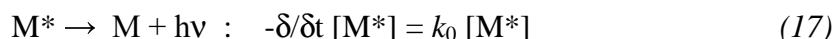
in which $\mu = -e \times r$. The oscillator strength is related to this dipole moment by the formula

$$f = (8\pi^2 m_e v / 3 h e^2) \cdot |\mu_{f,i}|^2 \quad (16)$$

Therefore the intensity of a certain transition can be estimated if the wavefunctions are known. The oscillator strengths of several transitions of trivalent lanthanide ions in solution have been calculated by Carnall and coworkers.¹²

Radiative rate of spontaneous emission

An electronically excited molecule may decay to the ground state due to the spontaneous emission of radiation. This emission can be characterized in terms of its total intensity and the time dependence of its intensity. Spontaneous emission is a random process, and such processes follow first-order kinetics, *i.e.* the rate of de-excitation of M^* depends on the first power of $[M^*]$.



The rate coefficient k_0 characterizes the rate of the spontaneous emission process, and is determined by the nature and properties of the emitting state. Integration yields

$$[M^*] = [M^*]_0 e^{-(k_0)t} \quad (18)$$

The natural lifetime τ_0 of a radiative process is defined as the reciprocal of the radiative rate coefficient.

$$\tau_0 = 1/k_0 \quad (19)$$

During the time $t = 0$ to $t = \tau_0$ the concentration of excited molecules falls to $1/e$ of its initial value, and therefore τ_0 is sometimes referred to as the $1/e$ lifetime. In the theory of photophysical processes k_0 is also known as the Einstein coefficient for spontaneous emission, which is usually given the symbol A_{nm} (the subscripts n and m refer to the upper and lower level of the transition). The Einstein coefficient (an Avogadro number of photons is called an einstein) is related to the integrated absorption coefficient A as follows

$$k_0 = A_{nm} = 2.881 \cdot 10^9 \nu_{n,m}^2 n^2 A \quad (20)$$

where $\nu_{n,m}$ is the wavenumber of the transition in cm^{-1} (which is approximated as ν_{max} , and which is taken to be identical to the absorption maximum), and n is the mean refractive index of the solvent over the absorption band. Rewriting this equation leads to a simple theoretical estimate of the radiative lifetimes

$$\tau_0 = 1/A_{nm} = (3.417 \times 10^8) / (\nu_{\text{max}}^2 n^2 A) \quad (21)$$

This equation suggests that the radiative lifetimes should decrease with ν_{max} . In fact rapid non-radiative processes compete with emission from the high electronically excited states, thereby reducing the observable intensity of already rapid emission processes.

Chapter 3

Near-Infrared and Visible Luminescence of Terphenyl-based Lanthanide Complexes Modified with Amide and Sulfonamide Pendant Arms[§]

3.1 Introduction

There is a worldwide interest in complexes of the trivalent rare earth or lanthanide cations for applications in fluoroimmunoassays,¹ laser systems,² and optical amplification.³ The unique luminescence properties of these rare earth cations and their wide range of emission bands (500 - 1550 nm)⁴ make them very interesting for such purposes. The lanthanide ions have narrow emission bands and relatively long luminescence lifetimes as a result of optical transitions within the 4f shell, which are in principle parity forbidden. Encapsulating ligands can enhance the luminescence properties by shielding the ion from quenchers such as

[§] Part of the work described in this chapter has been accepted for publication: Klink, S. I.; Hebbink, G. A.; Grave, L.; Peters, F. G. A.; van Veggel, F. C. J. M.; Reinhoudt, D. N.; Hofstraat, J. W. *Eur. J. Org. Chem.*, **2000**, in press.

hydroxyl groups of the solvent. Luminescent complexes of the lanthanide ions Eu^{3+} and Tb^{3+} are the most widely studied, and these particular complexes are used for example as long-lived luminescent probes in fluoroimmunoassays.⁵ These complexes show luminescence in the visible spectral region with relatively long luminescence lifetimes in the range of ms.^{6,7} Recently, there is an increasing interest in complexes of the near-infrared emitting lanthanide ions Yb^{3+} , Nd^{3+} , and Er^{3+} , which have emission bands ranging from 880 to 1550 nm. The Nd^{3+} and Yb^{3+} complexes are promising probes for fluoroimmunoassays and *in vivo* applications, because human tissue is relatively transparent for near-infrared light around 1000 nm. In optical telecommunication networks Er^{3+} -doped silica fiber amplifiers (EDFAs) are currently used for amplification of light with a wavelength of about 1550 nm,⁸ which corresponds to an optical transition of Er^{3+} ($^4\text{I}_{13/2} \rightarrow ^4\text{I}_{15/2}$ transition). The mechanism of such an optical amplifier is based on stimulated emission from the Er^{3+} $^4\text{I}_{13/2}$ excited state. Recently, a polymeric waveguide doped with NdCl_3 has been shown to amplify light of 1060 nm ($^4\text{F}_{3/2} \rightarrow ^4\text{I}_{11/2}$ transition).⁹

This work is part of our research that is concerned with the development of a polymer-based optical amplifier in which lanthanide complexes bearing antenna chromophores are incorporated in planar polymeric waveguides.^{3,10} By varying the lanthanide ion in the complex, various emission wavelengths become accessible, and hence optical signals of a range of wavelengths can be amplified. The development of stable, neutral lanthanide complexes in which the ion is shielded from the (quenching) environment is essential for our research. These lanthanide complexes should also allow efficient excitation. A general accepted way to accomplish this is to excite the lanthanide ion via an antenna chromophore, hence the incorporation of an antenna chromophore in the ligand is desirable. Furthermore, the complexes should have high luminescence quantum yields, and for practical purposes should be soluble in organic solvents and the polymer matrix.

Previously, our group has reported the synthesis of oxyacetate-functionalized *m*-terphenyl derivatives (H_3)**8** and (H_3)**9** which form overall neutral complexes with various lanthanide cations, such as Eu^{3+} , Yb^{3+} , Nd^{3+} , and Er^{3+} (see Figure 3.1).^{3,11,12,13} In methanol these *m*-terphenyl-based ligands provide an excellent shielding of the lanthanide ion leaving only room for one or two methanol molecules in the first coordination sphere. It was, among others, demonstrated that partial deuteration of the complex (Ln)**8** enhances the luminescence lifetime of the complexed lanthanide ion.¹¹ Unfortunately, the synthesis routes of these ligands do not allow the easy incorporation of an additional antenna chromophore. The triacid

monoamide calix[4]arene ligands¹⁴ can easily be functionalized with different antenna chromophores like triphenylene⁶ and fluorescein,¹⁵ (H₃)**10a** and (H₃)**10b** in Figure 3.1, respectively. Despite the relatively easy synthesis and good photophysical properties of these complexes, their limited solubility in organic solvents is a drawback.

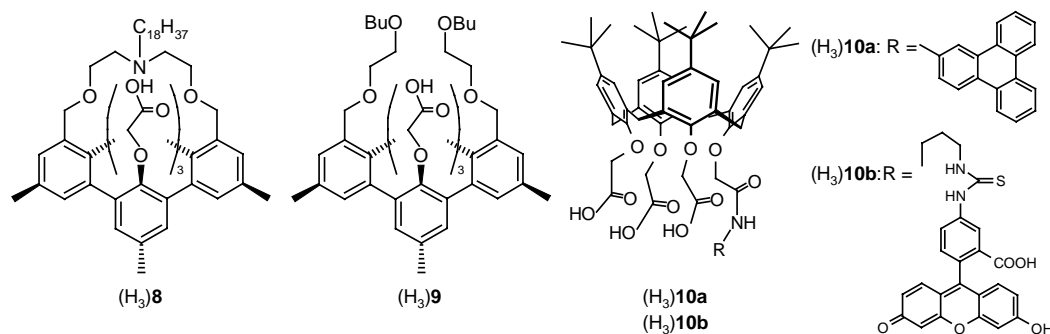


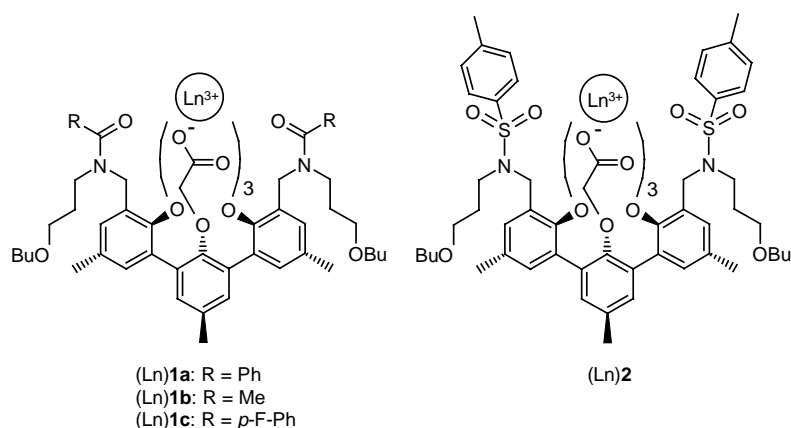
Figure 3.1: *m*-Terphenyl-based and antenna-functionalized calix[4]arene ligands for lanthanide complexation

In this chapter the synthesis and photophysical properties of *m*-terphenyl-based lanthanide complexes bearing amido and sulfonamido functionalities are presented. The *m*-terphenyl-based ligands have been designed to shield the lanthanide ion efficiently from the solvent and the resulting neutral complexes exhibit an enhanced solubility in organic solvents.¹¹ The influence of the metal coordinating functionalities on the photophysical properties of the complexed lanthanide ion has been investigated using Eu³⁺ and Tb³⁺ as models. Furthermore, the luminescence of the Dy³⁺ or Sm³⁺ complexes has been studied. For applications in optical telecommunication networks the 1550 nm transition of Er³⁺, the 1330 nm transition of Nd³⁺, and also the 980 nm transition of Yb³⁺ are of particular interest. The corresponding complexes of these near-infrared emitting lanthanide ions were synthesized and their photophysical properties were evaluated.

The ligands (H₃)**1a-c** and (H₃)**2** have been designed to provide eight hard oxygen donor atoms for encapsulation of the lanthanide ion: three ether oxygens and three negatively charged carboxylate oxygens, and two additional amide or sulfonamide oxygens (see Chart 3.1). The amide carbonyl oxygen is known to strongly coordinate to lanthanide ions.¹⁶ A route for the synthesis of these ligands has been developed, which allows the incorporation of different sensitizers at the amide and sulfonamide positions, without changing either the synthesis route or the coordinating nature of the ligand. To demonstrate this, the acetamido

and the benzamido group have been incorporated as coordinating moieties, and the luminescence properties of the complexes have been evaluated.

Chart 3.1



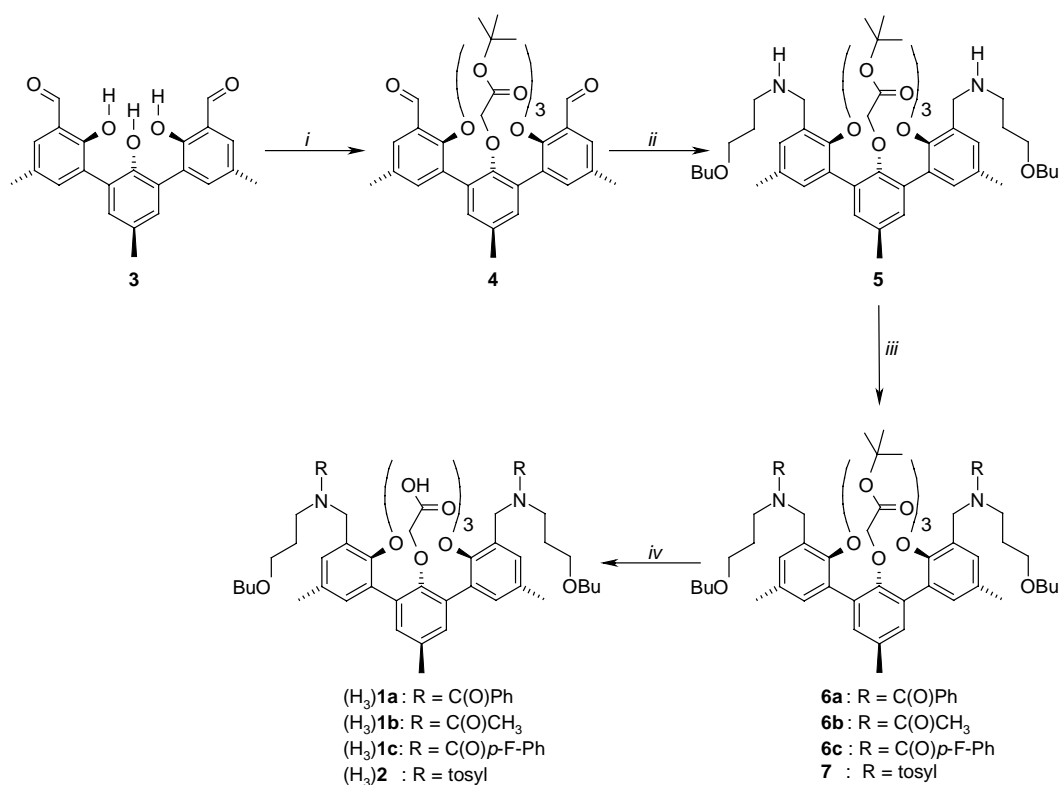
3.2 Results and Discussion

3.2.1 Synthesis

The ligands (H₃)**1a-c** were synthesized starting from the diformyl terphenyl **3**¹¹ (see Scheme 3.1). Diformyl terphenyl **3** was reacted with *tert*-butyl bromoacetate in acetonitrile in the presence of K₂CO₃ giving triester **4** in 90% yield. The ¹H NMR spectrum of **4** shows the signals at 1.38 and 1.21 ppm for the outer *tert*-butyl groups and the inner *tert*-butyl group, respectively, with a relative intensity of 2:1. Reductive amination of **4** with 3-*n*-butoxypropylamine and hydrogen in the presence of 10% Pd/C as a catalyst yielded the bisamine **5** in a quantitative yield. Reaction of **5** with the appropriate acid chloride in CH₂Cl₂ with Et₃N as a base gave the bis(amides) **6a-c** in 60-80% yield. Mild hydrolysis of the *tert*-butyl esters with trifluoroacetic acid gave the triacid derivatives (H₃)**1a-c** in quantitative yield. Complete hydrolysis was confirmed by the ¹H NMR spectra in which the signals for the *tert*-butyl groups were absent, and by the IR spectrum in which a peak around 1750 cm⁻¹ was observed for the carboxylic acids (ν_{C=O}).

The triacid sulfonamide ligand (H₃)**2** was synthesized analogously to (H₃)**1a-c** (see Scheme 3.1). Reaction of **5** with *p*-toluenesulfonyl chloride in CH₂Cl₂ with Et₃N as a base gave the bis(sulfonamide) **7** in 80% yield. Mild hydrolysis of the *tert*-butyl esters with trifluoroacetic acid gave (H₃)**2** in quantitative yield.

Scheme 3.1



Reaction conditions: i) *tert*-Butyl bromoacetate, K₂CO₃, CH₃CN; ii) *n*-Butoxy propylamine, H₂, 10% Pd/C, EtOH; iii) Appropriate acid chloride or *p*-toluenesulfonyl chloride, CH₂Cl₂, Et₃N; iv) TFA.

The corresponding lanthanide complexes were readily formed upon addition of lanthanide nitrate salts to solutions of the ligands in methanol in the presence of Et₃N as a base. FAB mass spectrometry (see Experimental) indicated that all complexes have a 1:1 stoichiometry.¹⁷ The IR spectra of the (Ln)**1a-c** complexes show that all carboxylic acids are deprotonated. The peak corresponding to the amide carbonyl is located at 1630 cm⁻¹ (ν_{NC=O}), and is not shifted relative to the amide carbonyl in the free ligand. In the IR spectra of the (Ln)**2** complexes the peaks of the coordinating sulfonamide carbonyls are not shifted relative to the free ligand (H₃)**2**.

3.2.2 Structure of the (Y)**1a**, (Y)**1c**, and (Y)**2** complexes

The diamagnetic complexes (Y)**1a**, (Y)**1c**, and (Y)**2** were characterized by NMR spectroscopy. Trivalent yttrium (Y³⁺) is generally accepted as a good diamagnetic model for the trivalent lanthanide ions, in particular the heavier lanthanide ions such as Tb³⁺, because of its similar ionic radius and indistinguishable coordination behavior. At room temperature the

spectrum of (Y)**1a** in DMSO- d_6 is broadened due to a hindered rotation around the tertiary amide and a hindered rotation of the phenyl groups. The spectrum taken at 100 °C is sharp (coalescence occurs at 60 °C), and a time-averaged C_s symmetry is apparent (see Figure 3.2). The benzyl protons and the protons at the α -position of the outer carboxylates in the (Y)**1a** complex appear as an AB system, whereas in the free ligand (H₃)**1a** these protons appear as singlets. These AB patterns confirm the rigidity of the complex and the coordination of the amide carbonyls to the lanthanide ion. The assignment of the peaks was confirmed by COSY¹⁸ and TOCSY¹⁹ experiments.

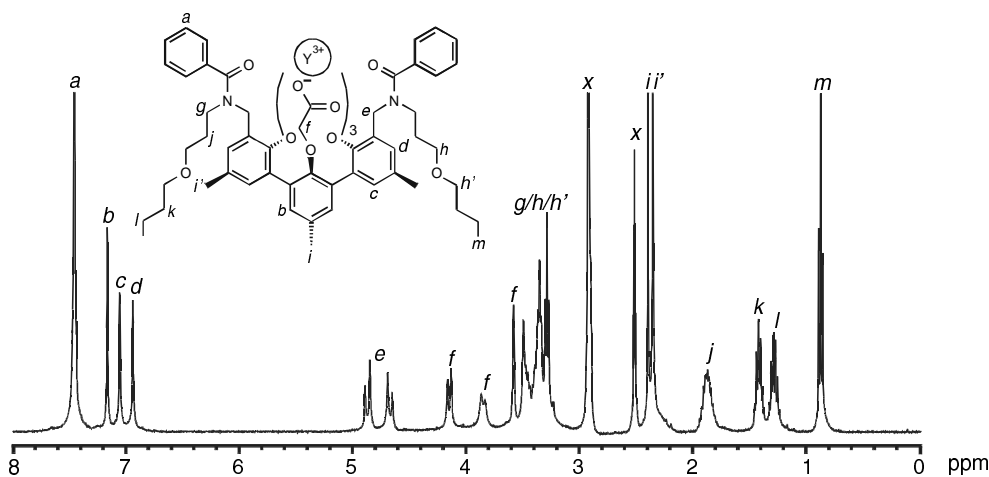


Figure 3.2: ^1H NMR (400 MHz) spectrum of (Y)**1a** in DMSO- d_6 at 100 °C.

The hindered rotation around the tertiary amide bond of the (Y)**1a** complex was further investigated with temperature dependent ^1H NMR and ^{19}F NMR studies of its derivative (Y)**1c**. This complex has fluorine atoms at the *para*-position of the benzoyl groups. The two substituents of the tertiary amide, *i.e.* the terphenyl moiety and the *n*-butoxypropyl moiety, can be *cis* and *trans* with respect to the amide carbonyl that is coordinated to the lanthanide ion. Molecular modeling simulations showed that this has consequences for the overall conformation of the complex. If the amide carbonyl is *trans* with respect to the *n*-propoxybutyl moiety, the benzoyl group must be pointed towards the *front* of the complex (the position of the carboxylic acid moiety of the inner terphenyl ring was arbitrarily designated as the front of the complex) to facilitate the coordination of the amide carbonyl to the lanthanide ion. If the amide carbonyl is *cis* with respect to the *n*-butoxypropyl moiety, the benzoyl group must be pointed towards the back of the complex (see Figure 3.3). This results in three possible conformational diastereomers of the complex: two isomers with C_s

symmetry (both benzoyl groups pointed either towards the back or the front of the complex) and one pair of enantiomers (one benzoyl group pointed to the front of the complex and one to the back).

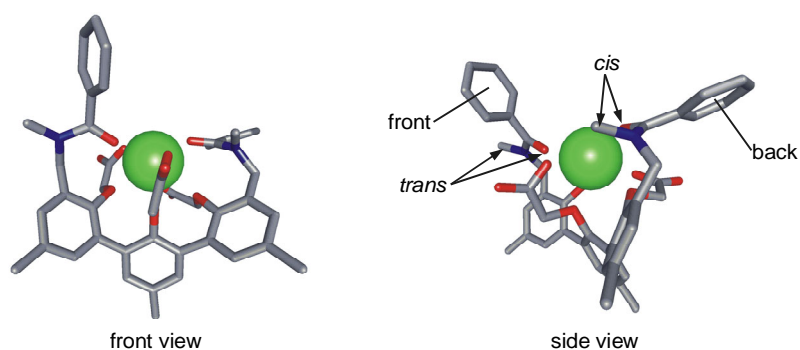


Figure 3.3: Typical structure of (Eu)**1a** obtained from a molecular modeling simulation in a box of OPLS methanol²⁰ using the CHARMM force field.²¹ In the simulation, the *n*-butoxypropyl moieties have been replaced by methyl groups. The hydrogen atoms have been omitted for clarity.

The ¹H NMR spectrum of (Y)**1c** at 30 °C is similar to that of (Y)**1a** and shows broadened signals for the protons that are in close vicinity to the amide carbonyls (see Figure 3.4). Upon raising the temperature the benzyl protons give rise to an AB system at 60 °C, whereas the protons at the α -position of the outer carboxylates give rise to an AB system at 80 °C.

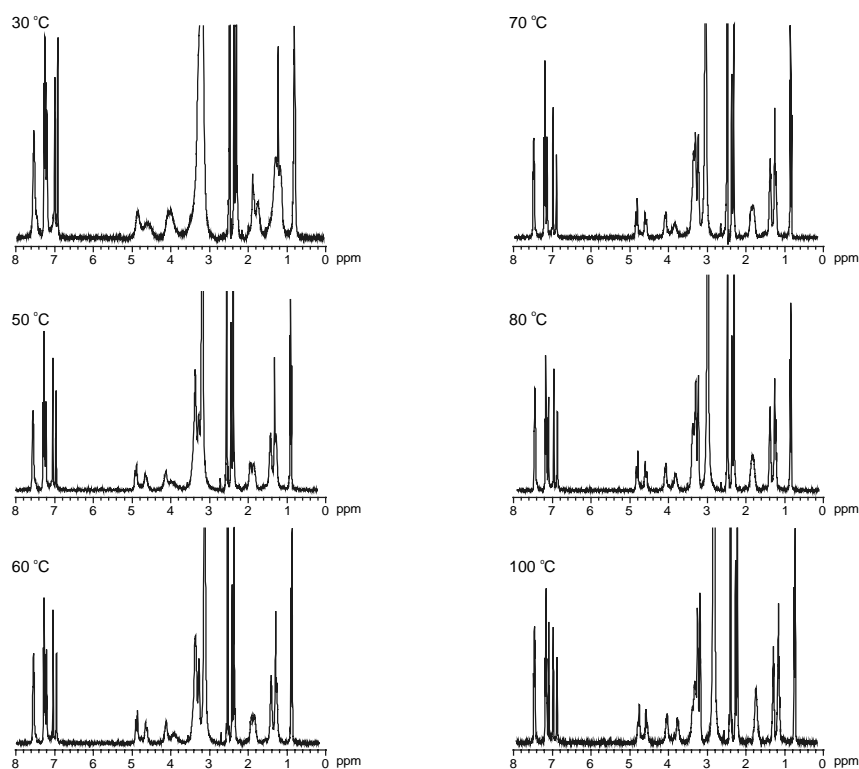


Figure 3.4: ¹H NMR spectra (400 MHz) of (Y)**1c** in DMSO-*d*₆ at different temperatures.

When the interconversion of the diastereomers, which involves a dissociation and recoordination of the amide carbonyls to the Y^{3+} ion, is slow on the NMR timescale, this can in principle give rise to four different signals in the ^{19}F NMR spectrum. The ^{19}F NMR spectrum of the (Y)**1c** complex at room temperature shows two peaks in a 3:1 ratio (see Figure 3.5). One possibility is that all isomers are present in solution and that three of the signals overlap, or that there are only two conformational isomers of the complex in solution with a preference for one of these isomers. Upon heating the sample, coalescence of the signals occurred at 60 °C, resulting in one signal. This is in agreement with the coalescence temperature observed in the 1H NMR spectra. The more rapid de- and recoordination, leads to a rapid interconversion between the isomers, resulting in one average F signal, thus apparent C_s symmetry of the complex.

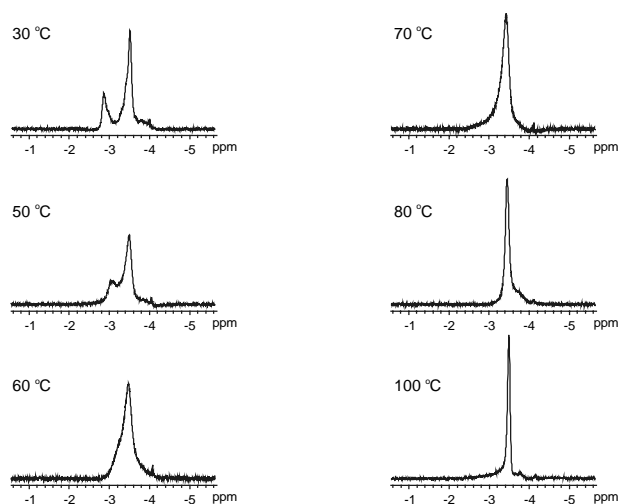


Figure 3.5: ^{19}F NMR spectra (400 MHz) of (Y)**1c** in $DMSO-d_6$ at different temperatures. Coalescence occurs at 60 °C. The chemical shifts are relative to trifluoroacetic acid. The spectra are not to scale

The 1H NMR spectrum of (Y)**2** is sharp at room temperature (see Figure 3.6) and is similar to the spectrum of (Y)**1a** at 100 °C. The observed AB pattern for the benzyl protons confirms the coordination of the sulfonamide oxygens to the lanthanide ion. Rotation around the sulfonamide bond appears to be rapid also at room temperature and no loss of the apparent C_s symmetry is observed despite the chirality generated at the sulfur atoms, due to the monodentate coordination of the sulfonamide oxygen.²² This can be attributed to the weaker sulfonamide coordination bonds as compared to the amide bonds, which allow a more rapid de- and recoordination equilibrium leading to the apparent C_s symmetry. The spectrum

shows two sharp doublets for the tosyl protons indicating that the tosyl groups can freely rotate at room temperature, contrary to the benzoyl groups in (Y)**1a**.

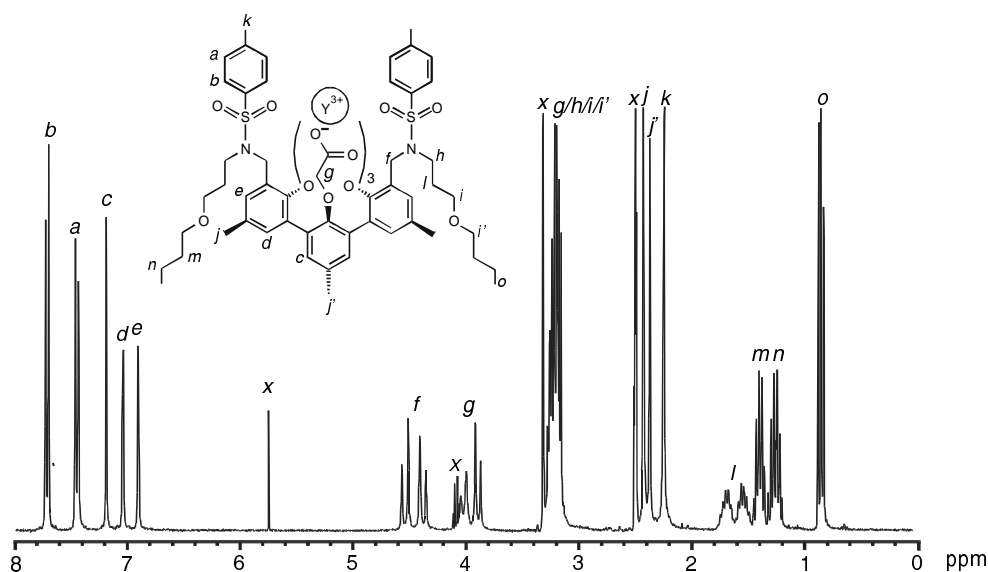


Figure 3.6: ^1H NMR (300 MHz) spectrum of (2)Y in $\text{DMSO}-d_6$ at room temperature.

It can be concluded from the NMR studies that due to the conformational and coordinating properties of the amide functions of the (Ln)**1a-c** complexes, these complexes can adopt different conformations in solution at room temperature. The (Ln)**2** complexes that contain the weaker coordinating sulfonamide groups exist in one (time-averaged) conformation in solution at room temperature.

3.2.3 ^{17}O NMR of the (Dy)**1a** complex in methanol

In order to establish the shielding capabilities of the ligand, the number of methanol molecules coordinated to the lanthanide ion in the (Dy)**1a** complex was determined by variable temperature ^{17}O NMR measurements. In this experiment, the Dy^{3+} -induced shift and line broadening of the ^{17}O signal of methanol at different temperatures is measured relative to the signal of pure methanol in order to prove the exchange between Dy^{3+} -bound and free methanol. The results of these measurements are summarized in Table 3.1. The observed ^{17}O signal of methanol shifts upfield with increasing temperature, while the line broadening of the signal at first increases and then again decreases. This behavior is characteristic for a transition of slow exchange between Dy^{3+} bound and bulk methanol molecules at 0 °C to fast exchange upon increase of the temperature.²³ Coalescence occurs probably at about 15 °C.

However, fast exchange is not yet completely reached at 55 °C. Extrapolation of the Dy³⁺-induced shift of the measured value of -1.70 ppm at this temperature for a [(Dy)**1c**]:[methanol] ratio of 1.14×10^{-3} to the induced shift for a [(Dy)**1c**]:[methanol] ratio of 1, is -1491 ppm.²⁴

Table 3.1: Chemical shift and linewidth of the ¹⁷O signal of methanol in the presence of 27.1 mM (Dy)**1c** as a function of the temperature.

Temperature (°C)	δ (ppm)	Linewidth (Hz)
0	-0.16	47.2
25	-1.04	73.2
35	-1.23	69.7
45	-1.72	58.2
55	-1.70	43.9

Previously, it has been shown that the Dy³⁺-induced ¹⁷O NMR shift of a Dy³⁺-coordinated oxygen atom is almost completely of contact origin ($\geq 85\%$) and that this shift is almost independent of the nature and the stoichiometry of the complex concerned.²⁵ The induced shift of a bound oxygen atom at 55 °C is -2347 ppm (determined from Dy³⁺-induced shifts of water).²⁶ This would mean that in the present case $-1491/-2347 = 0.6$ methanol molecules are bound to the Dy³⁺ ion. Taking into consideration that fast exchange is not completely reached at 55 °C, it can be concluded that one methanol molecule is bound to the complex.

3.2.4 Luminescence properties of the Eu³⁺ and Tb³⁺ complexes

The luminescence properties of the Eu³⁺ and Tb³⁺ complexes were evaluated to obtain structural information of the complexes. Previous work has shown that the terphenyl moiety, which is in close proximity of the lanthanide ion, can act as an antenna chromophore.¹¹ The transfer of energy from the antenna to the lanthanide ion is generally considered to take place through the triplet level of the chromophore via a Dexter mechanism, which is strongly distance dependent.²⁷ The terphenyl triplet energy state of $24,600 \text{ cm}^{-1}$ was estimated from the phosphorescence spectrum of (Gd)**1a** and (Gd)**2** at 77 K,²⁸ and is in agreement with previously reported values of $23,530 \text{ cm}^{-1}$ and $23,750 \text{ cm}^{-1}$ for the *m*-terphenyl moiety.^{3,29} The excitation spectra of (Eu)**1a** and (Eu)**2** show a band at 280 nm that corresponds to the absorption band of the terphenyl moiety, and clearly indicates that the Eu³⁺ ion can be excited

via the terphenyl moiety. The emission spectra of these complexes in methanol, excited at 300 nm, show the luminescence bands that correspond to the typical $\text{Eu}^{3+} \ ^5\text{D}_0 \rightarrow \ ^7\text{F}_n$ transitions, with the strongest emissions in the $\ ^5\text{D}_0 \rightarrow \ ^7\text{F}_1$ (around 593 nm) and $\ ^5\text{D}_0 \rightarrow \ ^7\text{F}_2$ (around 615 nm) transition regions (solid lines in Figures 3.7 and 3.8).

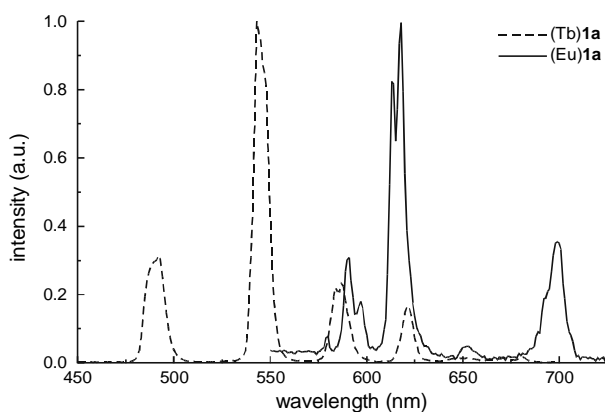


Figure 3.7: Emission spectra of the (Eu)**1a** (solid line) and (Tb)**1a** (dashed line) complexes in methanol (10^{-4} M) upon excitation of the terphenyl ligand at 300 nm.

The (Eu)**1b** complex has a similar emission spectrum (not shown). Deaeration of the samples only resulted in a slight increase in the luminescence intensity (less than 10%), indicating that the terphenyl triplet state is hardly quenched by oxygen and thus that the energy transfer to the Eu^{3+} ion is fast ($> 10^8 \text{ s}^{-1}$).³⁰

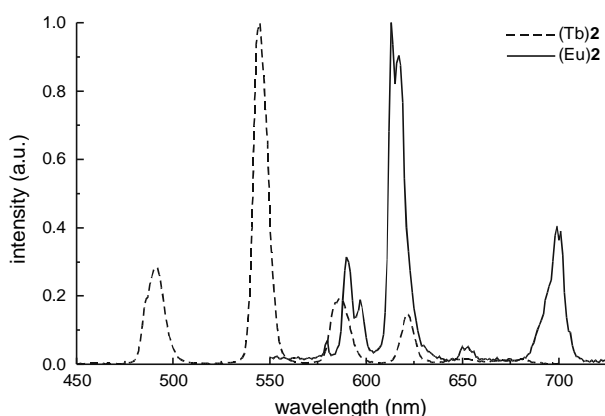


Figure 3.8: Emission spectra of the (Eu)**2** (solid line) and (Tb)**2** (dashed line) complexes in methanol (10^{-4} M) upon excitation of the terphenyl ligand at 300 nm.

For (Eu)**1a-b** and (Eu)**2** a peak is observed for the $\ ^5\text{D}_0 \rightarrow \ ^7\text{F}_0$ emission at 579 nm, indicating that the symmetry of the first coordination sphere is not centrosymmetric. Since the $\ ^7\text{F}_0$ state is non-degenerate, the single peak indicates that there is only one (time-averaged) luminescent

Eu³⁺ species in solution. The Eu³⁺ spectra further show a splitting of the ⁵D₀→⁷F₁ emission (around 593 nm) and a splitting of the ⁵D₀→⁷F₂ emission (around 615 nm) caused by the ligand field. Strictly, three sublevels are expected for the ⁷F₁ level and five sublevels for the ⁷F₂ level, when the Eu³⁺ ion is in a C_s symmetric environment. Under the given conditions, *i.e.* at room temperature and with an emission bandwidth of 1 nm, only two sublevels were observed for each of these J-levels. From these data the Eu(⁷F₁) and Eu(⁷F₂) energy levels can be determined (see Table 3.2). The values of the ligand field splitting are approximately 200 cm⁻¹ for the ⁷F₁ state and 130 cm⁻¹ for the ⁷F₂ state, and are in agreement with previously reported values for organic Eu³⁺ complexes.^{4,31}

Table 3.2: Eu(⁷F₁) and Eu(⁷F₂) energy levels (in cm⁻¹) relative to the Eu(⁷F₀) level in the *m*-terphenyl-based complexes, calculated from the luminescence spectra in methanol.

Energy level	(Eu) 1a (cm ⁻¹)	(Eu) 1b (cm ⁻¹)	(Eu) 2 (cm ⁻¹)
⁷ F ₁	321	292	292
	491	491	491
⁷ F ₂	928	928	928
	1060	1060	1060

Kirby and Richardson established that the intensity ratio of the ⁵D₀→⁷F₂ transition and the ⁵D₀→⁷F₁ transition is a good measure for the symmetry of the first coordination sphere of the Eu³⁺ ion.³² In a centrosymmetric environment the magnetic dipole ⁵D₀→⁷F₁ transition of Eu³⁺ is dominating, whereas distortion of the symmetry around the ion causes an intensity enhancement of electric dipole transitions such as the hypersensitive ⁵D₀→⁷F₂ transition. They have determined that this ratio is 8.0 for a single crystal Eu(DBM)₃.H₂O (DBM = 1,3-diphenyl-1,3-propanedionate) in which the Eu³⁺ ion has an asymmetric coordination sphere, whereas they found an intensity ratio of 0.67 for the centrosymmetric [Eu(ODA)₃] complex (ODA = oxydiacetate). In the present case, the (⁵D₀→⁷F₂)/(⁵D₀→⁷F₁) ratio is approximately 4 for all complexes, which is significantly higher than the value of 0.67. This can be expected since the first coordination sphere is not centrosymmetric, but has a time-averaged C_s symmetry, as could be concluded from the ¹H NMR data of the (Y)**1a** and (Y)**2** complexes. The emission spectrum of (**1a**)Eu in DMSO-*h*₆ (not shown) closely resembles the corresponding spectrum in methanol, demonstrating that the structure of the first coordination sphere is essentially the same in both solvents.

The (Tb)**1a** and (Tb)**2** complexes exhibit bright green luminescence in methanol upon excitation of the terphenyl unit at 300 nm (dashed lines in Figures 3.7 and 3.8). The peaks in the emission spectrum correspond to the $^5D_4 \rightarrow ^7F_n$ transitions, with the strongest emission corresponding to the $^5D_4 \rightarrow ^7F_5$ transition around 545 nm. The spectra show some structuring within the emission bands, but they are not as sensitive to the detailed structure of the first coordination sphere, as is the case for the Eu^{3+} spectra.³³

The time-resolved luminescence spectra of the (Eu)**1a-b**, (Eu)**2**, (Tb)**1a**, and (Tb)**2** complexes in methanol-*h*₁ show mono-exponential decays, with luminescence lifetimes of approximately 0.80 ms for the Eu^{3+} complexes and 1.80 ms for the Tb^{3+} complexes. The known sensitivity of Eu^{3+} and Tb^{3+} luminescence towards quenching by hydroxyl groups of the solvent³⁴ provides an experimental tool to estimate the degree of shielding by the ligands. An empirical relationship has been established that estimates the number of coordinated methanol molecules (*n*):^{35,36}

$$n = q(1/\tau_h - 1/\tau_d - k_{\text{corr}}) \quad (1)$$

where *q* is 2.1 for Eu^{3+} and 8.4 for Tb^{3+} , τ_h is the luminescence lifetime of the complex in methanol-*h*₁ and τ_d the luminescence lifetime of the complex in methanol-*d*₁, k_{corr} is a factor to correct for methanol molecules in the second sphere and is 0.125 ms⁻¹ for Eu^{3+} and 0.03 ms⁻¹ for Tb^{3+} . The luminescence lifetimes of the (Eu)**1a-b**, (Eu)**2**, (Tb)**1a**, and (Tb)**2** complexes are significantly longer than those of the free Eu^{3+} (0.27 ms) and Tb^{3+} (0.65 ms) in methanol-*h*₁, showing that effective solvent shielding has been achieved by complexation of the ions in the terphenyl ligands (see Table 3.3).

Table 3.3: Luminescence lifetimes of the Eu^{3+} and Tb^{3+} complexes measured in CH_3OH (τ_h) and CH_3OD (τ_d) as well as the number of coordinated solvent molecules (*n*) determined from equation (1).

Complex	τ_h (ms)	τ_d (ms)	<i>n</i>
(Eu) 1a	0.80	1.74	1.2 ± 0.5
(Eu) 1b	0.80	1.62	1.1 ± 0.5
(Eu) 2	0.68	1.79	1.7 ± 0.5
(Tb) 1a	1.83	2.68	1.2 ± 1.5
(Tb) 2	1.80	2.42	0.94 ± 1.5

Using equation (1), our experiments show that only one methanol molecule is coordinated to the complexed lanthanide ion in (Ln)**1a-b** and one or two methanol molecules are coordinated to the complexed lanthanide ion in (Ln)**2** (see Table 3.3).

A model for the structure which is in agreement with the photophysical data of the Eu^{3+} and Tb^{3+} complexes involves coordination of the lanthanide ion to three ether oxygens, three carboxylate oxygens, two amide oxygens, and one methanol molecule, in the case of the (Ln)**1a-b** complexes, resulting in a coordination number of nine for the first coordination sphere. This is in accordance with the experimentally determined coordination number of 9 of Eu^{3+} and Tb^{3+} ions in methanol.³⁷ These results are also supported by the results obtained from ^{17}O NMR measurements of the (Dy)**1a** complex, where it was found that one methanol molecule is bound to the complex. The model also applies to the (Ln)**2** complexes, but the photophysical data suggest that a coordinated sulfonamide oxygen can be temporarily replaced by a methanol molecule. Despite the fact that the ^1H NMR data of (Y)**1a** at room temperature indicate that the (Eu)**1a-b** complexes can be in different conformations due to the hindered rotation around the tertiary amide, the photophysical data clearly indicate that this does not affect the first coordination sphere of the Eu^{3+} ion. A change in amide C-substituent (acetyl or benzoyl) also does not alter the first coordination sphere.

3.2.5 Luminescence properties of the Dy^{3+} and Sm^{3+} complexes

Two other lanthanide ions that have emission bands in the visible region are Dy^{3+} and Sm^{3+} , but the luminescence of these ions is more sensitive to quenching by solvent hydroxyl groups than the Eu^{3+} and Tb^{3+} luminescence.³ Therefore, the emission spectra were recorded in $\text{DMSO-}h_6$, a strongly coordinating solvent without efficiently quenching hydroxyl groups.

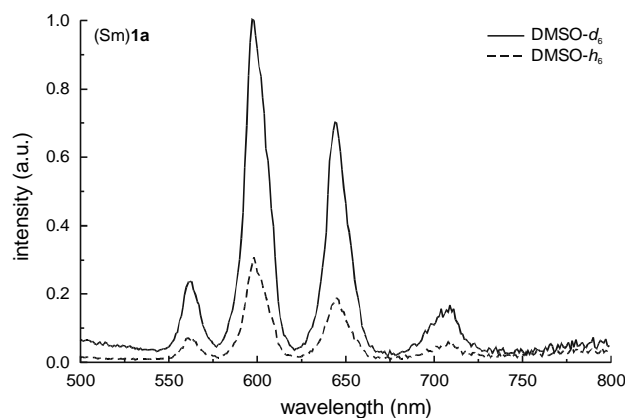


Figure 3.9: Emission spectra of 10^{-3} M solutions of (Sm)**1a** in $\text{DMSO-}h_6$ (dashed line) and $\text{DMSO-}d_6$ (solid line) upon excitation of the terphenyl ligand at 300 nm.

Upon excitation of the (Sm)**1a** (see Figure 3.9) and (Dy)**1a** (see Figure 3.10) complexes at 300 nm, the typical luminescence bands were observed, corresponding to the $^4F_{9/2} \rightarrow ^6H_j$ transitions, and $^4G_{5/2} \rightarrow ^6H_j$ transitions, respectively. The (Sm)**1a** complex shows two intense emission bands at 600 and 640 nm, and two weaker bands at 560 and 710 nm. The (Dy)**1a** complex shows four emission bands in the visible region, two strong bands at 475 and 575 nm and two weaker bands at 655 nm and at 745 nm.

The luminescence intensities increased dramatically upon changing the solvent from DMSO- h_6 (dashed lines in Figures 3.6 and 3.7) to DMSO- d_6 (solid lines in Figures 3.9 and 3.10) demonstrating the sensitivity of Dy^{3+} and Sm^{3+} towards quenching by C-H vibrations, although these vibrations are less energetic than O-H vibrations.³

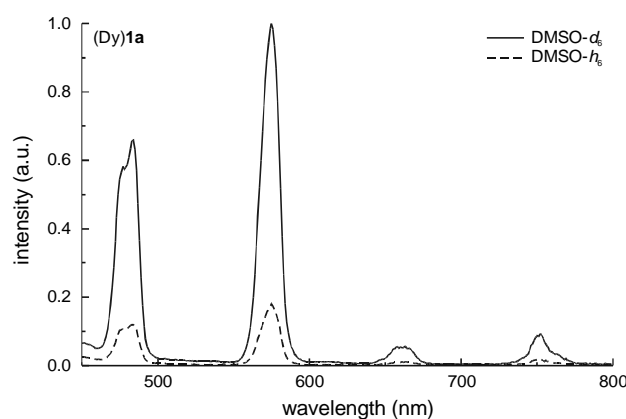


Figure 3.10: Emission spectra of 10^{-3} M solutions of (Dy)**1a** in DMSO- h_6 (dashed line) and DMSO- d_6 (solid line) upon excitation of the terphenyl ligand at 300 nm.

3.2.6 Luminescence properties of the Er^{3+} , Nd^{3+} , and Yb^{3+} complexes

Although sensitized emission has been studied in detail for Eu^{3+} and Tb^{3+} complexes,^{6,7,38} and efficient antenna chromophores with appropriate triplet energy levels have been reported, the field of sensitized near-infrared lanthanide luminescence is still relatively unexplored. The main difference between the sensitization of Eu^{3+} and Tb^{3+} and the sensitization of Nd^{3+} , Yb^{3+} , and Er^{3+} is that the former require chromophores with triplet states roughly above $22,000\text{ cm}^{-1}$, whereas the latter lanthanide ions can be excited via chromophores with much lower triplet states (see Figure 2.1). However, it has been reported that Nd^{3+} , Yb^{3+} , and Er^{3+} can also accept the excitation energy from chromophores with high lying triplet states. Indeed, after laser excitation at 350 nm sensitized emission at 1540 nm is observed for (Er)**1a** ($^4I_{13/2} \rightarrow ^4I_{15/2}$ transition), at 880, 1060, and 1330 nm for (Nd)**1a** ($^4F_{3/2} \rightarrow ^4I_{9/2}$, $^4I_{11/2}$, and $^4I_{13/2}$

transition, respectively), and at 980 nm for (Yb)1a (${}^2F_{5/2} \rightarrow {}^2F_{7/2}$ transition). The spectra are depicted in Figure 3.11.

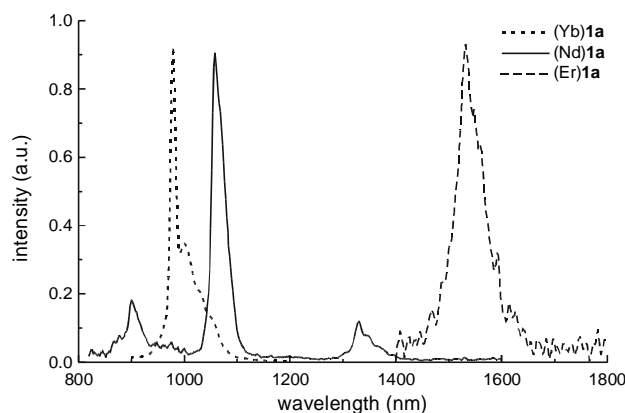


Figure 3.11: Near-infrared emission spectra of (Nd)1a, (Yb)1a and (Er)1a in DMSO- h_6 (10^{-3} M) upon laser excitation of the terphenyl ligand at 350 nm.

Time-resolved luminescence experiments showed luminescence lifetimes of the complexes in DMSO- h_6 (τ_h) and DMSO- d_6 (τ_d) in the range of microseconds (see Table 3.4), with the Yb $^{3+}$ complexes having the longest lifetimes and the Nd $^{3+}$ complexes the shortest. The lifetimes compare favorably to the recently published data on Yb $^{3+}$ and Nd $^{3+}$ in these solvents.^{39,40} Upon changing the solvent from DMSO- h_6 to DMSO- d_6 the lifetimes increase significantly indicating that for this class of lanthanide ions the C-H oscillators are efficient quenchers of the excited luminescent state. The relative quenching rate constants of the C-H oscillators of the solvent molecules (k_q , see Table 3.4) were calculated using equation (2).

$$k_q = 1/\tau_h - 1/\tau_d \quad (2)$$

The calculations show that the quenching rates are the highest for Nd $^{3+}$ complexes, and lowest for the Yb $^{3+}$ complexes. This is in accordance with the well-established energy gap law⁴¹ that states that the smaller the harmonic number of vibrational quanta that is required to match the energy gap between the lowest luminescent state and the highest non-luminescent state of the lanthanide ion, the more effective the vibronic quenching is. For the C-H vibration with vibrational quanta of 2950 cm^{-1} , the number of harmonics (n_h) necessary to match the energy gap is largest for Yb $^{3+}$ (${}^2F_{5/2} \rightarrow {}^2F_{7/2}$; $n_h = 3-4$), followed by Er $^{3+}$ (${}^4I_{13/2} \rightarrow {}^4I_{15/2}$; $n_h = 2-$

3) and smallest for Nd³⁺ (⁴F_{3/2}→⁴I_{15/2}: n_h = 1-2). For comparison the lifetimes of the Eu³⁺ complexes have been added to Table 3.4.

Table 3.4: Luminescence lifetimes measured in DMSO-*h*₆ (τ_h) and DMSO-*d*₆ (τ_d) as well as the quenching rate constants by the methyl groups of DMSO-*h*₆ (k_q) calculated with equation (2).

Complex	τ _h (μs)	τ _d (μs)	k _q (10 ⁴ s ⁻¹) ^a
(Yb)1a	9.1	19.9	6.0
(Yb)2	10.3	23.6	5.5
(Er)1a	2.1	3.3	16.3
(Er)2	2.4	3.5	13.3
(Nd)1a	1.2	2.5	47.1
(Nd)2	1.2	2.5	40.8
(Eu)1a	1.86 ms	2.30 ms	0.010
(Eu)2	1.87 ms	2.25 ms	0.009

The energy gap between the lowest luminescent state and highest non-luminescent state of Eu³⁺ (⁵D₀→⁷F₇: n_h = 6-7) is much larger than the energy gap of the NIR emitting lanthanide ions. The calculated quenching rate constants in Table 3.4 are not absolute values that allow direct comparison, because the C-D vibration also quenches the lanthanide excited state (albeit less efficient than the C-H vibration), and therefore the quenching rate constants are lower limits. The observed trend, however, demonstrates that quenching becomes rapidly more efficient when n_h decreases.

For future applications in polymer waveguide optical amplifiers the near-infrared emitting complexes must have high luminescence quantum yields. The intrinsic luminescence quantum yield (φ_{lum}) of the complexed ions is given by equation (3):

$$\phi_{\text{lum}} = \tau/\tau_0 \quad (3)$$

where τ₀ is the natural lifetime (*i.e.* the luminescence lifetime in the absence of quenching processes) and τ the observed luminescence lifetime. The natural lifetimes of the ⁴I_{13/2}→⁴I_{15/2} transition of Er³⁺ and the ²F_{5/2}→²F_{7/2} transition of Yb³⁺ have been calculated from their respective absorption spectra,⁴² and are 14 ms for (Er)1a and 2 ms for (Yb)1a. The natural lifetime of Nd³⁺ cannot be determined in this way, since the emissions do not involve a transition back to the ground state. Instead a literature value of 0.25 ms was taken for Nd³⁺.⁴³

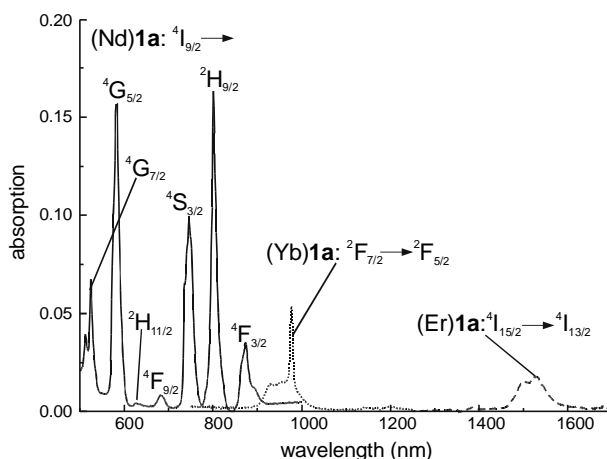


Figure 3.12: Part of the absorption spectra of the complexed lanthanide ions in (Nd)**1a**, (Er)**1a**, and (Yb)**1a** in DMSO- h_6 (10^{-2} M). The spectra have been corrected for the ligand absorption by subtracting the absorption spectrum of (**1a**)Gd, since Gd^{3+} has no absorptions in the 500 to 1700 nm region.

This leads to intrinsic luminescence quantum yields of 0.02% for (Er)**1a**, of 0.78% for (Yb)**1a**, and of 0.84% for (Nd)**1a** in DMSO- d_6 . These low luminescence quantum yields are caused by the fact that the C-H vibrations in the ligand are efficient quenchers. Deuteration of the ligands will improve the luminescence quantum yields, as has been demonstrated for Eu^{3+} complexes.^{3,11,44}

3.3 Conclusion

In summary, the *m*-terphenyl-based ligands reported here, bearing amide or sulfonamide functionalities form neutral complexes with trivalent lanthanide cations. The known luminescence behavior of Eu^{3+} was used to establish the structure of the complexes showing that the ligand occupies eight of the nine coordination sites of the ion, and a solvent molecule occupies the remaining coordination site. It has been demonstrated that by incorporating different lanthanide ions, various emission wavelengths become accessible, ranging from 500 to 1550 nm. The near-infrared emitting complexes exhibit sensitized-emission with a luminescence lifetime in the microsecond timescale. The complexes are very soluble in organic solvents, which is essential for the fabrication of polymer-based optical amplifiers. Further possible improvements of these complexes for future applications in optical amplifiers are deuteration of the ligands, and the incorporation of dyes to facilitate sensitized excitation in the visible region around 630 nm.

3.4 Experimental Section

3.4.1 Synthesis

General synthesis: Melting points were determined with a Reichert melting point apparatus and are uncorrected. Mass spectra were recorded on a Finnigan MAT 90 spectrometer using *m*-NBA (nitrobenzyl alcohol) as a matrix, unless stated otherwise. IR spectra were recorded with a Biorad 3200 or a Nicolet 5SXC FT-IR spectrophotometer using KBr pellets. Elemental analyses were performed on a Carlo Erba EA 1106 apparatus. ^1H NMR (250 MHz) and ^{13}C NMR (62.7 MHz) spectra were recorded with a Bruker AC 250 spectrometer in CDCl_3 unless stated otherwise, using residual CHCl_3 (7.26 ppm) and CDCl_3 (77.0 ppm) as the internal standard, respectively. ^1H NMR (400 MHz) and ^{19}F NMR (376.3 MHz) spectra were recorded with a Varian Unity 400 WB NMR spectrometer in $\text{DMSO-}d_6$ unless stated otherwise. ^{17}O NMR (40.68 MHz) spectra were recorded with a Varian Inova 300 NMR spectrometer in methanol. Preparative column chromatography separations were performed on Merck silica gel (particle size 0.040-0.063 mm, 230-400 mesh). CH_2Cl_2 , CHCl_3 , and hexane (mixture of isomers) were distilled from CaCl_2 and stored over molecular sieves (4 Å). Ethyl acetate was distilled from K_2CO_3 and stored over molecular sieves (4 Å). Triethylamine (Et_3N) was distilled *in vacuo* and stored over KOH. Acetonitrile and ethanol were of analytical grade and were dried over molecular sieves (4 Å) prior to use. *n*-Butoxypropylamine, *tert*-butyl bromoacetate, and the $\text{Ln}(\text{NO}_3)_3 \cdot 5\text{H}_2\text{O}$ salts were purchased from Aldrich and used without further purification. All reactions were carried out under an argon atmosphere. Standard workup involved washing the organic layers with water, drying over magnesium sulfate, filtration of the salts, and concentrating to dryness *in vacuo*.

2,6-Bis[3'-formyl-2'-((*tert*-butoxycarbonyl)methoxy)-5'-methylphenyl]-4-methyl-1-((*tert*-butoxycarbonyl)methoxy)benzene (4). To a mixture of **3** (1.9 g, 5.1 mmol) and K_2CO_3 (2.7 g, 20.2 mmol) in acetonitrile (250 mL) was added *tert*-butyl bromoacetate (3.2 g, 16.1 mmol) and the mixture was refluxed for 8 h. Subsequently the reaction mixture was filtered and the filtrate was concentrated *in vacuo*. The residue was redissolved in CH_2Cl_2 (200 mL) and washed twice with 0.5 N HCl, followed by standard workup. The crude product was purified by flash column chromatography (ethyl acetate/hexane 1:3 (v/v)) to give triester **4** as an off-white solid: yield 80%, m.p. 130-132 °C. ^1H NMR (CDCl_3): δ = 10.6 (s, 2H), 7.67 (d, J = 2.3

Hz, 2H), 7.43 (d, $J = 2.3$ Hz, 2H), 7.21 (s, 2H), 4.20 (s, 4H), 3.90 (s, 2H), 2.38 (s, 3H), 2.36 (s, 6H), 1.38 (s, 18H), 1.21 (s, 9H). ^{13}C NMR (CDCl_3): $\delta = 191.2, 167.7, 167.0, 157.0, 151.6, 138.6-127.9, 82.3, 81.4, 70.9, 69.7, 28.0, 27.8, 20.7, 20.6$. MS (FAB): m/z 741.2 [(M+Na) $^+$, calcd.: 741.3]. Anal. calcd. for $\text{C}_{41}\text{H}_{50}\text{O}_{11}$: C, 68.51, H, 7.01. Found: C, 68.75, H, 7.08.

2,6-Bis[3'-(*N*-*n*-butoxypropylaminomethyl)-2'-((*tert*-butoxycarbonyl)methoxy)-5'-methylphenyl]-4-methyl-1-((*tert*-butoxycarbonyl)methoxy)benzene (5). To a solution of **4** (1.54 g, 2.14 mmol) in ethanol (150 mL) was added *n*-butoxypropylamine (0.56 g, 4.28 mmol) and the solution was stirred at room temperature for 0.5 h. Subsequently 100 mg of Pd/C (10%) was added and the suspension was stirred overnight at room temperature under a hydrogen atmosphere. The reaction mixture was filtered over Hyflo filter aid and the filtrate was concentrated *in vacuo*. The bis(amine) **5** was obtained as a colorless oil in quantitative yield. ^1H NMR (CDCl_3): $\delta = 7.11$ (s, 2H), 7.08 (d, $J = 2.0$ Hz, 2H), 7.05 (d, $J = 2.0$ Hz, 2H), 4.12 (s, 4H), 3.94 (s, 2H), 3.86 (s, 4H), 3.49 (t, $J = 6.5$ Hz, 4H), 3.40 (t, $J = 6.5$ Hz, 4H), 2.73 (t, $J = 7.0$ Hz, 4H), 2.32 (s, 3H), 2.29 (s, 6H), 1.80 (m, 4H), 1.57 (m, 4H), 1.40 (s, 18H), 1.36 (m, 4H), 1.23 (s, 9H), 0.90 (t, $J = 7.2$ Hz, 6H). ^{13}C NMR (CDCl_3): $\delta = 168.3, 167.5, 152.6, 151.4, 133.1-130.2, 81.4, 80.8, 70.6, 70.4, 69.7, 69.3, 68.9, 53.4, 49.4, 46.8, 39.6, 33.4, 31.8, 30.1, 28.0, 27.8, 20.7, 19.3, 13.9$. MS (FAB): m/z 949.4 [(M+H) $^+$, calcd. for $\text{C}_{55}\text{H}_{85}\text{N}_2\text{O}_{11}$: 949.6].

Typical procedure for the synthesis of 6a-c and 7. To a solution of **5** (0.5 g, 0.53 mmol) and Et_3N (0.20 g, 2.0 mmol) in CH_2Cl_2 (75 mL) were added 3 mmol of the appropriate acid chloride or *p*-toluenesulfonyl chloride, and the resulting solution was stirred overnight at room temperature. After the addition of CH_2Cl_2 (100 mL), the reaction mixture was washed twice with 0.5 N HCl, followed by standard workup. The crude product was purified by flash column chromatography.

2,6-Bis[3'-(*N*-*n*-butoxy-propylbenzoylamidomethyl)-2'-((*tert*-butoxycarbonyl)-methoxy)-5'-methylphenyl]-4-methyl-1-((*tert*-butoxycarbonyl)methoxy)benzene (6a). The crude product was purified by flash column chromatography (ethyl acetate/hexane 2:3 (v/v)) to give the bis(benzoylamide) **6a** as a colorless oil: yield 80%. ^1H NMR (CDCl_3): $\delta = 7.54-7.31$ (m, 10H), 7.20-7.00 (m, 6H), 5.03 (s, 2H), 4.77 (s, 2H), 4.22-4.08 (m, 2H), 4.02-3.82 (m,

4H), 3.72-3.50 (m, 4H), 3.48-3.16 (m, 8H), 2.33 (s, 9H), 2.10-1.96 (m, 2H), 1.92-1.78 (m, 2H), 1.64-1.52 (m, 2H), 1.50-1.15 (m, 33H), 0.97-0.82 (m, 6H). ^{13}C NMR (CDCl_3): $\delta = 172.3, 167.9, 167.1, 151.9, 151.3, 136.5-126.6, 81.5, 80.9, 70.6, 70.4, 69.6, 68.4, 67.6, 60.4, 48.4, 46.3, 43.1, 42.3, 31.9, 28.7, 27.9, 21.0, 20.7, 19.3, 13.9$. MS (FAB): m/z 1157.6 $[(\text{M}+\text{H})^+]$, calcd. for $\text{C}_{69}\text{H}_{93}\text{N}_2\text{O}_{13}$: 1157.7].

2,6-Bis[3'-(*N*-*n*-butoxypropylacetamidomethyl)-2'-((*tert*-butoxycarbonyl)-methoxy)-5'-methylphenyl]-4-methyl-1-((*tert*-butoxycarbonyl)methoxy)benzene (6b). The crude product was purified by flash column chromatography (ethyl acetate/hexane 2:1 (v/v)) to give the bis(acetamide) **6b** as a colorless oil: yield 53%. ^1H NMR (CDCl_3): $\delta = 7.11-7.07$ (m, 2H), 7.00 (s, 2H), 6.90 (s, 1H), 6.78 (d, $J = 2.8$ Hz, 1H), 4.76 (s, 4H), 4.03 (s, 4H), 3.89-3.85 (m, 2H), 3.48-3.30 (m, 12H) 2.34-2.19 (m, 12H), 2.06 (s, 4H), 1.85-1.80 (m, 4H), 1.53-1.42 (m, 4H), 1.30-1.24 (m, 4H), 1.20-1.18 (m, 4H), 1.38 (s, 27H), 0.89-0.81 (m, 6H). ^{13}C NMR (CDCl_3): $\delta = 171.8, 171.2, 168.3, 168.2, 168.0, 167.2, 167.1, 167.4, 152.3, 151.9, 151.4, 133.8 - 126.1, 81.8, 81.0, 70.9, 70.8, 70.6, 70.2, 69.8, 68.5, 67.3, 48.0, 45.2, 44.0, 42.4, 38.5, 31.8, 28.5, 27.9, 21.7, 21.3, 20.9, 19.4, 13.9$. MS (FAB) m/z 1033.5 $[(\text{M}+\text{H})^+]$, calcd. for $\text{C}_{59}\text{H}_{89}\text{N}_2\text{O}_{13}$: 1033.6].

2,6-Bis[3'-(*N*-*n*-butoxypropyl-*p*-fluorobenzoylmethyl)-2'-((*tert*-butoxycarbonyl)-methoxy)-5'-methylphenyl]-4-methyl-1-((*tert*-butoxycarbonyl)methoxy)benzene (6c). The crude product was purified by flash column chromatography (ethyl acetate/hexane 2:1 (v/v)) to give the bis(*p*-F-benzoylamide) **6c** as a colorless oil: yield 73%. ^1H NMR (CDCl_3): $\delta = 7.56-7.40$ (m, 4H), 7.20-6.95 (m, 10H), 5.02 (s, 2H), 4.80 (s, 2H), 4.20-4.07 (m, 2H), 4.05-3.85 (m, 4H), 3.70-3.20 (m, 12H), 2.36 (s, 9H), 2.11-1.76 (m, 4H), 1.66-1.53 (m, 2H), 1.50-1.14 (m, 33H), 1.00-0.81 (m, 6H). ^{13}C NMR (CDCl_3): $\delta = 170.3, 167.0, 166.1, 163.8, 160.5, 150.9, 150.3, 132.4-126.0, 80.6, 80.0, 69.6, 69.2, 68.6, 67.5, 66.5, 59.3, 47.7, 45.2, 42.4, 41.5, 30.7, 27.7, 26.8, 19.9, 19.6, 18.2, 12.8$. MS (FAB) m/z 1215.6 $[(\text{M}+\text{Na})^+]$, calcd. for $\text{C}_{69}\text{H}_{90}\text{N}_2\text{O}_{13}\text{F}_2\text{Na}$: 1215.6].

2,6-Bis[3'-(*N*-*n*-butoxypropyl-*p*-toluenesulfonylamidemethyl)-2'-((*tert*-butoxy-carbonyl)methoxy)-5'-methylphenyl]-4-methyl-1-((*tert*-butoxycarbonyl)-methoxy)-benzene (7). The crude product was purified by flash column chromatography (ethyl acetate/hexane 1:3 (v/v)) to give the bis(sulfonamide) **7** as a colorless oil: yield 69%. ¹H NMR (CDCl₃): δ = 7.73 (d, *J* = 8.2 Hz, 4H), 7.27 (d, *J* = 8.3 Hz, 4H), 7.19 (d, *J* = 1.8 Hz, 2H), 7.07 (s, 2H), 7.03 (d, *J* = 1.8 Hz, 2H), 4.58 (s, 4H), 4.01 (s, 4H), 3.88 (s, 2H), 3.33-3.24 (m, 12 H), 2.40 (s, 6H), 2.29 (s, 3H), 2.25 (s, 6H), 1.74 - 1.63 (m, 4H), 1.52-1.38 (m, 4H), 1.32 (s, 18H), 1.27 (m, 4H), 1.23 (s, 9H), 0.86 (t, 6H, *J* = 7.0 Hz). ¹³C NMR (CDCl₃): δ = 168.1, 167.2, 152.0, 151.3, 143.0, 137.1-127.1, 81.5, 81.0, 70.5, 70.2, 69.6, 68.0, 46.9, 46.6, 31.7, 28.6, 27.9, 21.5, 20.8, 19.2, 13.9. MS (FAB): *m/z* 1280.1 [(M+Na)⁺, calcd. for C₆₉H₉₆N₂S₂O₁₅Na: 1279.6].

Typical preparation of the triacid ligands (H₃)1a-c and (H₃)2. A solution of 0.30 mmol of the ligands **6a-c** or **7** in TFA (50 mL) was stirred overnight at room temperature. Subsequently, toluene (25 mL) was added and the TFA/toluene mixture was azeotropically evaporated. The residue was taken up in CH₂Cl₂ (100 mL) and washed twice with 1 N HCl, followed by standard workup. The triacids were obtained as white solids in near quantitative yield.

2,6-Bis[3'-(*N*-*n*-butoxypropylbenzoylamidemethyl)-2'-((hydroxycarbonyl)-methoxy)-5'-methylphenyl]-4-methyl-1-((hydroxycarbonyl)methoxy)benzene ((H₃)1a). M.p.: 40-42 °C. ¹H NMR (CD₃OD): δ = 7.50-7.30 (m, 10H), 7.15-7.10 (m, 4H), 6.98 (s, 2H), 4.60 (s, 2H), 4.10-3.75 (m, 6H), 3.65-3.15 (m, 12H), 2.30 (s, 9H), 1.86 (m, 2H), 1.75 (m, 2H), 1.60-1.10 (m, 8H), 0.84-0.71 (m, 6H). ¹³C NMR (CD₃OD): δ = 174.6, 172.2, 172.0, 153.5, 153.0, 137.6-127.7, 71.8, 71.5, 69.9, 68.7, 44.6, 44.0, 32.9, 32.8, 29.5, 28.5, 21.0, 20.4, 14.3. MS (FAB): *m/z* 1012.0 [(M+Na)⁺, calcd.: 1011.5]. IR (KBr): 1738 (ν_{COO}), 1631 (ν_{NC=O}) cm⁻¹. Anal. calcd. for C₅₇H₆₈N₂O₁₃·1H₂O: C, 67.97, H, 7.01, N, 2.78. Found: C, 68.32, H, 7.03, N, 2.80.

2,6-Bis[3'-(*N*-*n*-butoxypropyl-acetamidemethyl)-2'-((hydroxycarbonyl)methoxy)-5'-methylphenyl]-4-methyl-1-((hydroxycarbonyl)methoxy)benzene ((H₃)1b). M.p.: 51-53 °C. ¹H NMR (CD₃OD): δ = 7.14-7.11 (m, 2H), 7.09-6.83 (m, 4H), 4.71 (s, 2H), 4.67 (s, 2H),

4.15-3.95 (m, 6H), 3.40-3.29 (m, 12H), 3.23-3.21 (m, 4H), 2.29 (s, 3H), 2.25 (s, 3H), 2.22 (s, 3H), 2.12 (s, 3H), 2.01 (s, 3H), 1.83-1.60 (m, 4H), 1.50-1.39 (m, 4H), 1.32-1.20 (m, 4H), 0.87-0.79 (m, 6H). ^{13}C NMR (CD_3OD): $\delta = 174.1, 173.7, 172.2, 153.4, 153.0, 152.4, 135.6 - 128.4, 71.8, 71.7, 70.6, 70.1, 69.5, 68.5, 46.5, 45.0, 44.0, 37.9, 32.9, 30.5, 29.4, 28.8, 21.8, 21.3, 21.0, 20.8, 20.4, 14.3$. MS (FAB) m/z 863.1 [(M-H) $^-$, calcd. for $\text{C}_{47}\text{H}_{63}\text{N}_2\text{O}_{13}$: 863.4]. IR (KBr): 1740 (ν_{COO}), 1630 ($\nu_{\text{NC=O}}$) cm^{-1} . Anal. calcd. for $\text{C}_{47}\text{H}_{64}\text{N}_2\text{O}_{13}\cdot\text{H}_2\text{O}$: C, 63.93, H, 7.53, N, 3.17. Found: C, 64.09, H, 7.74, N, 3.36.

2,6-Bis[3'-(*N*-*n*-butoxypropyl-*p*-fluorobenzoylamidemethyl)-2'-((hydroxycarbonyl)-methoxy)-5'-methylphenyl]-4-methyl-1-((hydroxycarbonyl)methoxy)benzene ((H₃)1c). M.p.: 73-75 °C. ^1H NMR (CD_3OD): $\delta = 7.40$ (s(b), 4H), 7.20-6.87 (m, 10H), 4.65 (s, 2H), 4.20-3.83 (m, 6H), 3.56-3.06 (m, 12H), 2.25 (s, 9H), 1.94-1.62 (m, 4H), 1.51-1.00 (m, 8H), 0.90-0.70 (m, 6H). ^{13}C NMR (CD_3OD): $\delta = 171.6, 170.0, 164.4, 161.1, 151.6, 151.2, 150.3, 133.6-127.6, 114.7, 114.4, 69.7-66.7, 46.2, 45.6, 42.7, 42.3, 36.8, 31.0, 27.5, 26.5, 19.0, 18.9, 18.4, 12.6$. MS (FAB): m/z 1047.4 [(M+Na) $^+$, calcd.: 1047.4]. IR (KBr): 1750 (ν_{COO}), 1635 ($\nu_{\text{NC=O}}$) cm^{-1} . Anal. calcd. for $\text{C}_{57}\text{H}_{66}\text{N}_2\text{O}_{13}\text{F}_2\cdot 0.5\text{H}_2\text{O}$: C, 66.20, H, 6.53, N, 2.71. Found: C, 66.20, H, 6.43, N, 2.88.

2,6-Bis[3'-(*N*-*n*-butoxypropyl-4-methylbenzene-sulfonylamidemethyl)-2'-((hydroxycarbonyl)methoxy)-5'-methylphenyl]-4-methyl-1-((hydroxycarbonyl)methoxy)-benzene ((H₃)2). M.p.: 60-62 °C. ^1H NMR (CD_3OD): $\delta = 7.73$ (d, $J = 7.7$ Hz, 4H), 7.38 (d, $J = 7.7$ Hz, 4H), 7.16 (s, 2H), 7.13 (s, 2H), 7.12 (s, 2H), 4.54 (s, 4H), 4.14 (s, 4H), 4.04 (s, 2H), 3.35-3.20 (m, 12H), 2.43 (s, 6H), 2.36 (s, 3H), 2.28 (s, 6H), 1.72-1.58 (m, 4H), 1.54-1.40 (m, 4H), 1.40-1.20 (m, 4H), 0.90 (t, $J = 7.2$ Hz, 6H). ^{13}C NMR (CD_3OD): $\delta 172.3, 170.5, 153.2, 152.1, 144.9 - 128.1, 71.7, 70.9, 69.1, 41.4, 32.8, 30.7, 29.8, 21.6, 20.9, 20.4, 14.5$. MS (FAB): $m/z = 1111.5$ [(M+Na) $^+$, calcd 1111.4]. IR (KBr): 1740 ($\text{C}=\text{O}_{\text{acid}}$), 1337, 1159 ($\text{S}=\text{O}$) cm^{-1} . Anal. calcd. for $\text{C}_{57}\text{H}_{72}\text{N}_2\text{O}_{15}\text{S}_2$: C, 62.85, H, 6.66, N, 2.57, S, 5.89. Found C, 62.50, H, 6.73, N, 3.06, S, 6.09.

Typical procedure for the preparation of the lanthanide complexes. To a solution of 0.05 mmol of triacids (H₃)1a-c or (H₃)2 and 0.25 mmol of Et₃N in methanol (20 mL) was added 0.07 mmol of the lanthanide nitrate salt. The resulting solution was stirred for 2 h, after which

the solvent was evaporated. The complex was redissolved in CHCl_3 and washed twice with water, followed by standard workup. The complexes were obtained as solids in quantitative yields. The complexes were characterized by FAB-MS spectrometry (see Table 3.5) and IR spectroscopy. The bis(amide) complexes (Ln)**1a-c** all gave similar IR spectra: a peak at 1640-1630 cm^{-1} ($\nu_{\text{NC=O}}$) with a shoulder around 1600 cm^{-1} (ν_{COO}). In the IR spectra of the bis(sulfonamide) complexes (Ln)**2** a peak at 1595-1600 cm^{-1} (ν_{COO}), and two peaks around 1330 and 1160 cm^{-1} ($\nu_{\text{S=O}}$) were observed.

Table 3.5: FAB-MS data of the *m*-terphenyl-based complexes. A mixture of dithiothreitol and dithioerythritol (5:1 (v/v)), known as *Magic Bullet*, was used as the matrix.

Complex	Measured (M+H) ⁺	Calcd. (M+H) ⁺	Complex	Measured (M+H) ⁺	Calcd. (M+H) ⁺
(Y) 1a	1075.9	1075.4	(Eu) 1b	1015.3	1015.3
(Eu) 1a	1139.6	1139.4	(Y) 1c	1111.5	1111.3
(Gd) 1a	1144.2	1144.3	(Y) 2	1260.3	1260.8
(Tb) 1a	1145.3	1145.4	(Eu) 2	1237.6	1237.3
(Er) 1a	1153.4	1153.4	(Gd) 2	1244.7	1244.3
(Yb) 1a	1160.2	1160.4	(Tb) 2	1267.2 ^a	1267.3 ^a
(Nd) 1a	1130.4	1130.4	(Er) 2	1254.3	1254.6
(Sm) 1a	1138.6	1138.4	(Yb) 2	1260.2	1260.4
(Dy) 1a	1150.3	1150.4	(Nd) 2	1230.0	1230.3

^a(M+Na)⁺

3.4.2 Photophysical studies

Visible region: Steady-state luminescence measurements were performed with a Photon Technology International (PTI) Alphascan spectrofluorimeter. The samples were excited with a 75 W quartz-tungsten-halogen lamp followed by a SPEX 1680 double monochromator. The emitted light was detected at an angle of 90° by a Hamamatsu R928 photomultiplier, and subsequently fed to a photon-counting interface. Time-resolved luminescence measurements were performed with an Edinburgh Analytical Instruments FL900 system. The excitation source consisted of a pulsed Xe-lamp (μs -pulsed output). The luminescence signal was detected by a Hamamatsu R928 photomultiplier and fed to a time-to-amplitude converter and a multichannel analyzer (Time Correlated Single Photon Detection).

NIR region: Steady state photoluminescence measurements were performed using the 351.1/363.8 nm lines of an Ar ion pump laser at a power of 60 mW for excitation. The laser

beam was modulated with an acousto-optic modulator at a frequency of 40 Hz. The luminescence signal was focused into a monochromator and detected with a liquid-nitrogen-cooled Ge detector, using standard lock-in techniques. Luminescence lifetime measurements (Edinburgh Analytical Instruments LP900 system) were performed by monitoring the luminescence decay after excitation with a 0.5 ns pulse of an LTB MSG 400 nitrogen laser ($\lambda_{\text{exc}}=337$ nm, pulse energy 20 μJ , 10 Hz repetition rate). Decay signals were recorded using a liquid-nitrogen-cooled Ge detector with a time resolution of 0.3 μs . The signals were averaged using a digitizing Tektronix oscilloscope. All decay curves were analyzed by deconvolution of the measured detector response and could be fitted with mono-exponential curves. The detector response was obtained by recording the signal of the NIR fluorescent dye IR 140 in methanol, which has a fluorescence lifetime (less than 1 ns) that is much shorter than the detector response.

3.4.3 Molecular dynamics and molecular modeling calculations

Initial structures as well as visualizations were carried out with Quanta 97.⁴⁵ The MM and MD calculations were run with CHARMM 24.²¹ Parameters were taken from Quanta 97 and point charges were assigned with the charge template option in Quanta. The phenoxy oxygen atoms were charged to $-0.45e$. The ligand was charged to -3 , with a small “excess” charge smoothed to non-polar carbons and hydrogens. The parameters for Eu^{3+} were $\epsilon = 0.050$ kcal/mol and $\sigma = 3.30$ Å.⁴⁶ The starting structures were minimized by ABNR (Adopted-Basis set Newton-Raphson) until the RMS on the energy gradient was ≤ 0.001 kcal·mol⁻¹Å⁻¹. No cutoff on the non-bonded interactions was applied in the gas-phase minimizations of the complexes. A constant dielectric constant with an ϵ of 1 was used.

Details of the MD simulations were as follows. The minimized complexes were placed in a cubic box of approximately 31 Å dimensions, initially filled 429 OPLS MeOHs.²⁰ Solvent molecules that overlap with the complexes were removed (based on heavy atom interatomic distances ≤ 2.3 Å). This in general resulted in removal of one methanol per one non-hydrogen atom of the systems under study. Full periodic boundary conditions were imposed. Before running the MD simulations the system was minimized by steepest descent, in order to remove the worst contacts, until the RMS on the energy gradient was ≤ 1.0 kcal·mol⁻¹Å⁻¹ or a maximum of 1000 steps was reached. During the simulation the non-bonded list was updated every 20 time steps with a cutoff of 14 Å. The van der Waals interactions were treated with a

switch function between 10 and 13 Å, whereas the shift function was applied to the electrostatic interactions (cutoff 13 Å). A constant dielectric constant and an ϵ of 1 were applied. The system was heated to 300 K in 5 ps, followed by 10 ps equilibration with scaling of the velocities within a temperature window of 10 degrees. After equilibration no scaling of the velocities was applied. No systematic deviation from the average temperature was observed. The production phase consisted of up to 500 ps and coordinates were saved regularly, *i.e.* every 100 time steps, for subsequent analysis. The verlet/leapfrog algorithm was used for the numerical integration. The SHAKE algorithm⁴⁷ on bonds involving hydrogen was applied, allowing a time step of 1 fs.

3.5 References and Notes

1. Mikkala, V.-M.; Helenius, M.; Hemmilä, I. K.; Kankare, J.; Takalo, H. *Helv. Chim. Acta* **1993**, *76*, 1361.
2. Iwamuro, M.; Hasegawa, Y.; Wada, Y.; Murakoshi, K.; Kitamura, T.; Nakashima, N.; Yamanaka, T.; Yanagida, S. *Chem. Lett.* **1997**, 1067.
3. Oude Wolbers, M. P.; van Veggel, F. C. J. M.; Snellink-Ruël, B. H. M.; Hofstraat, J. W.; Geurts, F. A. J.; Reinhoudt, D. N. *J. Chem. Soc., Perkin Trans. 2* **1998**, 2141.
4. Gschneider, Jr., K. A.; Eyring, L. *Handbook on the Physics and Chemistry of Rare Earths, Vol. 1, Metals*, North Holland Publishing Company, Amsterdam, 1978.
5. Hemmilä, I. K. *Applications of Fluorescence in Immunoassays*, Wiley and Sons, New York, 1991.
6. Steemers, F. J.; Verboom, W.; Reinhoudt, D. N.; van der Tol, E. B.; Verhoeven, J. W. *J. Am. Chem. Soc.* **1995**, *117*, 9408.
7. Sabbatini, N.; Guardigli, M.; Lehn, J.-M. *Coord. Chem. Rev.* **1993**, *123*, 201, and references cited herein.
8. Desurvire, E. *Phys. Today* **1994**, *97*, 20.
9. An, D.; Yue, Z.; Chen, R. T. *Appl. Phys. Lett.* **1998**, *72*, 2806.
10. Lin, S.; Feuerstein, R. J.; Mickelson, A. R. *J. Appl. Phys.* **1996**, *79*, 2868.
11. Oude Wolbers, M. P.; van Veggel, F. C. J. M.; Snellink-Ruël, B. H. M.; Hofstraat, J. W.; Geurts, F. A. J.; Reinhoudt, D. N. *J. Am. Chem. Soc.* **1997**, *119*, 138.

12. Oude Wolbers, M. P.; van Veggel, F. C. J. M.; Hofstraat, J. W.; Geurts, F. A. J.; Reinhoudt, D. N. *J. Chem. Soc., Perkin Trans. 2* **1997**, 2275.
13. Slooff, L. H.; Polman, A.; Oude Wolbers, M. P.; van Veggel, F. C. J. M.; Reinhoudt, D. N.; Hofstraat, J. W. *J. Appl. Phys.* **1998**, 83, 497.
14. Rudkevich, D. M.; Verboom, W.; van der Tol, E. B.; van Staveren, C.; Kaspersen, F.; Verhoeven, J. W.; Reinhoudt, D. N. *J. Chem. Soc., Perkin Trans. 2* **1995**, 131.
15. Oude Wolbers, M. P.; van Veggel, F. C. J. M.; Peters, F. G. A.; van Beelen, E. S. E.; Hofstraat, J. W.; Geurts, F. A. J.; Reinhoudt, D. N. *Chem. Eur. J.* **1998**, 4, 772.
16. Parker, D.; Williams, J. A. G. *J. Chem. Soc., Dalton Trans.* **1996**, 3613.
17. Satisfactory elemental analyses could not be obtained for the complexes, probably due to the incomplete combustion of lanthanide carbides and/or carbonates that may form during the combustion (see also ref. 11).
18. Bax, A.; Freeman, R. *J. Magn. Reson.* **1981**, 44, 542.
19. Bax, A.; Davis, D. G. *J. Magn. Reson.* **1985**, 65, 355.
20. Jorgensen, W. L. *J. Phys. Chem.* **1986**, 90, 1276.
21. (a) Brooks, B. R.; Bruccoleri, R. E.; Olafsen, B. D.; States, D. J.; Swaminathan, S.; Karplus, M. *J. Comput. Chem.* **1983**, 4, 187. (b) Momany, F. A.; Klimkowski, V. J.; Schäfer, L. *J. Comput. Chem.* **1990**, 11, 654. (c) Momany, F. A.; Rone, R.; Kunz, H.; Frey, R. F.; Newton, S. Q.; Schäfer, L. *J. Mol. Structure* **1993**, 286, 1.
22. Kim, W. D.; Kiefer, G. E.; Huskens, J.; Sherry, A. D. *Inorg. Chem.* **1997**, 36, 4128.
23. Lammers, H.; Maton, F.; Pubanz, D.; van Laren, M. W.; van Bekkum, H.; Merbach, A. E.; Muller, R. N.; Peters, J. A. *Inorg. Chem.* **1997**, 36, 2527.
24. The concentration of the complex in methanol is 27.1 mM, which corresponds to a [(Dy)**1c**]:[methanol] ratio of 1.14×10^{-3} .
25. Peters, J. A.; Huskens, J.; Raber, D. J. *Prog. Nucl. Magn. Reson. Spectrosc.* **1996**, 28, 283.
26. Johnson, L.; Verraest, D. L.; Besemer, A. C.; van Bekkum, H.; Peters, J. A. *Inorg. Chem.* **1996**, 35, 5703.
27. (a) Sato, S.; Wada, M. *Bull. Chem. Soc. Jpn.* **1970**, 43, 1955. (b) Kleinerman, M. J. *Chem. Phys.* **1969**, 51, 2370. (c) Dexter, D. L. *J. Chem. Phys.* **1953**, 21, 836.
28. Since the complexed Gd³⁺ ion has no energy levels below 32,000 cm⁻¹, it cannot depopulate the *m*-terphenyl triplet state via energy transfer.

29. Kira, A.; Thomas, J. K. *J. Phys. Chem.* **1974**, *78*, 196.
30. The energy transfer rate can be estimated from this oxygen dependence by using the Stern-Volmer equation for the diffusion-controlled oxygen quenching of the terphenyl triplet state: $I_0/I = 1 + k_{\text{diff}} \cdot \tau_T \cdot [\text{O}_2]$, where I_0 and I are the luminescence intensities in the absence and presence of oxygen, respectively, k_{diff} is taken as $10^{10} \text{ M}^{-1} \text{ s}^{-1}$, τ_T is the lifetime of the terphenyl triplet state, and $[\text{O}_2]$ is 2.1 mM, Murov, S. L.; Carmichael, I.; Hug, G. L. *Handbook of Photochemistry, 2nd Ed.*, Marcel Dekker, New York, **1993**.
31. Martin, N.; Bünzli, J.-C. G.; McKee, V.; Piguet, C.; Hopfgartner, G. *Inorg. Chem.* **1998**, *37*, 577.
32. (a) Kirby, A. F.; Foster, D.; Richardson, F. S. *Chem. Phys. Lett.* **1983**, *95*, 507. (b) Kirby, A. F.; Richardson, F. S. *J. Phys. Chem.* **1983**, *87*, 2544.
33. Richardson, F. S. *Chem. Rev.* **1982**, *82*, 541.
34. Kropp, J. L.; Windsor, M. W. *J. Chem. Phys.* **1965**, *42*, 1599.
35. (a) Horrocks, Jr., W. DeW.; Sudnick, D. R. *Acc. Chem. Res.* **1981**, *14*, 384. (b) Holz, R. C.; Chang, C. A.; Horrocks, Jr., W. DeW. *Inorg. Chem.* **1991**, *30*, 3270.
36. Beeby, A.; Clarkson, J. M.; Dickins, R. S.; Faulkner, S.; Parker, D.; Royle, L.; de Sousa, A. S.; Williams, J. A. G.; Woods, M. *J. Chem. Soc., Perkin Trans. 2* **1999**, 493.
37. Frey, S. T.; Horrocks, Jr., W. DeW. *Inorg. Chim. Acta* **1995**, *229*, 383, and references cited therein.
38. Takalo, H.; Hemmilä, I. K.; Sutela, T.; Latva, M. *Helv. Chim. Acta* **1996**, *79*, 789.
39. Beeby, A.; Faulkner, S. *Chem. Phys. Lett.* **1997**, *266*, 116.
40. (a) Hasegawa, Y.; Kimura, Y.; Murakoshi, K.; Wada, Y.; Kim, J.-H.; Nakashima, N.; Yamanaka, T.; Yanagida, S. *J. Phys. Chem.* **1996**, *100*, 10201. (b) Hasegawa, Y.; Murakoshi, K.; Wada, Y.; Yanagida, S.; Kim, J.-H.; Nakashima, N.; Yamanaka, T. *Chem. Phys. Lett.* **1996**, *248*, 8.
41. Stein, G.; Würzberg, E. *J. Chem. Phys.* **1975**, *62*, 208.
42. McCumber, D. E. *Phys. Rev.* **1964**, *134*, A299.
43. Weber, M. J. *Phys. Rev.* **1968**, *171*, 283.
44. (a) Dickins, R. S.; Parker, D.; de Sousa, A. S.; Williams, J. A. G. *J. Chem. Soc., Chem. Commun.* **1996**, 697. (b) Hemmilä, I. K.; Mikkala, V.-M.; Takalo, H. *J. Fluoresc.* **1995**, *5*, 159.
45. Quanta was bought from Molecular Simulations Inc., Burlington, MA, USA.

46. van Veggel, F. C. J. M.; Reinhoudt, D. N. *Chem. Eur. J.* **1999**, *5*, 90.
47. Berendsen, H. J. C.; Postma, J. P. M.; Dinola, A.; van Gunsteren, W. F.; Haak, J. R. *J. Chem. Phys.* **1984**, *81*, 3684.

Chapter 4

A Systematic Study of the Photophysical Processes in *m*-Terphenyl-Based Lanthanide Complexes Functionalized with a Triphenylene Sensitizer[§]

4.1 Introduction

The excitation of lanthanide ions by energy transfer from an organic antenna chromophore to obtain visible and near-infrared luminescence remains an intriguing concept that can be applied in many areas, varying from fluoroimmunoassays¹ to optical signal amplification.^{2,3} Provided that most of the excitation energy is transferred from the antenna chromophore to the luminescent lanthanide ion, this process is much more efficient than direct excitation, since the absorption coefficients of organic chromophores are several orders of magnitude (typically 3-5) larger than the intrinsically low molar absorption coefficients of trivalent lanthanide ions.⁴ A general strategy is to incorporate an antenna chromophore into a ligand

[§] The work described in this chapter has been published: Klink, S. I.; Hebbink, G. A.; Grave, L.; van Veggel, F. C. J. M.; Reinhoudt, D. N.; Slooff, L. H.; Polman, A.; Hofstraat, J. W. *J. Appl. Phys.* **1999**, *86*, 1181. Klink, S. I.; Grave, L.; Reinhoudt, D. N.; van Veggel, F. C. J. M.; Werts, M. H. V.; Geurts, F. A. J. *J. Phys. Chem. A* **2000**, in press.

system such as a calix[4]arene ionophore⁵ or DTPA,⁶ or to functionalize an antenna chromophore with lanthanide complexing moieties, such as a terpyridine that has been functionalized with carboxylate moieties.⁷

The sensitization pathway in luminescent lanthanide complexes generally consists of excitation of the antenna chromophore into its singlet excited state, subsequent intersystem crossing of the antenna to its triplet state, and energy transfer from the triplet to the lanthanide ion.^{8,9,10,11} This photophysical model is depicted in Figure 4.1.

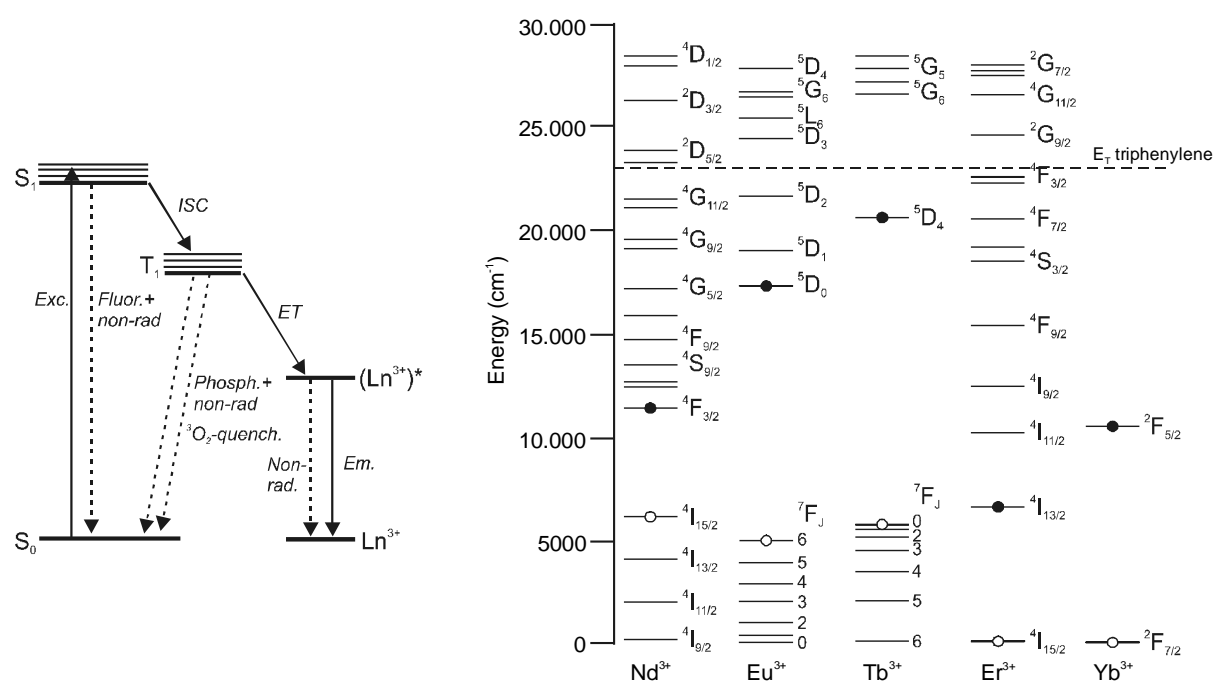


Figure 4.1: Left: Photophysical model describing the main pathways in the sensitization process. Right: Energy diagram of the 4f levels responsible for the lanthanide luminescence, where a filled circle denotes the lowest luminescent state, and an open circle denotes the highest non-luminescent state.¹²

The overall quantum yield of sensitized emission (ϕ_{SE}) is therefore the product of the triplet quantum yield (ϕ_{ISC}), the energy transfer quantum yield (ϕ_{ET}), and the intrinsic luminescence quantum yield of the lanthanide ion (ϕ_{lum}) (eq. 1).

$$\phi_{SE} = \phi_{ISC} \cdot \phi_{ET} \cdot \phi_{lum} \quad (1)$$

The efficient population of the antenna triplet state upon excitation into its first singlet excited state, requires a high absorption coefficient of the antenna at the excitation

wavelength and a high intersystem crossing yield. The complexed lanthanide ion also participates in the population of the triplet state by enhancing the intersystem crossing in the antenna chromophore via an external heavy atom effect.¹³ The subsequent transfer of the excitation energy from the triplet state to the lanthanide ion takes place via an electron exchange (Dexter) mechanism.¹⁴ This energy transfer mechanism is strongly distance dependent and the transfer rate diminishes rapidly at distances larger than 5 Å.

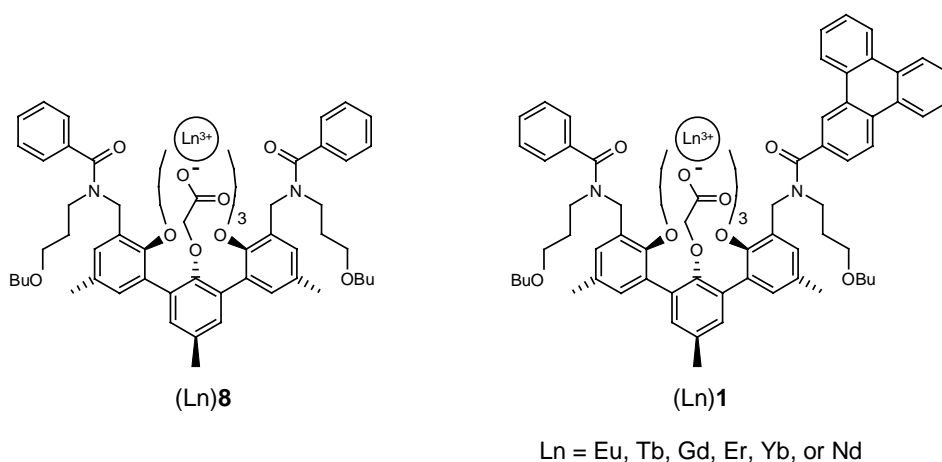
A further requirement of the antenna is that its triplet state should be matched with the main receiving excited state of the lanthanide ion, but it should be approximately 2,000 cm⁻¹ higher in energy to ensure a fast and irreversible energy transfer.⁸ The visible light emitting lanthanide ions Eu³⁺ and Tb³⁺ require antenna chromophores with triplet states of roughly around 22,000 cm⁻¹, because the receiving ⁵D₄ state of Tb³⁺ is at 20,500 cm⁻¹, whereas the receiving ⁵D₀ and ⁵D₁ states of Eu³⁺ are at 17,500 cm⁻¹ and 19,000 cm⁻¹, respectively (see Figure 4.1). If it is assumed that the antenna chromophore has a singlet-triplet energy gap of at least 5,000 cm⁻¹, which appears a lower limit for π-systems,¹⁵ the long wavelength absorption edge of the antenna (the 0-0 transition in the absorption spectrum) cannot be much above 370 nm for Tb³⁺, and 390 nm for Eu³⁺ complexes.⁵ Examples of sensitizers for Eu³⁺ and Tb³⁺, are β-diketonates,⁸ pyridine derivatives,⁷ carbostyryl-124,⁶ and triphenylene.⁵ The near-infrared (NIR) light emitting lanthanide ions Nd³⁺, Er³⁺, and Yb³⁺ have much lower lying luminescent states and require antenna chromophores with triplet states of around 14,000 cm⁻¹. By applying the same energetic considerations as for Eu³⁺ and Tb³⁺, it can be calculated that these lanthanide ions can be excited via antenna chromophores that have absorption bands in the 500 - 600 nm region. A recently reported example of such an antenna chromophore is fluorescein.^{3,16}

Previous work has shown that triphenylene can be incorporated in calix[4]arene-based ligands for lanthanide complexation, and that it is an efficient sensitizer for Eu³⁺ and Tb³⁺ luminescence. The antenna allows excitation up to 350 nm and it has a high intersystem crossing quantum yield (0.89).¹⁵ Tetraazatriphenylene which is a derivative of triphenylene has lanthanide ion coordinating properties, and forms 2:1 complexes with Eu³⁺ and Tb³⁺ in acetonitrile. The energy transfer process is very efficient in these complexes as could be concluded from the high overall luminescence quantum yields: 0.41 for the Eu³⁺ complex and 0.67 for the Tb³⁺ complex.¹⁷ Tetraazatriphenylene also forms 2:1 complexes with Nd³⁺, Er³⁺, and Yb³⁺, and these complexes exhibit sensitized near-infrared luminescence. However, in contrast to the luminescence of the Tb³⁺ and Eu³⁺ complexes, the luminescence intensity of

the near-infrared emitting complexes was sensitive to oxygen, implying that in these complexes the energy transfer is slower than in the Tb^{3+} and Eu^{3+} complexes.³²

In this chapter the synthesis of *m*-terphenyl-based triphenylene-functionalized lanthanide complexes is presented, as well as a systematic study of the photophysical processes of the corresponding visible light emitting Eu^{3+} and Tb^{3+} complexes and the NIR emitting Nd^{3+} , Yb^{3+} , and Er^{3+} complexes. The ligand (H_3)**1** is based on the *m*-terphenyl ligand (H_3)**8** reported in Chapter 3 in which one of the amido pendant arms has been functionalized with a triphenylene antenna chromophore. The lanthanide ion is encapsulated by eight hard oxygen donor atoms: three bidentate oxyacetate moieties and two amide oxygens. The triphenylene antenna chromophore is positioned in close proximity to the lanthanide ion upon coordination of the amide carbonyl.

Chart 4.1



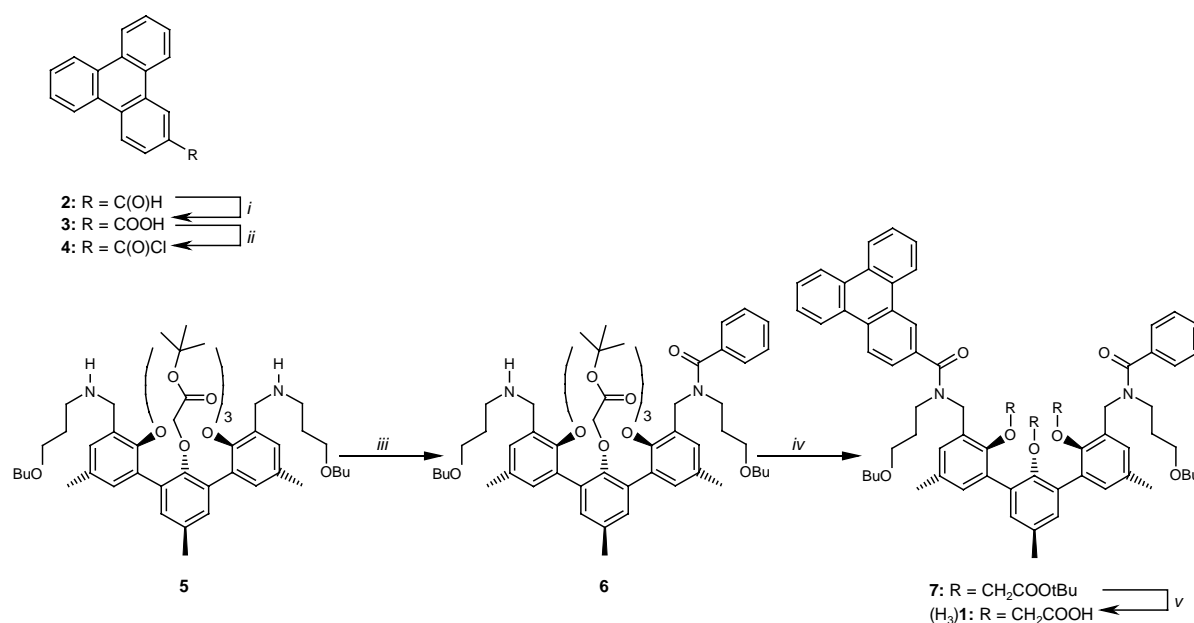
4.2 Results and Discussion

4.2.1 Synthesis

The triphenylene-functionalized ligand (H_3)**1** was synthesized in four steps starting from bis(amine) **5**¹⁸ and triphenylene aldehyde **2**⁵ (see Scheme 4.1). Reaction of bis(amine) **5** with 1.3 equivalents of benzoyl chloride gave the mono(amide) **6** in 20-30 % isolated yield. Triphenylene carboxylic acid **3** was synthesized in 80% yield by mild oxidation of triphenylene aldehyde **2**. Triphenylene carboxylic acid chloride **4** was prepared *in situ* with thionyl chloride (SOCl_2). After removal of the excess SOCl_2 , the triphenylene carboxylic acid

chloride **4** was reacted with mono(amide) **6** in dichloromethane in the presence of Et_3N , giving **7** in 60% yield. After quantitative hydrolysis of the *tert*-butyl esters of **7** with trifluoroacetic acid (TFA), the corresponding complexes were readily formed upon addition of the lanthanide nitrate salts to methanol solutions of the ligand in the presence of Et_3N as a base. FAB mass spectrometry indicated that the complexes have a 1:1 stoichiometry. The IR spectra confirm the presence of carboxylates ($\nu_{\text{COO}} = 1595\text{-}1600\text{ cm}^{-1}$).

Scheme 4.1



Reagents and conditions: i) $\text{H}_2\text{NSO}_3\text{H}$, NaClO_2 , $\text{CHCl}_3/\text{acetone}/\text{water}$, 3h, r.t. (80%); ii) SOCl_2 , reflux 4h (100%); iii) Benzoyl chloride, Et_3N , CH_2Cl_2 , 12 h, r.t. (20%); iv) Triphenylene carboxylic acid chloride **4**, Et_3N , CH_2Cl_2 , 12 h, r.t. (70%); v) TFA, 12 h, r.t. (100%).

4.2.2 Molecular dynamics studies

The structure of the (Ln)**1** complexes (Ln = Nd^{3+} , Eu^{3+} , Er^{3+} , Yb^{3+})¹⁹ was minimized in the gas phase and subjected to a molecular dynamics simulations (500 ps) in a cubic box of OPLS methanol²⁰ or DMSO²¹ using the CHARMM force field.²² The simulations show that the structures of the complexes are comparable in both solvent boxes: All eight donor atoms from the ligand (three phenol ether oxygens (PhO), three carboxylate oxygens (OCO), and two amide oxygens (NCO)) are coordinated to the lanthanide ion, and in addition one methanol or DMSO molecule is coordinated to the lanthanide ion. The PhO-Ln (typically 2.5

Å), OCO-Ln (typically 2.4 Å), and NCO-Ln (typically 2.3 Å) distances are comparable in this series of (Ln)**1** complexes, despite the small differences in ionic radii of the various lanthanides. In the present complexes the coordination geometry is not only controlled by steric hindrance and electrostatic interactions, but also by the conformational restraints of the ligand system. In the (Ln)**1** complexes, the average distance from the center of the lanthanide ion to the *center* of the sensitizer is approximately 8 Å. The coordination of the amide carbonyl to the lanthanide ion positions the bottom phenyl moiety of the triphenylene sensitizer at approximately 5 Å from the lanthanide ion.

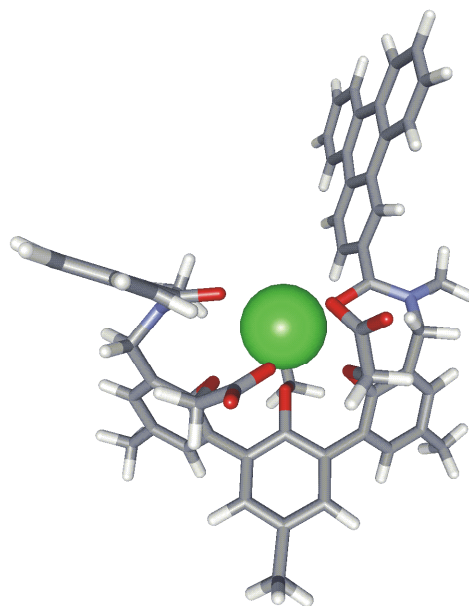


Figure 4.2: Typical structure of (Eu)**1**, subjected to a molecular dynamics simulation in a box of OPLS methanol (not shown) using the CHARMM force field. In this simulation, the *n*-butoxypropyl moieties have been replaced by methyl groups.

4.2.3 Sensitized emission of (Eu)**1** and (Tb)**1**

Upon excitation at 310 nm, the emission spectra of the (Eu)**1** complex in methanol show the typical narrow bands corresponding to the Eu^{3+} -centered ${}^5\text{D}_0 \rightarrow {}^7\text{F}_j$ transitions (solid line in Figure 4.3), with the strongest emission located around 615 nm originating from the ${}^5\text{D}_0 \rightarrow {}^7\text{F}_2$ transition. Scanning the excitation wavelength while monitoring the intensity of the Eu^{3+} emission at 615 nm, shows which transitions from the ground state, directly or indirectly, lead to population of the $\text{Eu}^{3+} {}^5\text{D}_0$ luminescent state. The resulting excitation spectrum (dashed line in Figure 4.3) shows a maximum around 300 nm and closely resembles the absorption spectrum of the antenna and proves that the lanthanide ion is excited via the triphenylene moiety.

The relative intensities and splitting of the (Eu)**1** emission bands are influenced by the symmetry of the ligand, and in particular by the symmetry of the first coordination sphere. Experimental data on a variety of Eu^{3+} complexes established that the emission band centered around 590 nm corresponding to the ${}^5\text{D}_0 \rightarrow {}^7\text{F}_1$ transition, which is a magnetic dipole transition, is relatively strong and largely independent of the coordination sphere, *i.e.* the ligand field. The emission band centered around 615 nm, corresponding to the ${}^5\text{D}_0 \rightarrow {}^7\text{F}_2$ transition, which is an electric dipole transition, is extremely sensitive to the symmetry of the coordination sphere and is therefore called *hypersensitive*.

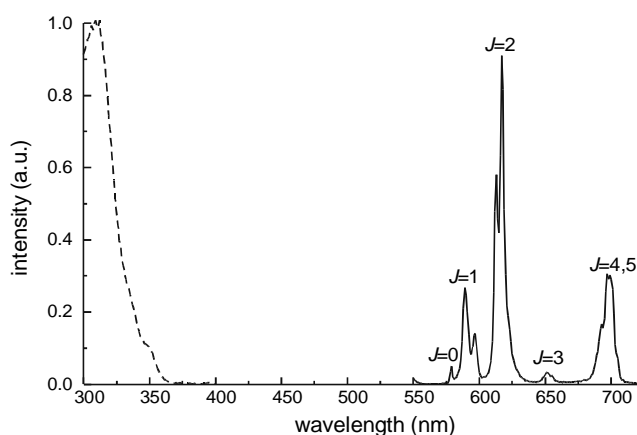


Figure 4.3: Excitation spectrum (dashed line, λ_{em} 615 nm) and emission spectrum (λ_{ex} 310 nm) of a 10^{-4} M solution of (Eu)**1** in methanol. The emission bands correspond to ${}^5\text{D}_0 \rightarrow {}^7\text{F}_j$ transitions and were recorded with a 1 nm emission bandwidth.

It has been established that the intensity ratio of the ${}^5\text{D}_0 \rightarrow {}^7\text{F}_2$ and the ${}^5\text{D}_0 \rightarrow {}^7\text{F}_1$ transitions is a measure of the symmetry of the coordination sphere.²³ In a centrosymmetric environment the magnetic dipole ${}^5\text{D}_0 \rightarrow {}^7\text{F}_1$ transition of Eu^{3+} is dominating, whereas distortion of the symmetry around the ion causes an intensity enhancement of the *hypersensitive* ${}^5\text{D}_0 \rightarrow {}^7\text{F}_2$ transition. Complexes with an asymmetric coordination sphere such as lanthanide-tris(β -diketonate) complexes have ${}^7\text{F}_2/{}^7\text{F}_1$ intensity ratios ranging from 8 to 12, whereas an intensity ratio of 0.67 has been reported for the centrosymmetric Eu-tris(oxydiacetate) complex.²³ In the present case the ${}^7\text{F}_2/{}^7\text{F}_1$ intensity ratio for (Eu)**1** is 4. This value is significantly higher than 0.67, which is not surprising, since the structures obtained from molecular modeling simulations showed that the first coordination spheres of the (Ln)**1** complexes have a (time-averaged) C_s symmetry.²⁴

The (Eu)**1** spectrum at room temperature shows a splitting of the ${}^5D_0 \rightarrow {}^7F_1$ emission and the ${}^5D_0 \rightarrow {}^7F_2$ emission, and a single peak at 580 nm corresponding to the ${}^5D_0 \rightarrow {}^7F_0$ transition. Lowering the temperature to 77 K did not alter the shape and splitting of the emission bands (not shown). The values of the ligand field splittings are small, approximately 200 cm^{-1} for the 7F_1 state and 130 cm^{-1} for the 7F_2 state, which is due to the shielding of the 4f-orbitals from the environment by an outer shell of 5s and 5p electrons.⁴ The $\text{Eu}^{3+} {}^7F_0$ state is non-degenerate and cannot be split by the ligand field, therefore the single peak at 580 nm indicates that there is only one (time-averaged) *luminescent* Eu^{3+} species in solution.

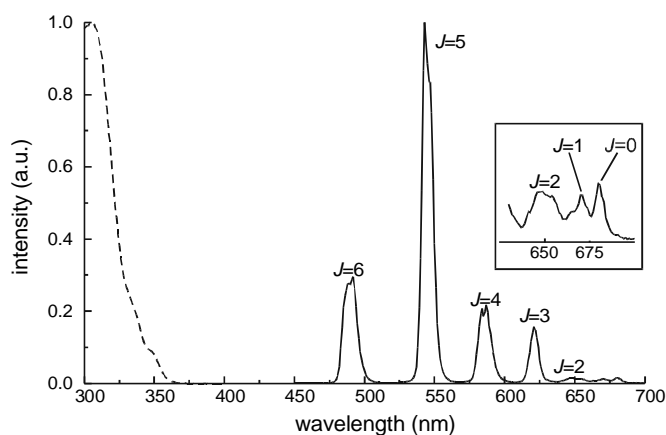


Figure 4.4: Excitation spectrum (dashed line, λ_{em} , 545 nm) and emission spectrum (λ_{ex} , 310 nm) of a 10^{-4} M solution of (Tb)**1** in methanol. The emission bands correspond to ${}^5D_4 \rightarrow {}^7F_j$ transitions and were recorded with a 1 nm emission bandwidth. The inset shows a magnification of the emission bands between 625 and 700 nm.

Photo-excitation of the antenna at 310 nm in the (Tb)**1** complex gives rise to the characteristic green Tb^{3+} emission corresponding to the ${}^5D_4 \rightarrow {}^7F_j$ transitions (solid line in Figure 4.4). The strongest emission is centered around 545 and corresponds to the hypersensitive ${}^5D_4 \rightarrow {}^7F_n$ transition. Monitoring the intensity of the 545 nm emission band, the excitation spectrum of (Tb)**1** proves the photosensitization via the antenna. The Tb^{3+} spectrum shows some fine-structure within the emission bands, but not as distinct as the Eu^{3+} spectrum.

The time-resolved luminescence spectra show mono-exponential decays with a luminescence lifetime of 0.86 ms for (Eu)**1** and 1.74 ms for (Tb)**1** in methanol (See Table 4.1). These lifetimes increase substantially in methanol- d_1 , caused by the well-known sensitivity of the Eu^{3+} and Tb^{3+} luminescence towards solvent hydroxyl groups.²⁵ An

empirical relationship has been established which estimates the number of coordinated methanol molecules (n):^{26,27}

$$n = q(1/\tau_h - 1/\tau_d - k_{\text{corr}}) \quad (2)$$

where q is 2.1 for Eu^{3+} and 8.4 for Tb^{3+} , τ_h is the luminescence lifetime of the complex in methanol- h_1 , τ_d the luminescence lifetime of the complex in methanol- d_1 , and k_{corr} is a term to correct for closely diffusing second-sphere methanol molecules which is 0.125 ms^{-1} for Eu^{3+} and 0.03 ms^{-1} for Tb^{3+} .²⁷ The calculations show that approximately 1 methanol molecule is coordinated to the lanthanide ion (See Table 4.1).

Table 4.1: Luminescence lifetimes of (Eu)**1** and (Tb)**1** measured in methanol- h_1 (τ_h), methanol- d_1 (τ_d), and DMSO- h_6 (τ_h), the number of coordinated methanol molecules (n) determined from equation (1), and the overall quantum yield of sensitized emission (ϕ_{SE}). Excitation at 310 nm, 10^{-4} M solutions.

Complex	τ_h (ms)	τ_d (ms)	n	ϕ_{SE}
(Eu) 1	0.86 ^a	2.21 ^b	1.2 ± 0.5	0.03 ^a
(Tb) 1	1.74 ^a	2.78 ^b	1.6 ± 1.5	0.15 ^a
(Eu) 1	1.89 ^c	n.d.	n.a.	0.02 ^c
(Tb) 1	2.21 ^c	n.d.	n.a.	0.03 ^c

^a in methanol- h_1 ; ^b in methanol- d_1 ; ^c in DMSO- h_6

The coordination number of Eu^{3+} and Tb^{3+} complexes in solution is usually 9,²⁸ which implies that all 8 donor atoms of the ligand are coordinated to the lanthanide ion. This is in excellent agreement with the results obtained from the molecular dynamics studies.

The photophysical properties of (Eu)**1** in methanol are in accordance with the data that were previously obtained for the symmetrical (Eu)**8** complex in methanol (see chapter 3), indicating that the substitution of one of the phenyl groups of (Eu)**8** by a triphenylene moiety indeed does not significantly alter the first coordination sphere of the lanthanide ion.

The efficiency of the overall sensitization process was assessed by determining the quantum yield of the sensitized emission, which is 0.03 for (Eu)**1** and 0.15 for (Tb)**1** in methanol. The emission spectra of these complexes in DMSO- h_6 , a strongly coordinating aprotic solvent, closely resemble the spectra in methanol, but surprisingly the overall quantum

yields are much lower: 0.02 for (Eu)**1** and 0.03 for (Tb)**1**. Time-resolved measurements showed that in DMSO the luminescence lifetimes are longer than in methanol- h_1 (See Table 4.1), therefore the sensitization process of the (Eu)**1** and (Tb)**1** complexes in DMSO must be much less effective than in methanol. The sensitization process will be discussed in more detail below.

4.2.4 Sensitized emission of (Nd)**1**, (Er)**1**, and (Yb)**1**

The NIR emitting lanthanide complexes in DMSO- d_6 exhibit the typical line-like lanthanide emission upon excitation of the triphenylene antenna chromophore, as is depicted in Figure 4.5. Emission bands at 880 (not shown in Figure 4.5), 1060, and 1330 nm (${}^4F_{3/2} \rightarrow {}^4I_{9/2}$, ${}^4I_{11/2}$, and ${}^4I_{13/2}$ transition, respectively) are observed for (Nd)**1**. The strongest emission is observed at 1060 nm, whereas the emissions at 880 and 1330 nm are weaker. The shape of the emission bands and the relative intensities are in agreement with previously reported spectra of organic Nd^{3+} complexes in solution.^{3,29,30} A single emission band centered at 1540 nm (${}^4I_{13/2} \rightarrow {}^4I_{15/2}$ transition) is observed for (Er)**1**. No emission was observed from higher excited states, such as green emission at 545 nm corresponding to the ${}^4S_{3/2} \rightarrow {}^4I_{15/2}$ transition, despite the fact that these states can be populated via the antenna triplet state. Apparently, the higher excited states relax non-radiatively to the ${}^4I_{13/2}$ state, from which radiative decay is observed.

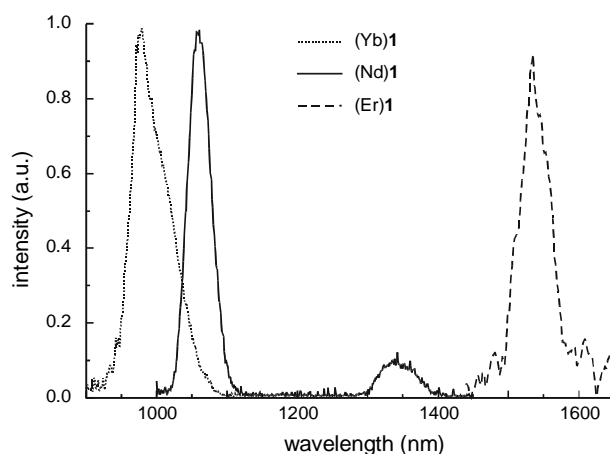


Figure 4.5: Emission spectra of 10^{-3} M solutions of the near-infrared emitting complexes (Yb)**1**, (Nd)**1** and (Er)**1** in DMSO- d_6 upon excitation at 320 nm recorded with a 15 nm emission bandwidth.

Upon excitation of (Yb)**1** at 310 nm, sensitized emission was observed at 980 nm (${}^2F_{5/2} \rightarrow {}^2F_{7/2}$ transition). A shoulder seems to be present at the lower energy side of the 980 nm

emission band, which is indicative of splitting of the $^2F_{7/2}$ manifold by the ligand field. Using laser excitation, an emission spectrum of (Yb)1 was obtained (solid line in Figure 4.6) with a higher resolution (6 nm) in which a sharp peak at 977 nm ($10,235\text{ cm}^{-1}$) is observed with a broad shoulder at 1005 nm ($9,950\text{ cm}^{-1}$). The same sharp peak at 977 nm is observed in the absorption spectrum (dotted line in Figure 4.6) together with a broad shoulder at 940 nm ($10,600\text{ cm}^{-1}$), which means that also the $^2F_{5/2}$ manifold is split by the ligand field. The shape of the luminescence and absorption spectra are similar to reported spectra of Yb^{3+} in both organic and inorganic matrices.^{31,32,33}

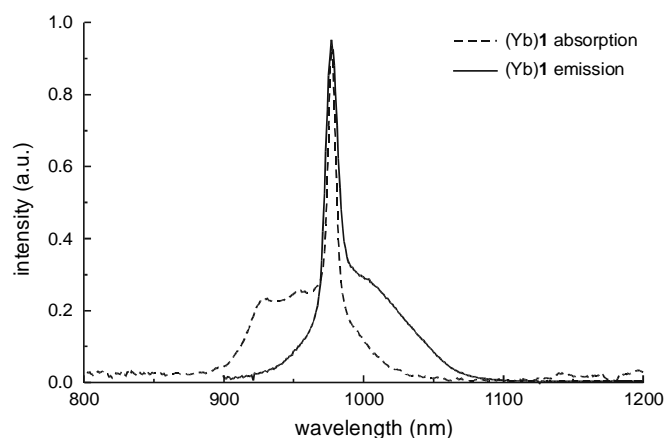


Figure 4.6: Absorption spectrum of a 10^{-2} M solution of (Yb)1 in DMSO (dashed line), and emission spectrum (solid line) of a 10^{-3} M solution of (Yb)1 in DMSO- d_6 upon laser excitation at 350 nm (Ar laser) recorded with a 6 nm emission bandwidth.

The luminescence decay curves obtained from time-resolved luminescence experiments could be fitted mono-exponentially with time-constants in the range of microseconds (See Table 4.2). The luminescence lifetime of (Yb)1 in DMSO- h_6 is the longest ($9.6\text{ }\mu\text{s}$), followed by that of (Er)1 ($2.4\text{ }\mu\text{s}$), and that of (Nd)1 ($1.5\text{ }\mu\text{s}$). The sensitivity of the NIR luminescent complexes towards quenching by the C-H vibrations became apparent when the solvent was changed to DMSO- d_6 . In DMSO- d_6 the luminescence lifetimes are significantly longer due to the fact that the C-D vibrations of the coordinated DMSO- d_6 molecule are less efficient quenchers of the lanthanide excited state than the C-H vibrations of a DMSO- h_6 molecule. According to the energy gap law¹² the smaller the number of vibrational quanta that is required to match the energy gap between the lowest luminescent state and the highest non-luminescent state of the lanthanide ion, the more effective the vibronic quenching will be.

The C-D vibration is less energetic than the C-H vibration, therefore more quanta are required to bridge the energy gap of the lanthanide ions. The natural radiative rate constants (k_0), *i.e.* the rate of spontaneous emission, of Er^{3+} and Yb^{3+} in these type of complexes in DMSO have been added to Table 4.2,³⁴ as well as a typical natural radiative rate constant of Nd^{3+} .³⁵ Since the observed rate constant k is the sum of the natural radiative rate constant k_0 and the nonradiative rate constant k_{nonr} , it is obvious from Table 4.2 that for the NIR emitting ions k is dominated by non-radiative deactivation of the luminescent state. This competition between non-radiative and radiative decay is most dramatic for Er^{3+} , because this ion has a very low k_0 of 71 s^{-1} .

Table 4.2: The luminescence lifetimes of the NIR emitting (Ln)**1** complexes in DMSO- h_6 ($\tau_h = 1/k_h$) and DMSO- d_6 ($\tau_d = 1/k_d$), as well as the natural lifetimes ($\tau_0 = 1/k_0$). Excitation at 337 nm, 1 mM solutions.

Complex	τ_h (μs)	k_h (s^{-1})	τ_d (μs)	k_d (s^{-1})	τ_0 (ms)	k_0 (s^{-1})
(Yb) 1	9.4	1.1×10^5	18.6	0.54×10^5	2.0	500
(Er) 1	2.4	4.2×10^5	3.4	2.9×10^5	14.0	71
(Nd) 1	1.4	7.1×10^5	2.5	4.0×10^5	0.25	4000

4.2.5 Antenna fluorescence and phosphorescence

The first step of the sensitization pathway is the population of the triphenylene triplet state ($^3\pi\pi^*$) via its singlet excited state ($^1\pi\pi^*$). In this step fluorescence and radiationless deactivation from the triphenylene $^1\pi\pi^*$ state compete with the spin-forbidden conversion to the $^3\pi\pi^*$ state. The shape of the UV-absorption spectra of the (Ln)**1** complexes in methanol are similar to that of ligand **7**, indicating that the lanthanide ion does not significantly influence the energy of the triphenylene $^1\pi\pi^*$ state. The $^1\pi\pi^*$ state energy of $29,000 \text{ cm}^{-1}$ (345 nm) was determined from the $0-0$ transition, which is clearly discernible in the absorption spectrum. Upon excitation of the (Ln)**1** complexes in methanol at 310 nm, a structured fluorescence band is observed at 375 nm that corresponds to fluorescence of the triphenylene moiety. Figure 4.7 shows the fluorescence intensities of the (Ln)**1** complexes relative to the ester-protected ligand **7**. The fluorescence quantum yields are summarized in Table 4.3. The presence of the lanthanide ion in close proximity of the antenna reduces the fluorescence intensity, but the effect is not the same for all the lanthanide ions.

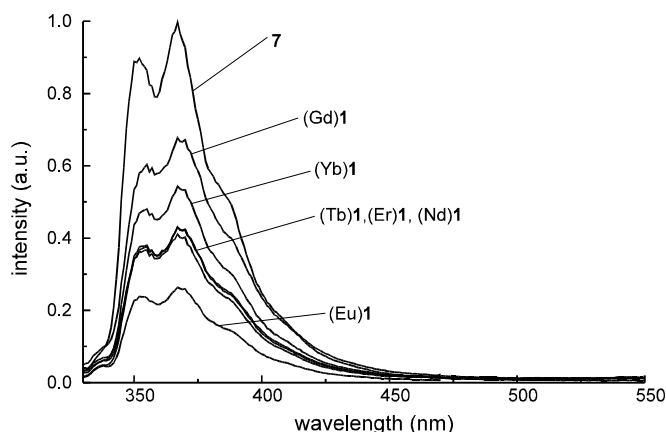


Figure 4.7: Fluorescence spectra of the triphenylene antenna in ligand **7** and in the (Ln)**1** complexes in methanol upon excitation at 310 nm. The intensities are relative to the fluorescence intensity of **7**.

The fluorescence quantum yield of ligand **7** is 0.019, but the fluorescence quantum yields of the triphenylene moiety in the (Ln)**1** complexes are even lower, <0.01. The fluorescence quantum yields are low, which is not surprising since triphenylene intrinsically has a high intersystem crossing quantum yield.¹⁵

Table 4.3: Fluorescence quantum yields of the triphenylene antenna chromophore in methanol (10^{-4} M, λ_{exc} . 310 nm).

Complex	$\phi_{flu, antenna}$	Complex	$\phi_{flu, antenna}$
7	0.019	(Yb) 1	0.012
(Eu) 1	0.0054	(Er) 1	0.0095
(Tb) 1	0.0086	(Nd) 1	0.0095
(Gd) 1	0.015		

The luminescence spectrum of (Gd)**1** in a methanol/ethanol glass at 77 K shows strong phosphorescence bands next to very weak fluorescence bands. Since Gd^{3+} has no energy levels below $32,000\text{ cm}^{-1}$, Gd^{3+} cannot accept any energy from the triphenylene triplet state. The ${}^3\pi\pi^*$ state energy of $22,830\text{ cm}^{-1}$ of the triphenylene moiety was determined from the $0-0$ transition in the phosphorescence spectrum (see Figure 4.8). This value is approximately 600 cm^{-1} lower in energy than the ${}^3\pi\pi^*$ state of unfunctionalized triphenylene ($23,400\text{ cm}^{-1}$), which is caused by the electron withdrawing amide carbonyl at the 2-position. Compared to the phosphorescence spectrum of ligand **7**, the antenna phosphorescence bands of (Gd)**1** have slightly shifted to the red. Furthermore, the decrease in the antenna fluorescence of (Gd)**1** is accompanied by an increased phosphorescence intensity.

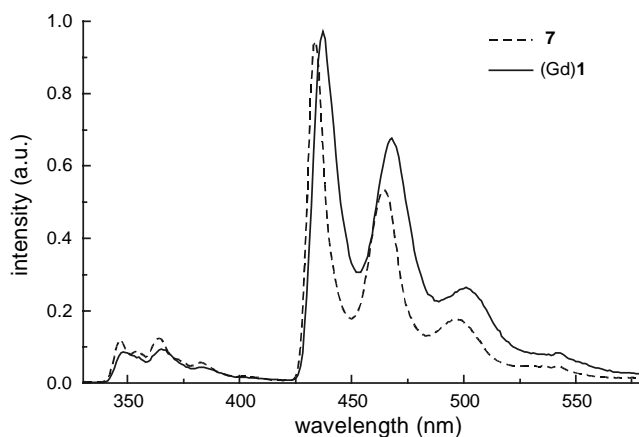


Figure 4.8: Total luminescence spectra of the triphenylene antenna in **7** (dashed line) and **(Gd)1** (solid line) taken in a methanol-ethanol glass at 77 K (excitation at 310 nm).

An *external heavy atom effect* can be induced by a heavy (paramagnetic) metal ion in close proximity of a chromophore, and increases the intersystem crossing yield of the chromophore, which results in a reduction of the fluorescence intensity and a concomitant increase in the phosphorescence intensity. This effect has been attributed to an enhanced spin-orbit coupling of the system which relaxes the selection rules for electronic transitions, but also to an exchange interaction of metal-unpaired electrons with the π -electrons of the organic chromophore. Tobita and coworkers¹³ have studied the influence of different lanthanide ions on the photophysical properties of the ligand (the antenna) in lanthanide-tris(methylsalicylate) and lanthanide-tris(benzoyltrifluoroacetato) complexes. They found that the decrease of the antenna fluorescence intensity depended on the magnetic properties of the lanthanide ion. The paramagnetic Gd^{3+} ion was found to lower the antenna triplet state lifetime more than the diamagnetic Lu^{3+} and La^{3+} ions. If these results were solely caused by spin-orbit coupling, then the effect should have increased with increasing atomic number Z . Since this was not the case, an additional exchange mechanism between the metal-unpaired electrons and the chromophore electrons was proposed. The exchange leads to mixing of the chromophore singlet and triplet state, ultimately resulting in more allowed singlet-triplet and triplet-singlet conversions. Also in the present case, the effect, *i.e.* the reduction of the antenna fluorescence, does not increase with increasing Z , which implies that a paramagnetic exchange mechanism may also be predominant.

In the case of **(Eu)1**, which has the lowest antenna fluorescence intensity, a photon-induced electron transfer may also play a role in the deactivation of the singlet excited state. Instead of radiative decay to the ground state, or intersystem crossing to the triplet state, an

electron is transferred to the Eu^{3+} ion upon excitation of the antenna into its singlet excited state, resulting in the transient formation of an antenna radical cation and Eu^{2+} . One of the reasons for the possible occurrence of this competing process³⁶ is the low reduction potential of Eu^{3+} in comparison with other trivalent lanthanide ions.³⁷

4.2.6 The intramolecular energy transfer process in (Eu)1 and (Tb)1

Since the energy transfer takes place through the triphenylene triplet state, oxygen may compete with the lanthanide ion as the acceptor for the excitation energy, and as a result the triplet state is quenched so that less lanthanide luminescence is obtained. The effect of oxygen on the sensitized luminescence intensity gives an indication of the energy transfer rate, since the competing oxygen quenching rate is equal to the product of the diffusion-controlled quenching rate constant and the oxygen concentration ($k_{\text{diff}}[\text{O}_2]$). However, deoxygenation of the (Eu)1 and (Tb)1 methanol solutions did not influence the luminescence intensity, which means that k_{ET} exceeds 10^7 s^{-1} .³⁸

The energy transfer process was further studied by probing the antenna's triplet state directly with the aid of transient absorption spectroscopy. To obtain the triplet-triplet absorption spectra of the complex, samples of (Gd)1 in deoxygenated DMSO were excited with 335 nm pulses and the changes in absorbance resulting from the population of the long-lived triplet state were monitored.

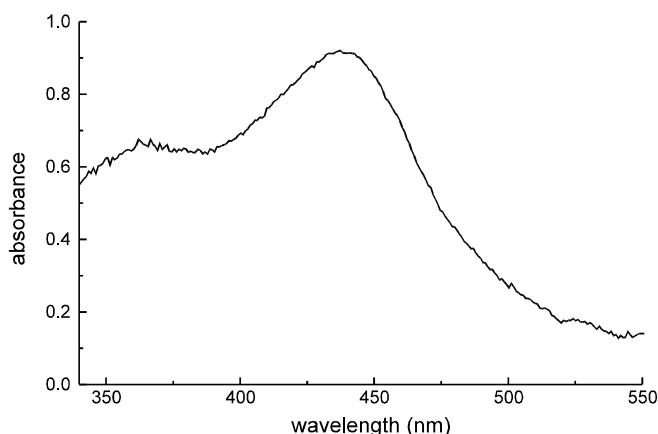


Figure 4.9: Transient absorption spectrum of (Gd)1 in methanol recorded 100 ns after the laser pulse (340 nm, energy <1 mJ).

As mentioned before, the (Gd)1 complex enables the study of the photophysical behavior of the antenna in the presence of a lanthanide ion, but in the absence of energy transfer. The

transient absorption spectrum of (Gd)**1** (See Figure 4.9) shows features at 360 and 440 nm, and is very similar to the transient absorption spectrum of unfunctionalized triphenylene, but slightly broadened. These absorption bands are due to triplet-triplet absorptions and therefore can be used to monitor the lifetime of the triplet state, which was 15.2 μs in the (Gd)**1** complex. This lifetime is the lifetime of the antenna's triplet state (τ_T) in the absence of energy transfer, thus $k_T = 1/\tau_T = 6.6 \times 10^4 \text{ s}^{-1}$.

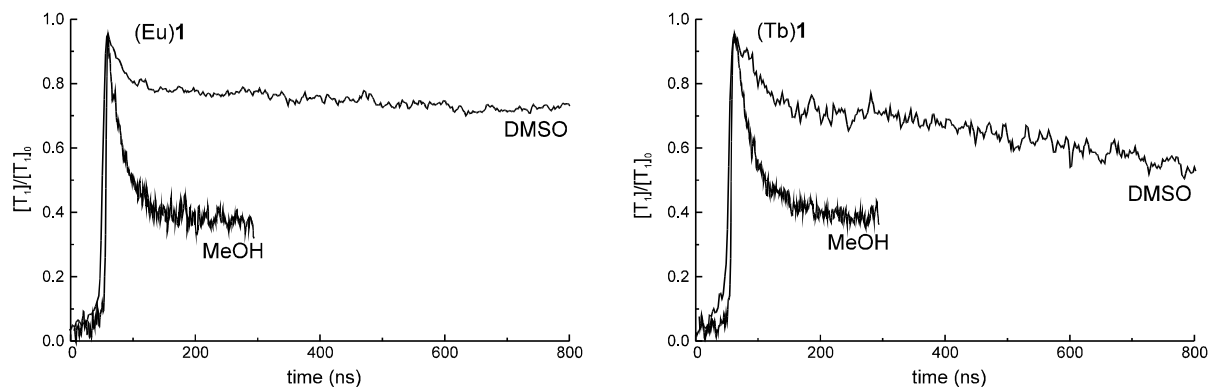


Figure 4.10: Kinetics of the transient absorption measurements obtained by singular value decomposition of the resulting data sets. The pump wavelength was 340 nm ($< 1 \text{ mJ/pulse}$). The corresponding transient absorption spectra were similar to the one shown in Figure 4.9. Left: (Eu)**1** in deoxygenated DMSO and methanol; Right: (Tb)**1** in deoxygenated DMSO and methanol.

The transient absorption spectra of the Tb(**1**) and Eu(**1**) complexes in the sub- μs domain show important details about the energy transfer process in DMSO and methanol. In DMSO the same absorption spectra are observed as for the (Gd)**1** complex, but triplet state kinetics of the antenna have become biexponential (see Figure 4.10): besides a ‘slow’ component (76%) having the same rate constant as observed for Gd(**1**), a second small component (24 %) is observed, which has a much faster decay (26 ns for both Tb(**1**) and Eu(**1**)).

The long triplet lifetimes would suggest that energy transfer to the lanthanide ion is extremely slow and an oxygen sensitivity of the lanthanide luminescence should have been observed. However, the intensity of the luminescence of both (Eu)**1** and (Tb)**1** is not influenced by deoxygenation. Therefore, we attribute this behavior to the presence of two distinct (conformational) populations of complexes: one in which energy transfer is absent and which is responsible for the observed long-lived triplets, and one in which the energy transfer to the lanthanide ion is relatively fast (responsible for the fast component), resulting in the sensitized luminescence. This is in line with the surprisingly low quantum yields of

sensitized luminescence of the complexes in DMSO. According to our transient absorption measurements the majority of complexes did not display efficient energy transfer. Changing to methanol as the solvent, the antenna triplet state kinetics shows the same biexponential behavior as in DMSO, but the contribution of the fast component has increased to 65 %. The corresponding short-lived triplet lifetime components are 29 ns and 26 ns for Tb(1) and Eu(1), respectively. Obviously the equilibrium between the dark and the luminescent forms of the complexes has been shifted towards the luminescent side. Indeed, it has already been noted that in methanol the overall luminescence quantum yields are higher than in DMSO.

To substantiate the proof of the presence of two distinct forms of complexes in solution, experiments with an external triplet quencher were performed. *cis*-Piperylene has a triplet state of $20,070\text{ cm}^{-1}$,^{15,39} which is approximately $2,800\text{ cm}^{-1}$ lower than that of triphenylene. Addition of increasing concentrations of piperylene to methanol solutions of (Eu)1 and (Tb)1 quenched the sensitized lanthanide luminescence upon excitation of the antenna at 310 nm (See Figures 4.11 a and b). This effect is more pronounced for Tb^{3+} than for Eu^{3+} , which may indicate that the energy transfer rate to Eu^{3+} is faster.

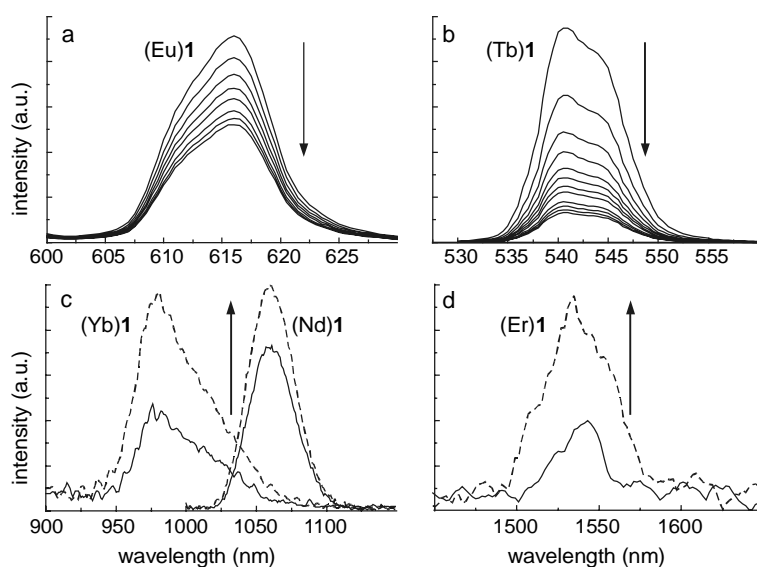


Figure 4.11: (a) Quenching of the 615 nm emission band of Eu^{3+} by piperylene; (b) Quenching of the 545 nm emission band of Tb^{3+} by piperylene. The arrows denote the effect of the increasing piperylene concentration in methanol; (c) Enhancement of the 980 nm emission band of Yb^{3+} , and 1060 nm emission band of Nd^{3+} upon deaeration; (d) enhancement of the 1550 nm emission band of Er^{3+} upon deaeration. The arrows denote the effect of deaeration of the DMSO-d_6 solutions.

With the Stern-Volmer equation (3) the lifetime of the quenched species, *i.e.* the triphenylene triplet state, can be calculated.

$$I_0/I = 1 + k_{\text{diff}} \cdot \tau_{\text{T}} \cdot [\text{Q}] = 1 + K_{\text{sv}}[\text{Q}] \quad (3)$$

In equation (3), I_0 is the lanthanide luminescence intensity without quencher, I is the lanthanide luminescence intensity, k_{diff} is the diffusion-controlled quenching rate constant, τ_{T} is the lifetime of the triphenylene triplet state, $[\text{Q}]$ is the concentration of the quencher, and K_{sv} is the product of k_{diff} and τ_{T} , the so-called Stern-Volmer constant. If the luminescence intensities are plotted against the quencher concentration, the slope of the fitted data is equal to the Stern-Volmer constant K_{sv} (see Figure 4.12). When for k_{diff} a value of $10^{10} \text{ M}^{-1} \text{ s}^{-1}$ is taken,¹⁵ the lifetime of the antenna triplet state can be calculated. This resulted in an antenna triplet lifetime of 11.3 ns for (Eu)**1** and 81.1 ns for (Tb)**1**.

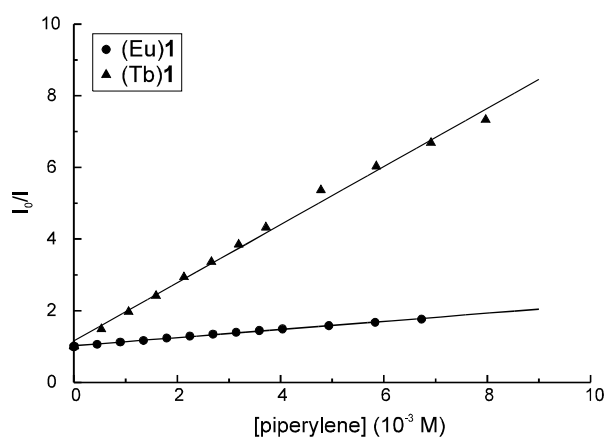


Figure 4.12: Stern-Volmer plot of quenching of triphenylene-sensitized Eu^{3+} and Tb^{3+} emission by piperylene: $I_0/I = 1 + k_{\text{diff}} \cdot \tau_{\text{triplet}} [\text{Q}] = 1 + K_{\text{sv}}[\text{Q}]$.

Since the antenna triplet lifetime is $15.2 \mu\text{s}$ in the absence of energy transfer (τ_{T} of (Gd)**1**), the deactivation of the antenna triplet is dominated by the rate of energy transfer to the lanthanide ion (k_{ET}), and thus it follows that

$$k_{\text{ET}} = 1/\tau_{\text{T}} \quad (4)$$

The intramolecular energy transfer rate in (Eu)**1** is $8.0 \times 10^7 \text{ s}^{-1}$, and $1.0 \times 10^7 \text{ s}^{-1}$ in (Tb)**1** (see Table 4.4).

Table 4.4: Quenching of sensitized (I)Ln luminescence by piperylene (pip) or oxygen (ox): Tabulated are triphenylene triplet state lifetimes (τ_T) using the Stern-Volmer equation, and energy transfer rates (k_{ET}).

Complex	τ_T (ns)	k_{ET} (s^{-1})	Relative k_{ET} (s^{-1})
(Eu) 1 (pip)	11.3	8.0×10^7	100
(Tb) 1 (pip)	81.1	1.0×10^7	13
(Nd) 1 (ox)	76.1	1.3×10^7	16
(Er) 1 (ox)	263.0	3.8×10^6	5
(Yb) 1 (ox)	202.2	4.9×10^6	6

Another way of studying the energy transfer is to monitor the early stages of the lanthanide luminescence using a streak camera and pulsed laser excitation. During the time that the energy transfer from the antenna to the lanthanide ion is in progress, the lanthanide luminescence intensity is expected to rise with a rate equal to the rate of the energy transfer. In these measurements it was found that the first 200 ns of the detected luminescence were completely dominated by the antenna fluorescence. Although the fluorescence has a low quantum yield, it has a very high radiative rate (*i.e.* the photons emitted per unit time) compared to the lanthanide luminescence. Therefore, on this short timescale, the lanthanide luminescence is relatively weak compared to the antenna fluorescence. After the antenna fluorescence signal had disappeared, no rise in the Tb^{3+} emission at 545 nm was observed for (Tb)**1**, signifying that the energy transfer to this ion is complete within 200 ns. This means that k_{ET} exceeds $2 \times 10^7 \text{ s}^{-1}$ (based on 99% energy transfer after 200 ns).

The (Eu)**1** complex exhibited an interesting behavior. After the disappearance of the antenna fluorescence, it shows emission from its $^5\text{D}_1$ state at 530 nm. This state decays with a time-constant of 2.1 μs , being converted non-radiatively into the $^5\text{D}_0$ state that is responsible for the typical Eu^{3+} emission observed in steady-state measurements (main emission at 615 nm), and radiatively to the $^7\text{F}_j$ manifold. This behavior is known for the sensitized emission of Eu^{3+} if the donating triplet level is above the $^5\text{D}_1$, as in the present case.^{9,10} The energy transfer from the antenna to the Eu^{3+} ion is faster than $2 \times 10^7 \text{ s}^{-1}$.

The transient absorption measurements, the piperylene quenching experiment, and the luminescence rise-time measurements, all show that the energy transfer rates in the (Eu)**1** and

(Tb)**1** complexes are in the order of 10^7 - 10^8 s⁻¹. The results of these measurements also support the hypothesis that two distinct conformations of the complexes occur in solution: one in which the energy transfer does not occur and which is responsible for the long-lived triplet lifetime observed by transient absorption spectroscopy, and one in which energy transfer to the lanthanide ion is fast and which is responsible for the short-lived triplet lifetime. In the non-luminescent isomer the antenna and lanthanide ion are probably further apart or the orientation of the lanthanide ion with respect to the antenna π -plane is unfavorable for energy transfer to occur.⁴⁰ In methanol the luminescent conformational isomer is slightly dominating, but still in 35% of the complexes (the non-luminescent conformational isomer) the energy is not transferred to the lanthanide ion. This explains the relatively low luminescence quantum yields that were measured for (Eu)**1** and (Tb)**1** in methanol: 0.03 and 0.15, respectively. Based on the measured luminescence lifetimes, an ISC yield of the antenna near unity, and an assumed complete energy transfer, the luminescence quantum yields can be expected to be as high as 0.29 for (Eu)**1** and 0.44 for (Tb)**1**.⁴¹ As mentioned before, the overall luminescence quantum yields of these complexes in DMSO are even lower, 0.02 for (Eu)**1** and 0.03 for (Tb)**1**. In this solvent the non-luminescent conformational isomer is dominating (according to the transient absorption measurements), resulting in an overall very inefficient energy transfer process. The decrease in the luminescence quantum yield when changing the solvent from methanol to DMSO is less dramatic for (Eu)**1** than for (Tb)**1**, because the significant increase of the (Eu)**1** luminescence lifetime partly compensates the inefficiency of the energy transfer process. For the (Eu)**1** complex in methanol and DMSO, energy may also be lost in the step preceding the energy transfer, *i.e.* the population of the triplet state. Based on the observation that the antenna fluorescence intensity of (Eu)**1** ($\phi_{\text{flu}} = 0.0054$) is lower than the antenna fluorescence intensity of (Tb)**1** ($\phi_{\text{flu}} = 0.0086$), a photon-induced electron transfer (a ligand-to-metal-charge-transfer (LMCT)) may also compete with the intersystem crossing to the triplet state in the former complex. Since, in general, the deactivation of such an LMCT state does not result in the population of the Eu³⁺ ⁵D₀ excited state,³⁶ a photon-induced electron transfer process will reduce the overall luminescence quantum yield.⁴²

The Stern-Volmer plot of the triplet quenching experiments only provides information on the *luminescent* conformational isomer of the complexes. From these experiments it was concluded that the energy transfer rate is significantly faster in the (Eu)**1** complex (8.0×10^7

s^{-1}) than in the (Tb)**1** complex ($1.0 \times 10^7 \text{ s}^{-1}$). However, based on the transient absorption measurements the energy transfer rates were approximately the same for the (Eu)**1** and (Tb)**1** complexes ($3.8 \times 10^7 \text{ s}^{-1}$). The explanation for this is that the values obtained from the piperylene quenching experiment are lower limits, because it was found that piperylene also quenched the luminescent states of Eu^{3+} and Tb^{3+} , albeit to a different extent.⁴³ Furthermore, the quenching of Tb^{3+} is more efficient, because the triplet state of *cis*-piperylene ($20,070 \text{ cm}^{-1}$) is just below the $^5\text{D}_4$ state of Tb^{3+} ($20,400 \text{ cm}^{-1}$), whereas it is higher in energy than the $^5\text{D}_1$ and $^5\text{D}_0$ states of Eu^{3+} ($19,000 \text{ cm}^{-1}$ and $17,500 \text{ cm}^{-1}$, respectively). As a result, the calculated energy transfer rate for (Tb)**1** as obtained from the quenching experiment has been underestimated more than the calculated energy transfer rate of (Eu)**1**. The photophysical processes and the rate constants in (Eu)**1** are summarized in Figure 4.13.

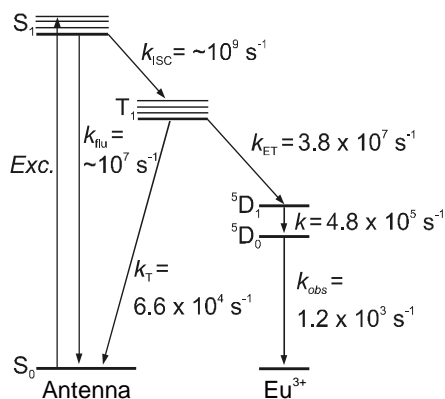


Figure 4.13: Schematic representation of the photophysical processes leading to sensitized luminescence of (Eu)**1** together with the rate constants of the processes.

4.2.7 The intramolecular energy transfer processes in (Nd)**1**, (Er)**1**, and (Yb)**1**

The energy transfer rates were determined in the NIR emitting complexes by measuring the influence of oxygen on the sensitized luminescence. The luminescence intensity is enhanced by 35% for (Nd)**1**, 120% for (Er)**1**, and 90% for (Yb)**1** upon deoxygenation of the $\text{DMSO}-d_6$ solutions (see Figures 4.10c and d), indicating that, contrary to the (Eu)**1** and (Tb)**1** complexes, oxygen quenching is competing with the energy transfer to the lanthanide ion. The Stern-Volmer equation can be used to estimate the antenna triplet state lifetimes and the energy transfer rates from this oxygen dependence. The diffusion-controlled quenching constant k_{diff} was taken as $10^{10} \text{ M}^{-1}\text{s}^{-1}$, and the oxygen concentration in DMSO was taken as

0.47 mM.¹⁵ The results are summarized in Table 4.4. The energy transfer to Yb³⁺ and Er³⁺ is significantly slower than the energy transfer to Nd³⁺.

Changing the solvent to methanol-*d*₄ would shift the equilibrium between the dark and luminescent conformational isomers of the complex towards the luminescent conformational isomer, as it has been shown for (Eu)**1** and (Tb)**1**, and would thus increase the quantum yield of the energy transfer (ϕ_{ET}). Unfortunately, the luminescence lifetimes of (Nd)**1**, (Yb)**1**, and (Er)**1** are significantly lower in methanol-*d*₄: for example the lifetimes of (Nd)**1** and (Er)**1** in methanol-*d*₄ are 0.89 μ s and 1.16 μ s, respectively. Thus changing the solvent from DMSO-*d*₆ to methanol-*d*₄ will not increase the *overall* luminescence quantum yield (ϕ_{SE}).

A special case is Yb³⁺, since it has only one excited state (²F_{5/2}), which is approximately 10,000 cm⁻¹ lower in energy than the antenna triplet state. It has been argued that the spectral overlap is therefore negligible.⁴⁴ Based on the fact that like Eu³⁺, Yb³⁺ is relatively easily reduced to Yb²⁺,³⁷ an internal redox mechanism has been proposed for the sensitized Yb³⁺ luminescence that takes place through the singlet state of the antenna chromophore.⁴⁴ The driving force $-\Delta G_{RET}$ of such a redox energy transfer can be estimated with the equation

$$\Delta G_{RET} = E(\text{Ant}^{\cdot+}/\text{Ant}) - E_{\text{Triph}^*} - E(\text{Ln}^{3+}/\text{Ln}^{2+}) \quad (5)$$

However, this mechanism is not operative in our system. In a cyclic voltammetry measurement on (Yb)**8** (see chart 4.1) in DMSO, no reduction was observed up to -1.90 V vs SCE. Since the oxidation potential of triphenylene is 1.55 V vs SCE,⁴⁵ $E(\text{Triph}^{\cdot+}/\text{Triph}) - E(\text{Yb}^{3+}/\text{Yb}^{2+})$ is >3.45 eV, whereas the energy of the triphenylene singlet excited state (E_{Triph^*}) is 3.6 eV. Therefore, there is almost no driving force for the photo-induced redox reaction in our system.

Moreover, if the redox energy transfer mechanism is operative, then the fluorescence of the triphenylene moiety of (Yb)**1** must not only be competing with intersystem crossing, but also with the energy transfer. Our photophysical data, *i.e.* the triphenylene fluorescence quantum yield and the oxygen dependence of the sensitized emission show that the energy transfer takes place via the triplet state. Therefore, the energy transfer mechanism is most likely an electron-exchange mechanism. The extremely small spectral overlap of the antenna phosphorescence spectrum and the Yb³⁺ absorption spectrum, causes the energy transfer to be slower than for example in the (Eu)**1** and (Nd)**1** complexes. The recently reported sensitized

near-infrared Nd^{3+} , Yb^{3+} , and Er^{3+} luminescence by energy transfer from the dye fluorescein was shown to be oxygen sensitive.¹⁶ Especially, the sensitized Yb^{3+} luminescence was very sensitive to oxygen, not only indicating that the energy transfer process proceeds via the triplet state, but also that it is very slow.

4.3 Conclusion

This study has shown that the (Ln)**1** complexes exist in solution in two conformational isomers: one in which energy transfer does not take place, and one in which the energy transfer takes place resulting in sensitized luminescence. Using quenching experiments to study this luminescent species, it was found that the energy transfer process is fast in the (Eu)**1** and (Tb)**1** complexes (no oxygen dependence), whereas it is slower in the NIR emitting complexes (oxygen dependence). The energy transfer rates can be improved by direct coordination of the antenna chromophore to the lanthanide ion, which would not only reduce the distance between donor and acceptor, but also the conformational freedom of the antenna relative to the lanthanide ion. This concept will be explored in chapter 5. An improvement of the spectral overlap of the NIR emitting lanthanide ions (especially Yb^{3+}) and the antenna can be achieved by incorporating antenna chromophores with lower lying triplet states. It has been shown that dyes like fluorescein can sensitize Er^{3+} , Yb^{3+} , and Nd^{3+} emission,^{3,16} and the next step is to incorporate these dyes in terphenyl-based ligands as will be presented in chapter 6.

4.4 Experimental Section

4.4.1 Synthesis

General synthesis: For a general description of the synthesis see paragraph 3.4.1 of chapter 3. Acetone was of analytical grade and was dried over molecular sieves (4 Å) prior to use.

Triphenylene-2-carboxylic acid (3). To a solution of triphenylene-2-carboxyaldehyde **2** (0.60 g, 2.34 mmol) in a mixture of CHCl_3 (30 mL) and acetone (90 mL) was subsequently

added a solution of H₂NSO₃H (0.50 g, 5.16 mmol) in water (1 mL) and a solution of NaClO₂ (0.50 g, 6.50 mmol) in water (1 mL). The resulting mixture was stirred for three hours at room temperature, after which it was concentrated *in vacuo* until the product precipitated. The solid was filtered off, washed thoroughly with water, and dried *in vacuo*. The product was obtained as an off-white solid, yield 80%. M.p.: >250 °C. ¹H NMR (DMSO-*d*₆): δ 9.29 (s, 1H), 8.94-8.74 (m, 5H), 8.19 (d, 1H, *J* = 8.0 Hz), 7.80-7.68 (m, 4H). ¹³C NMR (DMSO-*d*₆): 168.1, 133.2, 130.7, 130.2-128.2, 125.5-124.2. IR (KBr) 1684 cm⁻¹ (ν_{COOH}). MS (EI) *m/z* = 272.0 [M⁺, calcd. 272.1]. Anal. calcd. for C₁₉H₁₂O₂: C, 83.81, H, 4.44; found: C, 83.87, H, 4.46.

Mono(amide) terphenyl (6). To a solution of bis(amine) **5** (2.0 g, 2.11 mmol) and Et₃N (0.58 mL, 4.2 mmol) in CH₂Cl₂ (200 mL) was slowly added a solution of benzoyl chloride (0.41 g, 2.95 mmol) in CH₂Cl₂ (50 mL). The resulting solution was stirred overnight at room temperature. Subsequently, CH₂Cl₂ was added (100 mL) and the reaction mixture was washed twice with 5% K₂CO₃, followed by standard workup. The crude product was purified by flash column chromatography (MeOH/CH₂Cl₂ 1:9) to give mono(amide) **6** as a colorless oil in 30% yield. ¹H NMR (CDCl₃): δ 7.45-7.20 (m, 5H), 7.20-7.00 (m, 6H), 4.93-4.69 (m, 2H), 4.10-4.00 (m, 6H), 3.80-3.70 (m, 2H), 3.60-2.85 (m, 16H), 2.36 (s, 3H), 2.31 (s, 6H), 2.10-1.95 (m, 4H), 1.55-1.48 (m, 4H), 1.35 (s, 9H), 1.25 (s, 9H), 1.15 (s, 9H), 0.90-0.75 (m, 6H). ¹³C NMR (CDCl₃): δ 172.3, 167.9, 167.1, 151.9, 151.3, 136.5-126.6, 81.5, 80.9, 70.6, 70.4, 69.6, 68.56, 67.6, 48.4, 46.3, 31.9, 27.9, 21.0, 20.7, 19.3, 13.9. MS (FAB) *m/z* = 1053.5 [(M+H)⁺, calcd. for C₆₂H₈₉N₂O₁₂:1053.6].

Triphenylene-functionalized triester (7). A solution of triphenylene-2-carboxylic acid **3** (0.10 g, 0.37 mmol) in SOCl₂ (10 mL) was refluxed for 4 h. Subsequently, the excess SOCl₂ was removed *in vacuo*. The acid chloride **4** was redissolved in CH₂Cl₂ (5 mL) and added to a solution of mono(amide) **6** (0.30 g, 0.29 mmol) and Et₃N (0.10 g, 1.0 mmol) in CH₂Cl₂ (100 mL). The resulting solution was stirred overnight at room temperature. Subsequently CH₂Cl₂ was added (100 mL) and the reaction mixture was washed twice with 1 N HCl, followed by standard workup. The crude product was purified by flash column chromatography (ethyl acetate/hexane 2:3) to give **7** as a white solid in 60% yield. M.p.: 61-63 °C. ¹H NMR (CDCl₃): δ 8.86-8.60 (m, 6H), 8.29 (d, 1H, *J* = 8.0 Hz), 7.80-6.90 (m, 15H), 5.15 (s, 2H),

5.03 (s, 2H), 4.93 (s, 2H), 4.77 (s, 2H), 4.25-3.04 (m, 18H), 2.40-1.80 (m, 17H), 1.68-0.80 (m, 37H). ^{13}C NMR (CDCl_3): δ 172.3, 167.9, 167.1, 151.9, 151.3, 136.5-123.4, 81.5, 80.9, 70.6, 70.4, 69.6, 68.56, 67.6, 48.4, 46.3, 31.9, 27.9, 21.0, 20.7, 19.3, 13.9. MS (FAB) m/z = 1330.3 $[(\text{M}+\text{Na})^+]$, calcd. 1329.7]. Anal. calcd. for $\text{C}_{81}\text{H}_{98}\text{N}_2\text{O}_{13}$: C, 74.40, H, 7.55, N 2.14; found: C, 74.15, H, 7.48, N, 2.20.

Triphenylene-functionalized triacid ((H₃)1). A solution of triester **7** (0.20 g, 0.18 mmol) in TFA (15 mL) was stirred overnight at room temperature. Subsequently, toluene (15 mL) was added and the TFA/toluene mixture was azeotropically evaporated. The residue was taken up in CH_2Cl_2 (100 mL) and washed twice with 1 N HCl, followed by standard workup. The triacid (H₃)**1** was obtained as a white solid in quantitative yield. Mp: 102-104 °C. ^1H NMR (CD_3OD): δ 8.80-8.10 (m, 7H), 7.70-6.80 (m, 15H), 5.10-4.60 (m, 4H), 4.20-4.90 (m, 18H), 2.35-2.15 (m, 9H), 2.10-0.70 (m, 18H). MS (FAB) m/z = 1161.4 $[(\text{M}+\text{Na})^+]$, calcd. 1161.5]. Anal. calcd. for $\text{C}_{69}\text{H}_{74}\text{N}_2\text{O}_{13}\cdot\text{H}_2\text{O}$: C, 71.61, H, 6.62, N 2.42; found: C, 71.39, H, 6.50, N, 2.40.

General procedure for the preparation of the complexes. To a solution of 1.0 equiv. of triacid (H₃)**1** and 4.0 equiv. of Et_3N in methanol was added 1.1 equiv. of the lanthanide nitrate salt. The resulting solution was stirred for 2 h., after which the solvent was concentrated to dryness *in vacuo*. The complex was redissolved in CHCl_3 and washed twice with water, followed by standard workup. MS (FAB): (Eu)**1**: m/z = 1289.3 $[(\text{M}+\text{H})^+]$, calcd. 1289.4]; (Tb)**1**: m/z = 1295.2 $[(\text{M}+\text{H})^+]$, calcd. 1295.4]; (Gd)**1**: m/z = 1294.1 $[(\text{M}+\text{H})^+]$, calcd. 1294.4]; (Er)**1**: m/z = 1304.5 $[(\text{M}+\text{H})^+]$, calcd. 1304.4]; (Yb)**1**: m/z = 1310.4 $[(\text{M}+\text{H})^+]$, calcd. 1310.4]; (Nd)**1**: m/z = 1280.3 $[(\text{M}+\text{H})^+]$, calcd. 1280.4]. The complexes all gave similar IR spectra (in KBr): A peak at 1635 - 1630 cm^{-1} ($\nu_{\text{NC=O}}$) with a shoulder around 1600 - 1590 cm^{-1} (ν_{COO}).

4.4.2 Photophysical studies

See paragraph 3.4.2 of chapter 3 for a general description of the photophysical studies.

Quantum yield measurements. The quantum yield of the triphenylene fluorescence and the quantum yield of the overall sensitized lanthanide emission were determined relative to a reference solution of quinine sulfate in 1 M H_2SO_4 ($\phi = 0.546$), and corrected for the refractive index of the solvent.⁴⁶ The absorption of the solutions was 0.1 at the excitation

wavelength (310 nm). The solvents were of spectroscopical grade. Deaeration of the samples was performed by purging the solutions thoroughly with argon for 15-20 minutes.

Transient absorption spectroscopy. The 340 nm pump light was delivered by a frequency-doubled tunable optical parametric oscillator system (Coherent Infinity XPO). The width of the pulse was approximately 2 ns (FWHM) and its energy was less than 1 mJ/pulse. For recording the transient absorption spectra at a definite time after the laser pulse, the probe light from a flashlamp (EG&G FX504, 2.5 μ s pulsewidth) went via the sample through a spectrograph (Acton SpectraPro 150) to a gated intensified charge-coupled device camera (Princeton Instruments ICC-576-G/RB-EM). This system was also used to obtain kinetic data in the microsecond domain by recording a set of transient spectra at increasing time intervals. Alternatively, the flashlamp was used in combination with the streak camera system (Hamamatsu) as the detector to simultaneously probe wavelength and time-dependence of the transient signals in the sub-microsecond domain. The streak images containing the transient absorbance data were subjected to principal component analysis by means of singular value decomposition. All datasets contained only one significant component. This component was used in the reconstruction of the transient absorption spectrum of this single component in the top of the excitation pulse and its kinetics.

4.4.3 Electrochemical measurements

Cyclic voltammetry was performed in a three-electrode cell containing a platinum work electrode, a platinum counter electrode, and a Ag/AgCl reference electrode, with an Autolab PGSTA10 (ECOCHEMIE, Utrecht, The Netherlands). The ferrocene/ferricenium redox couple was used as an internal standard ($E^0 = 0.44$ V vs SCE in DMSO).⁴⁷ The solvent DMSO was of spectroscopical grade and was deoxygenated by purging with nitrogen. The ground electrolyte was Bu_4NPF_6 (0.1 M). The measurements were performed in a glove box under a nitrogen atmosphere. The cyclic voltammograms were recorded at a scan rate of 100 mV/s.

4.4.4 Molecular dynamics and molecular modeling calculations

See paragraph 3.4.3 of chapter 3 for the description of the molecular mechanics and molecular dynamics calculations. For the molecular dynamics calculations in OPLS DMSO, the minimized structures were placed in a rectangular box ($31.49 \text{ \AA} \times 31.49 \text{ \AA} \times 47.23 \text{ \AA}$), initially filled with 400 OPLS DMSOs.²¹ The same protocol was used as described for the

molecular dynamics calculations in OPLS MeOH.

4.5 References and Notes

1. Mikkala, V.-M.; Helenius, M.; Hemmilä, I.; Kankare, J.; Takalo, H. *Helv. Chim. Acta* **1993**, *76*, 1361.
2. Slooff, L. H.; Polman, A.; Oude Wolbers, M. P.; van Veggel, F. C. J. M.; Reinhoudt, D. N.; Hofstraat, J. W. *J. Appl. Phys.* **1997**, *83*, 497.
3. Oude Wolbers, M. P.; van Veggel, F. C. J. M.; Peters, F. G. A.; van Beelen, E. S. E.; Hofstraat, J. W.; Geurts, F. A. J.; Reinhoudt, D. N. *Chem. Eur. J.* **1998**, *4*, 772.
4. (a) Gschneider, K. A.; Eyring, L. R. *Handbook on the Physics and Chemistry of Rare Earths*, North Holland Publishing Company, Amsterdam, **1979**. (b) Sabbatini, N.; Guardigli, M.; Lehn, J.-M. *Coord. Chem. Rev.* **1993**, *123*, 201, and references cited therein.
5. Steemers, F. J.; Verboom, W.; Reinhoudt, D. N.; van der Tol, E. B.; Verhoeven, J. W. *J. Am. Chem. Soc.* **1995**, *117*, 9408.
6. (a) Selvin, P. R.; Rana, T. M.; Hearst, J. E. *J. Am. Chem. Soc.* **1994**, *116*, 6029. (b) Li, M.; Selvin, P. R. *Proc. Natl. Acad. Sci. USA* **1994**, *91*, 10024.
7. Mikkala, V.-M.; Helenius, M.; Hemmilä, I.; Kankare, J.; Takalo, H. *Helv. Chim. Acta* **1993**, *76*, 1361.
8. Sato, S.; Wada, M. *Bull. Chem. Soc. Jpn.* **1970**, *43*, 1955.
9. Crosby, G. A.; Whan, R. E.; Alire, R. M. *J. Chem. Phys.* **1961**, *34*, 743.
10. Tanaka, M.; Yamaguchi, G.; Shiokawa, J.; Yamanaka, C. *Bull. Chem. Soc. Jpn.* **1970**, *43*, 549.
11. Haynes, A. V.; Drickamer, H. G. *J. Chem. Phys.* **1982**, *76*, 114.
12. Stein, G.; Würzberg, E. *J. Chem. Phys.* **1975**, *62*, 208.
13. (a) Tobita, S.; Arakawa, M.; Tanaka, I. *J. Phys. Chem.* **1984**, *88*, 2697. (b) Tobita, S.; Arakawa, M.; Tanaka, I. *J. Phys. Chem.* **1985**, *89*, 5649.
14. Dexter, D. L. *J. Chem. Phys.* **1953**, *21*, 836.
15. Murov, S. L.; Carmichael, I.; Hug, G. L. *Handbook of Photochemistry, 2nd Ed.*, Marcel Dekker, New York, **1993**.
16. Werts, M. H. V.; Hofstraat, J. W.; Geurts, F. A. J.; Verhoeven, J. W. *Chem. Phys. Lett.*

- 1997, 276, 196.
17. van der Tol, E. B.; van Ramesdonk, H. J.; Verhoeven, J. W.; Steemers, F. J.; Kerver, E. G.; Verboom, W.; Reinhoudt, D. N. *Chem. Eur. J.* **1998**, *4*, 2315.
 18. Klink, S. I.; Hebbink, G. A.; Grave, L.; Peters, F. G. A.; van Veggel, F. C. J. M.; Reinhoudt, D. N.; Hofstraat, J. W. *Eur. J. Org. Chem.*, **2000**, in press.
 19. The Lennart Jones parameters for the Ln³⁺ ions were taken from: van Veggel, F. C. J. M.; Reinhoudt, D. N. *Chem. Eur. J.* **1999**, *5*, 90.
 20. Jorgensen, W. L. *J. Phys. Chem.* **1986**, *90*, 1276.
 21. Jorgensen, W. L. BOSS Version 3.5 Biochemical and Organic Simulation System User's Manual, **1994**.
 22. (a) Brooks, B. R.; Bruccoleri, R. E.; Olafsen, B. D.; States, D. J.; Swaminathan, S.; Karplus, M. *J. Comput. Chem.* **1983**, *4*, 187. (b) Momany, F. A.; Klimkowski, V. J.; Schäfer, L. *J. Comput. Chem.* **1990**, *11*, 654. (c) Momany, F. A.; Rone, R.; Kunz, H.; Frey, R. F.; Newton, S. Q.; Schäfer, L. *J. Mol. Structure* **1993**, *286*, 1. The Lennart Jones parameters for the Ln³⁺ ions were taken from: van Veggel, F. C. J. M.; Reinhoudt, D. N. *Chem. Eur. J.* **1999**, *5*, 90.
 23. (a) Kirby, A. F.; Foster, D.; Richardson, F. S. *Chem. Phys. Lett.* **1983**, *95*, 507. (b) Kirby, A. F.; Richardson, F. S. *J. Phys. Chem.* **1983**, *87*, 2544.
 24. The ¹H NMR spectrum of (Y)**8** in DMSO-*d*₆ shows that this type of complexes have a (time-averaged) C_s symmetry. See also chapter 3.
 25. (a) Kropp, J. L.; Windsor, M. W. *J. Chem. Phys.* **1963**, *39*, 2769. (b) Kropp, J. L.; Windsor, M. W. *J. Chem. Phys.* **1965**, *42*, 1599. (c) Kropp, J. L.; Windsor, M. W. *J. Chem. Phys.* **1966**, *45*, 761.
 26. (a) Horrocks, W. DeW., Jr.; Sudnick, D. R. *Acc. Chem. Res.* **1981**, *14*, 384. (b) Holz, R. C.; Chang, C. A.; Horrocks, W. DeW., Jr. *Inorg. Chem.* **1991**, *30*, 3270.
 27. Beeby, A.; Clarkson, J. M.; Dickins, R. S.; Faulkner, S.; Parker, D.; Royle, L.; de Sousa, A. S.; Williams, J. A. G.; Woods, M. *J. Chem. Soc., Perkin Trans. 2* **1999**, 493.
 28. Frey, S. T.; Horrocks, Jr., W. DeW. *Inorg. Chim. Acta* **1995**, *229*, 383, and references cited therein.
 29. (a) Hasegawa, Y.; Kimura, Y.; Murakoshi, K.; Wada, Y.; Kim, J-H.; Nakashima, N.; Yamanaka, T.; Yanagida, S. *J. Phys. Chem.* **1996**, *100*, 10201. (b) Hasegawa, Y.; Murakoshi, K.; Wada, Y.; Yanagida, S.; Kim, J-H.; Nakashima, N.; Yamanaka, T.

- Chem. Phys. Lett.* **1996**, 248, 8.
30. Beeby, A.; Faulkner, S. *Chem. Phys. Lett.* **1997**, 266, 116.
 31. (a) Carnall, W. T.; Goodman, G. L.; Rajnak, K.; Rana, R. S. *J. Chem. Phys.* **1989**, 90, 3443. (b) Beeby, A.; Dickins, R.; Faulkner, S.; Parker, D.; Williams, J. A. G. *Chem. Commun.* **1997**, 1401.
 32. Steemers, F. J.; Verboom, W.; Hofstraat, J. W.; Geurts, F. A. J.; Reinhoudt, D. N. *Tetrahedron Lett.* **1998**, 39, 7583.
 33. Crosby, G. A.; Kasha, M. *Spectrochim. Acta* **1958**, 10, 377.
 34. Klink, S. I.; Hebbink, G. A.; Grave, L.; van Veggel, F. C. J. M.; Reinhoudt, D. N.; Slooff, L. H.; Polman, A.; Hofstraat, J. W. *J. Appl. Phys.* **1999**, 86, 1181.
 35. Weber, M. J. *Phys. Rev.* **1968**, 171, 283.
 36. (a) Sabbatini, N.; Perathoner, S.; Lattanzi, G.; Dellonte, S.; Balzani, V. *J. Phys. Chem.* **1987**, 91, 6136. (b) Steemers, F. J.; Meuris, H. G.; Verboom, W.; Reinhoudt, D. N. *J. Org. Chem.* **1997**, 62, 4229.
 37. The reduction potentials of Eu^{3+} and Yb^{3+} in water are -0.35 V and -1.05 V (vs NHE), respectively. Bard, A. J.; Parsons, R.; Jordan, J. *Standard Potentials in Aqueous Solution*, Marcel Dekker Inc., New York, **1985**.
 38. k_{diff} is taken as $10^{10} \text{ M}^{-1}\text{s}^{-1}$, $[\text{O}_2]$ in methanol is 2.1 mM (ref. 15). Since $k_{\text{ox}} = k_{\text{diff}}[\text{O}_2] = 2 \times 10^7 \text{ s}^{-1}$, and there is no oxygen effect: $k_{\text{ET}} > k_{\text{ox}}$, which means that k_{ET} exceeds 10^7 s^{-1} .
 39. Bhaumik, M. L.; El-Sayed *J. Chem. Phys.* **1965**, 42, 787.
 40. Bhattacharyya, S.; Sousa, L. R.; Ghosh, S. *Chem. Phys. Lett.* **1998**, 297, 154.
 41. $\phi_{\text{SE}} = \phi_{\text{ISC}} \cdot \phi_{\text{ET}} \cdot \phi_{\text{lum}} = \phi_{\text{ISC}} \cdot \phi_{\text{ET}} \cdot \tau/\tau_0$. Typical values of the natural lifetime τ_0 of Eu^{3+} and Tb^{3+} are 3 ms and 4 ms, respectively. If ϕ_{ISC} and ϕ_{ET} are taken as 1, then based on the luminescence lifetimes ϕ_{SE} is 0.29 for (Eu)**1** and 0.44 for (Tb)**1**.
 42. It can be demonstrated that a photon-induced electron transfer process may indeed be the additional cause of the low luminescence quantum yield of (Eu)**1**. The antenna fluorescence lifetime of (Tb)**1** was measured to be approximately 1 ns. Using the equation $\phi_{\text{flu}} = k_{\text{flu}}/(k_{\text{flu}} + k_{\text{ISC}}) = k_{\text{flu}} \cdot \tau_{\text{flu}}$, it follows that $k_{\text{flu}} = 0.86 \times 10^7 \text{ s}^{-1}$ and $k_{\text{ISC}} = 9.9 \times 10^8 \text{ s}^{-1}$. It can furthermore be calculated that $\phi_{\text{ISC}} \approx 0.99$. If it is assumed that k_{flu} and k_{ISC} are the same for (Eu)**1** as for (Tb)**1**, then the rate of the photon-induced electron transfer (k_{PET}) can be calculated via $\phi_{\text{flu}} = k_{\text{flu}}/(k_{\text{flu}} + k_{\text{ISC}} + k_{\text{PET}})$, resulting in $k_{\text{PET}} = 5.9 \times$

10^8 s^{-1} . As a result, the intersystem crossing yield of (Eu)**1** is lower than that of (Tb)**1** with $\phi_{\text{ISC}} \approx 0.63$.

43. van der Tol, E. B., *Design and Photophysics of Luminescent Labels for Use in Time-Resolved Biological Assays*, PhD Thesis, University of Amsterdam, **1998**.
44. Horrocks Jr., W.D.; Bolender, J. P.; Smith, W. D.; Supkowski, R. M. *J. Am. Chem. Soc.* **1997**, *119*, 5972, and references cited therein.
45. Pysh, E. S.; Yang, N. C. *J. Am. Chem. Soc.* **1963**, *85*, 2124.
46. Demas, N. J.; Crosby, G. A. *J. Phys. Chem.* **1971**, *75*, 991.
47. Barrette, W. C., Jr.; Johnson, H. W., Jr.; Sawyer, D. T. *Anal. Chem.* **1984**, *56*, 1890.

Chapter 5

Sensitized Luminescence of Ternary Eu³⁺ and Nd³⁺ Complexes

5.1 Introduction

As was pointed out in chapter 4, in general the population of the excited state of a luminescent lanthanide ion occurs via energy transfer from an organic antenna chromophore. This sensitization process is much more efficient than direct excitation of the lanthanide ion, since the absorption coefficients of organic chromophores are several orders of magnitude larger (typically 3-5) than the intrinsically low molar absorption coefficients of trivalent lanthanide ions.¹ The efficiency of the sensitization process depends on the distance between the sensitizer and lanthanide ion, and specific energetic requirements of the sensitizer that are imposed by the photophysics of the sensitization process. It has generally been accepted that the transfer of excitation energy from the antenna to the lanthanide ion usually takes place via the antenna triplet state^{2,3,4,5} by an electron-exchange mechanism (also known as a Dexter mechanism).⁶ According to Dexter's theory the rate constant for energy transfer (k_{ET}) is given by equation (1).

$$k_{\text{ET}} = (2\pi/\hbar)Z^2 \cdot \int F_d(\nu)\epsilon_a(\nu)d\nu \quad (1)$$

The first term $(2\pi/\hbar)Z^2$ is related to the specific orbital interactions, and is therefore strongly dependent on the distance between donor and acceptor. Dexter derived that $Z^2 \sim e^{-2R/L}$, where R is the distance between donor and acceptor, and L is the sum of the van der Waals radii of the donor and acceptor. The second term $\int F_d(\nu)\epsilon_a(\nu)d\nu$ is the spectral overlap integral, where F_d is the emission spectrum of the triplet state of the sensitizer (the phosphorescence spectrum) and $\epsilon_a(\nu)$ is the absorption spectrum of the 4f-transitions of the lanthanide ion. The integrals of the phosphorescence and the absorption spectra are both normalized, so that $\int F_d(\nu)d\nu = 1$ and $\int \epsilon_a(\nu)d\nu = 1$. In other words, the spectral overlap integral is a measure of the matching of the energy levels of the donor and the acceptor, and does *not* depend on the absorption coefficients of the donor and the acceptor.

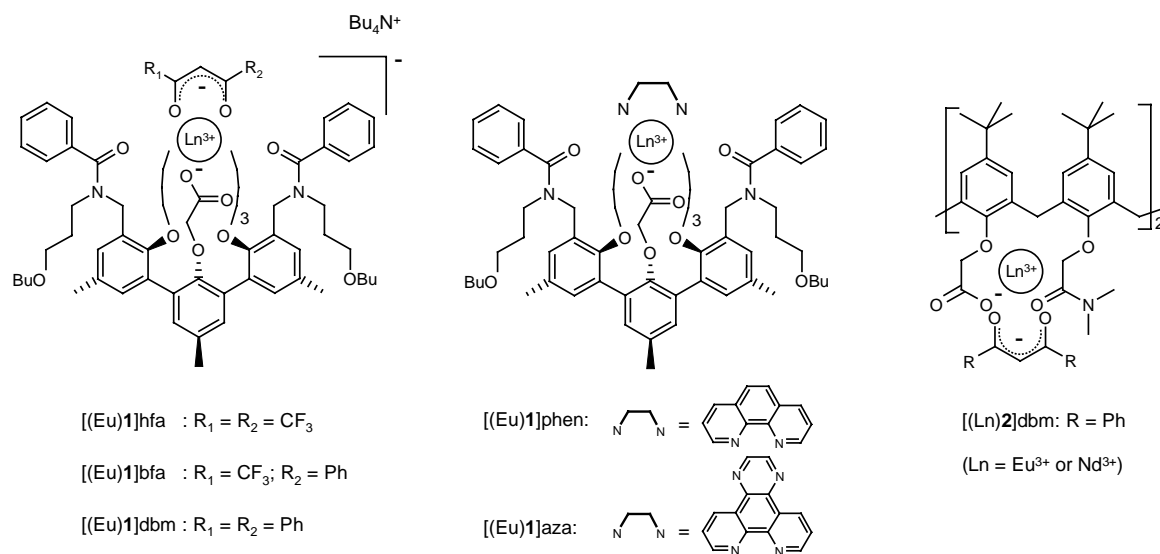
In the triphenylene-functionalized lanthanide complexes described in chapter 4, the antenna is positioned in close proximity to the lanthanide ion, but it is still not in direct contact with the ion. The system can be optimized by introducing antenna chromophores with chelating properties that allow direct coordination of the sensitizer to the lanthanide ion. Examples of such antenna chromophores are β -diketonates. In the well-known Eu^{3+} and Tb^{3+} β -diketonate complexes, the coordinated β -diketonate ligands act as antenna chromophores for the sensitized lanthanide luminescence.⁷ The excitation wavelength and also the energy transfer efficiency is strongly influenced by the two substituents at the propanedione skeleton of the β -diketonate ligands.⁸ In the lanthanide-tris(β -diketonate) complexes, the lanthanide ion is coordinated by only six oxygen donor atoms provided by the ligands leaving room for two solvent molecules, usually water. In the lanthanide-tetrakis(β -diketonate) complexes however, the coordination sphere of the lanthanide ion is saturated (eight oxygen donor atoms). Alternatively, the fourth (charged) β -diketonate ligand can be replaced by a neutral donor ligand, such as the bidentate ligand 1,10-phenanthroline.⁹ Another recent example is the complex of $\text{Eu}(\text{fod})_3$ and Michler's ketone in benzene.^{10,11} Upon coordination to the Eu^{3+} ion, a bathochromic shift of the absorption band of Michler's ketone to 420 nm is observed, allowing visible light excitation with a high overall quantum yield of sensitized emission ($\phi_{\text{SE}} = 0.17$).

Tetraazatriphenylene has lanthanide ion coordinating properties and forms 2:1 complexes with Eu^{3+} and Tb^{3+} in acetonitrile.¹² The energy transfer process is very efficient in these

complexes as could be concluded from the high overall luminescence quantum yields: 0.41 for the Eu^{3+} complex and 0.67 for the Tb^{3+} complex. Tetraazatriphenylene also forms 2:1 complexes with Nd^{3+} , Er^{3+} , and Yb^{3+} , and these complexes exhibit sensitized near-infrared luminescence.¹³

In the ternary complexes of Eu^{3+} and Nd^{3+} described in this chapter, the sensitizing properties of β -diketonates and tetraazatriphenylene have been combined with the complexing properties of *m*-terphenyl- and calix[4]arene-based ligands (see Chart 5.1). In chapter 3, it has been shown that the lanthanide ion in the *m*-terphenyl-based ligand (Ln)**1** is coordinated by eight hard oxygen donor atoms, and that the ninth coordination site of the lanthanide ion is occupied by a solvent molecule. In principle this site can also be occupied by an antenna chromophore bearing neutral or negatively charged coordinating groups, which bring the antenna in direct contact with the lanthanide ion.

Chart 5.1



The calix[4]arene-based ligand (H_2)**2**, is a derivative of the previously reported triacid-monoamide-calix[4]arene ionophores.^{14,15} The lanthanide ion in the $[(\text{Ln})\mathbf{2}]^+$ complex depicted in Chart 5.1, is encapsulated by eight hard oxygen donor atoms: four ether oxygen atoms, two negatively charged carboxylate oxygens and two amide oxygens. Coordination of the β -diketonate to the complexed lanthanide ion results in ternary complexes that are overall neutral.

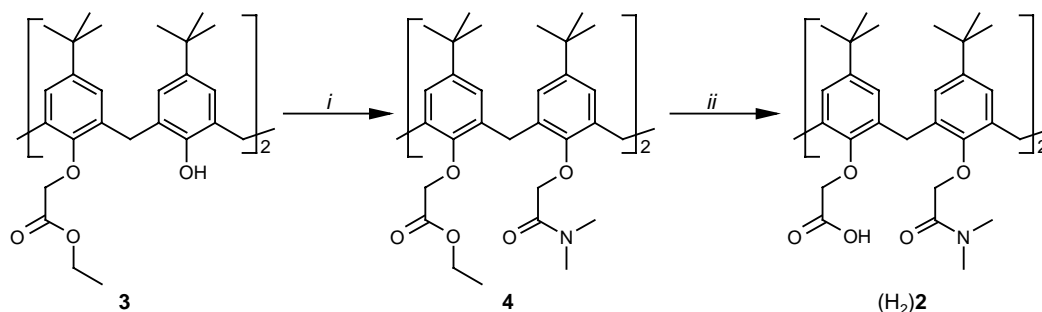
5.2 Results and Discussion

5.2.1 Synthesis

The synthesis of the *m*-terphenyl-based (Ln)**1** complexes has been described in chapter 3. The ternary [(Ln)**1**] β -diketonate complexes were prepared by mixing one equivalent of the tetrabutylammonium salt of the appropriate β -diketonate and one equivalent of (Ln)**1** in dichloromethane, and subsequent removal of the solvent. The neutral tetraazatriphenylene and phenanthroline ternary complexes were prepared in a similar way. The *m*-terphenyl-based ternary complexes have been characterized by mass spectrometry and IR spectroscopy (see the experimental section). The FAB mass spectra show the expected 1:1:1 stoichiometry (ligand : Ln³⁺ : sensitizer) of the ternary complexes.

The synthesis of the calix[4]arene-based ligand (H₂)**2** starting from the diester calix[4]arene **3** is depicted in Scheme 5.1. Alkylation of the diester calix[4]arene **3** with 2-chloro-*N,N*-dimethylacetamide gave precursor **4** in 80% yield.

Scheme 5.1



Reagents and conditions: i) 2-Chloro-*N,N*-dimethylacetamide, CH₃CN, K₂CO₃, reflux, 80%; ii) K₂CO₃, methanol/water, 2h, reflux, 95%.

The ethylester moieties of **4** were hydrolyzed under basic conditions with K₂CO₃ in a water/methanol solution in nearly quantitative yield. Complete hydrolysis was confirmed by the ¹H NMR spectra in which the signals for the ethyl groups were absent, and by the IR spectrum in which a peak around 1750 cm⁻¹ was observed for the carboxylic acids (ν_{COOH}). The corresponding complexes were prepared by addition of the appropriate Ln(NO₃)₃ salt to a solution of (H₂)**2** in methanol in the presence of Et₃N as a base. Finally, the ternary

complexes were prepared in a similar way as the *m*-terphenyl-based ternary complexes. The [(Ln)**2**]NO3 and [(Ln)**2**]dbm complexes have been characterized by mass spectrometry and IR spectroscopy (see the experimental section).

5.2.2 Molecular mechanics studies

The structure of the *m*-terphenyl-based ternary complex [(Eu)**1**]hfa and the calix[4]arene-based [(Eu)**2**]dbm were minimized in the gas phase using the CHARMM force field.¹⁶ The simulations show that the complexed Eu^{3+} ion is coordinated by ten oxygen donor atoms (see Figure 5.1). In the [(Eu)**1**]hfa complex all eight donor atoms from the ligand, three phenol ether oxygens, three carboxylate oxygens, and two amide oxygens, are coordinated to the lanthanide ion, in addition to the two oxygen donor atoms of the β -diketonate moiety. In the [(Eu)**2**]dbm complex all eight donor atoms from the ligand, four phenol ether oxygens, two carboxylate oxygens, and two amide oxygens, are coordinated to the lanthanide ion, in addition to the two oxygen donor atoms of the β -diketonate moiety.

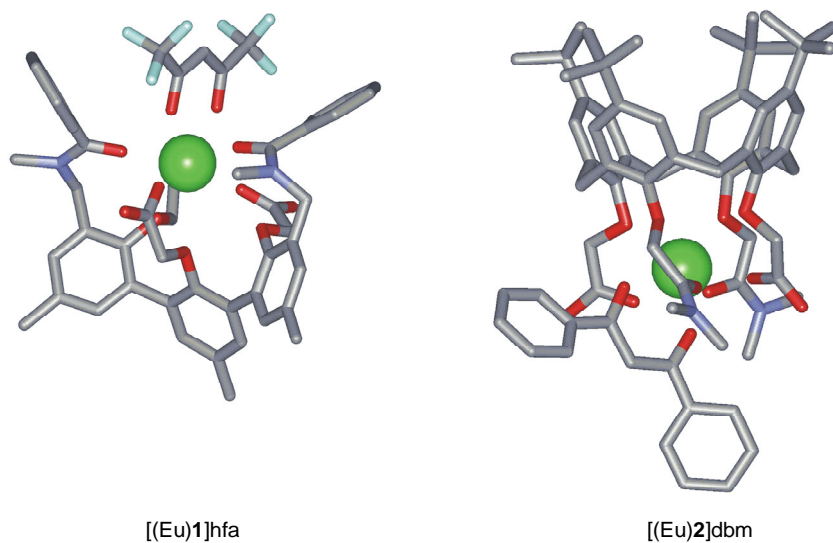


Figure 5.1: Minimized structures of [(Eu)**1**]hfa and [(Eu)**2**]dbm obtained from gas-phase optimizations. In the optimization, the *n*-butoxypropyl moieties of [(Eu)**1**]hfa have been replaced by methyl groups. The hydrogen atoms of both complexes have been omitted for clarity.

Although, the coordination number of Eu^{3+} in organic complexes in solution is generally eight or nine, for example, the coordination number of (Eu)**1** in methanol is nine (see chapter 3), coordination numbers of ten have also been reported.¹⁷

5.2.3 Monitoring the formation of the ternary complex

The formation of the ternary complexes can be studied by monitoring the sensitized luminescence intensity as a function of the amount of ternary complex in solution. In this way the formation of the two ternary complexes [(Eu)**1**]aza and [(Eu)**1**]bfa was examined in more detail. Figure 5.2 shows the titration experiments, in which small amounts of a (Eu)**1** stock solution were added to a solution of tetraazatriphenylene¹⁸ or (deprotonated) bfa.¹⁹ The complexes were excited in the absorption bands of the antenna chromophores, which reside at longer wavelengths where the (Eu)**1** complex itself has no absorption bands. Upon addition of increasing concentrations of (Eu)**1** to the antenna chromophores, the sensitized Eu³⁺ emission increased (see Figure 5.2).

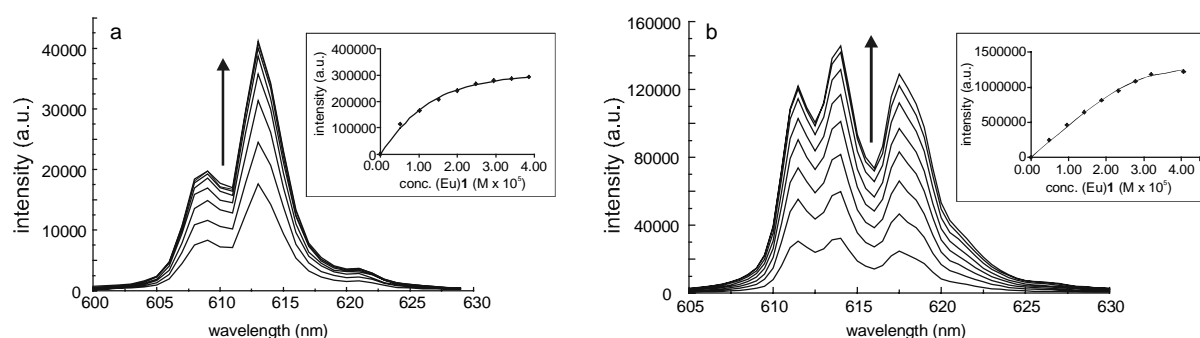


Figure 5.2: The increase in the sensitized ${}^5D_0 \rightarrow {}^7F_2$ emission intensity upon the addition of increasing concentrations of (Eu)**1** to the tetraazatriphenylene (a) and bfa (b) antenna chromophores in dichloromethane. The insets show the formation of the ternary complexes as a function of the sensitized luminescence intensity. The solid lines are the theoretical curves for a 1:1 complex with $K = 1.43 \times 10^5 M^{-1}$ for [(Eu)**1**]aza and $K = 5.04 \times 10^5 M^{-1}$ for [(Eu)**1**]bfa, respectively.

During the titration experiment, the absorption bands did not change (the dilution had been taken in account) indicating that upon coordination to (Eu)**1**, the singlet excited states of the antenna chromophores are not affected significantly by the Eu³⁺ ion. Analysis of the titration data yields the formation constant of the 1:1 ((Eu)**1**:antenna) ternary complexes, $K = 1.43 \times 10^5 M^{-1}$ for [(Eu)**1**]aza and $K = 5.04 \times 10^5 M^{-1}$ for [(Eu)**1**]bfa.

For the luminescence measurements (*vide supra*) the desired concentration of the ternary complexes would be $10^{-5} M$, in order to keep the absorption of samples below 0.2 at the excitation wavelength. The formation constant of [(Eu)**1**]bfa of $5.04 \times 10^5 M^{-1}$ implies that under these conditions the amount of ternary complex in solution is 64%. The addition of

extra amounts of (Eu)**1** to the [(Eu)**1**]bfa solution will shift the equilibrium towards the formation of the ternary complex, and the sensitized emission intensity is expected to increase. However, the sensitized luminescence intensity did not increase when extra (Eu)**1** (to a concentration of 10^{-4} M) was added to a 10^{-5} M solution of [(Eu)**1**]bfa. Therefore, the formation constant as obtained from the titration experiment is probably a lower limit of the actual formation constant. An explanation is that in this experiment two equivalents of base (NBu₄OH) were used to deprotonate the bfa antenna. Since this base can also coordinate to (Eu)**1**, it competes with the coordination of the bfa antenna.

The *m*-terphenyl-based ternary complexes were prepared as described in paragraph 5.2.1, and redissolved in dichloromethane to a concentration of 10^{-5} M. At this concentration, the β -diketonate ternary complexes are probably not dissociated. In the case of azatriphenylene and the phenanthroline ternary complexes, also free (Ln)**1** and antenna are in solution. Since the formation constant of [(Eu)**1**]aza is 1.43×10^5 M⁻¹, the amount of ternary complex in solution is only 44%. It is likely that [(Tb)**1**]aza and [(Eu)**1**]phen have similar formation constants. The emission, excitation spectra and lifetimes represent the photophysical properties of the ternary complex, because only the complex exhibits sensitized luminescence. The luminescence quantum yields have to be corrected for the amount of ternary complex in solution, because some of the excitation energy is lost when free antenna chromophores are excited.

5.2.4 Photophysical properties of the *m*-terphenyl-based ternary Eu³⁺ complexes

Upon photo-excitation the population of the triplet state is very high in these sensitizers with intersystem crossing yields in the order of 0.90.²⁰ The triplet energies of the coordinated sensitizers have been obtained from the literature and are depicted in Figure 5.3 (see also Table 5.1), as well as the 4f-energy levels of Eu³⁺. This figure clearly shows that the triplet states of the sensitizers are all higher in energy than the ⁵D₁ level of Eu³⁺ at approximately 19,000 cm⁻¹.

Emission spectra of the ternary Eu³⁺ complexes

The emission spectra of ternary *m*-terphenyl-based Eu³⁺ complexes in dichloromethane, excited at 330 nm, show the sensitized luminescence bands that correspond to the typical

$\text{Eu}^{3+} \ ^5\text{D}_0 \rightarrow \ ^7\text{F}_n$ transitions (see Figure 5.4). The strongest emission is observed around 615 nm corresponding to the *hypersensitive* $\ ^5\text{D}_0 \rightarrow \ ^7\text{F}_2$ transition. The excitation spectra of these ternary complexes closely follow the absorption spectra of the coordinated sensitizers (not shown), and thus prove that the Eu^{3+} luminescent state is populated via the antenna. From the excitation spectra it can be seen that the dbm antenna allows the longest wavelength excitation of up to 400 nm.

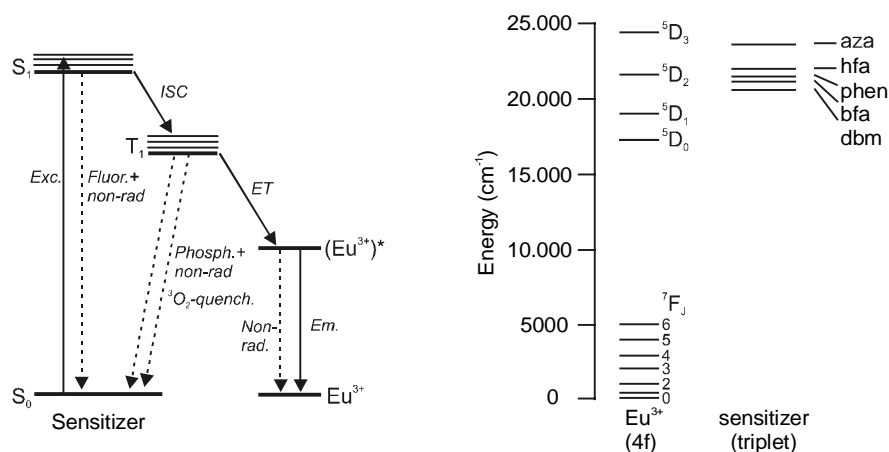


Figure 5.3: Left: Schematic representation of the photophysical pathway of the sensitization process. Right: The relevant $4f$ energy levels of Eu^{3+} as well as the triplet state energies of the sensitizers. For an explanation of the abbreviations of the sensitizers: see Chart 5.1.

Except for $[(\text{Eu})\mathbf{1}]\text{hfa}$, a single small peak is observed for the $\ ^5\text{D}_0 \rightarrow \ ^7\text{F}_0$ emission at 579 nm. Since the $\ ^7\text{F}_0$ state is non-degenerate, the single peak indicates that there is only one (time-averaged) luminescent Eu^{3+} species in solution. For the $[(\text{Eu})\mathbf{1}]\text{hfa}$ complex, a shoulder is observed on the high energy side of the peak, indicating a second luminescent species in solution (*vide infra*). The Eu^{3+} spectra further show some splitting of the $\ ^5\text{D}_0 \rightarrow \ ^7\text{F}_1$ emissions (around 593 nm) and the $\ ^5\text{D}_0 \rightarrow \ ^7\text{F}_2$ emissions (around 615 nm) in the order of $100\text{-}200\ \text{cm}^{-1}$ caused by the ligand field.

The intensity ratio of the $\ ^5\text{D}_0 \rightarrow \ ^7\text{F}_2$ transition and the $\ ^5\text{D}_0 \rightarrow \ ^7\text{F}_1$ transition is a good measure of the symmetry of the first coordination sphere of the Eu^{3+} ion.²¹ In a centrosymmetric environment the magnetic dipole $\ ^5\text{D}_0 \rightarrow \ ^7\text{F}_1$ transition of Eu^{3+} is dominating, whereas distortion of the symmetry around the ion causes an intensity enhancement of electric dipole transitions such as the *hypersensitive* $\ ^5\text{D}_0 \rightarrow \ ^7\text{F}_2$ transition. For the ‘bare’ $(\text{Ln})\mathbf{1}$ complex in dichloromethane, the $\ ^7\text{F}_2/\ ^7\text{F}_1$ intensity ratio is 3.5. This ratio is in correspondence with the

ratio of 4.0 that was found for this complex in methanol (see also chapter 3).

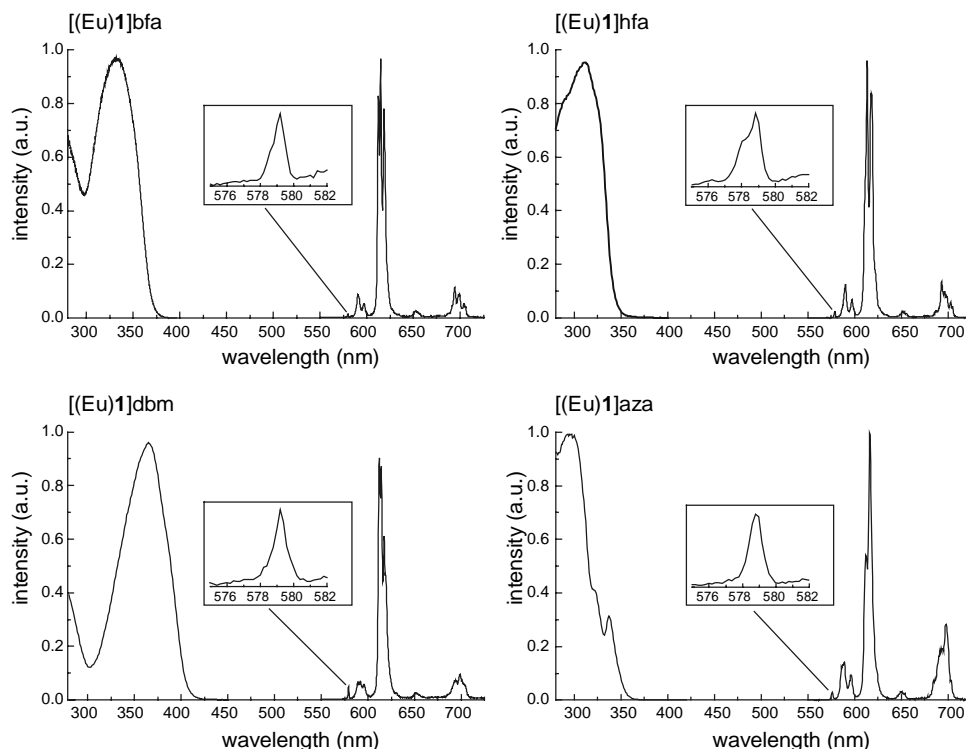


Figure 5.4: The normalized excitation ($\lambda_{em} = 615$ nm) and emission spectra of [(Eu1)bfa], [(Eu1)hfa], [(Eu1)dbm], and [(Eu1)aza] in dichloromethane. The inset shows a magnification of the ${}^5D_0 \rightarrow {}^7F_0$ emission at 579 nm. The spectra were taken with a spectral bandwidth of 0.5 nm.

For the ternary β -diketonate complexes these ratios are significantly higher, around 10 (see Table 5.1), indicating that the structure and symmetry of the first coordination sphere of Eu^{3+} have changed. The obtained ${}^7F_2/{}^7F_1$ intensity ratios are in line with reported literature values for Eu-tris(β -diketonate) complexes. For example, the ${}^7F_2/{}^7F_1$ intensity ratio for a single crystal $\text{Eu}(\text{dbm})_3 \cdot \text{H}_2\text{O}$ is 8.0.²¹

A typical feature of Eu-tris(β -diketonate) complexes is the domination of the ${}^5D_0 \rightarrow {}^7F_2$ transition in the emission spectrum, with the rest of the emission bands being weak. Also in the emission spectra of the β -diketonate ternary complexes, the intensity of the ${}^5D_0 \rightarrow {}^7F_2$ transition is dominating: the ${}^5D_0 \rightarrow {}^7F_2$ emission for example of [(Eu1)bfa] constitutes of almost 80% of its total emission intensity.

The coordination of tetraazatriphenylene and phenanthroline causes a much smaller increase in the relative intensity of the *hypersensitive* transition, with ${}^7F_2/{}^7F_1$ ratios of approximately 5. The weaker coordinating (neutral) nitrogen donor atoms apparently have a

smaller influence on the Eu^{3+} ion than the charged oxygen donor atoms of the β -diketonate moieties.

Table 5.1: The triplet energies of the sensitizers and photophysical data of the ternary Eu^{3+} complexes in dichloromethane (10^{-5} M).

Complex	E_{T} sensitizer (cm^{-1})	${}^7\text{F}_2/{}^7\text{F}_1$ ^a	ϕ_{SE} ^b	${}^5\text{D}_0$ τ (ms) ^d	${}^5\text{D}_1$ τ (μs) ^d
[(Eu)1]hfa	22,000	9.0	0.26	1.27	1.51
[(Eu)1]bfa	21,400	11.4	0.29	1.08	1.53
[(Eu)1]dbm	20,600	10.1	0.03	0.38	0.36
[(Eu)1]phen	21,480	4.9	0.04 (0.09) ^c	0.93	n.d.
[(Eu)1]aza	23,800	5.4	0.03 (0.07) ^c	0.71	2.97

^aIntensity ratio of the ${}^5\text{D}_0 \rightarrow {}^7\text{F}_2$ emission and the ${}^5\text{D}_0 \rightarrow {}^7\text{F}_1$ emission. ^bThe measured quantum yield of the sensitized Eu^{3+} emission. ^c ϕ_{SE} corrected for the amount of ternary complex in solution (see main text). ^dLuminescence lifetime of the Eu^{3+} emission.

Quantum yield of the sensitized luminescence

The quantum yields of the sensitized lanthanide emission were determined relative to a reference solution of quinine sulfate in 1 M H_2SO_4 ($\phi = 0.546$), and corrected for the refractive index of the solvent.²² All quantum yields were measured with aerated solutions. The results have been summarized in Table 5.1 and show that the bfa antenna is clearly the most efficient sensitizer for Eu^{3+} with a quantum yield of 0.29, followed by the hfa antenna with a quantum yield of 0.26. The dbm antenna and, rather unexpectedly, also the tetraazatriphenylene antenna are less efficient sensitizers for Eu^{3+} with luminescence quantum yields of only 0.03, and 0.07, respectively.

The overall quantum yield of the sensitized luminescence depends on the intersystem crossing quantum yield, the efficiency of the energy transfer process, and the quantum yield of the lanthanide luminescence. It was already mentioned that the investigated antenna chromophores have intersystem crossing quantum yields that are close to unity. Further information about the energy transfer process and the subsequent population and decay of the Eu^{3+} luminescent state could be provided by time-resolved luminescence measurements.

Luminescence lifetimes of the ternary complexes

The luminescence lifetimes were measured using pulsed laser excitation of the complexes at 337 nm and a streak camera to monitor the Eu^{3+} ${}^5\text{D}_0$ emission at 615 nm. The observed

luminescence decays were mono-exponential with lifetimes of 1.27 ms for [(Eu)**1**]hfa and 1.08 ms for [(Eu)**1**]bfa, and slightly lower lifetimes of 0.93 ms for [(Eu)**1**]phen and 0.71 ms for [(Eu)**1**]aza (see Table 5.1). Compared to these complexes, [(Eu)**1**]dbm has a relatively short lifetime of 0.38 ms (*vide infra*). These lifetimes are comparable to the lifetime of (Eu)**1** in methanol (0.80 ms).

By monitoring the early stages of the lanthanide luminescence, the process of energy transfer can be studied. During the time that the energy transfer from the antenna to the lanthanide ion is in progress, the lanthanide luminescence intensity is expected to rise with a rate equal to the rate of the energy transfer. In these measurements it was found that directly after the laser pulse, the ternary Eu^{3+} complexes exhibited emission from the $\text{Eu}^{3+} {}^5\text{D}_1$ state at 560 nm. This state decays with a time-constant in the order of microseconds (see Table 5.1), being converted non-radiatively into the ${}^5\text{D}_0$ state that is responsible for the typical Eu^{3+} emission observed in steady-state measurements (main emission at 615 nm), and radiatively to the ${}^7\text{F}_j$ manifold, *e.g.* the 530 nm emission. The rise-time of the ${}^5\text{D}_0$ emission was indeed in accordance with the decay time of the ${}^5\text{D}_1$ state. It is known in the literature that if the triplet energy level of the antenna is above the ${}^5\text{D}_1$ state of Eu^{3+} , then the ${}^5\text{D}_0$ state is populated primarily by non-radiative energy transfer from the ${}^5\text{D}_1$ state, with a decay time in the order of a few microseconds.²³

Discussion

The emission spectra and the mono-exponential lifetimes of the ternary complexes (except for [(Eu)**1**]hfa) prove that there is only one luminescent Eu^{3+} species in solution. In the emission spectrum of the [(Eu)**1**]hfa complex a shoulder was observed on the high energy side of the ${}^5\text{D}_0 \rightarrow {}^7\text{F}_0$ emission band at 579 nm, thus indicating a second luminescent Eu^{3+} species in solution. However, the two species have the same luminescence lifetime, and must therefore be very similar. Probably different conformations of the complex exist in solution that slowly interconvert on the luminescence timescale (see also chapter 3).

The differences in the luminescence quantum yields for the β -diketonate ternary complexes can be explained in terms of the antenna triplet state energies. Sato and Wada found that in Eu-tris(β -diketonate) complexes, the triplet energy level of the donating β -diketonate ligand should be approximately $2,000 \text{ cm}^{-1}$ above the ${}^5\text{D}_1$ level of Eu^{3+} (at $\sim 19,000 \text{ cm}^{-1}$) in order to obtain the highest luminescence quantum yields.² A larger energy difference

leads to a drop in the luminescence quantum yield, because the spectral overlap becomes smaller. On the other hand, a smaller energy difference reduces the quantum yield because of a thermally activated energy back-transfer process. For the hfa and bfa antenna chromophores the energy difference with the 5D_1 state is approximately 3,000 and 2,400 cm^{-1} , resulting in a slightly higher quantum yield for [(Eu)**1**]bfa than for [(Eu)**1**]hfa. In the case of [(Eu)**1**]dbm, the energy difference is only 1,600 cm^{-1} and the low luminescence quantum yield can be explained by a thermally activated energy back-transfer process. An indication for such an energy back-transfer process, is a reduced Eu^{3+} luminescence lifetime, since the Eu^{3+} luminescent state is depopulated by an additional process. As mentioned before, the [(Eu)**1**]dbm complex has indeed a much shorter lifetime of the 5D_0 and 5D_1 states than the other complexes. The luminescent 5D_0 state of [(Eu)**1**]dbm is depopulated via the 5D_1 state and subsequent energy back-transfer to the dbm antenna.

In other systems (the 2:1 complexes in acetonitrile) quantum yields of 0.41 and 0.67 have measured for the tetraazatriphenylene-sensitized Eu^{3+} and Tb^{3+} luminescence, respectively.¹² Compared to these systems, the sensitization process is less efficient in the [(Eu)**1**]aza complex ($\phi_{\text{SE}} = 0.07$). Also the quantum yield of the corresponding Tb^{3+} complex [(Tb)**1**]aza is moderate: 0.15. The phenanthroline antenna has the same coordinating moieties as tetraazatriphenylene, and [(Eu)**1**]phen has the same moderate sensitized luminescence quantum yield as [(Eu)**1**]aza.

The luminescence lifetimes of [(Eu)**1**]aza (0.73 ms), [(Tb)**1**]aza (2.08 ms), and [(Eu)**1**]phen (0.93 ms) are similar to the lifetimes of the ‘bare’ complexes in methanol (~0.80 ms, see chapter 3), and therefore deactivation processes of the lanthanide luminescent state are apparently not the problem. The effect of oxygen on the sensitized luminescence intensity gives an indication of the energy transfer rate. Dissolved oxygen may be competing with the lanthanide ion as an alternative acceptor of the excitation energy from the triplet, if the energy transfer rate is in the same order of magnitude as the oxygen quenching rate. Deoxygenation of the samples did not increase the sensitized luminescence intensity of both [(Eu)**1**]aza and [(Tb)**1**]aza, and therefore the energy transfer is fast and must exceed 10^7 s^{-1} .²⁴

It is possible, that although the *intrinsic* intersystem crossing quantum yield of tetraazatriphenylene and 1,10-phenanthroline is close to unity, this yield is smaller in the ternary complex due to a competing process. Based on the redox potentials of the *m*-terphenyl unit and the antenna chromophores this process may very well be a photon-induced electron transfer from the *m*-terphenyl unit of the ligand to the antenna. In this way the *m*-terphenyl

ligand also deactivates the singlet state, so that less triplet excited antenna species are formed from which the energy can be transferred to the lanthanide ion.

5.2.5 Luminescence of the calix[4]arene-based ternary complexes

The terphenyl-based ternary complexes described in the previous paragraph are negatively charged. For the use of these complexes as optically active dopants in polymers, e.g. polymeric optical amplifiers, neutral complexes are more desirable (see chapter 3). The calix[4]arene-based lanthanide complexes are positively charged and become neutral upon coordination of the β -diketonate antenna. The dbm antenna was chosen, because it allows excitation up to 400 nm.

Upon excitation at 300 nm of the calix[4]arene moiety of the precursor complex [(Eu)2]NO₃ in dichloromethane, the Eu³⁺ emission bands were observed corresponding to the ⁵D₀→⁷F_n transitions (see Figure 5.5). The hypersensitive ⁵D₀→⁷F₂ emission at 624 nm is dominating the spectrum. The excitation spectrum of [(Eu)2]NO₃ corresponds to the absorption spectrum of the calix[4]arene moiety and shows an additional small band at 393 nm, corresponding to the ⁷F₀→⁵L₆ transition of Eu³⁺.

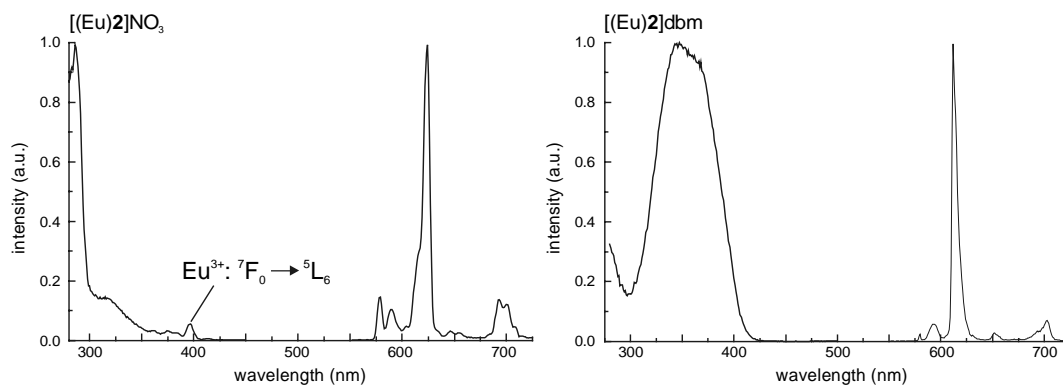


Figure 5.5: The excitation and emission spectra of [(Eu)2]NO₃ and [(Eu)2]dbm in dichloromethane. The spectra were taken with a spectral bandwidth of 1.0 nm.

Upon excitation at 360 nm of the antenna of [(Eu)2]dbm in dichloromethane, the Eu³⁺ emission bands are observed corresponding to the ⁵D₀→⁷F_n transitions (see Figure 5.5). As is the case for the *m*-terphenyl-based ternary β -diketonate complexes, the hypersensitive ⁵D₀→⁷F₂ emission is dominating the spectrum. Compared to the emission spectrum of [(Eu)2]NO₃, there is a clear reduction of the relative intensity of the ⁵D₀→⁷F₀ emission at 579

nm. The excitation spectrum of [(Eu)**2**]dbm corresponds to the absorption spectrum of the dbm antenna and proves that the Eu^{3+} ion is excited via the antenna. The luminescence quantum yield of [(Eu)**2**]dbm is very low, less than 0.01. This is even lower than that of the corresponding *m*-terphenyl-based complex [(Eu)**1**]dbm. Apparently, the energy back-transfer process is more efficient in [(Eu)**2**]dbm, which is in line with the extremely short luminescence lifetime of 0.087 ms. For comparison, the luminescence lifetime of the $\text{Eu}(\text{dbm})_3$ complex in an EPA²⁵ solution at room temperature is 0.15 ms with a luminescence quantum yield of approximately 0.01.²⁶

The near-infrared emitting ternary Nd^{3+} complex [(Nd)**2**]dbm in dichloromethane exhibits the typical line-like lanthanide emission upon excitation of the dbm antenna chromophore (see Figure 5.6). Emission bands at 880 (not shown), 1060, and 1330 nm ($^4\text{F}_{3/2} \rightarrow ^4\text{I}_{9/2}$, $^4\text{I}_{11/2}$, and $^4\text{I}_{13/2}$ transitions, respectively) are observed for [(Nd)**2**]dbm. As usual, the strongest emission is observed at 1060 nm.

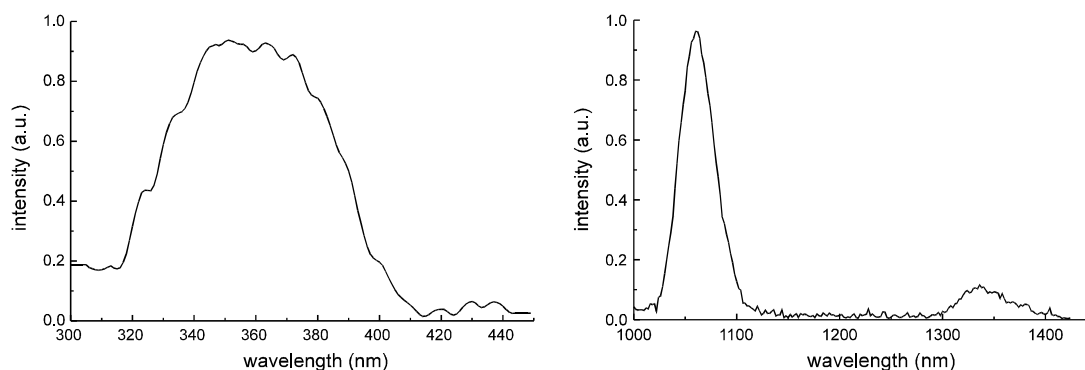


Figure 5.6: The excitation and emission spectra of [(Nd)**2**]dbm in dichloromethane (10^{-5} M).

5.3 Conclusion

By bringing the antenna chromophore in direct contact with the Eu^{3+} ion in the ternary complexes, the sensitization process has become more efficient compared to the triphenylene-functionalized Eu^{3+} complex described in chapter 4. However, the ternary complexes are intrinsically less stable and require antenna chromophores with strongly coordinating moieties, which limits the choice of antenna chromophores and the experimental conditions. In the case of the ternary β -diketonate complexes, the high sensitized Eu^{3+} luminescence quantum yields of 0.26 and 0.29 for [(Eu)**1**]hfa and [(Eu)**1**]bfa, respectively, outweigh their

limitations. The ternary complexes demonstrate that the efficiency of the energy transfer process is not only determined by the distance from the antenna to the lanthanide ion, but also by certain energetic requirements (energy back-transfer), and by the redox properties of the system (photon-induced electron transfer).

5.4 Experimental Section

5.4.1 Synthesis

General synthesis: See paragraph 3.4.1 of chapter 3 for a general description of the synthesis. Diester calix[4]arene **3** and tetraazatriphenylene were synthesized according to literature procedures.^{12,27} All reactions were carried out under an argon atmosphere. Standard workup involved washing the organic layers with water, drying over magnesium sulfate, filtration of the salts, and concentrating to dryness *in vacuo*.

25,27-Bis(*N,N*-dimethylcarbonylmethoxy)-5,11,17,23-tetrakis(1,1-dimethylethyl)-26,28-bis(ethoxycarbonylmethoxy) (4). To a mixture of **3** (2.0 g, 2.4 mmol) and K₂CO₃ (0.84 g, 6.1 mmol) in acetonitrile (100 mL) was added 2-chloro-*N,N*-dimethylacetamide (0.65 g, 5.4 mmol) and the mixture was refluxed for 14 h. Subsequently, the reaction mixture was allowed to cool down to room temperature, and was filtered. The filtrate was concentrated to dryness *in vacuo*. The residue was redissolved in CH₂Cl₂ (200 mL) and washed twice with 1 N HCl, followed by standard workup. The crude product was recrystallized from acetonitrile to give **4** as a white solid: yield 80%, m.p. 103-106 °C. ¹H NMR (CDCl₃): δ = 6.87 (s, 4H), 6.70 (s, 4H), 5.01-4.73 (m, 12H), 4.14 (q, 4H, *J* = 8.45 Hz), 3.23 (AB, 4H, *J* = 12.7 Hz), 3.07 (s, 6H), 2.98 (s, 6H), 1.28 (t, 6H, *J* = 8.4 Hz), 1.15 (s, 18H), 1.04 (s, 18H). ¹³C NMR (CDCl₃): δ = 170.6, 168.6, 153.5, 152.6, 144.9, 144.3, 133.5, 132.6, 126.0-124.0, 72.0, 70.8, 59.7, 36.0, 35.1, 33.2, 32.0-30.0, 13.5. MS (FAB): *m/z* = 991.9 [(M+H)⁺, calcd. 991.6]. Anal. calcd. for C₆₀H₈₂N₂O₁₀·0.40CH₃CN: C, 72.47, H, 8.32, N, 3.34. Found: C, 72.11, H, 8.07, N, 2.99 (the presence of CH₃CN in the sample was confirmed by the ¹H NMR spectrum of **4**, δ_{CH₃} = 1.98 ppm).

25,27-Bis(*N,N*-dimethylcarbonylmethoxy)-5,11,17,23-tetrakis(1,1-dimethylethyl)-26,28-bis(hydroxycarbonylmethoxy) ((H₂)2**).** A mixture of **4** (2.0 g, 2.4 mmol) and K₂CO₃ (0.84 g, 6.1 mmol) in a 5:1 methanol/water solution (100 mL) was refluxed for 2 h. Subsequently, the solvents were removed *in vacuo*. The residue was redissolved in CH₂Cl₂ (200 mL) and washed twice with 1 N HCl, followed by standard workup. The crude product was recrystallized from acetonitrile to give (H₂)**2** as a white solid: yield 95%, m.p. 248-250 °C. ¹H NMR (CDCl₃): δ = 7.14 (s, 4H), 6.63 (s, 4H), 4.80 (s, 4H), 4.67 (AB, 4H, *J* = 12.6 Hz), 4.64 (s, 4H), 3.30 (AB, 4H, *J* = 12.6 Hz), 3.03 (d, 12H, *J* = 4.2 Hz), 1.33 (s, 18H), 0.87 (s, 18H). ¹³C NMR (CDCl₃): δ = 169.2, 166.5, 151.7, 149.8, 145.5, 144.3, 132.9, 130.5, 124.3, 123.8, 71.7, 70.8, 35.1, 34.5, 32.9-32.0, 30.0-28.9. MS (FAB): *m/z* 935.6 [(M+H)⁺, calcd.: 935.5]. Anal. calcd. for C₅₆H₇₄N₂O₁₀: C, 71.92, H, 7.98, N, 3.00. Found: C, 71.85, H, 7.86, N, 3.14.

General procedure for the preparation of the [(Ln)2**]NO₃ complexes.** To a solution of 0.05 mmol of the bisacid (H₂)**2** and 0.20 mmol of Et₃N in methanol (20 mL) was added 0.07 mmol of the lanthanide nitrate salt. The resulting solution was stirred for 2 h, after which the solvent was evaporated. The complex was redissolved in CHCl₃ and washed twice with water, followed by standard workup. The [(Ln)**2**]NO₃ complexes were obtained as solids in quantitative yields. The complexes were characterized by FAB-MS spectrometry (see Table 5.2) and IR spectroscopy. The [(Ln)**2**]NO₃ complexes gave similar IR spectra: A peak at 1640-1630 cm⁻¹ (ν_{NC=O}) with a shoulder around 1590-1600 cm⁻¹ (ν_{COO}).

General procedure for the preparation of the calix[4]arene-based ternary complexes. The ternary complexes were prepared by stirring a dichloromethane solution (10 mL) of 0.030 mmol of the appropriate [(Ln)**2**]NO₃ complex, 0.030 mmol dbm, and 30 μL of a 1 M aqueous NBu₄OH solution for 1 h. Subsequently, dichloromethane was added (50 mL) and the organic layer was washed once with water, followed by standard workup. The ternary complexes were obtained as solids, and were characterized by FAB-MS spectroscopy (see Table 5.2) and IR spectroscopy. The ternary [(Ln)**2**]dbm complexes gave similar IR spectra: a peak at 1650-1640 cm⁻¹ (ν_{NC=O} and ν_{C=O,β-diketone}) and a peak at 1600 cm⁻¹ (ν_{COO}).

General procedure for the preparation of the *m*-terphenyl-based complexes. The ternary β-diketonate complexes were prepared by mixing a dichloromethane solution (10 mL)

of (Eu)**1** (30 mg, 0.026 mmol), 0.026 mmol of the appropriate β -diketone, and 27 μ L of a 1 M aqueous NBu_4OH solution. After stirring for 0.5 h, the solvent was removed *in vacuo*. The neutral azatriphenylene and phenanthroline ternary complexes were prepared in a similar way. The complexes were characterized by FAB-MS spectrometry (see Table 5.2) and IR spectroscopy. The IR spectra of the β -diketonate complexes show a peak at 1650-1640 cm^{-1} ($\nu_{\text{NC=O}}$ and $\nu_{\text{C=O},\beta\text{-diketone}}$), with a shoulder around 1610-1600 cm^{-1} (ν_{COO}), whereas the IR spectra of [(Ln)**1**]aza and [(Ln)**1**]phen show a peak at 1635-1630 cm^{-1} ($\nu_{\text{NC=O}}$) with a shoulder around 1590-1600 cm^{-1} (ν_{COO}).

Table 5.2: Mass spectra (FAB): A mixture of dithiothreitol and dithioerythritol (5:1 (v/v)), known as Magic Bullet was used as the matrix.

Complex	Measured m/z	Calcd. m/z
$\text{N}(\text{Bu})_4[(\text{Eu})\mathbf{1}]\text{hfa}$	1343.0 ($\text{M}-\text{N}(\text{Bu})_4^-$)	1343.4
$\text{N}(\text{Bu})_4[(\text{Eu})\mathbf{1}]\text{bfa}$	1351.3 ($\text{M}-\text{N}(\text{Bu})_4^-$)	1351.4
$\text{N}(\text{Bu})_4[(\text{Eu})\mathbf{1}]\text{dbm}$	1359.4 ($\text{M}-\text{N}(\text{Bu})_4^-$)	1359.4
[(Eu) 1]phen	1261.9 ($\text{M}-\text{CH}_2\text{COO}^+$)	1261.4
[(Eu) 1]aza	1371.0 ($\text{M}+\text{H}^+$)	1371.4
[(Tb) 1]aza	1377.4 ($\text{M}+\text{H}^+$)	1377.5
[(Eu) 2] NO_3	1085.1 ($\text{M}-\text{NO}_3^+$)	1085.4
[(Eu) 2]dbm	1331.5 ($\text{M}+\text{Na}^+$)	1331.5
[(Nd) 2] NO_3	1076.5 ($\text{M}-\text{NO}_3^+$)	1076.4
[(Nd) 2]dbm	1322.4 ($\text{M}+\text{Na}^+$)	1322.5

5.4.2 Photophysical studies

Steady-state luminescence measurements were performed with a Photon Technology International (PTI) Alphascan spectrofluorimeter (see paragraph 3.4.2 of chapter 3) or an Edinburgh FS900 spectrofluorimeter. In the Edinburgh FS900 spectrofluorimeter, the samples were excited by a 450 W xenon lamp followed by a single monochromator. The emitted light was detected at an angle of 90° by a Hamamatsu R928 photomultiplier, and subsequently fed to a photon-counting interface.

The luminescence lifetimes were measured using pulsed laser excitation of the complexes with an LTB MSG 400 nitrogen laser ($\lambda_{\text{exc.}}$ 337 nm) and a streak camera system (Hamamatsu) as the detector to simultaneously probe wavelength and time-dependence of the luminescence

signals in the millisecond and microsecond domain. The streak images containing the luminescence decay curves could be fitted with mono-exponential functions. The absorptions of the solutions were typically 0.1 at the excitation wavelength. The solvents were of spectroscopical grade. Deaeration of the samples was performed by purging the solutions with argon for a duration of 10 minutes.

5.4.3 Molecular mechanics calculations

See paragraph 3.4.3 of chapter 3 for a description of the molecular mechanics calculations.

5.5 References and Notes

1. (a) Gschneider, K. A.; Eyring, L. R. *Handbook on the Physics and Chemistry of Rare Earths*, North Holland Publishing Company, Amsterdam, **1979**. (b) Sabbatini, N.; Guardigli, M.; Lehn, J.-M. *Coord. Chem. Rev.* **1993**, *123*, 201, and references cited therein.
2. Sato, S.; Wada, M. *Bull. Chem. Soc. Jpn.* **1970**, *43*, 1955.
3. Crosby, G. A.; Whan, R. E.; Alire, R. M. *J. Chem. Phys.* **1961**, *34*, 743.
4. Tanaka, M.; Yamaguchi, G.; Shiokawa, J.; Yamanaka, C. *Bull. Chem. Soc. Jpn.* **1970**, *43*, 549.
5. Haynes, A. V.; Drickamer, H. G. *J. Chem. Phys.* **1982**, *76*, 114.
6. Dexter, D. L. *J. Chem. Phys.* **1953**, *21*, 836.
7. Weissman, S. I. *J. Chem. Phys.* **1942**, *10*, 214.
8. Filipescu, N.; Sager, W. F.; Serafin, F. A. *J. Phys. Chem.* **1964**, *68*, 3324.
9. Frey, S. T.; Gong, M. L.; Horrocks, Jr., W. DeW. *Inorg. Chem.* **1994**, *33*, 3229.
10. fod = 6,6,7,7,8,8,8-heptafluoro-2,2-dimethyloctane-3,5-dione; Michler's ketone = 4,4'-bis(*N,N*-dimethylamino)benzophenone.
11. Werts, M. H. V.; Duin, M. A.; Hofstraat, J. W.; Verhoeven, J. W. *Chem. Commun.* **1999**, 799.
12. van der Tol, E. B.; van Ramesdonk, H. J.; Verhoeven, J. W.; Steemers, F. J.; Kerver, E. G.; Verboom, W.; Reinhoudt, D. N. *Chem. Eur. J.* **1998**, *4*, 2315.
13. Steemers, F. J.; Verboom, W.; Hofstraat, J. W.; Geurts, F. A. J.; Reinhoudt, D. N.

- Tetrahedron Lett.* **1998**, *39*, 7583.
14. Rudkevich, D. M.; Verboom, W.; van der Tol, E. B.; van Staveren, C.; Kaspersen, F.; Verhoeven, J. W.; Reinhoudt, D. N. *J. Chem. Soc., Perkin Trans. 2* **1995**, 131.
 15. Steemers, F. J.; Verboom, W.; Reinhoudt, D. N.; van der Tol, E. B.; Verhoeven, J. W. *J. Am. Chem. Soc.* **1995**, *117*, 9408.
 16. (a) Brooks, B. R.; Bruccoleri, R. E.; Olafsen, B. D.; States, D. J.; Swaminathan, S.; Karplus, M. *J. Comput. Chem.* **1983**, *4*, 187. (b) Momany, F. A.; Klimkowski, V. J.; Schäfer, L. *J. Comput. Chem.* **1990**, *11*, 654. (c) Momany, F. A.; Rone, R.; Kunz, H.; Frey, R. F.; Newton, S. Q.; Schäfer, L. *J. Mol. Structure* **1993**, *286*, 1.
 17. Frey, S. T.; Horrocks Jr., W. DeW. *Inorg. Chim. Acta.* **1995**, *229*, 383.
 18. To 2.5 mL of a 1.05×10^{-5} M solution of tetraazatriphenylene in CH_2Cl_2 , 25 μL aliquots of a (Eu)**1** solution (5.2×10^{-4} M) were added.
 19. To 2.6 mL of a 3.05×10^{-5} M solution of (deprotonated) bfa in CH_2Cl_2 , 25 μL aliquots of a (Eu)**1** solution (5.08×10^{-4} M) were added. The bfa stock solution was prepared by mixing in CH_2Cl_2 (10 mL), bfa (13.18 mg, 6.10×10^{-2} mmol) with 120 μL (1.2×10^{-2} mmol) of a 1 M aqueous solution of Bu_4NOH . The solvents were removed *in vacuo*, subsequently dichloromethane was added (10 mL) and the mixture was concentrated to dryness. This was repeated twice. Finally, the deprotonated bfa antenna was redissolved in CH_2Cl_2 to a concentration of 3.05×10^{-5} M.
 20. Murov, S. L.; Carmichael, I.; Hug, G. L. *Handbook of photochemistry, 2nd Ed.*, Marcel Dekker, New York, **1993**.
 21. (a) Kirby, A. F.; Foster, D.; Richardson, F. S. *Chem. Phys. Lett.* **1983**, *95*, 507. (b) Kirby, A. F.; Richardson, F. S. *J. Phys. Chem.* **1983**, *87*, 2544.
 22. Demas, N. J.; Crosby, G. A. *J. Phys. Chem.* **1971**, *75*, 991.
 23. Tanaka, M.; Yamaguchi, G.; Shiokawa, J.; Yamanaka, C. *Bull. Chem. Soc. Jpn.* **1970**, *43*, 549.
 24. The competing oxygen quenching rate is equal to the product of the diffusion-controlled quenching rate constant and the oxygen concentration ($k_{\text{diff}}[\text{O}_2]$); k_{diff} is taken as $10^{10} \text{ M}^{-1} \text{ s}^{-1}$, $[\text{O}_2]$ in dichloromethane is 2.2 mM (ref. 20). Since $k_{\text{ox}} = k_{\text{diff}}[\text{O}_2] = 2 \times 10^7 \text{ s}^{-1}$, and there is no oxygen effect: $k_{\text{ET}} > k_{\text{ox}}$, which means that k_{ET} exceeds 10^7 s^{-1} .
 25. EPA = 5:5:2 (v/v) ether/isopentane/ethanol

26. Bhaumik, M. L. *J. Chem. Phys.* **1964**, *40*, 3711.
27. Collins, E. M.; McKervey, M. A. Madigan, E.; Moran, M. B.; Owens, M.; Ferguson, G.; Harris, S. J. *J. Chem. Soc., Perkin Trans. 1* **1991**, 3137.

Chapter 6

Fluorescent Dyes as Sensitizers for Near- Infrared Nd³⁺ Emission

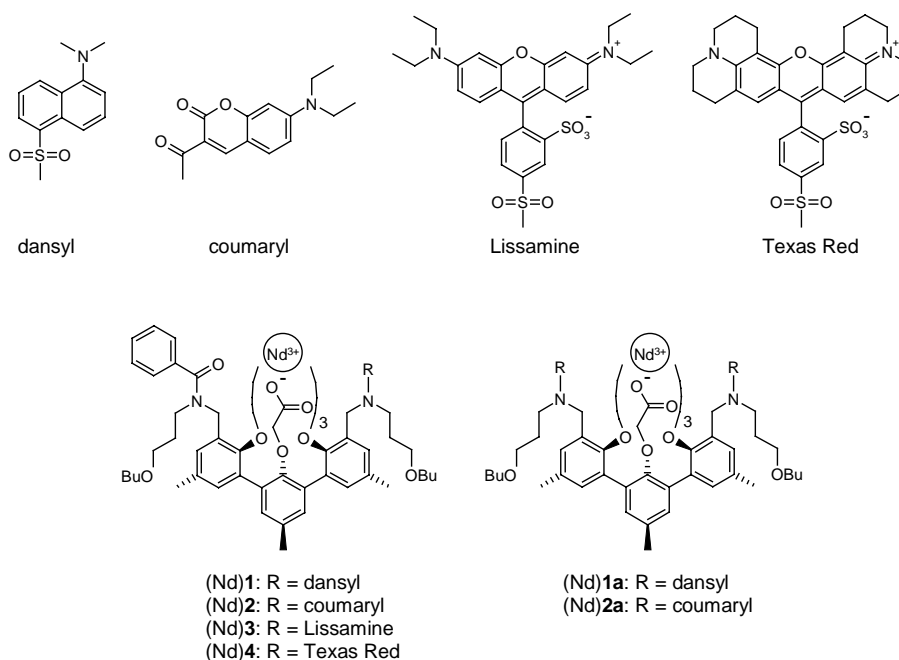
6.1 Introduction

As was outlined in the previous chapters, organic complexes of the trivalent lanthanide ions Nd³⁺ and Er³⁺ exhibit near-infrared luminescence at wavelengths (at 1330 nm and 1550 nm, respectively) that are of interest for applications in optical telecommunication networks. The ultimate goal of this research is the development of polymeric optical amplifiers based on these organic lanthanide complexes. The advantage of polymer-based optical amplifiers is that they can be integrated into existing polymeric optical components such as splitters, switches, and multiplexers.¹ For such an application, an efficient population of the lanthanide luminescent state is required, which can be achieved by the incorporation of an antenna chromophore into the lanthanide complex. The preferable excitation window of these antenna-functionalized lanthanide complexes should be in the visible region around 530 nm, which would allow the use of green diode lasers as excitation sources. Green diode laser systems are very compact and available at relatively low costs.

The population of the lanthanide luminescent state via an organic antenna chromophore with a much higher extinction coefficient is a well established strategy to overcome the intrinsically low absorption coefficients of lanthanide ions.^{2,3} Upon excitation of the antenna into its singlet excited state and subsequent intersystem crossing to its triplet state, the energy is transferred from the triplet state to the lanthanide ion. The excitation window of the antenna chromophore is limited by the energetic constraints imposed by the photophysics of sensitized lanthanide luminescence (see Chapter 2). As a result, the energy of the antenna singlet excited state, and thus the excitation window is limited to the region that is at least $5,000\text{ cm}^{-1}$ higher in energy than the lanthanide luminescent state.⁴ For example, the excitation window of the visible light emitting Eu^{3+} and Tb^{3+} complexes is limited to the near-UV region.⁴ The near-infrared luminescent lanthanide ions Nd^{3+} , Yb^{3+} , and Er^{3+} , have much lower lying luminescent states, and by applying the same energetic considerations it follows that in principle these lanthanide ions can be excited via antenna chromophores that have absorption bands in the visible spectral region up to approximately 500-600 nm.

As was mentioned before, a key step in the sensitization process is the intersystem crossing from the antenna singlet excited state to the triplet state.⁵ Although some of the first sensitizers for Nd^{3+} , Er^{3+} , and Yb^{3+} luminescence, such as β -diketonates^{6,7} and triphenylene^{8,9} (see also chapters 4 and 5) have the desired high intersystem crossing yields, a drawback of these sensitizers is that they require near-UV excitation and that they have relatively high lying triplet energy levels. The energy difference between the triplet state of these sensitizers and the lanthanide luminescent state is approximately $10,000\text{ cm}^{-1}$. A few sensitizers for Nd^{3+} , Er^{3+} , and Yb^{3+} have been reported that allow visible light excitation. Among them are porphyrins,¹⁰ the triphenylmethane derivative xylene orange,¹¹ and the xanthene dyes eosin and fluorescein.¹² These sensitizers have broad absorption bands in the visible region with high absorption coefficients. Werts *et al.* have incorporated eosin and fluorescein into a DTPA (diethylenetriaminepentaacetic acid) ligand and the corresponding Nd^{3+} , Er^{3+} , and Yb^{3+} complexes exhibited sensitized near-infrared luminescence in D_2O .¹² The main pathway of the energy transfer process proceeds via the eosin and fluorescein triplet states, as could be concluded from the oxygen dependence of the sensitized lanthanide emission intensity. Whereas eosin is known as a triplet sensitizer with an intersystem crossing yield of 0.33, fluorescein is strongly fluorescent ($\phi_{\text{flu}} = 0.97$) and has a low intersystem crossing yield of 0.02.¹³ It was therefore surprising that fluorescein also sensitizes the luminescence of Nd^{3+} , Er^{3+} , and Yb^{3+} . Recently, Oude Wolbers *et al.* have covalently functionalized a calix[4]arene-

based ionophore with a fluorescein moiety.¹⁴ The resulting Nd³⁺ and Yb³⁺ complexes exhibited near-infrared luminescence in organic solutions (DMSO-*h*₆ and methanol-*d*₄) upon excitation of the fluorescein antenna. Upon closer examination of the antenna properties, it was found that the fluorescence of the fluorescein moiety in the complex was reduced considerably compared to that of the free ligand. This indicates the presence of an *external heavy atom effect*¹⁵ induced by the lanthanide ion. Such an effect increases the intersystem crossing rate of the antenna chromophore, which enhances the overall efficiency of the sensitization process.

Chart 6.1


The research described in this chapter is focussed on the application of fluorescent dyes as photosensitizers for Nd³⁺ luminescence. The incorporated dyes dansyl, coumaryl, Lissamine, and Texas Red (see Chart 6.1) have intense absorption bands in the visible region with triplet states that are high enough in energy to populate the Nd³⁺ luminescent state (the ⁴F_{3/2} state), which has an energy of 11,400 cm⁻¹ (see Figure 6.1). Lissamine and Texas Red have broad absorption bands in the visible region that enable excitation with a green diode laser, *i.e.* at 530 nm. These dyes are known for their excellent fluorescence properties with high fluorescence quantum yields, and therefore have low intersystem crossing yields (ϕ_{isc} is typically less than 0.02).^{13,16} At first sight, this would make them less perfect candidates as antenna chromophores for the sensitization of lanthanide ions. However, it has been shown

that the complexed lanthanide ion can increase the intersystem crossing rate of the antenna chromophore by an *external heavy atom effect*.¹⁵

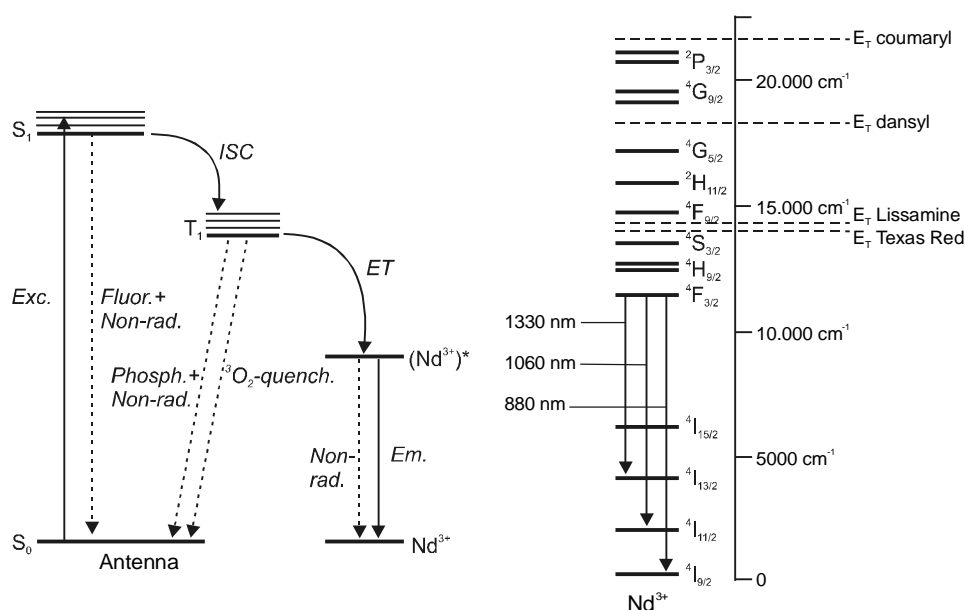


Figure 6.1: Photophysical model that describes the sensitization process (left). Upon excitation of the antenna chromophore into its singlet excited state, intersystem crossing takes place to the triplet state, which is followed by energy transfer to the 4f states of the Nd³⁺ ion, and subsequent emission. A detailed scheme of the 4f energy levels of Nd³⁺ as well as the approximate triplet energies of the incorporated dyes^{13,16,17} is depicted on the right.

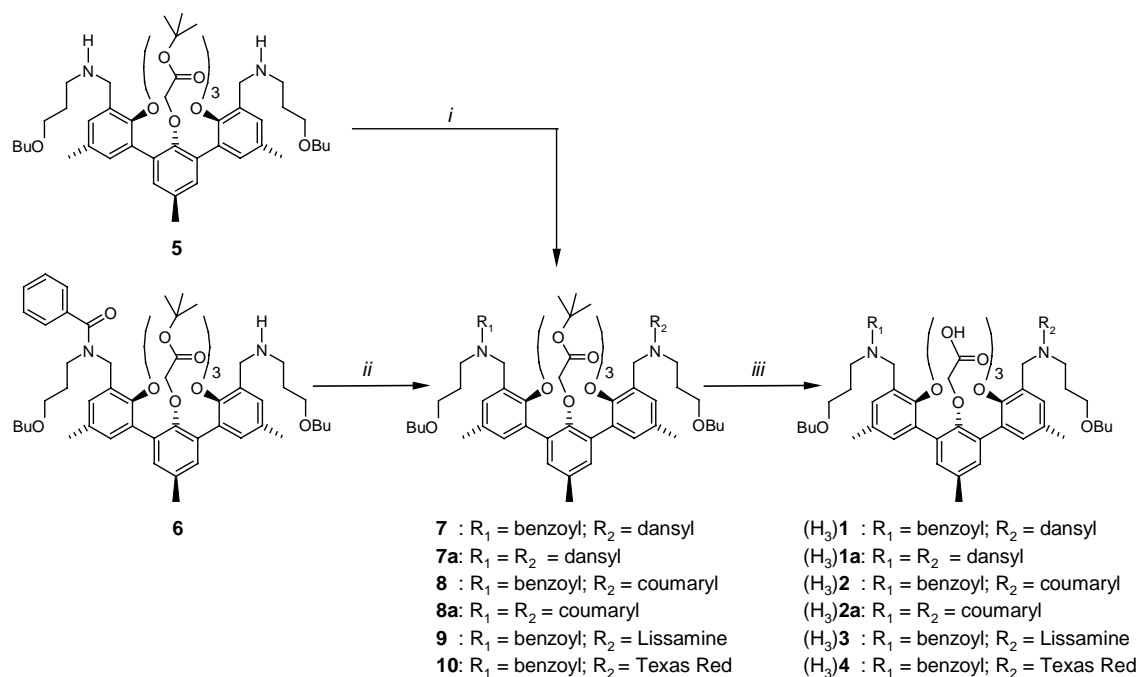
The photophysical properties of these dye-functionalized Nd³⁺ complexes have been investigated, in particular the sensitized Nd³⁺ emission and the antenna fluorescence. Furthermore, the luminescence characteristics of complexes bearing two antenna chromophores instead of only one, namely (Nd)**1a** and (Nd)**2a** (see Chart 6.1), have also been studied. These complexes have been synthesized in order to investigate whether the incorporation of an additional antenna chromophore improves the efficiency of the sensitization process.

6.2 Results and Discussion

6.2.1 Synthesis

In chapters 3 and 4, a synthesis route has been described that allows easy (mono-) functionalization of the *m*-terphenyl ligands with antenna chromophores that bear a carboxylic acid or a sulfonyl chloride moiety. The synthesis of the dye-functionalized ligands was carried out accordingly as is depicted in Scheme 6.1. The triacid dye-functionalized ligands were synthesized starting from the bis(amine) terphenyl **5** or mono(amide) terphenyl **6**.

Scheme 6.1



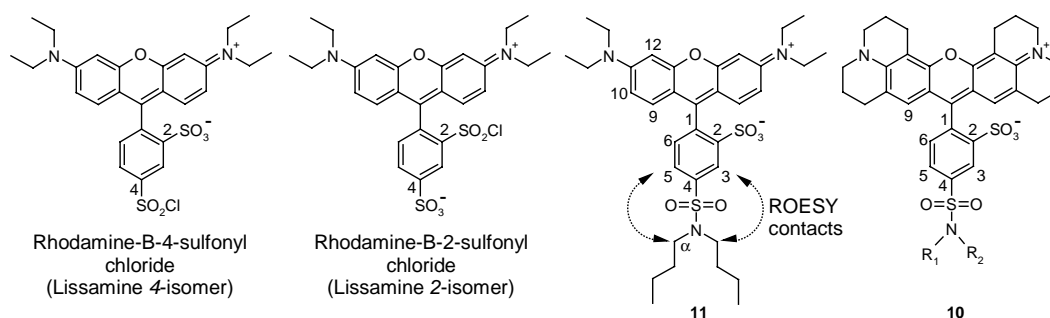
Reagents and conditions: i) Dansyl chloride, Et₃N, CH₂Cl₂, rt; or 7-diethylaminocoumarin-3-acetic acid, EDC, DMAP, CH₂Cl₂, rt; ii) Appropriate sulfonyl chloride, Et₃N, CH₂Cl₂, rt; or 7-diethylaminocoumarin-3-acetic acid, EDC, DMAP, CH₂Cl₂, rt; iii) TFA.

Dansyl chloride was reacted with **6** or **5** to give the mono(dansyl) triester **7** and bis(dansyl) triester **7a** after flash column chromatography in 60 % and 80 % isolated yield, respectively. The ¹H NMR spectra of **7** and **7a** show four doublets and one multiplet in the region from 8.6 to 7.1 ppm for the protons of the dansyl moiety with a correct integral ratio compared to the signals of the benzylic protons (4H) of the terphenyl moiety. The coumaryl triesters **8** and **8a**

were synthesized by a DMAP (4-dimethylaminopyridine) catalyzed EDC (1-(3-dimethylaminopropyl)3-ethylcarbodiimide) coupling of 7-dimethylamino-coumarin-3-acetic acid and **6** or **5** in CH_2Cl_2 . The coumaryl triester **8** was isolated after preparative thin layer chromatography in 52 % yield and the bis(coumaryl) triester **8a** was isolated after flash column chromatography in 48 % yield. Formation of the amide bond was evident from the ^1H NMR spectra of these compounds. The ^1H NMR spectrum of the mono-functionalized compound **8** shows additional multiplet signals in the region around 5 ppm (compared to the ^1H NMR spectrum of **6**) corresponding to two benzylic protons of the newly formed amide moiety. In the ^1H NMR spectrum of the bis-functionalized compound **8a** multiplet signals around 5 ppm are present corresponding to four benzylic protons of the two amide moieties.

The terphenyl triester ligands functionalized with the Rhodamine-B derivatives Lissamine and Texas Red were synthesized by reacting mono(amide) terphenyl **6** with the commercially available sulfonyl chloride isomer mixtures of the appropriate dye.

Chart 6.2



*Chemical structures of the Rhodamine-B derivatives Rhodamine-B-4-sulfonyl chloride, Rhodamine-B-2-sulfonyl chloride, dibutyl Lissamine **11**, and the Texas Red moiety of **10**. The observed ROESY contacts (400 MHz) are indicated in the structure of **11**.*

Compound **11** was synthesized as a reference compound from di-*n*-butylamine and the Lissamine isomer mixture (see Chart 6.2) in CH_2Cl_2 in the presence of Et_3N as a base. One of the possible isomers (the 4- or the 2-isomer) of **11** was isolated after preparative thin layer chromatography in 40 % yield. The ^1H NMR spectrum of the isolated product **11** shows one set of signals for the Lissamine moiety (see Table 6.1), indicating that it is one compound and not a mixture of isomers. The assignment of the peaks was verified by a 2D-COSY¹⁸ experiment. The 2D-ROESY¹⁹ spectrum of **11** shows contacts between the α -protons of the

di-*n*-butyl tail and the H3 and H5 protons of the Lissamine moiety (see Chart 6.2), proving that the isolated product **11** is the 4-isomer.

Table 6.1: Selected ¹H NMR data (300 MHz) of the compounds **9**, **10**, and **11** in CDCl₃ (see also Chart 6.2).

Compound	H3	H5	H10	H12
Lissamine triester 9	8.85 (s)	8.00 (d, <i>J</i> = 8.5 Hz)	6.81 (d, <i>J</i> = 8.5 Hz)	6.69 (s)
Texas Red triester 10	8.81 (s)	7.90 (d, <i>J</i> = 7.8 Hz)	n.a.	n.a.
Dibutyl Lissamine 11	8.74 (s)	7.91 (d, <i>J</i> = 8.0 Hz)	6.77 (d, <i>J</i> = 8.0 Hz)	6.66 (s)

Mono(amide) **6** was reacted with 2 equivalents of the Lissamine isomer mixture, and only one of the two possible isomers (the 2-isomer or the 4-isomer) of Lissamine triester **9** was isolated in 44% yield. The coupling of the dye was confirmed by mass spectrometry (FAB): the spectrum shows an intense peak at 1618.8 that can be attributed to (M+H)⁺. The ¹H NMR spectrum of triester **9** shows one set of signals for the protons of the Lissamine moiety (see Table 6.1) that is nearly identical to that of dibutyl Lissamine **11**, indicating that the sulfonamide moiety of triester **9** is at the same position of the Lissamine phenyl ring as the sulfonamide moiety of **11**. For the synthesis of the Texas Red triester **10**, mono(amide) terphenyl **6** was reacted with 2 equivalents of the Texas Red sulfonyl chloride isomer mixture, resulting in an isolated yield of **10** of 46% after preparative thin layer chromatography. The ¹H NMR spectrum of triester **10** shows one set of signals for the protons of the Texas Red moiety (see Table 6.1), and the chemical shifts of the H3 and H5 protons are almost identical to the chemical shifts of the corresponding protons of Lissamine triester **9** and dibutyl Lissamine **11**. This shows that the isolated Texas Red triester **10** is also the 4-isomer.

Mild hydrolysis of the *tert*-butyl esters of the compounds **7-10** with trifluoroacetic acid at room temperature gave the corresponding triacid ligands in nearly quantitative yields. The corresponding Nd³⁺ complexes were prepared at room temperature by addition of a solution of Nd(NO₃)₃ in methanol to a solution of the appropriate ligand in methanol in the presence of Et₃N as a base. Mass spectrometry (FAB) showed that the complexes had the expected 1:1 stoichiometry (see Experimental Section). The IR spectra of the complexes (except for (Nd)**1a**) show an intense peak around 1630 cm⁻¹ corresponding to the amide carbonyl, with a shoulder around 1600 cm⁻¹, indicating that the carboxylic acids are deprotonated. The spectra

of (Nd)**1**, (Nd)**1a**, (Nd)**3**, and (Nd)**4** further show peaks around 1330 and 1160 cm^{-1} corresponding to the sulfonamides.

6.2.2 Molecular dynamics studies

The structure of the complexes (Nd)**1**, (Nd)**2**, (Nd)**3**, and (Nd)**4** were minimized in the gas phase and subjected to molecular dynamics simulations (500 ps) in a cubic box of OPLS DMSO²⁰ using the CHARMM force field.²¹ The simulations show that the lanthanide ion is coordinated by the eight oxygen donor atoms provided by the ligand: three bidentate oxyacetate moieties, in addition to one sulfonamide oxygen and one amide oxygen ((Nd)**1**, (Nd)**3**, and (Nd)**4**), or two amide oxygens ((Nd)**2**). One DMSO molecule occupies the ninth coordination site of the Nd^{3+} ion. The average distances from the sensitizer to the Nd^{3+} ion in the different complexes are tabulated in Table 6.2. The mechanism by which the energy is transferred from the antenna to the lanthanide ion is generally accepted to be an electron-exchange mechanism.²² In view of this mechanism, the distance of the Lissamine or Texas Red moiety to the lanthanide ion is relatively large. Strictly, an electron-exchange (Dexter) mechanism is only efficient at distances shorter than 5 Å, but Dexter has shown that energy transfer can still take place at distances of up to 10 Å.²²

Table 6.2: Approximate distances from the antenna chromophore to the complexed Nd^{3+} ion in the different complexes obtained from the molecular dynamics simulations in a box of OPLS DMSO.

Complex	Distance (Å)	Complex	Distance (Å)
(Nd) 1	5	(Nd) 3	10 ^a
(Nd) 2	5	(Nd) 4	10 ^a

^aAverage distance from the Nd^{3+} ion to the center of the xanthene moiety

6.2.3 Photophysical properties of the mono-dye-functionalized complexes

Sensitized Nd^{3+} luminescence

The incorporated fluorescent dyes have broad and intense absorption bands ranging from the near-UV to the visible region of the electromagnetic spectrum: dansyl has an absorption maximum at 345 nm ($\epsilon = 4.2 \times 10^3 \text{ M}^{-1}\text{cm}^{-1}$), coumaryl at 400 nm ($\epsilon = 2.2 \times 10^4 \text{ M}^{-1}\text{cm}^{-1}$), and the Rhodamine-B derivatives Lissamine and Texas Red at 568 nm ($\epsilon = 8.8 \times 10^4 \text{ M}^{-1}\text{cm}^{-1}$) and 590 nm ($\epsilon = 8.5 \times 10^4 \text{ M}^{-1}\text{cm}^{-1}$), respectively. Upon excitation of the antenna chromophores of the four mono-functionalized complexes (Nd)**1** to (Nd)**4** in DMSO-*d*₆, the

characteristic emission bands of Nd³⁺ are observed at 880, 1060, and 1330 nm. The intense emission band at 1060 nm corresponds to the $^4F_{3/2} \rightarrow ^4I_{11/2}$ transition, and constitutes of approximately 60% of the total emission intensity. The two weaker emission bands at 880 nm and at 1330 nm correspond to the $^4F_{3/2} \rightarrow ^4I_{9/2}$ and $^4F_{3/2} \rightarrow ^4I_{13/2}$ transitions, respectively. The excitation spectra of the complexes were recorded by monitoring the intensity of 1060 nm emission band as a function of the excitation wavelength. The resulting excitation spectra closely resemble the absorption spectra of the incorporated antenna chromophores (see Figure 6.2), and prove that excitation of the antenna is the main photophysical pathway leading to Nd³⁺ luminescence. It can furthermore be seen from Figure 6.2 that excitation of the Lissamine and Texas Red antenna chromophores at 530 nm, which would be the wavelength of a green diode laser, indeed results in sensitized Nd³⁺ luminescence.

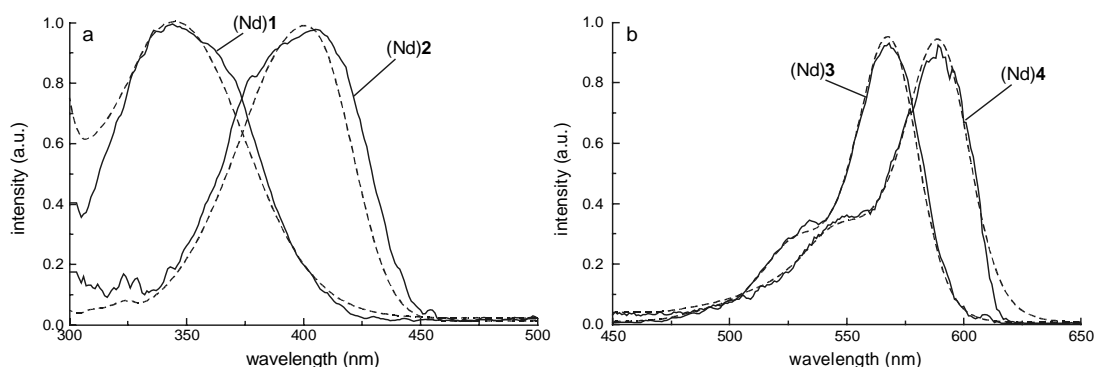


Figure 6.2: Normalized excitation spectra (solid lines) of the dye-functionalized complexes (Nd)**1** and (Nd)**2** (a) and (Nd)**3** and (Nd)**4** (b) in DMSO-*d*₆ while monitoring the intensity of the 1060 emission of Nd³⁺, as well as the normalized absorption spectra of the dyes (dashed lines).

These steady state luminescence spectra were taken of dilute solutions of the complexes (10^{-5} - 10^{-6} M), and demonstrate the effectiveness of using energy transfer for the population of the Nd³⁺ luminescent state. Direct excitation of the complexed Nd³⁺ ions would require concentrations of the samples of up to 1.0 M in order to observe any Nd³⁺ luminescence in solution^{23,24} as a result of the low absorption coefficients of the intra-4f transitions which are typically less than $10 \text{ M}^{-1}\text{cm}^{-1}$.² Furthermore, these low concentrations avoid the possible aggregation of the complexes since especially Rhodamine-B dyes tend to form dimers at higher concentrations.²⁵ The absence of such aggregation under the experimental conditions was confirmed by the fact that the sensitized Nd³⁺ emission intensity of the (Nd)**3** and (Nd)**4**

complexes increased linearly with increasing absorbance of the samples up to an absorbance of 0.6 at the excitation wavelength.

In order to probe which dye is the most efficient sensitizer for Nd^{3+} , the emission intensities of the various dye-functionalized Nd^{3+} complexes were compared as follows: dilute oxygenated $\text{DMSO}-d_6$ solutions were used and the complexes were excited into the absorption maxima of the incorporated dyes (see also Table 6.3). Furthermore, corrections were made for the absorbances of the samples (which were typically around 0.3) and differences in the excitation intensity as a function of the wavelength employing Rhodamine-B as a quantum counter. Under these conditions the emission intensities are proportional to the quantum yields of sensitized emission. The sensitized emission intensities of the dye-functionalized Nd^{3+} complexes are depicted in Figure 6.3 and show that in this series of fluorescent dyes dansyl is the most efficient sensitizer, followed by both Rhodamine-B derivatives Lissamine and Texas Red, and that coumaryl is the least efficient sensitizer (see also Table 6.3).

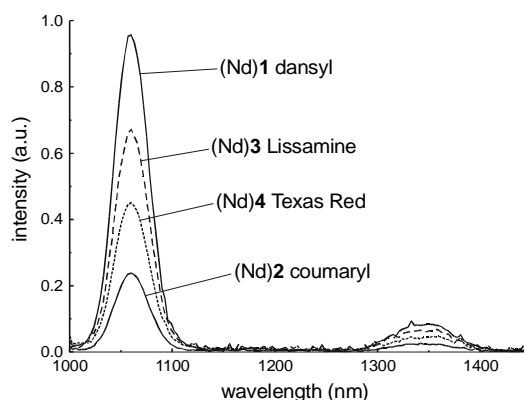


Figure 6.3: Sensitized Nd^{3+} luminescence intensities of the different dye-functionalized Nd^{3+} complexes in $\text{DMSO}-d_6$ upon excitation into the absorption maxima of the incorporated dyes. The spectra have been corrected for the differences in the excitation intensity (see main text).

The quantum yield of the sensitized emission depends on the photophysical properties of the dyes (in particular the triplet state energy and intersystem crossing rate), the distance between the dye and the lanthanide ion, and the photophysical properties of the lanthanide ion. In general, the quantum yield of sensitized emission (ϕ_{SE}) is the product of the triplet quantum yield (ϕ_{ISC}), the energy transfer quantum yield (ϕ_{ET}), and the intrinsic luminescence quantum yield of the lanthanide ion (ϕ_{lum}), hence:

$$\Phi_{SE} = \Phi_{ISC} \cdot \Phi_{ET} \cdot \Phi_{lum} \quad (1)$$

The intrinsic luminescence quantum yield of the complexed Nd³⁺ ions in the different complexes can be compared by measuring the luminescence lifetimes τ , that are directly related to Φ_{lum} via:

$$\Phi_{lum} = k_{rad} \cdot \tau \quad (2)$$

where k_{rad} is the radiative rate of the Nd³⁺ emission, which is likely to be nearly identical for the Nd³⁺ ions in the different complexes.

Luminescence lifetimes

The luminescence lifetimes of the complexes in DMSO-*d*₆ upon laser excitation at 337 nm are equal within the experimental error: around 2.20 μ s (see Table 6.2). These luminescence lifetimes are in line with the lifetimes of the *m*-terphenyl-based Nd³⁺ complexes described in Chapter 3, and the recently reported lifetime of Nd(OAc)₃ of 2.33 μ s in DMSO-*d*₆.²³ The energy gap between the lowest excited state (⁴F_{3/2}) and the highest ground state (⁴I_{7/2}) of Nd³⁺ is relatively small ($\Delta E \approx 5,300 \text{ cm}^{-1}$), and non-radiative deactivation of the Nd³⁺ excited state by the first overtone of the C-H vibration, which has vibrational quanta of 2950 cm^{-1} , is therefore very efficient. Previous work has indeed shown that non-radiative deactivation of the Nd³⁺ luminescent state by high-frequency oscillators such as the C-H vibration of the ligands is the dominating deactivation process (see chapter 3).

Table 6.3: Sensitized emission intensity relative to the emission of (Nd)I and luminescence lifetimes of the four different dye-functionalized complexes in DMSO-*d*₆.

Complex	Antenna $\epsilon \text{ M}^{-1}\text{cm}^{-1}$ (λ_{max})	Sensitized emission Intensities ^a	τ_{Nd} (μ s) ^b
(Nd)1	4.2×10^3 (345 nm)	1.0	2.21
(Nd)2	2.2×10^4 (400 nm)	0.29	2.16
(Nd)3	8.8×10^4 (568 nm)	0.75	2.21
(Nd)4	8.5×10^4 (590 nm)	0.53	2.26

^aIntensities of the 1060 and 1330 nm emission bands relative to (Nd)I. ^b λ_{exc} . 337 nm; λ_{em} .1060 nm; error $\approx 10\%$

Since the measured luminescence lifetimes are identical within the experimental error, also ϕ_{lum} is nearly identical for the four complexes. The differences in sensitized emission intensity of the four dye-functionalized complexes are therefore caused by differences in the intersystem crossing process (ϕ_{ISC}) and the energy transfer process (ϕ_{ET}).

Oxygen dependence of the sensitized emission

The effect of oxygen on the sensitized luminescence intensity gives an indication of the energy transfer rate, because oxygen may compete with the lanthanide ion as the acceptor for the excitation energy, resulting in less sensitized lanthanide luminescence. Whereas for most of the complexes no oxygen effect was observed upon deoxygenation of the samples, the luminescence intensity of (Nd)2 was oxygen dependent (an increase of 20% upon deoxygenation of the solvent). This indicates that the transfer of excitation energy from the coumaryl antenna to the Nd^{3+} ion is slower than for the other antenna chromophores.

Antenna fluorescence

The antenna processes that are competing with intersystem crossing from the singlet state to the triplet state, are fluorescence and non-radiative decay (see Figure 6.1).

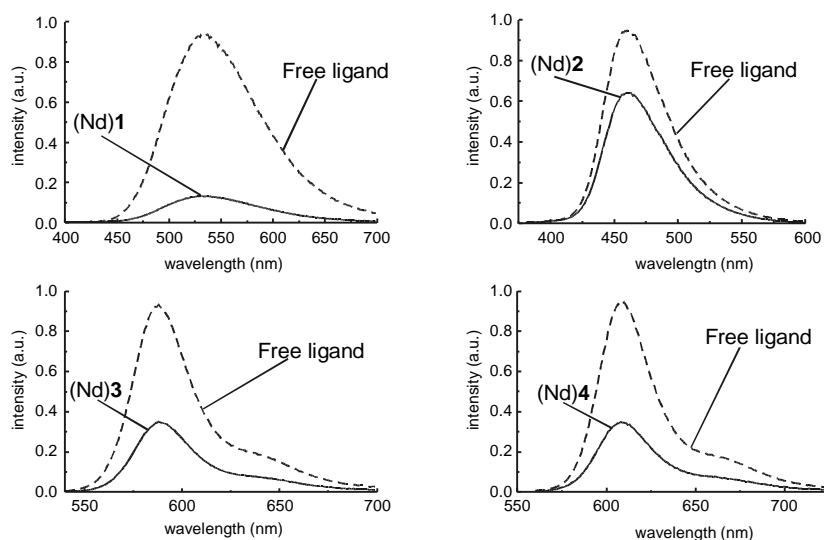


Figure 6.4: The antenna fluorescence intensities of the complexes relative to the antenna fluorescence intensities of the free ligands in DMSO.

The shape and the emission maxima of the fluorescence spectra of the antenna moieties in the complexes and in the free ligands are similar, indicating that the complexed Nd³⁺ ion does not significantly affect the energy of the antenna singlet state (see Figure 6.4). However, the fluorescence intensities of the antenna moieties in the complexes are significantly reduced compared to the fluorescence intensities of the antenna moieties in the free ligands. The reduction of the fluorescence intensity is the largest for dansyl: more than 80%. Lissamine and Texas Red have similar reductions of the fluorescence intensity (more than 60%), whereas coumaryl has the smallest reduction (40%) in the fluorescence intensity.

The reduction of the fluorescence intensity of the antenna in the complex is caused by an external heavy atom effect induced by the heavy and paramagnetic Nd³⁺ ion in close proximity to the antenna chromophore. Such an effect increases the intersystem crossing *rate* of the chromophore, generally resulting in a reduction of the fluorescence intensity.^{15,26} The reduction of the antenna fluorescence intensities of the present Nd³⁺ complexes can therefore be considered to be a measure of the increased intersystem crossing *yield* of the antenna chromophores. More information can be obtained from time-resolved fluorescence measurements. The fluorescence lifetimes of the antenna moieties in the complexes and free ligands are mono-exponential with lifetimes in the nanosecond region (see Table 6.4). The decreased fluorescence lifetimes of the antenna moieties in the complexes are in line with the observed reduction of the fluorescence intensities. The intersystem crossing rates can be estimated via equation (3).²⁷

$$k_{ISC} = 1/\tau_{flu,complex} - 1/\tau_{flu,freelig} \quad (3)$$

The results have been summarized in Table 6.4. The external heavy atom effect is among other factors dependent on the distance between the antenna chromophore and the lanthanide ion. Based on this and the results from the molecular modeling simulations, one would expect similar effects for (Nd)**1** and (Nd)**2**, and smaller effects for (Nd)**3** and (Nd)**4**. The complexes (Nd)**1** and (Nd)**2** indeed have similar intersystem crossing rates, whereas the intersystem crossing rate of (Nd)**4** is smaller. An exception is (Nd)**3** which has a similar intersystem crossing rate as (Nd)**1** and (Nd)**2**, despite the difference in antenna-lanthanide distance. This shows that also other factors like structural differences of the dyes play an important role.

Table 6.4: Fluorescence intensities of the dye moieties in the complexes relative to fluorescence intensities of the dye moieties in the free ligands, the fluorescence lifetimes of the dye moieties in the complexes and free ligands, as well as the estimated intersystem crossing rates using equation (3).

Complex	I/I_0	τ_{flu} complex (ns)	τ_{flu} free ligand (ns)	k_{ISC} (s^{-1})
(Nd)1	0.14	2.37	16.7	3.6×10^8
(Nd)2	0.60	0.90	1.28	3.5×10^8
(Nd)3	0.30	1.22	2.60	4.35×10^8
(Nd)4	0.40	2.50	4.27	1.66×10^8

Whether the large enhancement in the intersystem crossing rate (k_{ISC}) also results in a large increase of the intersystem crossing quantum yield (Φ_{ISC}) depends on the rates of the competing processes, namely the radiative and non-radiative decay of the singlet excited state of the antenna.²⁸ The increase in the intersystem crossing quantum yield is the largest for the dansyl antenna because of its relatively long fluorescence lifetime (16.7 ns). The lifetime of the coumaryl antenna is much shorter (1.28 ns), therefore the overall effect is smaller.

Concluding remarks

In this series of investigated fluorescent dyes, the dansyl antenna chromophore is the most efficient sensitizer for Nd^{3+} . Based on the fluorescence properties of the dansyl moiety in the complex, this dye has the largest increase in the intersystem crossing yield as a result of an external heavy atom effect. The least efficient sensitizer is the coumaryl antenna. The sensitized emission intensity of the coumaryl-functionalized complex (Nd)2 is not only oxygen sensitive, but also the increase of the intersystem crossing yield was the smallest. Despite the relative large distance (10 Å) from the antenna chromophore to the Nd^{3+} ion in (Nd)3 and (Nd)4, the energy transfer process in these complexes was not sensitive to oxygen and a significant external heavy atom effect was observed. However, the comparison of the efficiency of the sensitization process of the different dye-functionalized complexes in terms of the intersystem crossing process and the energy transfer process is complicated, because the dyes are structurally different and have different photophysical properties.

6.2.4 Photophysical properties of the bis-dye-functionalized complexes

For an efficient excitation process high absorption coefficients are desirable. It has been shown above that the dansyl antenna is the most efficient sensitizer for Nd^{3+} . Unfortunately,

the absorption coefficient of dansyl is relatively low ($\epsilon = 4.2 \times 10^3 \text{ M}^{-1}\text{cm}^{-1}$ at 345 nm), especially when it is compared to the absorption coefficients of Lissamine and Texas Red ($\epsilon = 8.8 \times 10^4 \text{ M}^{-1}\text{cm}^{-1}$ at 568 nm, and $\epsilon = 8.5 \times 10^4 \text{ M}^{-1}\text{cm}^{-1}$ 590 nm, respectively). The bis-functionalized complexes (Nd)**1a** and (Nd)**2a** have been synthesized in order to double the effective absorption coefficients compared to the mono-functionalized (Nd)**1** and (Nd)**2** complexes. Under the experimental conditions, i.e. using a Xe lamp as the excitation source and dilute solutions, it is not likely that both antenna chromophores of (Nd)**1a** and (Nd)**2a** will be excited simultaneously. The incorporation of the additional antenna chromophore will therefore double the probability of the absorption of a photon compared to the mono-functionalized complexes. The absorption spectra of the mono- and bis-functionalized complexes are similar (not shown), but as expected the absorption coefficients of the latter complexes are twice as high, 8.5×10^3 and $4.4 \times 10^4 \text{ M}^{-1}\text{cm}^{-1}$, for (Nd)**1a** and (Nd)**2a** respectively.

Using the same methods as described above, the sensitized luminescence intensities of the mono- and bis-functionalized complexes have been compared. The sensitized emission intensities of the mono- and bis-functionalized complexes are approximately equal (see Figure 6.5). As expected, the Nd³⁺ lifetimes are similar within the experimental error (see Table 6.5). One should bear in mind that the spectra have been corrected for the absorbance of the samples, and it shows that the incorporation of the second antenna chromophore does not affect the quantum yield of sensitized emission, but that it increases the luminescence efficiencies ($\epsilon \times \phi_{\text{SE}}$) by a factor of two.

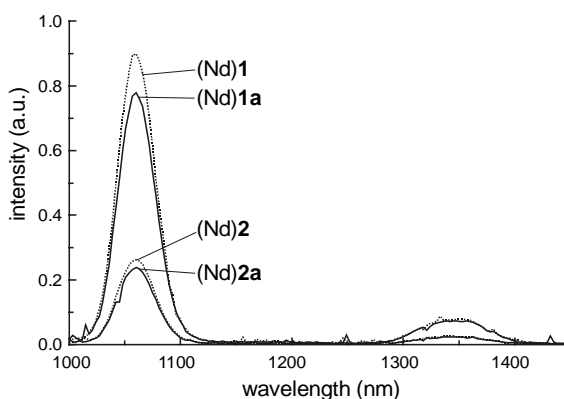


Figure 6.5: Sensitized Nd³⁺ luminescence intensities of the mono- and bis-functionalized Nd³⁺ complexes in DMSO-d₆ upon excitation into the absorption maxima of the incorporated dyes. The spectra have been corrected for the absorbance of the samples and differences in the excitation intensity (see main text).

The two antenna chromophores are positioned in close proximity to each other and thus may interact, for example resulting in quenching of the singlet excited state. For the coumaryl antenna chromophores of (Nd)**2a**, this is evidently not the case since the antenna fluorescence lifetimes and emission intensities of (Nd)**2** and (Nd)**2a** are comparable, as are the lifetimes and emission intensities of the corresponding free ligands. The conformation of the complex is probably such that one coumaryl moiety points towards the front of the complex, and the other towards the back (see chapter 3). In this conformation the two coumaryl antenna chromophores are not likely to interact with each other.²⁹

Table 6.5: Fluorescence intensities of the dye moieties in the bis-functionalized complexes relative to fluorescence intensities of the dye moieties in the corresponding free ligands, as well as the fluorescence lifetimes of the dye moieties in the complexes and free ligands.

Complex	τ_{Nd} (μs) ^a	I/I_0	τ_{flu} complex (ns)	τ_{flu} free ligand (ns)
(Nd) 1a	2.15	0.30	13.5 (47%) 2.37 (53%)	16.9
(Nd) 2a	2.39	0.58	0.88	1.26

^a error $\approx 10\%$

However, there seems to be an interaction between the two dansyl antenna chromophores of (Nd)**1a**, as can be concluded from the bi-exponential fluorescence lifetimes. Since the fluorescence lifetime of the dansyl moieties in the free ligand is mono-exponential, this interaction does not take place in the free ligand. Apparently the more rigid conformation of the complex imposed by the coordination of the sulfonamides to the Nd^{3+} ion, forces the dansyl moieties to be in close proximity to each other. Surprisingly, this interaction does not negatively influence the overall sensitization process compared to the mono-functionalized dansyl complex.

6.3 Conclusion

Despite their low intersystem crossing quantum yields, fluorescent dyes can be used as sensitizers for near-infrared Nd^{3+} emission due to an external heavy atom effect induced by the Nd^{3+} ion. Intramolecular energy transfer from the organic dyes dansyl, coumaryl, Lissamine, and Texas Red to Nd^{3+} has been established in the corresponding four *m*-terphenyl-based dye-functionalized Nd^{3+} complexes. The sensitization process is the most efficient in the dansyl complex (Nd)**1**, followed by the Lissamine (Nd)**3** and Texas Red (Nd)**3**

complexes, and least efficient in the coumaryl complex (Nd)**2**. The complexed lanthanide ion was found to enhance the intersystem crossing rate of the antenna via an external heavy atom effect, as could be concluded from the reduced fluorescence intensities and lifetimes of the antenna in the complexes compared to the fluorescence intensities and lifetimes of the antenna in the free ligands. For the dansyl antenna, this results in a high intersystem crossing yield because of its relatively long-lived singlet excited state. The incorporation of an additional dansyl antenna increases the absorption coefficient of the resulting complex and also the luminescence efficiency ($\epsilon \times \phi_{SE}$) of the system. A drawback is that the excitation window is limited to 400 nm. For future applications, the Lissamine antenna is the most attractive sensitizer, because it allows excitation at 530 nm, and because the luminescence efficiency is higher.

6.4 Experimental Section

6.4.1 Synthesis

General synthesis: See paragraph 3.4.1 of chapter 3 for a general experimental description. Dansyl chloride was purchased from Aldrich and used without further purification. The dyes Lissamine (sulfonyl chloride mixture of isomers), Texas Red (sulfonyl chloride mixture of isomers), and 7-diethylaminocoumarin-4-acetic acid were purchased from Molecular Probes and used without further purification. Di-n-butylamine was purchased from Aldrich and used without further purification. Flash column chromatography was performed on Merck silica gel (particle size 0.040-0.063 mm, 230-400 mesh). Preparative thin layer chromatography separations were performed on Merck aluminum oxide 150F₂₅₄ plates with a layer thickness of 1.5 mm. Standard workup involved washing the organic layers with water, drying over magnesium sulfate, filtration of the salts, and concentrating to dryness *in vacuo*.

Mono(dansyl) triester (7). To a solution of mono(amide) **6** (0.63 g, 0.59 mmol) and Et₃N (0.22 g, 2.2 mmol) in CH₂Cl₂ (30 mL) was added dansyl chloride (0.18 g, 0.65 mmol). The resulting solution was stirred overnight at rt. The reaction mixture was diluted with CH₂Cl₂ (100 mL) and successively washed with 0.5 N HCl and 0.5 N KOH, followed by standard workup. The crude product was purified by flash column chromatography (EtOAc/hexane

45:55 (v/v)) to give **7** as a light-green solid in 51% yield: m.p.: 43-45 °C. ¹H NMR (CDCl₃): δ 8.54 (d, 1H, *J* = 8.5 Hz), 8.44 (d, 1H, *J* = 8.5 Hz), 8.25 (d, 1H, *J* = 8.5 Hz), 7.63-7.48 (m, 2H), 7.45-7.30 (m, 5H), 7.20 (d, 1H, *J* = 8.5 Hz), 7.17-6.95 (m, 6H), 5.06-4.71 (m, 4H), 4.18-3.82 (m, 6H), 3.68-3.14 (m, 12H), 2.91 (s, 6H), 2.34 (s, 3H), 2.11 (s, 6H), 2.08-1.71 (m, 4H), 1.60-1.15 (m, 35H), 0.97-0.80 (m, 6H). ¹³C NMR (CDCl₃): δ 172.3, 167.9, 167.1, 136.5-126.6, 122.9, 129.3, 125.1, 81.5, 80.4, 70.6-67.6, 46.9, 31.8, 27.9, 21.0, 19.2, 14.2. MS (FAB) *m/z* = 1308.7; [(M+Na)⁺, calcd.: 1308.7]. Anal. calcd. for: C₇₄H₉₉N₃O₁₄S·0.5CH₂Cl₂: C, 67.32, H, 7.58, N, 3.16, S, 2.41. Found: C, 67.49, H, 7.60, N, 3.25, S, 2.12.

Bis(dansyl) triester (7a). To a solution of bis(amine) **5** (1.00 g, 1.00 mmol) and Et₃N (1.32 g, 13.2 mmol) in CH₂Cl₂ (100 mL) was added dansyl chloride (0.63 g, 2.20 mmol). The resulting solution was stirred overnight at rt. The reaction mixture was diluted with CH₂Cl₂ (100 mL) and successively washed with 0.5 N HCl and 0.5 N KOH, followed by standard workup. The crude product was purified by flash column chromatography (gradient from hexane to EtOAc/hexane 40:60(v/v)) to give **7a** as a light-green solid in 80% yield. M.p.: 49-51 °C. ¹H NMR (CDCl₃): δ 8.51 (d, 2H, *J* = 8.5 Hz), 8.39 (d, 2H, *J* = 8.5 Hz), 8.22 (d, 2H, *J* = 8.5 Hz), 7.60-7.40 (m, 4H), 7.18 (d, 2H, *J* = 8.5 Hz), 7.04 (s, 2H), 6.97-6.92 (m, 4H), 4.77 (s, 4H), 3.98 (s, 4H), 3.86 (s, 2H), 3.50-3.10 (m, 12H), 2.87 (s, 12H), 2.30 (s, 3H), 2.09 (s, 6H), 1.85-1.55 (m, 8H), 1.40-1.15 (m, 31H), 0.86 (t, 6H, *J* = 7.2 Hz). ¹³C NMR (CDCl₃): δ 167.5, 166.6, 151.2, 151.6, 150.7, 135.1, 132.8, 132.6-127.4, 122.6, 119.4, 114.6, 81.1, 80.5, 69.9-67.5, 44.9, 44.6, 31.2, 27.6-27.3, 20.1, 18.7, 13.4. MS (FAB) *m/z* = 1437.1 [(M+Na)⁺ calcd.: 1437.7]. Anal. calcd. for: C₇₉H₁₀₆N₄O₁₅S₂·1CH₂Cl₂: C, 64.03, H, 7.25, N, 3.73, S, 4.27. Found C, 64.31, H, 7.40, N, 3.98, S, 4.09.

Mono(coumaryl) triester (8). A solution of mono(amide) **6** (0.40 g, 0.38 mmol) and DMAP (0.11 g, 0.57 mmol) in CH₂Cl₂ (10 mL) was cooled to 0 °C. Subsequently, 7-diethylaminocoumarin-4-acetic acid (0.100 g, 0.38 mmol) and EDC·HCl (0.11 g, 0.57 mmol) were added to the solution. The reaction mixture was stirred overnight at rt. The reaction mixture was diluted with CH₂Cl₂ (100 mL), and successively washed with 0.5 N HCl and 1 N NaOH, followed by standard workup. The crude product was purified by flash column chromatography (EtOAc/hexane 1:1 (v/v)) to give **8** as a green-yellow oil in 47% yield. ¹H NMR (CDCl₃): δ 7.80-7.62 (m, 1H), 7.53-6.98 (m, 12H), 6.67-6.40 (m, 2H), 5.09-4.71 (m,

4H), 4.22-3.80 (m, 6H), 3.71-3.13 (m, 16H), 2.40-2.20 (m, 9H), 2.09-1.76 (m, 4H), 1.70-1.04 (m, 41H), 0.98-0.67 (m, 6H). ¹³C NMR (CDCl₃): δ 167.9, 159.3, 156.7, 152.0, 151.2, 142.7, 134.0-126.7, 109.3, 107.8, 97.4, 81.3, 81.1, 70.0-6.1, 44.6, 31.7, 28.0-26.0, 20.6, 19.4, 13.8, 12.1. MS (FAB) *m/z* = 1318.6; [(M+Na)⁺, calcd. for C₇₆H₁₀₁N₃O₁₅Na: 1318.7].

Bis(coumaryl) triester (8a). A solution of bis(amine) **5** (0.73 g, 0.77 mmol) and DMAP (0.14 g, 1.15 mmol) in CH₂Cl₂ (10 mL) was cooled to 0 °C. Subsequently, 7-diethylaminocoumarin-4-acetic acid (0.20 g, 0.77 mmol) and EDC·HCl (0.22 g, 1.15 mmol) were added to the solution. The reaction mixture was stirred overnight at rt. The reaction mixture was diluted with CH₂Cl₂ (100 mL) and washed twice with 5% K₂CO₃, followed by standard workup. The crude product was purified by preparative thin layer chromatography (MeOH/CH₂Cl₂ 10:90 (v/v)) to give **8a** as a green-yellow oil in 48% yield. ¹H NMR (CDCl₃): δ 7.70-7.56 (m, 2H), 7.32-6.90 (m, 8H), 6.55-6.35 (m, 4H), 5.25-4.63 (m, 4H), 4.09-3.70 (m, 6H), 3.50-3.10 (m, 20H), 2.30-2.10 (m, 9H), 1.90-1.70 (m, 4H), 1.50-0.90 (m, 47H), 0.76 (t, 3H, *J* = 12.5 Hz), (t, 3H, *J* = 12.5 Hz). ¹³C NMR (CDCl₃): δ 167.2, 159.4, 156.9, 152.0, 151.2, 133.7-128.5, 109.2, 107.9, 97.2, 81.6, 81.0, 70.6-67.5, 44.9, 42.7, 31.5, 31.7, 28.6-27.4, 20.9, 19.4, 14.0, 12.4. MS (FAB) *m/z* = 1457.7 [(M+Na)⁺, calcd. for C₈₃H₁₁₀N₄O₁₇Na: 1457.7].

Lissamine triester (9). To a solution of mono(amide) **6** (0.13 g, 0.12 mmol) and Et₃N (0.05 g, 0.50 mmol) in CH₂Cl₂ (50 mL) was added Lissamine sulfonyl chloride (0.14 g, 0.25 mmol). The resulting solution was stirred overnight at rt. The reaction mixture was diluted with CH₂Cl₂ (100 mL) and successively washed with 1 N HCl, 0.5 N KOH and 1 N HCl, followed by standard workup. The crude product was purified by preparative thin layer chromatography (MeOH/CH₂Cl₂ 5:95 (v/v)) to give **9** as a dark-purple solid in 44% yield. M.p.: 171-173°C. ¹H NMR (CDCl₃): δ 8.85 (s, 1H), 8.00 (d, 1H, *J* = 8.5 Hz), 7.43-6.80 (m, 14H), 6.81 (d, 2H, *J* = 8.5 Hz), 6.69 (s, 2H), 5.10-4.65 (m, 4H), 4.20-3.85 (m, 6H), 3.70-3.20 (m, 20H), 2.25 (s, 9H), 2.05-1.65 (m, 8H), 1.60-1.10 (m, 43H), 0.90-0.70 (m, 6H). ¹³C NMR (CDCl₃): δ 172.3, 168.6, 166.8, 159.0, 157.4, 148.1, 141.3, 133.2-126.1, 113.9, 112.8, 95.1, 81.0, 80.5, 70.3-67.6, 49.2, 46.7, 31.2, 28.6-27.0, 20.4-18.8, 13.4, 12.1. MS (FAB) *m/z* = 1615.8 [(M+Na)⁺, calcd.: 1615.0]. Anal. calcd. for C₈₉H₁₁₆N₄O₁₈S₂·1H₂O: C, 66.31, H, 7.38, N, 3.48, S, 3.98. Found: C, 65.94, H, 7.39, N, 3.84, S, 4.03.

Texas Red triester (10). To a solution of mono(amide) **6** (84 mg, 0.08 mmol) and Et₃N (34 mg, 0.32 mmol) in CH₂Cl₂ (25 mL) was added Texas Red sulfonyl chloride (100 mg, 0.16 mmol). The resulting solution was stirred overnight at rt. The reaction mixture was diluted with CH₂Cl₂ (100 mL) and successively washed with 1 N HCl and 1 N KOH, followed by standard workup. The crude product was purified by preparative thin layer chromatography (MeOH/CH₂Cl₂ 5:95 (v/v)) to give **10** as a dark-purple solid in 46% yield. M.p.: 126-128 °C. ¹H NMR (CD₂Cl₂): δ 8.81 (s, 1H), 7.90 (d, 1H, *J* = 7.8 Hz), 7.45-6.90 (m, 12H), 6.74 (s, 2H), 5.00-4.60 (m, 4H), 4.13-3.80 (m, 6H), 3.60-2.60 (m, 22H), 2.26 (s, 9H), 2.10-1.60 (m, 10H), 1.45-1.10 (m, 43H), 0.90-0.70 (m, 6H). ¹³C NMR (CDCl₃): δ 172.8, 167.5, 155.7, 151.8, 148.9, 140.9, 136.2-122.5, 113.3, 104.0, 81.1, 70.1-67.6, 50.4, 49.9, 46.7-42.6, 31.3, 28.6, 26.9, 20.5-18.9, 13.4. MS (FAB) *m/z* = 1640.5 [(M+Na)⁺, calcd.: 1640.8]. Anal. calcd. for C₉₃H₁₁₆N₄O₁₈S₂·1H₂O: C, 67.29, H, 7.16, N, 3.37, S, 3.86. Found: C, 66.82, H, 7.20, N, 3.41, S, 3.65.

Dibutyl Lissamine (11). To a solution of di-*n*-butylamine (56 mg, 0.12 mmol) and Et₃N (45 mg, 0.44 mmol) in CH₂Cl₂ (50 mL) was added Lissamine (0.50 g, 0.87 mmol). The resulting solution was stirred overnight at rt. The reaction mixture was diluted with CH₂Cl₂ (100 mL) and washed twice with 0.5 N HCl, followed by standard workup. The crude product was purified by preparative thin layer chromatography (MeOH/CH₂Cl₂ 5:95) to give **11** as a dark-red solid in 40% yield. M.p.: 168-170 °C. ¹H NMR (CDCl₃): δ 8.74 (s, 1H), 7.91 (d, 1H, *J* = 8.0 Hz), 7.26 (d, 2H, *J* = 8.0 Hz), 7.17 (d, 1H, *J* = 8.0 Hz), 6.77 (d, 2H, *J* = 8.0 Hz), 6.66 (s, 2H), 3.60-3.45 (m, 8H), 3.31-3.20 (m, 4H), 1.70-1.50 (m, 4H), 1.40-1.25 (m, 16H), 0.93 (t, 6H, *J* = 7.2 Hz). ¹³C NMR (CDCl₃): δ 158.4, 157.3, 155.0, 147.9, 141.2, 132.9, 129.2, 126.6, 113.8, 112.9, 95.5, 48.1, 45.4, 30.7, 19.4, 13.3, 12.1. MS (FAB) *m/z* = 670.3 [(M+H)⁺, calcd. 670.3]. Anal. calcd. for: C₃₅H₄₇N₃O₆S₂·0.33CH₂Cl₂: C, 60.80, H, 6.88, N, 6.02, S, 9.19; found: C, 60.51, H, 6.84, N, 6.04, S, 8.93.

Typical procedure for the synthesis of the triacids (H₃)1-(H₃)4. A solution of 0.10 mmol of the ligands in TFA (25 mL) was stirred overnight at rt. Subsequently, toluene (10 mL) was added, and the TFA/toluene mixture was azeotropically evaporated. The residue was taken up in CH₂Cl₂ (100 mL) and washed twice with 1 N HCl, followed by standard workup. The triacids were obtained as colored solids in nearly quantitative yield.

Mono(dansyl) triacid ((H₃)1). Light-green solid: m.p.: 83-85 °C. ¹H NMR (CD₃OD): δ 8.56 (d, 1H, *J* = 8.1 Hz), 8.33 (d, 1H, *J* = 8.1 Hz), 8.22 (d, 1H, *J* = 7.0 Hz), 7.65-7.53 (m, 2H), 7.50-7.33 (m, 5H), 7.29 (d, 1H, *J* = 7.0 Hz), 7.20-6.71 (m, 6H), 5.0-4.64 (m, 4H), 4.27-3.85 (m, 6H), 3.63-3.07 (m, 12H), 2.88 (s, 6H), 2.36 (s, 6H), 2.06 (s, 3H), 2.00-1.62 (m, 4H), 1.60-1.18 (m, 8H), 0.96-0.80 (m, 6H). MS (FAB) *m/z* = 1140.5 [(M+Na)⁺], calcd.1140.5. Anal. calcd. for: C₆₂H₇₅N₃O₁₄S·2H₂O: C, 64.51, H, 6.90, N, 3.64, S, 2.78. Found: 64.63, H, 6.71, N, 3.73, S, 2.41.

Bis(dansyl) triacid ((H₃)1a). Light-green solid: m.p.: 78-80 °C. ¹H NMR (CD₃OD): δ 8.46 (d, 2H, *J* = 8.5 Hz), 8.24 (d, 2H, *J* = 8.5 Hz), 8.12 (d, 2H, *J* = 8.5 Hz), 7.60-7.40 (m, 4H), 7.18 (d, 2H, *J* = 8.5 Hz), 7.05 (s, 2H), 6.90 (s, 2H), 6.70 (s, 2H), 4.63 (s, 4H), 4.05-3.80 (m, 6H), 3.40-3.00 (m, 12H), 2.82 (s, 12H), 2.25 (s, 3H), 1.96 (s, 6H), 1.66-1.62 (m, 4H), 1.40-1.12 (m, 8H), 0.78 (t, 6H, *J* = 7.5 Hz). MS (FAB) *m/z* = 1247.6 [(M+H)⁺]; calcd. 1247.5]. Anal. calcd. for: C₆₇H₈₂N₄O₁₅S₂·2H₂O: C, 62.70, H, 6.75, N, 4.36, S, 5.00. Found: C,62.43, H, 7.53, N, 4.52, S, 4.74.

Mono(coumaryl) triacid ((H₃)2). Green-yellow solid: m.p.: 94-96 °C. ¹H NMR (CD₃OD): δ 7.94-7.75 (m, 1H), 7.50-7.32 (m, 5H), 7.23-6.97 (m, 5H), 6.80-6.67 (m, 2H), 6.60-6.50 (m, 2H), 4.98-4.65 (m, 4H), 4.30-3.87 (m, 6H), 3.65-3.10 (m, 16H), 2.47-2.23 (m, 9H), 2.00-1.70 (m, 4H), 1.63-1.00 (m, 14H), 0.97-0.67 (m, 6H).). MS (FAB) *m/z* = 1150.5 [(M+Na)⁺], calcd.1150.5]. Anal. calcd. for: C₆₄H₇₇N₃O₁₅·3H₂O: C, 65.01, H, 7.08, N, 3.55. Found: C, 65.29, H, 7.43, N, 3.61.

Bis(coumaryl) triacid ((H₃)2a). Green-yellow solid: m.p.: 118-120 °C. ¹H NMR (CD₃OD): δ 7.84-7.62 (m, 2H), 7.35-6.90 (m, 8H), 6.70-6.55 (m, 2H), 6.59-6.35 (m, 2H), 4.90-4.60 (m, 4H), 4.10-3.90 (m, 6H), 3.60-3.05 (m, 20H), 2.30-2.10 (m, 9H), 1.90-1.70 (m, 4H), 1.50-0.93 (m, 20H), 0.83 (t, 3H, *J* = 8.0 Hz), 0.62 (t, 3H, *J* = 8.0 Hz). MS (FAB) *m/z* = 1289.4 [(M+Na)⁺]; calcd. 1289.6]. Anal. calcd. for: C₇₁H₈₆N₄O₁₇·4H₂O: C, 63.66, H, 7.07, N, 4.18. Found: C, 63.35, H, 7.36, N, 4.45.

Lissamine triacid ((H₃)3). Dark-purple solid: mp 145-147 °C. ¹H NMR (CD₃OD): δ 8.86 (s, 1H), 8.07 (d, 1H), 7.55-7.35 (m, 5H), 7.30-7.10 (m, 9H), 7.10-6.90 (m, 4H), 4.70 (s, 4H),

4.40-4.00 (m, 6H), 3.80-3.20 (m, 20H), 2.49 (s, 9H), 2.00-1.70 (m, 4H), 1.65-1.45 (m, 4H), 1.45-1.20 (m, 16H), 1.00-0.80 (m, 6H). MS (FAB) $m/z = 1447.6$; $[(M+Na)^+]$, calcd.: 1447.2]. Anal. calcd. for: $C_{77}H_{92}N_4S_2O_{18} \cdot 2H_2O$: C, 63.27, H, 6.62, N, 3.83, S, 4.39. Found: C, 63.16, H, 6.71, N, 3.88, S, 4.04.

Texas Red triacid ((H₃)4). Dark-purple solid: m.p.: 126-128 °C. ¹H NMR (CD₃OD): δ ¹H NMR (CD₃OD): δ 8.80 (s, 1H), 8.01 (d, 1H, $J = 7.8$ Hz), 7.40-6.87 (m, 12H), 6.57 (s, 2H), 5.00-4.60 (m, 4H), 4.15-3.80 (m, 6H), 3.60-2.60 (m, 22H), 2.26 (s, 9H), 2.10-1.60 (m, 10H), 1.45-1.10 (m, 16H), 0.90-0.70 (m, 6H). MS (FAB) $m/z = 1496.7$; $[(M+Na)^+]$, calcd.: 1496.6]. Anal. calcd. for: $C_{81}H_{92}N_4S_2O_{18}S_2 \cdot 2H_2O$: C, 64.44, H, 6.41, N, 3.71, S, 4.25. Found: C, 64.24, H, 6.53, N, 3.68, S, 3.98.

General procedure for the preparation of the complexes. To a solution of 1.0 equiv. of the triacid ligand and 4.0 equiv. of Et₃N in methanol was added 1.3 equiv. of the lanthanide nitrate salt. The resulting solution was stirred for 2 h, after which the solvent was concentrated to dryness. The complex was redissolved in ethyl acetate and washed twice with water to remove the excess lanthanide salt, followed by standard workup. The complexes were obtained as solids in nearly quantitative yields. The complexes were characterized by FAB mass spectrometry (see Table 6.3). The complexes all gave similar IR spectra: a peak at 1630 cm^{-1} ($\nu_{NC=O}$) with a shoulder around 1600 cm^{-1} (ν_{COO}).

Table 6.3: Mass spectra (FAB): A mixture of dithiothreitol and dithioerythritol (5:1 (v/v)), known as Magic Bullet, was used as the matrix.

Complex	m/z	calcd.
(Nd)1	1257.4 (M+H) ⁺	1257.4
(Nd)1a	1386.7 (M+H) ⁺	1386.4
(Nd)2	1267.4 (M+H) ⁺	1267.4
(Nd)2a	1406.3 (M+H) ⁺	1406.5
(Nd)3	1565.8 (M) ⁺	1565.5
(Nd)4	1612.5 (M) ⁺	1612.5

6.4.2 Photophysical studies

For a general description of the photophysical studies see paragraph 3.4.2 of chapter 3.

6.4.3 Molecular dynamics and molecular modeling calculations

See paragraph 3.4.3 of chapter 3 for description of the molecular mechanics and molecular dynamics calculations. For the molecular dynamics calculations in OPLS DMSO, the minimized structures were placed in a rectangular box (31.49 Å × 31.49 Å × 47.23 Å), initially filled with 400 OPLS DMSOs.²⁰ The same protocol was used as described for the molecular dynamics calculations in OPLS MeOH.

6.5 References and Notes

1. Miniscalco, W. J. *J. Lightwave Technol.* **1991**, *9*, 234.
2. Gschneider, K. A.; Eyring, L. R. *Handbook on the Physics and Chemistry of Rare Earths*, North Holland Publishing Company, Amsterdam, **1979**.
3. Sabbatini, N.; Guardigli, M.; Lehn, J.-M. *Coord. Chem. Rev.* **1993**, *123*, 201
4. Steemers, F. J.; Verboom, W.; Reinhoudt, D. N.; van der Tol, E. B.; Verhoeven, J. W. *J. Am. Chem. Soc.* **1995**, *117*, 9408.
5. (a) Sato, S.; Wada, M. *Bull. Chem. Soc. Jpn.* **1970**, *43*, 1955. (b) Haynes, A. V.; Drickamer, H. G. *J. Chem. Phys.* **1982**, *76*, 114.
6. (a) Beeby, A.; Dickins, R.; Faulkner, S.; Parker, D.; Williams, J. A. G. *Chem. Commun.* **1997**, 1401. (b) Crosby, G. A.; Kasha, M. *Spectrochim. Acta* **1958**, *10*, 337. (c) Meshkova, S. B.; Topilova, Z. M.; Bolshoy, D. V.; Beltyukova, Tsvirko, M. P. *Acta Phys, Pol. A*, **1999**, *95*, 983.
7. Iwamuro, M.; Hasegawa, Y.; Wada, Y.; Murakoshi, K.; Kitamura, T.; Nakashima, N.; Yamanaka, T.; Yanagida, S. *Chem. Lett.* **1997**, 1067.
8. Klink, S. I.; Hebbink, G. A.; Grave, L.; van Veggel, F. C. J. M.; Reinhoudt, D. N.; Slooff, L. H.; Polman, A.; Hofstraat, J. W. *J. Appl. Phys.* **1999**, *86*, 1181.
9. Steemers, F. J.; Verboom, W.; Hofstraat, J. W.; Geurts, F. A. J.; Reinhoudt, D. N. *Tetrahedron Lett.* **1998**, *39*, 7583.
10. Gaiduk, M. I.; Grigoryants, V. V.; Mironov, A. F.; Rmyantseva, V. D.; Chissov, V. I.; Sukhin, G. M. *J. Photochem. Photobiol. B* **1990**, *7*, 15.

11. Meshkova, S. B.; Rusakova, N. V.; Bolshoi, D. V. *Acta Chim. Hung.* **1992**, 129, 317.
12. Werts, M. H. V.; Hofstraat, J. W.; Geurts, F. A. J.; Verhoeven, J. W. *Chem. Phys. Lett.* **1997**, 276, 196.
13. Murov, S. L.; Carmichael, I.; Hug, G. L. *Handbook of Photochemistry, 2nd Ed.*, Marcel Dekker, New York, **1993**.
14. Oude Wolbers, M. P.; van Veggel, F. C. J. M.; Peters, F. G. A.; van Beelen, E. S. E.; Hofstraat, J. W.; Geurts, F. A. J.; Reinhoudt, D. N. *Chem. Eur. J.* **1998**, 4, 772.
15. Streck, W.; Wierzchaczewski, M. *Chem. Phys.* **1981**, 58, 185.
16. Mantulin W. W.; Song, P.-S. *J. Am. Chem. Soc.* **1973**, 95, 5122.
17. Chambers, R.; Kearns, D. R. *Photochem. Photobiol.* **1969**, 10, 215.
18. Bax, A.; Freeman, R. *J. Magn. Reson.* **1981**, 44, 542.
19. Bax, A.; Davis, D. G. *J. Magn. Reson.* **1985**, 63, 207.
20. Jorgenson, W. L. BOSS Version 3.5 Biochemical and Organic Simulation System User's Manual, **1994**.
21. (a) Brooks, B. R.; Bruccoleri, R. E.; Olafsen, B. D.; States, D. J.; Swaminathan, S.; Karplus, M. *J. Comput. Chem.* **1983**, 4, 187. (b) Momany, F. A.; Klimkowski, V. J.; Schäfer, L. *J. Comput. Chem.* **1990**, 11, 654. (c) Momany, F. A.; Rone, R.; Kunz, H.; Frey, R. F.; Newton, S. Q.; Schäfer, L. *J. Mol. Structure* **1993**, 286, 1.
22. Dexter, D. L. *J. Chem. Phys.* **1953**, 21, 836.
23. Beeby, A.; Faulkner, S. *Chem. Phys. Lett.* **1997**, 266, 116.
24. Hasegawa, Y.; Murakoshi, K.; Wada, Y.; Yanagida, S.; Kim, J.-H.; Nakashima, N.; Yamanaka, T. *Chem. Phys. Lett.* **1996**, 248, 8.
25. (a) Selwyn, J. E.; Steinfeld, J. I. *J. Phys. Chem.* **1972**, 76, 762. (b) Chambers, R. W.; Kajiwara, T.; Kearns, D. R. *J. Phys. Chem.* **1974**, 78, 380.
26. (a) Tobita, S.; Arakawa, M.; Tanaka, I. *J. Phys. Chem.* **1984**, 88, 2697. (b) Tobita, S.; Arakawa, M.; Tanaka, I. *J. Phys. Chem.* **1985**, 89, 5649.
27. Based on the low intersystem crossing yields of the antenna chromophores, it can be assumed that k_{ISC} is negligible in the free ligand then: $1/\tau_{flu, freelig} = k_{flu} + k_{nonrad}$, and $1/\tau_{flu, complex} = k_{flu} + k_{nonrad} + k_{ISC}$. It follows that $k_{ISC} = 1/\tau_{flu, complex} - 1/\tau_{flu, freelig}$.
28. $\Phi_{ISC} = k_{ISC} / (k_{ISC} + k_{rad} + k_{nonrad})$
29. Bourson, J.; Pouget, J.; Valeur, B. *J. Phys. Chem.* **1993**, 97, 4552.

Chapter 7

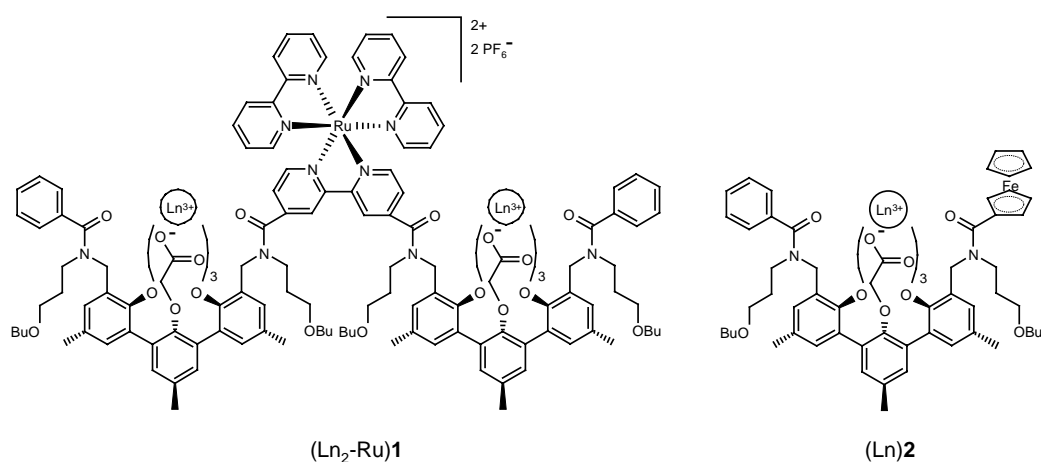
Ferrocene and Ru-tris(bipyridine) as a New Class of Photosensitizers for Near-Infrared Yb³⁺ and Nd³⁺ Luminescence

7.1 Introduction

Well-known examples of solid state laser systems and optical amplifiers based on lanthanide ions are the Nd:YAG laser¹ and Er³⁺-doped fiber amplifiers.² In these inorganic systems the lanthanide excited state is populated by direct excitation into their narrow absorption bands. The absorption coefficients are typically less than 10 M⁻¹cm⁻¹ as a result of the forbidden character of the optical transitions of lanthanide ions.³ In order to increase the excitation efficiency of Er³⁺ in inorganic matrices, its emission can be sensitized by energy transfer from co-doped Yb³⁺ which has a broader absorption band (at 980 nm) with a higher absorption coefficient.⁴ Organic lanthanide complexes have the advantage that they can be functionalized with an organic antenna chromophore (the *sensitizer*), usually consisting of a conjugated π -system, that can absorb the excitation light and subsequently donate the excitation energy to the lanthanide ion. This strategy has been described in the previous chapters. Until now the research has focused on organic conjugated molecules as sensitizers, such as β -diketonates,^{5,6} polyaromatic systems such as naphthalene,⁷ triphenylene,^{8,9} and

porphyrins,¹⁰ and dyes like xylenol orange¹¹ and fluorescein.^{12,13} A new class of potential antenna chromophores for the sensitization of Er^{3+} , Nd^{3+} , and Yb^{3+} are organo d-metal complexes, e.g. ruthenium-tris(bipyridine) ($[\text{Ru}(\text{bpy})_3]^{2+}$) and ferrocene. $[\text{Ru}(\text{bpy})_3]^{2+}$ and ferrocene have absorption bands in the visible region, and triplet states at $17,400\text{ cm}^{-1}$ and $13,300\text{ cm}^{-1}$, respectively.^{14,15} The $[\text{Ru}(\text{bpy})_3]^{2+}$ complex has a metal-to-ligand charge transfer (MLCT) band in the visible region with a maximum around 450 nm and would allow excitation up to 500 nm. Upon excitation into this $^1\text{MLCT}$ band, a rapid intersystem crossing process ($>10^{10}\text{ s}^{-1}$) takes place to the $^3\text{MLCT}$ state with a triplet quantum yield that is almost unity. The $[\text{Ru}(\text{bpy})_3]^{2+}$ complexes are known to emit light of around 630 nm from this $^3\text{MLCT}$ state that is long-lived (up to μs in deoxygenated solvents). Compared to $[\text{Ru}(\text{bpy})_3]^{2+}$, ferrocene has only weak absorption bands in the visible region, but it has a very low lying triplet state that closely matches the receiving luminescent states of Nd^{3+} and Yb^{3+} . The photophysical properties of ferrocene, e.g. the intersystem crossing rate, are not well-known, since both the ferrocene singlet and triplet states do not exhibit any luminescence.¹⁶

Chart 7.1



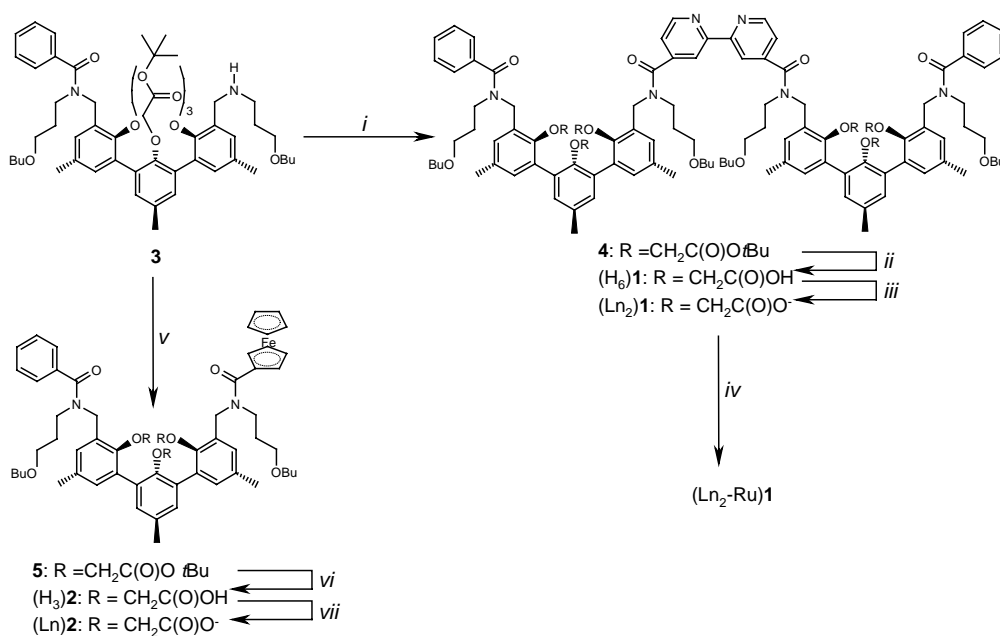
In this chapter the synthesis and photophysical properties of ferrocene- and ruthenium-tris(bipyridine)-functionalized lanthanide complexes are reported. The complexes exhibit lanthanide-centered near-infrared luminescence upon excitation of the d-metal complex. This is the first example of the population of the lanthanide luminescent by energy transfer from an organo-d-metal complex in organic systems. These systems are based on *m*-terphenyl-based lanthanide complexes that are covalently linked to ferrocene or ruthenium-tris(bipyridine) (see Chart 7.1).

7.2 Results and Discussion

7.2.1 Synthesis

The heteronuclear $[(\text{Ln}_2\text{-Ru})\mathbf{1}](\text{PF}_6)_2$ and $(\text{Ln})\mathbf{2}$ complexes were synthesized starting from mono(amide) $\mathbf{3}$ (see Chapter 4), in four and three steps, respectively (see Scheme 7.1). 2,2'-Bipyridine-4,4'-dicarboxylic acid chloride was reacted with mono(amide) $\mathbf{3}$ giving the ester protected ligand $\mathbf{4}$ in 72% yield. The ^1H NMR spectrum clearly shows the multiplet signals originating from the coupled bipyridine moiety.

Scheme 7.1



Reagents and Conditions: i) 2,2'-Bipyridine-4,4'-dicarboxylic acid chloride, Et_3N , CH_2Cl_2 , rt, 12 h (72%); ii) TFA, rt, 12 h (100%); iii) $\text{Ln}(\text{NO}_3)_3$, Et_3N , MeOH, rt, 4 h (100%); iv) $\text{Ru}(\text{bpy})_2\text{Cl}_2$, AgPF_6 , acetone, reflux, 12h; v) Ferrocenecarboxylic acid chloride, Et_3N , CH_2Cl_2 , rt, 12 h (83%); vi) TFA, rt, 12 h (100%); vii) $\text{Ln}(\text{NO}_3)_3$, Et_3N , MeOH, rt, 4 h (100%).

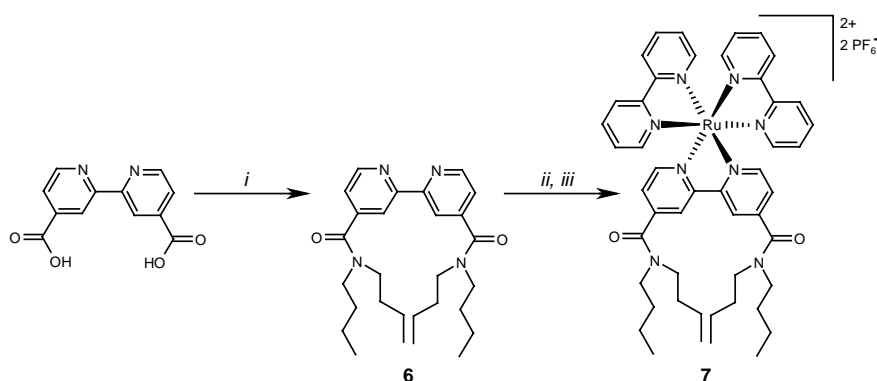
The *tert*-butylesters of $\mathbf{4}$ were hydrolyzed with trifluoroacetic acid in quantitative yield. The corresponding lanthanide complexes were prepared by adding the appropriate lanthanide nitrate salts to methanol solutions of the ligand in the presence of triethylamine as a base. FAB Mass spectra indicate that the dinuclear complexes $(\text{Ln}_2)\mathbf{1}$ have the expected 2:1 (lanthanide:ligand) stoichiometry. The IR spectra confirm the presence of carboxylates.

Finally, the $[\text{Ru}(\text{bpy})_2]^{2+}$ moiety was introduced in the dinuclear complexes $(\text{Ln}_2)\mathbf{1}$ by activating $\text{Ru}(\text{bpy})_2\text{Cl}_2$ with AgPF_6^{17} in deaerated acetone, and subsequent reaction with the $(\text{Ln}_2)\mathbf{1}$ complexes. During the reaction, the mixture turned from dark green to dark red. After purification by Sephadex column chromatography, the $[(\text{Ln}_2\text{-Ru})\mathbf{1}](\text{PF}_6)_2$ complexes were obtained as red solids in 40-60% yield. The complexes were characterized by MALDI-TOF spectrometry and IR spectroscopy (see experimental).

Ferrocenecarboxylic acid chloride was reacted with mono(amide) **3** giving **5** in 83% yield. After hydrolysis of the *tert*-butylesters of **5** with trifluoroacetic acid in quantitative yield, the corresponding complexes were formed analogously to the $(\text{Ln}_2)\mathbf{1}$ complexes. FAB Mass spectra indicate that the $(\text{Ln})\mathbf{2}$ complexes have a 1:1 (lanthanide:ligand) stoichiometry. The IR spectra confirm the presence of carboxylates.

Compound **7** is the bis(amide)-functionalized Ru-bpy antenna moiety of the $[(\text{Ln}_2\text{-Ru})\mathbf{1}]^{2+}$ complexes. The synthesis of this reference **7** is depicted in Scheme 7.2, and was synthesized in two steps. Reaction of 2,2'-bipyridine-4,4'-dicarboxylic acid chloride with di-*n*-butylamine gave **6** in 83% yield. For the coupling of **6** to $\text{Ru}(\text{bpy})_2\text{Cl}_2$ an alternative reaction procedure was used: **6** was reacted with $\text{Ru}(\text{bpy})_2\text{Cl}_2$ in a mixture of THF and water (9:1) under reflux conditions. Reference compound **7** was obtained by redissolving the reaction mixture in water and subsequent addition of a concentrated NH_4PF_6 solution, after which the compound precipitated as an orange-red solid in 34% yield.

Scheme 7.2



Reagents and Conditions: i) Di-*n*-butylamine, Et_3N , CH_2Cl_2 , rt, 12 h (83%); ii) $\text{Ru}(\text{bpy})_2\text{Cl}_2$, THF/water, reflux, 12 h; iii) NH_4PF_6 .

7.2.2 Photophysical properties of the $[(\text{Ln}_2\text{-Ru})\mathbf{1}]^{2+}$ complexes

Absorption spectra

The absorption spectrum of the $[(\text{Nd}_2\text{-Ru})\mathbf{1}]^{2+}$ complex shows the characteristic bands of the Ru-bpy antenna: the MLCT $d \rightarrow \pi^*$ transition at 450 nm ($\epsilon = 13,900 \text{ M}^{-1}\text{cm}^{-1}$) and the shoulder at 340 nm corresponding to the d-metal centered absorption (see Figure 7.1).¹⁴

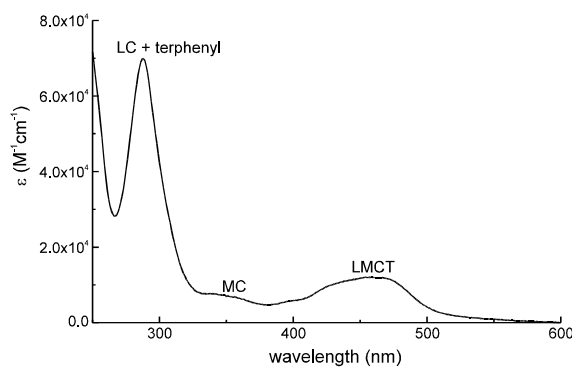


Figure 7.1: Absorption spectrum of $[(\text{Nd}_2\text{-Ru})\mathbf{1}]^{2+}$ in acetonitrile at room temperature.

The intense band at 290 nm can be assigned to $\pi \rightarrow \pi^*$ transitions of the terphenyl and bipyridine moieties.¹⁴ The spectrum is similar to that of reference compound **7**, indicating that the complexed lanthanide ions do not significantly influence the energy levels of the Ru-bpy antenna. The $[(\text{Yb}_2\text{-Ru})\mathbf{1}]^{2+}$ and $[(\text{Gd}_2\text{-Ru})\mathbf{1}]^{2+}$ complexes (not shown) have similar absorption spectra as the $[(\text{Nd}_2\text{-Ru})\mathbf{1}]^{2+}$ complex.

$[(\text{Ln}_2\text{-Ru})\mathbf{1}]^{2+}$ luminescence

Photo-excitation of the $[(\text{Nd}_2\text{-Ru})\mathbf{1}]^{2+}$ complex in $\text{DMSO-}d_6$ (10^{-5} M) at 450 nm resulted in Nd^{3+} -centered near-infrared luminescence. Figure 7.2 shows the near-infrared spectrum with emission bands at 1060 and 1330 nm corresponding to the ${}^4\text{F}_{3/2} \rightarrow {}^4\text{I}_{11/2}$ and ${}^4\text{I}_{13/2}$ transitions, respectively. The observed emission band at 880 nm corresponding to the ${}^4\text{F}_{3/2} \rightarrow {}^4\text{I}_{9/2}$ transition is not shown in Figure 7.2. The 1060 nm emission band is superimposed on the tail of the broad emission band of the Ru-bpy antenna (vide infra). The excitation spectrum of $[(\text{Nd}_2\text{-Ru})\mathbf{1}]^{2+}$ was obtained by monitoring the intensity of the emission band at 1060 nm, while scanning the excitation wavelength. The excitation spectrum closely resembles the absorption spectrum of the Ru-bpy antenna (see Figure 7.2), which proves that the Nd^{3+} ions are excited via the antenna.¹⁸

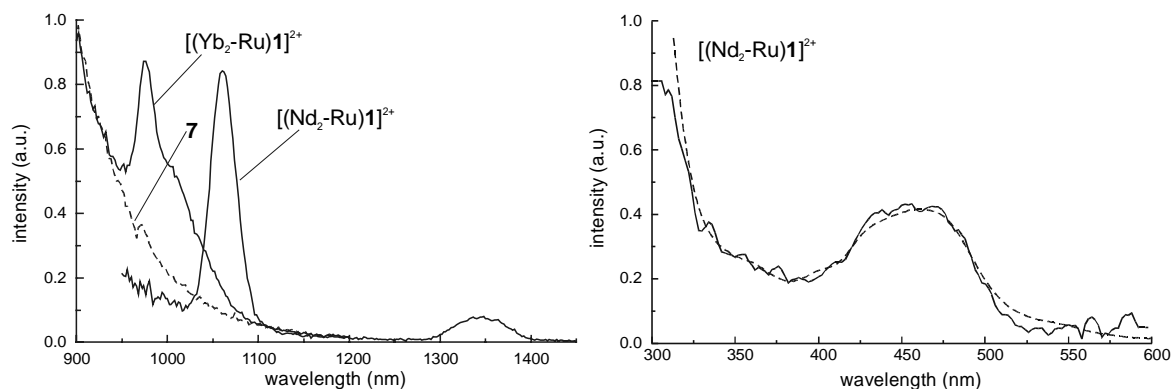


Figure 7.2: Left: Ln^{3+} -centered luminescence spectrum of $[(\text{Nd}_2\text{-Ru})\mathbf{1}]^{2+}$ and $[(\text{Yb}_2\text{-Ru})\mathbf{1}]^{2+}$ in $\text{DMSO-}d_6$ (10^{-5} M) upon excitation at 450 nm, as well as the tail of the antenna luminescence of **7**. Right: The excitation spectrum of Nd^{3+} luminescence (solid line) of $[(\text{Nd}_2\text{-Ru})\mathbf{1}]^{2+}$ in $\text{DMSO-}d_6$ (10^{-5} M) while monitoring the 1060 nm emission band. The dashed line is the absorption spectrum of $[(\text{Nd}_2\text{-Ru})\mathbf{1}]^{2+}$ in $\text{DMSO-}d_6$.

The lifetime of the Nd^{3+} -centered luminescence is 2.10 μs , which is the same as the lifetimes previously obtained for mononuclear *m*-terphenyl-based Nd^{3+} complexes¹⁹ and the reported lifetime of $\text{Nd}(\text{OAc})_3$ of 2.33 μs ²⁰ in $\text{DMSO-}d_6$. This indicates that the two complexed Nd^{3+} ions do not quench each other. Deoxygenation led to a small increase (20 %) of the sensitized Nd^{3+} luminescence, but did not influence the Nd^{3+} luminescence lifetime.

Upon excitation at 450 nm of the $[(\text{Yb}_2\text{-Ru})\mathbf{1}]^{2+}$ complex in $\text{DMSO-}d_6$ Yb^{3+} -centered luminescence was observed at 975 nm corresponding to the ${}^4\text{F}_{5/2} \rightarrow {}^4\text{F}_{7/2}$ transition. Although the Yb^{3+} luminescence is superimposed on the tail of the Ru-bpy luminescence, the characteristic shoulder at 1005 nm is clearly discernible. As is the case for the $[(\text{Nd}_2\text{-Ru})\mathbf{1}]^{2+}$ complex, the excitation spectrum of $[(\text{Yb}_2\text{-Ru})\mathbf{1}]^{2+}$ closely follows the absorption spectrum of the antenna, proving that the Yb^{3+} ions¹⁸ are excited via the antenna. The luminescence lifetime of the Yb^{3+} luminescence is 17.9 μs , and in line with previously determined lifetimes of *m*-terphenyl-based Yb^{3+} complexes.¹⁹ Also in this complex there is no concentration quenching between the two complexed Yb^{3+} ions. Deoxygenation of the solvent did neither increase the sensitized Yb^{3+} luminescence, nor did it influence its luminescence lifetime.

The ${}^3\text{MLCT}$ state of the antenna, which is the donating energy level in the energy transfer process, still exhibits luminescence. Therefore, the sensitization process and in particular the energy transfer process, has been studied in detail by measuring the intensity of the antenna luminescence and by time-resolved luminescence measurements of the antenna and

lanthanide luminescence. The main pathways of the sensitization process, as well the 4f energy states of Nd^{3+} and Yb^{3+} are depicted in Figure 7.3.

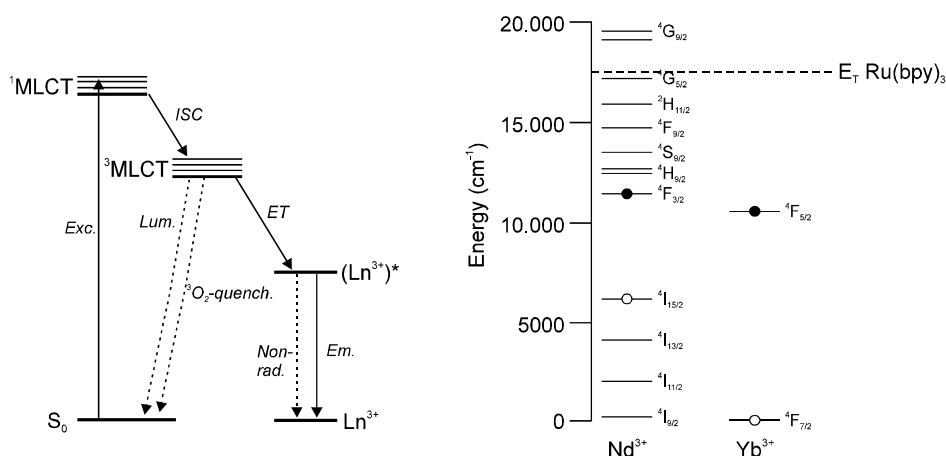


Figure 7.3: Right: Photophysical model describing the main pathways in the sensitization process. Left: Energy diagram of the 4f levels of Nd^{3+} and Yb^{3+} , where the filled circle denotes the lowest luminescent state, and the open circle denotes the highest non-luminescent state (adapted from Stein, G.; Würzberg, E. J. Chem. Phys. 1975, 62, 208).

Ru-bpy antenna luminescence

The antenna luminescence intensities of $[(\text{Nd}_2\text{-Ru})\mathbf{1}]^{2+}$ and $[(\text{Yb}_2\text{-Ru})\mathbf{1}]^{2+}$ were compared to the intensities of the reference complexes $[(\text{Gd}_2\text{-Ru})\mathbf{1}]^{2+}$ and **7**. In $[(\text{Gd}_2\text{-Ru})\mathbf{1}]^{2+}$ there is no intramolecular energy transfer process, because Gd^{3+} has no energy levels below $32,000\text{ cm}^{-1}$, and therefore cannot accept any energy from the antenna triplet state. Upon excitation at 450 nm in (aerated) $\text{DMSO-}d_6$ a broad emission band at 660 nm that originates from the $^3\text{MLCT}$ state of the Ru-bpy antenna is observed for all the complexes. Deoxygenation of the samples significantly increased the luminescence intensities: approximately 40% for $[(\text{Gd}_2\text{-Ru})\mathbf{1}]^{2+}$, $[(\text{Yb}_2\text{-Ru})\mathbf{1}]^{2+}$, and **7** and 20% for $[(\text{Nd}_2\text{-Ru})\mathbf{1}]^{2+}$. It is well known from literature that oxygen quenches the long-lived Ru-bpy luminescent state, and also in our systems oxygen quenching of the $^3\text{MLCT}$ state is a competing process. Figure 7.4 shows the luminescence intensities of the $[(\text{Ln}_2\text{-Ru})\mathbf{1}]^{2+}$ complexes relative to **7** in deoxygenated DMSO. The comparable photophysical properties of the antenna of $[(\text{Gd}_2\text{-Ru})\mathbf{1}]^{2+}$ and **7** indicate that the (heavy and paramagnetic) lanthanide ions do not influence the radiative transition of the $^3\text{MLCT}$ state to the ground state via an *external heavy atom effect*.²¹ The clearly lower antenna luminescence intensity of the $[(\text{Nd}_2\text{-Ru})\mathbf{1}]^{2+}$ antenna compared to the $[(\text{Gd}_2\text{-Ru})\mathbf{1}]^{2+}$ antenna is in accordance with the fact that the antenna $^3\text{MLCT}$ state of the former complex is also

depopulated by energy transfer to the Nd^{3+} ions. A surprising result is that the antenna luminescence of $[(\text{Yb}_2\text{-Ru})\mathbf{1}]^{2+}$ is not reduced relative to $[(\text{Gd}_2\text{-Ru})\mathbf{1}]^{2+}$. This may indicate that the rate of the energy transfer process is at least an order of magnitude slower than the rate of the competing processes, and that thus the quantum yield of the energy transfer process is much lower for $[(\text{Yb}_2\text{-Ru})\mathbf{1}]^{2+}$ than for $[(\text{Nd}_2\text{-Ru})\mathbf{1}]^{2+}$.

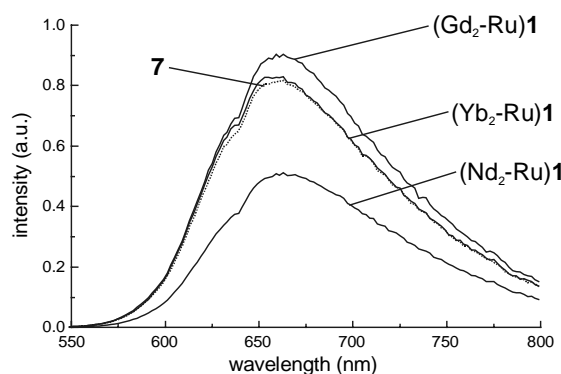


Figure 7.4: Emission spectra of $\text{Ru}(\text{bpy})_3$ -centered luminescence of $[(\text{Gd}_2\text{-Ru})\mathbf{1}]^{2+}$, $[(\text{Yb}_2\text{-Ru})\mathbf{1}]^{2+}$, and $[(\text{Nd}_2\text{-Ru})\mathbf{1}]^{2+}$ in deoxygenated $\text{DMSO-}d_6$ (10^{-5} M) upon excitation at 450 nm, as well as the emission spectrum of reference compound **7** (dashed line).

Time-resolved luminescence measurements

The processes that deactivate the antenna $^3\text{MLCT}$ state, i.e. radiative decay, energy transfer, and quenching by oxygen, were studied with time-resolved luminescence measurements. Upon excitation at 337 nm, the decay of the antenna luminescence of the complexes is mono-exponential with time-constants in the nanosecond to microsecond range. As expected the luminescence lifetimes increase upon deoxygenation of the solvent (see Table 7.1). The luminescence lifetime of the antenna $[(\text{Nd}_2\text{-Ru})\mathbf{1}]^{2+}$ is shorter than that of $[(\text{Gd}_2\text{-Ru})\mathbf{1}]^{2+}$, caused by the intramolecular energy transfer process. The oxygen quenching rate k_{ox} of the $^3\text{MLCT}$ state was calculated from $k_{\text{ox}} = 1/\tau_{\text{RuGd,ox}} - 1/\tau_{\text{RuGd,deox}} = 0.52 \times 10^6 \text{ s}^{-1}$. Since the oxygen concentration in DMSO is 0.47 mM at room temperature, the molar quenching rate constant (k_{q}) is $1.1 \times 10^9 \text{ M}^{-1}\text{s}^{-1}$. Diffusion-controlled oxygen quenching rate constants are typically in the order of $10^9\text{-}10^{10} \text{ M}^{-1}\text{s}^{-1}$,¹⁵ and this shows that also in the present case the oxygen quenching process is diffusion controlled.

The Ru-bpy luminescence lifetime 0.77 μs of $[(\text{Gd}_2\text{-Ru})\mathbf{1}]^{2+}$ in deoxygenated DMSO represents the $^3\text{MLCT}$ state lifetime in the absence of both oxygen quenching and energy transfer, and is thus the sum of the non-radiative and radiative decay of the $^3\text{MLCT}$ state,

hence $k_{\text{rad}} + k_{\text{nonrad}} = 1/\tau_{\text{RuGd}} = 1.30 \times 10^6 \text{ s}^{-1}$. The energy transfer rate (k_{ET}) in the [(Nd₂-Ru)**1**]²⁺ complex can then be calculated from $k_{\text{ET}} = 1/\tau_{\text{RuNd}} - 1/\tau_{\text{RuGd}} = 1.08 \times 10^6 \text{ s}^{-1}$. Obviously, the energy transfer to the Yb³⁺ ions in [(Yb₂-Ru)**1**]²⁺ cannot be calculated in the same way as for [(Nd₂-Ru)**1**]²⁺ (*vide infra*).

Table 7.1: Luminescence lifetimes of the Ru-bpy antenna and the lanthanide luminescence in deoxygenated and oxygenated DMSO (10⁻⁵ M) upon excitation at 337 nm.

Complex	Ln ³⁺	Ln ³⁺	Ru-bpy	Ru-bpy	Ru-bpy	
	$\tau_{\text{ox}} (\mu\text{s})^{\text{a}}$	$\tau_{\text{deox}} (\mu\text{s})^{\text{a}}$	$\tau_{\text{ox}} (\mu\text{s})$	$\tau_{\text{deox}} (\mu\text{s})$	$\tau_{\text{deox}}/\tau_{\text{ox}}$	$(I_{\text{deox}}/I_{\text{ox}})^{\text{b}}$
7	n.a.	n.a.	0.51	0.74	1.45	(1.40)
[(Gd ₂ -Ru) 1] ²⁺	n.a.	n.a.	0.55	0.77	1.40	(1.35)
[(Nd ₂ -Ru) 1] ²⁺	2.17 (0.37)	2.10 (0.42)	0.37	0.42	1.14	(1.20)
[(Yb ₂ -Ru) 1] ²⁺	17.9	18.2	0.53	0.78	1.47	(1.50)

^aLuminescence rise-time in parentheses; ^bRatio of the Ru-bpy luminescence intensity in deoxygenated and oxygenated DMSO ($\lambda_{\text{exc.}} 450 \text{ nm}$).

During the time that the energy transfer from the antenna triplet state to the lanthanide ion is in progress, the lanthanide luminescence intensity is expected to rise with a rate equal to the decay rate of antenna triplet state. Upon excitation of the antenna of [(Nd₂-Ru)**1**]²⁺ in deoxygenated DMSO, the Nd³⁺ emission rises with a time-constant of 0.42 μs . Since this is exactly the decay time of the antenna ³MLCT state, this further proves that the antenna ³MLCT state is the donating energy level (see Figure 7.3). In aerated DMSO the Nd³⁺ emission rises with a time-constant of 0.37 μs , which is the decay time of the antenna ³MLCT state under these conditions.

The rise-time of the Yb³⁺ luminescence at 980 nm could not be measured because the first microseconds (after the laser pulse) of the time-resolved emission spectrum are dominated by the decay of the Ru-bpy antenna luminescence. This is not surprising since the emission spectrum shows that there is an appreciable amount of antenna luminescence at 980 nm (see Figure 7.2). Upon excitation at 337 nm a bi-exponential decay is observed at 980 nm for [(Yb₂-Ru)**1**]²⁺ in aerated DMSO-*d*₆ with time-constants of 0.53 μs and 17.9 μs , corresponding to the Ru-bpy-centered luminescence and the Yb³⁺-centered luminescence, respectively, which are overlapping. In deoxygenated DMSO-*d*₆, the same bi-exponential decay is observed after excitation at 337 nm with an increased lifetime of 0.72 μs

corresponding to the Ru-bpy decay and a lifetime of 18.2 μs corresponding to the Yb³⁺ luminescence are observed.

The energy transfer rates are relatively slow, $\sim 10^6 \text{ s}^{-1}$ for [(Nd₂-Ru)1]²⁺ and 10^4 - 10^5 s^{-1} for [(Yb₂-Ru)1]²⁺, which may be caused by the distance from the Ln³⁺ ions to the metal center of the antenna. The energy transfer process involves an *electron-exchange* mechanism that can be visualized as the simultaneous exchange of two electrons between the LUMO of the donor and the LUMO of the acceptor, and the HOMO of the acceptor and the HOMO of the donor. In the present system, such a mechanism requires a physical overlap between the 4f orbitals of the lanthanide ion and the HOMO and LUMO of the antenna.

In the literature, there is still some discussion whether the promoted electron of an excited Ru(bpy)₃ complex is localized on a single bpy ligand or delocalized over the three bpy ligands.^{14,22} In the present complex the bpy moiety that is closest to the lanthanide ions has been modified with amide groups that are para with respect to the ruthenium coordinating nitrogen atoms. Comparison of the luminescence spectra of these amide functionalized [(Ln₂-Ru)1]²⁺ complexes in DMSO with the standard [Ru(bpy)₃]²⁺ complex shows that the emission maximum of the amide-functionalized complexes has shifted to the red: from 634 nm to 666 nm ($\Delta E = \sim 700 \text{ cm}^{-1}$). The amide groups stabilize the ³MLCT state of the Ru-bpy antenna, and probably the LUMO is localized on the amide-functionalized bpy moiety, which is closest to the Ln³⁺ ions ($\sim 5 \text{ \AA}$). However, the antenna HOMO is localized on the Ru^{II} center,¹⁴ which is further away from the lanthanide ions ($>5 \text{ \AA}$). Since the electron-exchange mechanism is strongly distance dependent (the optimal distance is $<5 \text{ \AA}$), this will result in a slow energy transfer rate.

Compared to [(Nd₂-Ru)1]²⁺, the energy transfer rate in [(Yb₂-Ru)1]²⁺ will be even lower because of the larger energy difference between the triplet state and the receiving state of Yb³⁺, resulting in a much smaller spectral overlap. In the [(Nd₂-Ru)1]²⁺ complex the energy transfer probably takes place via the ⁴G_{5/2} state at 17,100 cm^{-1} , whereas in [(Yb₂-Ru)1]²⁺ it can only take place to the ²F_{5/2} state at 10,240 cm^{-1} (see Figure 7.3).

7.2.3 Photophysical properties of the (Ln)2 complexes

Absorption and sensitized luminescence spectra

The absorption spectrum of (Nd)2 in DMSO above 300 nm (see Figure 7.5) shows the characteristic ferrocene absorptions, e.g. at 325 nm and 440 nm, that correspond to d-d transitions.²³ The absorption spectrum of (Yb)2 has a similar shape (not shown).

Aerated $\text{DMSO-}d_6$ solutions of the (Nd)**2** and (Yb)**2** complexes (10^{-4} M) exhibit the typical line-like lanthanide emission upon excitation of the ferrocene antenna at 320 nm. At room temperature sensitized emission at 1060 and 1330 nm (${}^4\text{F}_{3/2} \rightarrow {}^4\text{I}_{11/2}$, and ${}^4\text{I}_{13/2}$ transition, respectively) is observed for (Nd)**2**, and at 980 nm (${}^2\text{F}_{5/2} \rightarrow {}^2\text{F}_{7/2}$ transition) for (Yb)**2** (see Figure 7.5). The excitation spectra of (Nd)**2** and (Yb)**2**, closely follow the absorption spectrum of the ferrocene antenna and confirm that excitation takes place via the antenna.

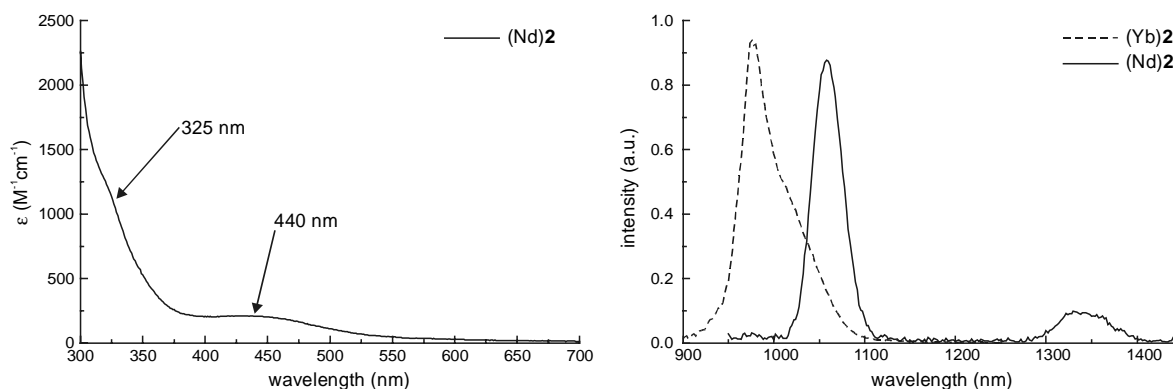
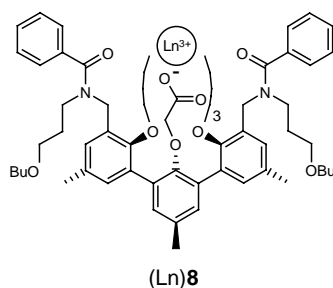


Figure 7.5: (Left) Absorption spectrum of (Nd)**2** in DMSO at room temperature. (Right) Emission spectra of (Yb)**2** and (Nd)**2** in $\text{DMSO-}d_6$ (10^{-4} M) upon excitation at 320 nm.

The terphenyl moiety can also act as an antenna chromophore for the sensitized lanthanide luminescence (see Chapter 3). In order to determine the role of the terphenyl moiety in the sensitization process, the sensitized lanthanide emission of (Ln)**2** was compared to the emission of the reference complexes (Ln)**8** upon excitation at 320 nm (see Chart 7.2 and Figure 7.6).

Chart 7.2



The reference complexes exhibited very little sensitized lanthanide luminescence upon excitation at 320 nm, indicating that at this excitation wavelength the majority of the

lanthanide ions (>90%) in the (Ln)**2** complexes are excited via the ferrocene antenna. Deoxygenation of the samples had a small effect on the sensitized luminescence intensity of (Nd)**2** and (Yb)**2**, although the effect was more pronounced for (Nd)**2** indicating that the energy transfer process is faster in (Yb)**2** than in (Nd)**2** (see Figure 7.6). Upon excitation at 337 nm the lanthanide luminescence decay curves could be fitted mono-exponentially with lifetimes of 2.0 μs for (Nd)**2** and 18.8 μs for (Yb)**2**. Deoxygenation of the solvent did not influence these luminescence lifetimes.

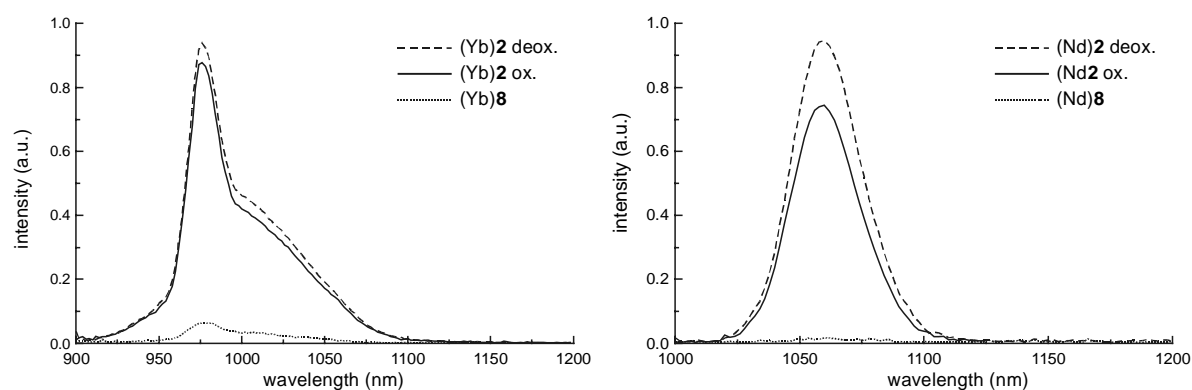


Figure 7.6: The emission spectra of (Yb)**2** and (Nd)**2** in deoxygenated and oxygenated DMSO- d_6 (10^{-4} M) upon excitation at 320 nm, as well as the emission spectra of the reference complexes (Yb)**8** and (Nd)**8** in DMSO- d_6 (10^{-4} M) upon excitation at 320 nm.

The overall sensitization process, which is the product of the intersystem crossing yield, the energy transfer yield (ϕ_{ET}), and the intrinsic lanthanide luminescence yield, is more efficient for (Yb)**2** than for (Nd)**2**, since $I_{\text{Yb}}/I_{\text{Nd}} = \sim 4$.²⁴ The intersystem crossing yield of the ferrocene antenna can be expected to be the same in both complexes, and judging from the luminescence lifetimes the intrinsic lanthanide luminescence yields appear to be the same.²⁵ The difference is therefore probably caused by differences in the energy transfer process, as is illustrated by the larger influence of oxygen on the sensitized emission intensity of (Nd)**2** than of (Yb)**2**.

As was recently proposed for the sensitization of Yb^{3+} , the energy transfer process in (Yb)**2** may take place through the singlet state of the antenna chromophore via an internal redox mechanism.²⁶ Such a mechanism is not possible for the (Nd)**2** complex, since Nd^{3+} has a significantly more negative reduction potential than Yb^{3+} . The driving force $-\Delta G_{\text{RET}}$ of such a photon-induced redox transfer can be estimated by $\Delta G_{\text{RET}} = E(\text{Fc}/\text{Fc}^+) - E(\text{Fc}^*) - E(\text{Yb}^{3+}/\text{Yb}^{2+})$. Cyclic voltammetry experiments showed that $E(\text{Fc}/\text{Fc}^+) - E(\text{Yb}^{3+}/\text{Yb}^{2+}) \geq 2.52$

eV.²⁷ In the present experiments the (Yb)**2** complex was excited at 325 nm into a Fe-localized excited state. If the energy transfer process takes place directly from this state then $E(\text{Fc}^*)$ is 3.85 eV, which means that there is a net driving force of ≤ 1.33 eV. However, if the non-radiative decay to the lowest excited singlet state is fast, and the energy transfer thus takes place from this state, then the $E(\text{Fc}^*)$ is 2.4 eV. If this is the case, then there is no net driving force for the photo-induced redox transfer. Our experiments show that there is some oxygen dependence of the sensitized Yb^{3+} luminescence indicating the participation of the ferrocene triplet state. Furthermore, excitation into a lower band of ferrocene at 440 nm (in which case $E(\text{Fc}^*)$ is 2.8 eV) also resulted in sensitized Yb^{3+} luminescence. Based on these energetic considerations, it can be concluded that the sensitization of Yb^{3+} in (Yb)**2** proceeds via the ferrocene triplet state, but energy transfer from the singlet state cannot be excluded.

7.3 Conclusion

It has been demonstrated that $[\text{Ru}(\text{bpy})_3]^{2+}$ and ferrocene can sensitize near-infrared Nd^{3+} and Yb^{3+} luminescence in organic systems. The excitation spectra show that energy transfer takes place from the Ru-bpy antenna to the luminescent ions in the trinuclear $[(\text{Ln}_2\text{-Ru})\mathbf{1}]^{2+}$ complexes, resulting in Nd^{3+} - and Yb^{3+} -centered near-infrared luminescence. The $^3\text{MLCT}$ of the antenna is the donating energy level, as could be concluded from the fact that the lanthanide luminescence rises with the decay of the $^3\text{MLCT}$ state. The energy transfer to lanthanide ions was found to be relatively slow in comparison with the competing processes. This may be related to the relatively large distance from the lanthanide ions to the Ru^{II} center of the antenna. The ferrocene-functionalized (Nd)**2** and (Yb)**2** complexes exhibited near-infrared luminescence upon excitation of the ferrocene moiety. This process is more efficient in the (Yb)**2** complex, than in (Nd)**2**. The sensitization of Yb^{3+} in (Yb)**2** proceeds via the ferrocene triplet state, but energy transfer from the singlet state cannot be excluded.

7.4 Experimental Section

7.4.1 Synthesis

General synthesis: See paragraph 3.4.1 of chapter 3 for a general description of the synthesis. Acetone was of analytical grade and was dried over molecular sieves (4 Å) prior to use. 2,2'-Bipyridine-4,4'-dicarboxylic acid and di-*n*-butylamine were purchased from Aldrich and used without further purification. The compound Ru(bpy)Cl₂ was synthesized according to a literature procedure.²⁸

The identification of the [(Ln₂-Ru)**1**](PF₆)₂ complexes was confirmed by Matrix Assisted Laser Desorption Ionisation Time-of-Flight (MALDI-TOF) mass spectrometry²⁹ using a PerSeptive Biosystems Voyager-DE-RP MALDI-TOF mass spectrometer (PerSeptive Biosystems, Inc., Framingham, MA, USA) equipped with delayed extraction³⁰. A 337 nm UV nitrogen laser producing 3 ns pulses was used and the mass spectra were obtained in the linear and reflection mode. The samples were prepared by mixing 10 µl of a chloroform solution of the sample with 30 µl of a solution of 3 mg/l 2,5-dihydroxybenzoic acid in chloroform. One µl of the solution was loaded on a gold-sample plate, the solvent was removed in warm air and the sample transferred to the vacuum of the mass spectrometer for analysis.

Bipyridine bis(terphenyl) ester (4). To a mixture of 2,2'-bipyridine-4,4'-dicarboxylic acid (74 mg, 0.30 mmol) in THF (50 mL) was added SOCl₂ (5 mL), and the mixture was refluxed for three hours, after which the solvent and excess SOCl₂ were removed *in vacuo*. The resulting brown solid was redissolved in CH₂Cl₂ (50 mL) and subsequently, a solution of **3** (0.58 g, 0.55 mmol) and Et₃N (0.08 mL, 0.55 mmol) in CH₂Cl₂ (10 mL) was slowly added. The resulting solution was stirred overnight at room temperature. Subsequently, CH₂Cl₂ (100 mL) was added and the reaction mixture was first washed with 1 N HCl and then with 5% K₂CO₃, followed by standard workup. The crude product was purified by flash column chromatography (4% MeOH in CH₂Cl₂ (v/v)) to give **4** as an oil in 72% yield. ¹H NMR (CDCl₃): δ = 8.78-8.60 (m, 6 H), 7.52-7.32 (m, 10 H), 7.20-6.96 (m, 12 H), 5.04 (s, 2H), 5.00 (s, 2H), 4.78 (s, 2H), 4.75 (s, 2H), 4.20-4.08 (m, 4 H), 4.03-3.82 (m, 8 H), 3.70-3.17 (m, 24H), 2.33 (s, 18H), 2.10-1.62 (m, 16 H), 1.46-1.16 (m, 62 H), 0.98-0.76 (m, 12 H). ¹³C NMR (CDCl₃): δ = 171.8, 169.3, 167.4, 166.5, 155.5, 151.9, 151.4, 150.7, 148.8, 144.9,

136.3-126.1, 120.5, 118.1, 81.0, 80.4, 70.0-66.8, 65.2, 47.9-41.7, 31.1, 27.4, 20.4, 20.1, 18.7, 14.6, 13.3. MS (FAB): $m/z = 2315.3 [(M+H)^+]$, calcd. for C₁₃₆H₁₈₀N₆O₂₆: 2315.3].

Bipyridine bis(terphenyl) acid ((H₆)1). A solution of **4** (80 mg, 0.035 mmol) in TFA (25 mL) was stirred overnight at room temperature. Subsequently, toluene (15 mL) was added and the TFA/toluene mixture was evaporated azeotropically. The residue was taken up in CH₂Cl₂ (100 mL) and washed twice with 1 N HCl, followed by standard workup. The bipyridine-bis(terphenyl) acid (H₆)1 was obtained as an off-white solid in quantitative yield. M.p.: 103-105 °C. ¹H NMR (DMSO-d₆): δ = 8.83-8.62 (m, 2 H), 8.42-8.30 (m, 2 H), 7.60-7.27 (m, 12 H), 7.20-6.80 (m, 12 H), 4.96-4.75 (m, 4H), 4.70-4.50 (m, 4H), 4.20-3.80 (m, 12 H), 3.60-2.90 (m, 24H), 2.30 (s, 18H), 1.93-1.60 (m, 8 H), 1.54-0.56 (m, 28 H). IR (KBr): 1750 cm⁻¹ (ν_{COOH}). MS (FAB): $m/z = 2000.0 [(M+Na)^+]$, calcd. 1999.9]. Anal. calcd. for C₁₁₂H₁₃₂N₆O₂₆·1H₂O: C, 67.39, H, 6.77, N, 4.21. Found, C, 67.12, H, 6.89, N, 4.24.

Typical procedure for the preparation of the lanthanide complexes (Ln₂)1. To a solution of (H₆)1 (100 mg, 0.05 mmol) and Et₃N (0.07 mL, 0.50 mmol) in methanol (20 mL) was added 0.15 mmol of the lanthanide nitrate salt. The resulting solution was refluxed for 2 h, and subsequently stirred at room temperature for 2 h, after which the solvent was evaporated. The complex was redissolved in CHCl₃ and washed twice with water, followed by standard workup. The complexes were obtained as solids in nearly quantitative yields. The complexes were characterized by IR spectroscopy and FAB-MS spectrometry. The dinuclear complexes (Ln₂)1 all gave similar IR spectra: A peak at 1640-1630 cm⁻¹ (ν_{NC(O)}) with a shoulder around 1600 cm⁻¹ (ν_{COO}). FAB-MS data: (Nd₂)1: $m/z = 2259.6 [(M+H)^+]$, calcd. for C₁₁₂H₁₂₇O₂₆N₆Nd₂: 2259.7]; (Yb₂)1: $m/z = 2319.2 [(M+H)^+]$, calcd. for C₁₁₂H₁₂₇O₂₆N₆Yb₂: 2319.8]; (Gd₂)1: $m/z = 2288.1 [(M+H)^+]$, calcd. for C₁₁₂H₁₂₇O₂₆N₆Gd₂: 2287.7].

Typical procedure for the preparation of the [(Ln₂-Ru)1](PF₆)₂ complexes. To a solution of Ru(bpy)₂Cl₂ (26 mg, 0.05 mmol) in deaerated acetone (20 mL) was added AgPF₆ (38 mg, 0.15 mmol), and the resulting mixture was stirred for 1 h. The reaction mixture was filtered to remove the AgCl, and the filtrate was added to a solution of (Ln₂)1 (0.03 mmol) in acetone (10 mL), after which the reaction mixture was refluxed overnight. The solvent was removed in vacuo and the crude product was purified with Sephadex (LH20) column chromatography (MeOH/CH₂Cl₂ 1:1 (v/v)). [(Nd₂-Ru)1](PF₆)₂: yield 64%. IR (KBr): 1636 (ν_{NC(O)}), 1590

(ν_{COO}), 842 ($\nu_{\text{bpyC-H,para}}$) cm^{-1} . MALDI-TOF: $m/z = 2815.3$ [(M-PF₆)⁺, calcd. for C₁₃₂H₁₄₂O₂₆N₁₀Nd₂RuPF₆: $m/z = 2815.6$]. [(Yb₂-Ru)1](PF₆)₂: yield 67%. IR (KBr): 1636 ($\nu_{\text{NC(O)}}$), 1590 (ν_{COO}), 842 ($\nu_{\text{bpyC-H,para}}$) cm^{-1} . MALDI-TOF: $m/z = 2879.0$ [(M-PF₆)⁺, calcd. for C₁₃₂H₁₄₂O₂₆N₁₀Yb₂RuPF₆: $m/z = 2878.8$]. [(Gd₂-Ru)1](PF₆)₂: yield: 46%. IR(KBr): 1629 ($\nu_{\text{NC(O)}}$), 1590 (ν_{COO}), 842 ($\nu_{\text{bpyC-H,para}}$) cm^{-1} . MALDI-TOF: $m/z = 2847.2$ [(M-PF₆)⁺, calcd. for C₁₃₂H₁₄₂O₂₆N₁₀Gd₂RuPF₆: $m/z = 2847.7$].

Bipyridine bis(dibutylamide) (6). To a mixture of 2,2'-bipyridine-4,4'-dicarboxylic acid (100 mg, 0.41 mmol) in THF (75 mL) was added SOCl₂ (5 mL), and the mixture was refluxed for 3 h, after which the solvent and excess SOCl₂ were removed in vacuo. The resulting brown solid was redissolved in CH₂Cl₂ (50 mL) and subsequently, a solution of di-n-butylamine (0.28 mL, 1.64 mmol) and Et₃N (0.23 mL, 1.64 mmol) in CH₂Cl₂ (10 mL) was slowly added. The resulting solution was stirred overnight at room temperature. The reaction mixture was washed with 1 N HCl and 5% K₂CO₃, followed by standard workup. The crude product was purified by recrystallization from CH₂Cl₂/ether to give **6** as a white solid: yield 77%. Mp: 123-125 °C. ¹H NMR (CDCl₃): $\delta = 8.75$ (d, 2 H, $J = 2.4$ Hz), 8.41 (s, 2 H), 7.32 (d, 2 H, $J = 2.4$ Hz), 3.53 (t, 4H, $J = 7.7$ Hz), 3.21 (t, 4H, $J = 7.7$ Hz), 1.78-1.37 (m, 12H), 1.25-1.08 (m, 4H), 1.02 (t, 6H, $J = 7.5$ Hz), 0.80 (t, 6H, $J = 7.5$ Hz). ¹³C NMR (CDCl₃): $\delta = 168.5$, 155.3, 149.1, 145.4, 120.7, 117.8, 48.2, 44.1, 30.3, 29.1, 19.7, 19.2, 13.4, 13.1. MS (FAB): $m/z = 467.3$ [(M+H)⁺, calcd. 467.3]. Anal. calcd. for C₂₈H₄₂N₄O₂: C, 72.07, H, 9.07, N, 12.01. Found: C, 71.92, H, 9.16, N, 12.21.

Reference compound (7). To a solution of **6** (10 mg, 0.02 mmol) in a mixture of THF (9 mL) and water (1 mL) was added Ru(bpy)₂Cl₂ (11 mg, 0.02 mmol), and the resulting solution was refluxed for 12 h. Subsequently, the solvents were evaporated and the reaction mixture was redissolved in water. Upon addition of a concentrated aqueous solution of NH₄PF₆, the product was obtained as a red-orange precipitate in 34% yield. ¹H NMR (CDCl₃): $\delta = 8.27$ (d, 4H, $J = 4.1$ Hz), 8.19 (s, 2H), 7.95 (t, 4H, $J = 6.9$ Hz), 7.77 (t, 4H, $J = 5.4$ Hz), 7.71 (d, 2H, $J = 2.4$ Hz), 7.48-7.40 (m, 4H), 7.35 (d, 2H, $J = 2.8$ Hz), 3.60-3.43 (m, 4H), 3.40-3.12 (m, 4H), 1.66-1.07 (m, 16H), 0.90 (t, 6H, $J = 7.2$ Hz), 0.70 (t, 3H, $J = 7.2$ Hz). MS (FAB): $m/z = 1025.3$ [(M-PF₆)⁺ calcd. for C₄₈H₅₈N₈O₂RuPF₆: 1025.3].

Ferrocene terphenyl ester (5). To a mixture of ferrocenecarboxylic acid (0.16 g, 0.68 mmol) in CH₂Cl₂ (50 mL) was added oxalyl chloride (0.50 mL), and the reaction mixture was refluxed for 3 h. The excess oxalyl chloride and the solvent were removed *in vacuo*. The solid was redissolved in CH₂Cl₂ (50 mL), and subsequently a solution of **3** (0.60 g, 0.57 mmol) and Et₃N (0.32 mL, 2.27 mmol) in CH₂Cl₂ (10 mL) was slowly added. The resulting solution was stirred overnight at room temperature. Subsequently, CH₂Cl₂ (100 mL) was added and the reaction mixture was washed twice with 1 N HCl, followed by standard workup. The crude product was purified by flash column chromatography (2% MeOH in CH₂Cl₂ (v/v)) to give **5** as a dark-yellow oil in 83% yield. ¹H NMR (CDCl₃): δ = 7.52-7.30 (m, 5H), 7.22-6.96 (m, 6H), 5.14-4.60 (m, 6H), 4.40-3.73 (m, 13H), 3.86-3.18 (m, 12H), 2.35 (s, 9H), 2.10-1.81 (m, 4H), 1.63-1.49 (m, 4H), 1.47-1.21 (m, 31H), 1.00-0.82 (m, 6H). ¹³C NMR (CDCl₃): δ = 171.7, 167.6, 166.7, 151.4, 150.9, 136.3-126.1, 81.0, 80.4, 70.3, 69.8, 69.2, 68.2, 67.2, 47.9-41.7, 31.1, 27.4, 20.4, 20.1, 18.7, 14.6, 13.3. MS (FAB): *m/z* = 1264.5 [(M)⁺, calcd. for C₇₃H₉₆N₂O₁₃Fe: 1264.6].

Ferrocene terphenyl triacid ((H₃)2**).** A solution of **5** (0.59 g, 0.12 mmol) in TFA (25 mL) was stirred overnight at room temperature. Subsequently toluene (15 mL) was added and the TFA/toluene mixture was azeotropically evaporated. The residue was taken up in CH₂Cl₂ (100 mL) and washed twice with 1 N HCl, followed by standard workup. The ferrocene terphenyl acid (H₃)**2** was obtained as a yellow solid in quantitative yield. M.p.: 81-83 °C. ¹H NMR (CD₃OD): δ = 7.43-7.23 (m, 5H), 7.21-6.85 (m, 6H), 5.10-4.42 (m, 6H), 4.40-3.73 (m, 13H), 3.60-3.06 (m, 12H), 2.30 (s, 9H), 2.00-1.63 (m, 4H), 1.55-1.06 (m, 8H), 0.94-0.68 (m, 6H). IR (KBr): 1750 cm⁻¹ (ν_{COOH}). MS (FAB): *m/z* = 1097.5 [(M)⁺, calcd.: 1097.4]. Anal. calcd. for C₆₁H₇₂N₂O₁₃Fe·1.5H₂O: C, 65.18, H, 6.72, N, 2.49. Found: C, 65.05, H, 6.33, N, 2.53.

Typical procedure for the preparation of the lanthanide complexes (Ln)2**.** To a solution of (H₃)**2** (35 mg, 0.03 mmol) and Et₃N (0.02 mL, 0.15 mmol) in methanol (20 mL) was added 0.04 mmol of the lanthanide nitrate salt. The resulting solution was stirred at room temperature for 3 h, after which the solvent was evaporated. The complex was redissolved in CHCl₃ and washed twice with water, followed by standard workup. The complexes were obtained as yellow solids in near quantitative yields. The complexes were characterized by IR spectroscopy and FAB-MS spectrometry. The (Ln)**2** complexes all gave similar IR spectra: A

peak at 1640-1630 cm^{-1} ($\nu_{\text{NC=O}}$) with a shoulder around 1590 cm^{-1} (ν_{COO}). FAB-MS data: (Nd)**2**: $m/z = 1238.1$ [(M+H)⁺, calcd. for $\text{C}_{61}\text{H}_{69}\text{O}_{13}\text{N}_2\text{FeNd}$: 1235.3]; (Yb)**2**: $m/z = 1268.4$ [(M+H)⁺, calcd. for $\text{C}_{61}\text{H}_{69}\text{O}_{13}\text{N}_2\text{FeYb}$: 1267.4].

7.4.2 Photophysical measurements

See the experimental section of Chapter 3 (photophysical studies) for a general description of the photophysical measurements. The Ru-bpy antenna luminescence lifetime measurements were performed by monitoring the luminescence decay after excitation with a 0.5 ns pulse of a LTB MSG 400 nitrogen laser ($\lambda_{\text{exc}}=337$ nm, pulse energy 20 μJ , 10 Hz repetition rate) with a streak camera system (Hamamatsu) as the detector to simultaneously probe wavelength and time-dependence of the signals. The streak images containing the luminescence data were subjected to principal component analysis by means of singular value decomposition. All the datasets contained only one significant component.

7.4.3 Electrochemical measurements

See paragraph 4.4.3 of chapter 4 for a description of the cyclic voltammetry measurements.

7.5 References and Notes

1. Moncorge, R.; Merkle, L. D.; Zandi, B. *MRS Bull.* **1999**, *24*, 21, and references cited therein.
2. Desurvire, E. *Phys. Today* **1994**, *97*, 20.
3. Gschneider Jr., K.A.; Eyring, L. *Handbook on the Physics and Chemistry of Rare Earths*, North Holland Publishing Company, Amsterdam, **1979**.
4. Hsu, K.; Miller, C. M.; Kringlebotn, J. T.; Taylor, E. M.; Townsend, J.; Payne, D. N. *Optics Lett.* **1994**, *19*, 886.
5. Iwamuro, M.; Hasegawa, Y.; Wada, Y.; Murakoshi, K.; Kitamura, T.; Nakashima, N.; Yamanaka, T.; Yanagida, S. *Chem. Lett.* **1997**, 1067.
6. (a) Crosby, G. A.; Kasha, M. *Spectrochim. Acta* **1958**, *10*, 377. (b) Meshkova, S. B.; Topilova, Z. M.; Bolshoy, D. V.; Beltyukova, S. V.; Tsvirko, M. P.; Venchikov, V. Ya. *Acta Phys. Pol. A* **1999**, *95*, 983.

7. Beeby, A.; Dickins, R.; Faulkner, S.; Parker, D.; Williams, J. A. G. *Chem. Commun.* **1997**, 1401.
8. Klink, S. I.; Hebbink, G. A.; Grave, L.; van Veggel, F. C. J. M.; Reinhoudt, D. N.; Slooff, L. H.; Polman, A.; Hofstraat, J. W. *J. Appl. Phys.* **1999**, *86*, 1181.
9. Steemers, F. J.; Verboom, W.; Hofstraat, J. W.; Geurts, F. A. J.; Reinhoudt, D. N. *Tetrahedron Lett.* **1998**, *39*, 7583.
10. Gaiduk, M. I.; Grigoryants, V. V.; Mironov, A. F.; Rmyantseva, V. D.; Chissov, V. I.; Sukhin, G. M. *J. Photochem. Photobiol. B* **1990**, *7*, 15.
11. Meshkova, S. B.; Rusakova, N. V.; Bolshoi, D. V. *Acta Chim. Hung.* **1992**, *129*, 317.
12. Oude Wolbers, M. P.; van Veggel, F. C. J. M.; Peters, F. G. A.; van Beelen, E. S. E.; Hofstraat, J. W.; Geurts, F. A. J.; Reinhoudt, D. N. *Chem. Eur. J.* **1998**, *4*, 772.
13. Werts, M. H. V.; Hofstraat, J. W.; Geurts, F. A. J.; Verhoeven, J. W. *Chem. Phys. Lett.* **1997**, *276*, 196.
14. Juris, A.; Balzani, V.; Barigelleti, F.; Campagna, S.; Belser, P.; von Zelewsky, A. *Coord. Chem. Rev.* **1988**, *84*, 85.
15. Murov, S. L.; Carmichael, I.; Hug, G. L. *Handbook of Photochemistry, 2nd Ed.*, Marcel Dekker, New York, **1993**.
16. Herkstroeter, W. G. *J. Am. Chem. Soc.* **1975**, *97*, 4161, and reference cited therein.
17. Connor, J. A.; Meyer, T. J.; Sullivan, B. P. *Inorg. Chem.* **1979**, *18*, 1388.
18. Under the experimental conditions it is not likely that both lanthanide ions in the complex will be excited at the same time.
19. See Chapter 3.
20. Beeby, A.; Faulkner, S. *Chem. Phys. Lett.* **1997**, *266*, 116.
21. (a) Streck, W.; Wierzchaczewski, M. *Chem. Phys.* **1981**, *58*, 185. (b) Tobita, S.; Arakawa, M.; Tanaka, I. *J. Phys. Chem.* **1984**, *88*, 2697. (c) Tobita, S.; Arakawa, M.; Tanaka, I. *J. Phys. Chem.* **1985**, *89*, 5649.
22. Balzani, V.; Juris, A.; Venturi, M. *Chem. Rev.* **1996**, *96*, 759.
23. (a) Sohn, Y. S.; Hendrickson, D. N.; Gray, H. B. *J. Am. Chem. Soc.* **1971**, *93*, 3603. (b) Rohmer, M.-M.; Veillard, A.; Wood, M. H. *Chem. Phys. Lett.* **1974**, *29*, 466.
24. Including the 880 nm emission band.
25. When the observed lifetimes (τ) are compared to the natural lifetimes, with $\tau_0 = 2.0$ ms for Yb³⁺ and $\tau_0 = 0.25$ ms for Nd³⁺, it can be calculated that the intrinsic lanthanide luminescence quantum yield ($= \tau/\tau_0$) is approximately the same for both complexes.

26. Horrocks Jr., W. D.; Bolender, J. P.; Smith, W. D.; Supkowski, R. M. *J. Am. Chem. Soc.* **1997**, *119*, 5972.
27. In the cyclic voltammetry measurement on (Yb)**8** in DMSO, no reduction was observed up to -1.90 V vs SCE. The oxidation potential of the ferrocene moiety of (H₃)**2** in DMSO was determined by cyclic voltammetry and is 0.62 V vs SCE.
28. Sullivan, B. P.; Salmon, D. J.; Meyer, T. J. *Inorg. Chem.* **1978**, *10*, 3334.
29. (a) Karas, M.; Bachmann, D.; Bahr, U.; Hillenkamp, F. *Int. J. Mass Spec. Ion Proc.* **1987**, *78*, 53. (b) Hillenkamp, F.; Karas, M. *Anal. Chem.* **1991**, *63*, 1193A.
30. Vestal, M. L.; Juhasz, P.; Martin, S.A. *Rapid Commun. Mass Spectrom.* **1995**, *9*, 1044.

Appendix

Towards Polymer Optical Amplifiers Based on Lissamine-Functionalized Nd³⁺ Complexes[§]

A1. Introduction

The goal of the research described in this thesis has been the development of a sensitizer-functionalized near-infrared light emitting lanthanide complex for applications in polymeric optical signal amplifiers, *i.e.* planar polymeric waveguides doped with the lanthanide complex. The main advantage of polymer-based waveguides is that standard lithography techniques can be used to make specific waveguide structures. In this way, polymer-based amplifiers can be monolithically integrated with other existing polymer-based functionalities such as splitters, switches, and multiplexers.

The mechanism of an optical signal amplifier is based on the mechanism of stimulated emission by the optical signal from an excited state of a luminescent species, for example Er³⁺, resulting in a second photon that has the same frequency, direction and phase as the

[§] Part of the work described in this appendix has been published: Slooff, L. H.; Polman, A.; Klink, S. I.; Hebbink, G. A.; Grave, L.; van Veggel, F. C. J. M.; Reinhoudt, D. N.; Hofstraat, J. W. *Optical Mat.* **2000**, *14*, 101.

optical signal. An important element of this mechanism is that there must be a population inversion between the excited state and the ground state of the luminescent species, i.e. that more species are in the excited state than in the ground state.

As has been studied in this thesis, an efficient excitation of luminescent lanthanide complexes can be achieved by incorporating an antenna chromophore (or a sensitizer) into the complexes. In this way the lanthanide ion is excited indirectly by energy transfer from the antenna chromophore to the lanthanide ion.

In chapter 4 it has been shown that *m*-terphenyl-based complexes of Nd^{3+} and Er^{3+} functionalized with a triphenylene antenna chromophore, exhibit sensitized near-infrared luminescence in solution. The main problem associated with the near-infrared emitting lanthanide ions in organic matrices, appears to be the non-radiative deactivation of the luminescent states. The luminescence lifetimes of the organic Er^{3+} and Nd^{3+} complexes are dominated by the non-radiative decay originating from quenching by high frequency oscillators such as the C-H vibrations of the ligand and the solvent, resulting in lifetimes in the μs range.

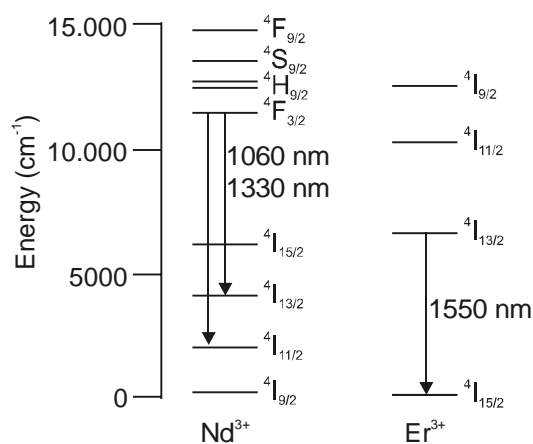


Figure A1: Part of the 4f energy levels of Nd^{3+} and Er^{3+} .

The radiative rate (the rate of spontaneous emission) of Nd^{3+} (typically $k_{\text{rad}} = 4,000 \text{ s}^{-1}$) is much higher than the radiative rate of Er^{3+} (typically $k_{\text{rad}} = 100 \text{ s}^{-1}$). The competition between the radiative decay and non-radiative decay is therefore more favorable for Nd^{3+} than for Er^{3+} , resulting in a higher intrinsic luminescence quantum yield for Nd^{3+} . Therefore Nd^{3+} complexes are initially more attractive for applications in polymer-based optical amplifiers than Er^{3+} complexes.

Another advantage of the 1060 nm and 1330 nm emissions of Nd³⁺ (⁴F_{3/2}→⁴I_{13/2}, ⁴I_{11/2} transition, respectively) is that these transitions take place to energy levels just above the ground state (see Figure A1). These levels are rapidly depopulated non-radiatively to the ground state (the ⁴I_{9/2} state), keeping the ⁴I_{11/2} or ⁴I_{13/2} state empty. As a result, in such a 4-level laser system, the population inversion is achieved immediately upon pumping.

A2. Recently Reported Organic Systems Based on Nd³⁺

For applications in organic laser systems and optical amplifiers operating in the near-infrared region, most attention in the literature has indeed been paid to Nd³⁺ complexes. For example, Hasagawa and coworkers work on the development of liquid laser systems based on Nd-tris(β-diketonato) complexes. In order to increase the luminescence lifetimes, they have replaced all the C-H groups in the Nd-tris(β-diketonato) complexes with C-D groups.¹ This is a well-established principle to improve the luminescence lifetimes of the complexed lanthanide ions.^{2,3} For example, upon direct excitation of the complexed Nd³⁺ ion at 532 nm, the luminescence lifetime of the deuterated Nd(hfa)₃ (hfa = hexafluoroacetyl-acetonate) complex ranged from 0.70 μs in methanol-*d*₄ to 6.30 μs in DMSO-*d*₆.¹ Although in most of their studies, the Nd³⁺ complexes are excited by direct (laser) excitation into the absorption bands of the lanthanide ion, Hasegawa *et al.* have also shown that their complexes can exhibit sensitized Nd³⁺ emission.⁴

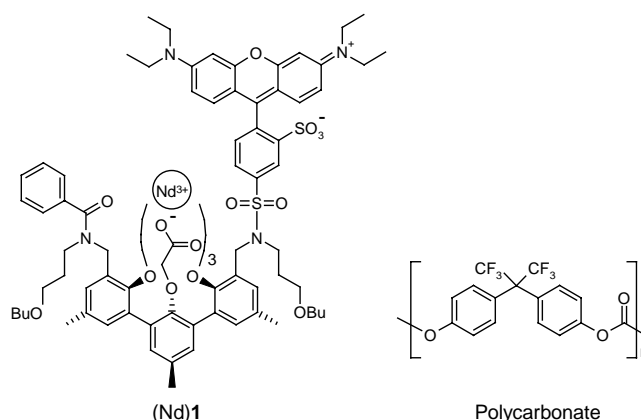
Lin *et al.* have fabricated a fluorinated polyimide waveguide doped with Nd(hfa)₃ for the potential amplification of light of 1060 nm.⁵ Upon direct excitation of the complexed Nd³⁺ ion, emission bands are observed at 880, 1060, and 1330 nm. The luminescence lifetime of the Nd³⁺ complex was approximately 1 μs. Chen and coworkers have successfully demonstrated a NdCl₃-doped polymeric optical amplifier operating at 1060 nm (⁴F_{3/2}→⁴I_{11/2} transition).⁶ The polymer matrix was a photolime-gelatin-thin-film, a polymer that is being used for optical elements, such as for example wavelength division multiplexers and display holograms. The Nd³⁺ ions were excited by direct excitation into the absorption band at 796 nm.

A3. Choice of the Polymer Matrix and the Nd³⁺ Complex

The antenna-functionalized Nd³⁺ complex

In the previous chapters various antenna chromophores for the sensitization of near-infrared Nd³⁺ luminescence have been studied: triphenylene (chapter 4), the β -diketonate dbm (chapter 5), fluorescent dyes *e.g.* Lissamine (chapter 6), and d-metal complexes *e.g.* Ru(bpy)₃ (chapter 7). From these antenna chromophores, Lissamine is the best candidate, because it allows excitation with visible light at 530 nm, which is also the wavelength of a green diode laser. Such a diode laser is compact and relatively inexpensive. In this appendix the first results of planar (partially) fluorinated polycarbonate waveguides doped with the Lissamine-functionalized complex (Nd)**1** are described (see Chart A1).

Chart A1



The polymer matrix

An optical waveguide is a structure that confines and guides a light beam by total internal reflection. This can be accomplished by surrounding a high refractive index material (*the waveguide core*), by a lower index material (*the cladding*). The material of the waveguide core and the cladding should of course be transparent to the excitation and signal wavelength, should dissolve large amounts of the lanthanide complex, and should allow further modification into other waveguide structures. The partially fluorinated polycarbonate polymer⁷ (see Chart A1) is transparent in the near-infrared region and is able to dissolve large amounts of the Lissamine-functionalized complex (Nd)**1** complex. The polymer waveguide is covered on one side by a SiO₂ layer and on the other side by air.

A4. Results and Discussion

Fabrication of the waveguides

The polycarbonate waveguides were made by spincoating a cyclohexyl acetate solution of (Nd)1 and the polycarbonate polymer or a cyclohexyl acetate solution of only the polycarbonate polymer onto a Si substrate covered with a 3 μm thick thermally grown SiO₂ layer. Spincoating was performed for 30 seconds at a spinrate of 3,000 s⁻¹, and was followed by a thermal annealing at 190 °C in vacuum for one hour. The thickness of the polymer layers was 3.55 μm .

Optical properties of the waveguide

The optical loss measurements were performed on an undoped (partially) fluorinated polycarbonate waveguide using the prism coupling technique.⁸ The result is shown in Figure A2. The background loss at the Nd³⁺ emission wavelengths is < 0.05 dB/cm and 0.08 dB at 1305 nm.

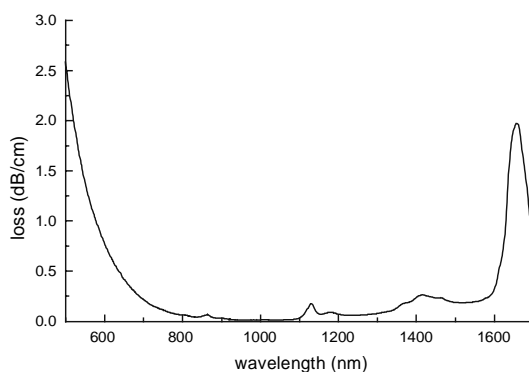


Figure A2: Optical loss spectrum of the undoped partially fluorinated polycarbonate waveguide.

This indicates that these waveguides are ideally suited for planar waveguide applications. The peaks around 1650 nm (C-H) 1400 nm (C-H, O-H), and 1150 nm (C-H) are due to overtone absorptions by C-H and O-H bonds.

The refractive index of the Nd-doped polymeric waveguide has been measured with ellipsometry, and was found to be similar to that of the undoped polymer waveguide except for the wavelength region around 580 nm, indicating that the spincoating technique leads to Nd-doped waveguides layers with similar density as pure waveguide layers. The deviation of the refractive index in the region around 580 nm is caused by the high absorption of the Lissamine antenna.

Figure A3 shows the emission spectrum of the 3 wt.% (Nd)1-doped polycarbonate waveguide after excitation at 515 nm. The planar waveguide was excited from the top with a rectangular spot near the entrance facet of the waveguide and the luminescence was collected at the output facet. The spectrum clearly shows the 890 and 1060 nm emission bands corresponding to the ${}^4F_{3/2} \rightarrow {}^4I_{9/2}$, and ${}^4I_{11/2}$, respectively. Spectra taken in the near-infrared region (not shown) also show the 1340 nm luminescence (${}^4F_{3/2} \rightarrow {}^4I_{13/2}$). The luminescence decay is mono-exponential with a lifetime of 0.8 μ s. This is comparable to the luminescence lifetime (1.2 μ s) of the *m*-terphenyl-based Nd^{3+} complex in a DMSO- h_6 solution described in chapter 3. As expected, also in a solid organic matrix the luminescence lifetime is thus dominated by non-radiative decay.

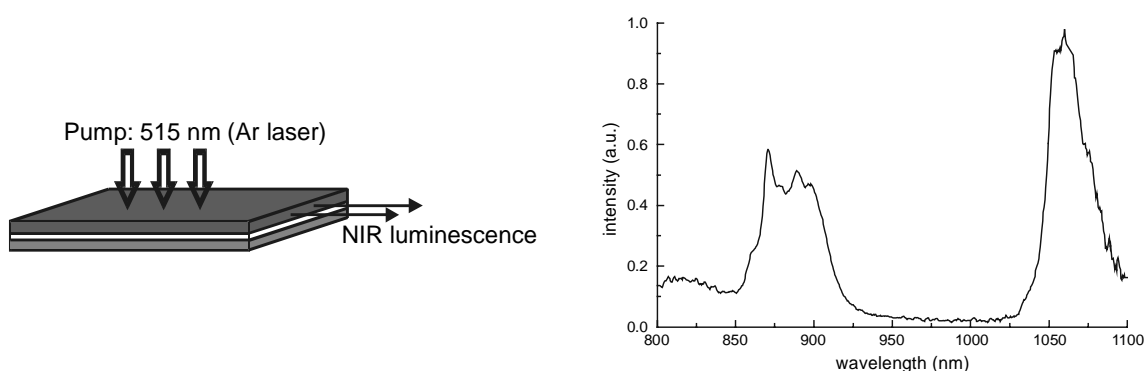


Figure A3: Left: Schematic representation of the polymer waveguide. Right: Luminescence spectrum of the (Nd)1 doped waveguide upon excitation from the top at 515 nm.

The high absorption coefficient of the Lissamine antenna, that is necessary for an efficient excitation of the Nd^{3+} ion, also strongly influences the optical properties of the polymer waveguide, in particular the refractive index and the transparency of the waveguide at 580 nm. As a result of the high absorption around 580 nm, the (Nd)1 complexes in the waveguide cannot be excited by coupling of the excitation light into the waveguide, because all the light will be absorbed within the first millimeters of the waveguide. Therefore in these steady state luminescence measurements the waveguide was pumped from the top. Ongoing research is being concerned with the solution of this problem and to find a way to excite the waveguide over its entire length.

A5. Conclusion

A Lissamine-functionalized Nd³⁺ complex has successfully been incorporated into a planar polycarbonate waveguide. Sensitized near-infrared Nd³⁺ emission was observed upon excitation of the Lissamine antenna with a luminescence lifetime of 0.8 μ s. Due to the high absorption coefficient of the antenna, the waveguide is not transparent at the excitation wavelength. For this reason the waveguide was excited from the top. Other ways of excitation are currently under investigation, as well as a study to the photostability of the complexes in the waveguides.

A6. Experimental Section

Characterization of the optical properties of the polymer

The real and imaginary parts of the refractive index of the polymer waveguide were measured using a variable angle spectroscopic ellipsometer.⁹ The optical losses were measured using the sliding prism method.⁸ Diiodomethane was used as an index matching liquid for optimum output coupling. A white light source as well as lasers operating at 633, 838, 1305, and 1565 nm were used.

The steady state luminescence measurements were performed using the 515 nm line of an Ar laser as the excitation source operating at an intensity of 40 mW. The planar waveguide, which had a total length of 25 mm, was pumped from the top with a rectangular spot (5x15 mm²) near the entrance facet of the waveguide. The luminescence was collected at the output facet, using a multi-mode optical fiber. The fiber was led into an objective in front of the monochromator, and the emitted luminescence was detected with a photomultiplier tube or a liquid-nitrogen-cooled Ge detector. The time-resolved luminescence measurements were performed using a photomultiplier tube and a photon counting system. The time resolution of the system was 0.1 μ s.

A7. References and Notes

1. Hasegawa, Y.; Kimura, Y.; Murakoshi, K.; Wada, Y.; Kim, J.-H.; Nakashima, N.; Yamanaka, T.; Yanagida, S. *J. Phys. Chem.* **1996**, *100*, 10201.
2. Oude Wolbers, M. P.; van Veggel, F. C. J. M.; Snellink-Ruël, B. H. M.; Hofstraat, J. W.; Geurts, F. A. J.; Reinhoudt, D. N. *J. Am. Chem. Soc.* **1997**, *119*, 138.
3. Hemmilä, I.; Mikkala, V.-M.; Takalo, H. *J. Fluorescence* **1995**, *5*, 159.
4. Iwamuro, M.; Hasegawa, Y.; Wada, Y.; Murakoshi, K.; Kitamura, T.; Nakashima, N.; Yamanaka, T.; Yanagida, S. *Chem. Lett.* **1997**, 1067.
5. Lin, S.; Feuerstein, R. J.; Mickelson, A. R. *J. Appl. Phys.* **1996**, *79*, 2868.
6. (a) Chen, R.T.; Lee, M.; Natarajan, S.; Lin, C.; Ho, Z. Z.; Robinson, D. *IEEE Photon. Technol. Lett.* **1993**, *5*, 1328. (b) An, D.; Yue, Z.; Chen, R. T. *Appl. Phys. Lett.* **1998**, *72*, 2806.
7. Woudenberg, R. H.; Boonstra, T. O. *Polymers comprising a fluorinated carbonate moiety*, International patent, deposited September 3, **1998**, #WO 9838237.
8. Weber, H. P.; Dunn, F. A.; Leibolt, W. N. *Appl. Opt.* **1973**, *12*, 755.
9. Aspnes, D. E. in *Handbook of Optical Constants of Solids*, Ed. Palik, E., Academic Press, Orlando, **1985**.

Summary

The work described in this thesis deals with the synthesis, characterization, and photophysical studies of luminescent lanthanide complexes that are based on *m*-terphenyl and calix[4]arene building blocks. The primary role of the organic ligand is to form stable complexes with lanthanide ions and to shield the lanthanide ion from its environment. This is necessary, because high-frequency vibrations, such as O-H vibrations, can efficiently quench the lanthanide luminescent state. An important feature of the complexes is that they have been functionalized with a light harvesting unit, the so-called *antenna chromophore* or *sensitizer*. Such a unit can efficiently capture the excitation light and subsequently donate this energy to the lanthanide ion. The subsequent lanthanide emission bands are characteristic for the complexed lanthanide ion, and can range from 500 to 1550 nm. Some of the characteristic optical transitions of lanthanide ions can be used to amplify near-infrared light with a wavelength of 1330 and 1550 nm. These wavelength regions play an important role in optical telecommunication networks, where data is transported as light pulses through glass fibers. The ultimate goal of this research is to develop a polymer-based optical amplifier that operates in the near-infrared region. By complexation of *inorganic* lanthanide ions, that have emission bands in the near-infrared region, in *organic* antenna-functionalized ligands, the lanthanide ions can be excited efficiently, and the complexes can be processed into polymer materials.

In chapter 1 the goal of the thesis has been formulated and the framework in which the research has been performed.

In chapter 2 a general background has been given concerning the photophysical properties of trivalent lanthanide ions. Although lanthanide ions can also be excited directly, the excitation via an antenna chromophore is preferred, because lanthanide ions have very low absorption coefficients. Much attention has therefore been paid to the sensitization process, which involves excitation of the antenna into its singlet excited state, intersystem crossing to the triplet state, and subsequent energy transfer to the lanthanide ion. Moreover, the coordination properties of lanthanide ions have been discussed, and the concomitant demands on the ligands for the formation of stable lanthanide complexes. Finally, a short overview has been given of (primarily) macrocyclic polydentate ligands and their corresponding luminescent lanthanide complexes.

Chapter 3 deals with the design and synthesis of novel *m*-terphenyl ligands that contain three bidentate oxyacetate moieties and two sulfonamide or amide groups for the coordination and shielding of the lanthanide ion. The terphenyl moiety, which is in close proximity to the lanthanide ion, was used as the antenna chromophore. An important aspect of the developed synthesis route of the ligands is that also other antenna chromophores can easily be incorporated at the amide and sulfonamide substituents. The conformational properties of the complexes were studied using (temperature dependent) ^1H NMR and ^{19}F NMR spectroscopy. Moreover, the composition of the first coordination sphere was studied using ^{17}O NMR and luminescence spectroscopy. On average, one methanol molecule is coordinated to the lanthanide ion, implying that the eight donor atoms of the ligand are coordinated to the lanthanide ion. The sensitized luminescence of the visible light emitting Eu^{3+} , Tb^{3+} , Dy^{3+} , and Sm^{3+} complexes is described. The Er^{3+} , Yb^{3+} , and Nd^{3+} complexes exhibit room temperature luminescence in the near-infrared (NIR) region. Compared to the visible light emitting lanthanide ions Eu^{3+} and Tb^{3+} , the luminescent states of the NIR light emitting lanthanide ions are lower in energy, and the energy gaps between the lowest excited state and highest ground state are smaller. As a result of the small energy gaps, the luminescent states are also efficiently deactivated by quenching by C-H vibrations, resulting in low overall luminescence quantum yields.

The *m*-terphenyl ligand described in chapter 4 has covalently been functionalized with a triphenylene antenna chromophore. The efficiency of the overall sensitization process in the Eu^{3+} and Tb^{3+} complexes, as well as the efficiency of the individual steps in the sensitization pathway, have been studied in detail. For example, the triplet state from which the energy transfer takes place to the lanthanide ion was monitored directly by transient absorption spectroscopy, and indirectly by triplet quencher experiments and by studying the kinetics of the lanthanide luminescence. These experiments indicate that there are two conformational isomers of the complexes in solution: one in which the energy transfer is fast resulting in lanthanide luminescence, and one in which the energy transfer does not take place at all. As a result the overall luminescence quantum yields are low.

The triplet energy of the antenna in the Er^{3+} and Nd^{3+} complexes is donated to energy levels of the lanthanide ion that are above the lowest excited state. However, only emission from the lowest excited state was observed. Molecular oxygen that is dissolved in the solvent can deactivate the triplet state by collisional quenching if the energy transfer to the lanthanide ion is not fast enough. This effect was not observed for the Eu^{3+} and Tb^{3+} complexes, but it

was observed for the NIR emitting complexes, and indicates that the energy transfer is slower in the latter complexes.

One of the possibilities to improve the system described in chapter 4 is to bring the sensitizer in even closer proximity to the lanthanide ion. In chapter 5 this has been achieved in a non-covalent fashion. Antenna chromophores with chelating properties, β -diketonates, tetraazatriphenylene, and 1,10 phenanthroline, coordinate directly to the lanthanide ion in the *m*-terphenyl complex. This chapter mainly focuses on the sensitized luminescence of *ternary* Eu^{3+} complexes, because their emission spectra are very sensitive to their environments and the kinetics of the energy transfer is well-known. In the case of the (negatively charged) β -diketonate ternary complexes high overall quantum yields were obtained implying that the sensitization process is efficient in these systems. However, the ternary complexes are less stable than the covalent system described in chapter 4. The synthesis of neutral calix[4]arene-based ternary complexes is also described. The luminescence of the corresponding Eu^{3+} and Nd^{3+} complexes is briefly discussed.

Compared to the visible light emitting lanthanide ions (Eu^{3+} and Tb^{3+}), the NIR light emitting lanthanide ions (Er^{3+} , Yb^{3+} , and Nd^{3+}) have relatively low lying luminescent states. In principle, sensitizers can be used that have lower triplet *and* singlet energies, and thus may allow excitation with visible light. In chapter 6 four different dyes (dansyl, coumaryl, and the Rhodamine-B derivatives Lissamine and Texas Red) have been studied as sensitizers for Nd^{3+} . The incorporated fluorescent dyes have strong absorption bands in the visible region. Although these dyes have low intersystem crossing quantum yields, sensitized Nd^{3+} luminescence was observed for all the dyes. It has been demonstrated that the complexed Nd^{3+} ion increases the intersystem crossing rate, and thus facilitates the population of the triplet state. The Lissamine dye is the most promising antenna. This antenna has a high absorption coefficient and allows excitation at 530 nm, which is the wavelength of a green diode laser.

In chapter 7 a new class of sensitizers for the sensitization of near-infrared Nd^{3+} and Yb^{3+} emission has been demonstrated: the organo-*d*-metal complexes Ru-tris(bipyridine) $[\text{Ru}(\text{bpy})_3]^{2+}$ and ferrocene. $[\text{Ru}(\text{bpy})_3]^{2+}$ allows excitation with visible light, has a high intersystem crossing quantum yield, and is chemically very robust. Ferrocene has a triplet energy level that matches the luminescent states of Nd^{3+} and Yb^{3+} . Sensitized Nd^{3+} and Yb^{3+} luminescence was observed following the excitation of organo-d-metal antennas. The energy transfer process has been studied in detail for the $[\text{Ru}(\text{bpy})_3]^{2+}$ -functionalized Nd^{3+} complex.

The sensitized Nd³⁺ luminescence rose with the decay time of the antenna phosphorescence, proving that the antenna triplet state is the donating energy level. The energy transfer rate is $\sim 10^6 \text{ s}^{-1}$, which is relatively slow. This is probably due to the relatively large distance from the lanthanide ion to the Ru^{II} center.

Finally, a dye-functionalized Nd³⁺ complex has been incorporated in a planar polymer waveguide. The fabrication of the doped waveguide and its optical properties have been presented in the appendix. These studies have demonstrated that our Lissamine-functionalized Nd³⁺ complex can be processed into polymer materials with losing its optical properties.

Samenvatting

Het onderzoek dat is beschreven in dit proefschrift heeft als centraal thema de synthese, karakterisering en bestudering van de optische eigenschappen van luminescente lanthanide-complexen die gebaseerd zijn op *m*-terphenyl- en calix[4]areeneenheden. De functie van het *m*-terphenyl- of calix[4]areenligand is het vormen van een stabiel complex met een lanthanide-ion en dit af te schermen van zijn omgeving. Een dergelijke afscherming is noodzakelijk, omdat hoog-energetische rekvibraties, zoals de O-H-rekvibratie, de luminescentie van een lanthanide-ion efficiënt kunnen uitdoven. De liganden zijn bovendien gefunctionaliseerd met een antenne-chromofoor (de *sensitizer*), die op efficiënte wijze het excitatielicht kan opvangen en deze energie vervolgens kan overdragen op het lanthanide-ion, wat uiteindelijk resulteert in lanthanide-luminescentie. De emissiebanden zijn karakteristiek voor het gecomplexeerde lanthanide-ion en kunnen variëren van 500 tot 1550 nm. Enkele optische overgangen van lanthanide-ionen kunnen gebruikt worden voor het versterken van nabij-infrarode lichtsignalen die een golflengte hebben van 1330 of 1550 nm. Lichtpulsen met deze golflengtes worden gebruikt in optische telekommunikatie-netwerken om data door glasvezels te versturen. Het uiteindelijke doel van het onderzoek is het ontwikkelen van een polymere optische versterker dat nabij-infrarode lichtsignalen kan versterken. Door een *anorganisch* lanthanide-ion dat emissiebanden heeft in het nabij-infrarode gebied te complexeren in een *organisch* ligand dat tevens gefunctionaliseerd is met een antenne-chromofoor kan het lanthanide-ion efficiënt aangeslagen worden en kan het complex verwerkt worden in polymeren.

In hoofdstuk 1 is het doel van dit onderzoek omschreven en het kader waarin het onderzoek is uitgevoerd.

In hoofdstuk 2 zijn de fotofysische eigenschappen van de driewaardige lanthanide-ionen behandeld. Hoewel lanthanide-ionen ook op directe wijze aangeslagen kunnen worden, worden de lanthanide-ionen bij voorkeur via een antenne-chromofoor aangeslagen, omdat lanthanide-ionen zelf zeer lage absorptie-coëfficiënten hebben. De afzonderlijke stappen in het zogenaamde sensitisatieproces, te weten het aanslaan van de antenne in zijn singlet aangeslagen toestand, de *intersystem crossing* naar de triplet toestand en de energieoverdracht naar het lanthanide-ion, zijn in dit hoofdstuk uitvoerig behandeld.

Verder zijn in dit theoretische hoofdstuk de coördinatie-eigenschappen van lanthanide-ionen behandeld en de eisen waaraan het ligand moet voldoen om stabiele en afgeschermd

lanthanide-complexen te verkrijgen. Tenslotte is een kort overzicht gegeven van (hoofdzakelijk macrocyclische) polydentaatliganden en de overeenkomstige luminescente lanthanide-complexen.

Hoofdstuk 3 beschrijft de synthese van nieuwe *m*-terfenylliganden die drie bidentaat oxyacetaatgroepen en twee amide- of twee sulfonamidegroepen bezitten voor het complexeren en afschermen van het lanthanide-ion. De terfenyl-eenheid, die zich dicht bij het lanthanide-ion bevindt, is als antenne-chromofoor gebruikt. Een belangrijk aspect van de ontwikkelde syntheseroute is dat ook andere antenne-chromoforen ingebouwd kunnen worden en wel op de posities van de amide- of sulfonamidesubstituenten. De conformationele eigenschappen van de complexen zijn bestudeerd met behulp van (variabele temperatuur) ^1H -NMR- en ^{19}F -NMR-metingen. Bovendien is de eerste coördinatiesfeer van het lanthanide-ion bestudeerd met behulp van ^{17}O -NMR-metingen en luminescentiespectroscopie. Gemiddeld is er één methanol gebonden aan het lanthanide-ion, wat impliceert dat de acht donoratomen van het ligand inderdaad gebonden zijn aan het lanthanide-ion. Vervolgens zijn de optische eigenschappen van de Eu^{3+} -, Tb^{3+} -, Dy^{3+} -, en Sm^{3+} -complexen, die zichtbaar licht uitzenden, onderzocht. De Er^{3+} -, Yb^{3+} -, en Nd^{3+} -complexen vertonen bij kamertemperatuur luminescentie in het nabij-infrarode gebied. Vergeleken met Eu^{3+} en Tb^{3+} is bij Er^{3+} , Yb^{3+} en Nd^{3+} het energieverval tussen de aangeslagen toestand van het lanthanide-ion en de grondtoestand klein. Door dit geringe energieverval zijn deze lanthanide-ionen erg gevoelig voor uitdoving door C-H-vibraties, wat resulteert in lage luminescentie-kwantumopbrengsten.

Het *m*-terfenylligand dat beschreven is in hoofdstuk 4 is covalent gefunctionaliseerd met trifenyleen als antenne-chromofoor. Het sensitisatieproces in de Eu^{3+} - en Tb^{3+} -complexen is in detail bestudeerd. Zo is de efficiëntie van het gehele proces bepaald, alsmede de efficiëntie van de afzonderlijke stappen. Het verval van de triplet aangeslagen toestand van de antenne, dat mede wordt bepaald door het energieoverdrachtsproces, is op een directe manier via *transient absorption*-metingen en op een indirecte manier door middel van triplet uitdoving-experimenten, bestudeerd. De resultaten van deze experimenten wijzen erop dat er in oplossing twee conformationele isomeren van het complex bestaan: één isomeer waarin de energie-overdracht snel is en dat dus luminescentie vertoont en één isomeer waarin de energie-overdracht niet plaatsvindt. Dit heeft geleid tot lage luminescentie-kwantumopbrengsten.

Hoewel in de Er^{3+} -en Nd^{3+} -complexen energieoverdracht plaatsvindt naar energieniveaus van het lanthanide-ion die zich boven de laagste aangeslagen toestand bevinden, werd alleen luminescentie waargenomen die afkomstig is van het laagste aangeslagen niveau. Indien de

energieoverdracht naar het lanthanide ion niet snel genoeg is, kan de tripletenergie van de antenne ook overgedragen worden aan zuurstof (een triplet uitdover) dat aanwezig is in het oplosmiddel. Een dergelijk effect werd niet waargenomen bij de Eu^{3+} - en Tb^{3+} -complexen, maar wel bij de nabij-infrarood licht-uitzendende complexen. Dit geeft aan dat in deze laatste complexen de energieoverdracht langzamer is.

In hoofdstuk 5 is het systeem dat beschreven is in hoofdstuk 4 verbeterd door de antenne direkt te laten coördineren aan het lanthanide-ion. In deze *ternaire* complexen worden de antenne en het lanthanide-complex slechts bij elkaar gehouden door niet-covalente interacties. De gekozen antennes, diverse β -diketonaten, tetraazatrifenyleen, en 1,10-fenantroline, bezitten de daartoe benodigde coördinerende eigenschappen. In dit hoofdstuk zijn voornamelijk de ternaire Eu^{3+} -complexen bestudeerd, omdat de vorm van de Eu^{3+} -luminescentiespectra sterk beïnvloed wordt door de eerste coördinatiesfeer en omdat het verloop van het energieoverdrachtsproces bekend is. De ternaire (negatief geladen) β -diketonaat-complexen hebben hoge luminescentie-kwantumopbrengsten, wat inhoudt dat het sensitisatieproces inderdaad efficiënt is. Een nadeel van deze ternaire complexen is de verminderde stabiliteit ten opzichte van het covalente systeem dat beschreven is in hoofdstuk 4. In hoofdstuk 5 is tevens de synthese van neutrale ternaire calix[4]areen-complexen beschreven. De overeenkomstige Eu^{3+} - en Nd^{3+} -complexen vertonen gesensitiseerde luminescentie en de spectra zijn kort behandeld.

Vergeleken met Eu^{3+} and Tb^{3+} hebben Er^{3+} , Yb^{3+} en Nd^{3+} lager gelegen luminescente niveaus. Daarom kunnen deze ionen, in tegenstelling tot Eu^{3+} en Tb^{3+} , aangeslagen worden via antenne-chromoforen die absorptiebanden hebben in het zichtbare gebied. In hoofdstuk 6 zijn vier verschillende kleurstoffen (dansyl, coumaryl en de rhodamine-B-derivaten Lissamine en Texas Red) bestudeerd als sensitizer voor Nd^{3+} . Deze kleurstoffen hebben intense absorptiebanden in het zichtbare gebied. Hoewel deze fluorescente kleurstoffen lage *intersystem crossing*-kwantumopbrengsten hebben, werd in alle gevallen gesensitiseerde Nd^{3+} -luminescentie waargenomen. Er is aangetoond dat het Nd^{3+} -ion de *intersystem crossing*-snelheid verhoogt, en dus helpt bij de populatie van de triplet aangeslagen toestand van de antenne. Uiteindelijk is Lissamine de beste keuze, omdat het een hoge absorptiecoëfficiënt bezit en de antenne aangeslagen kan worden met licht met een golflengte van 530 nm. Voor toekomstige toepassingen is dat de gewenste excitatie-golflengte.

In hoofdstuk 7 is een nieuwe klasse van antenne-chromoforen gepresenteerd, namelijk de organo-*d*-metaal complexen ruthenium-tris(bipyridine) ($[\text{Ru}(\text{bpy})_3]^{2+}$) en ferrocen. De

$[\text{Ru}(\text{bpy})_3]^{2+}$ -antenne kan aangeslagen worden met zichtbaar licht, heeft een hoge *intersystem crossing*-kwantumopbrengst en is chemisch inert. Ferroceen heeft een triplet-energie die past bij de energie van de luminescente niveaus van Nd^{3+} en Yb^{3+} . Beide antennes kunnen de luminescentie van Nd^{3+} en Yb^{3+} sensitiseren. Het energieoverdrachtsproces is in detail bestudeerd voor het $[\text{Ru}(\text{bpy})_3]^{2+}$ -gefunctionaliseerde Nd^{3+} -complex. De Nd^{3+} -luminescentie groeit in met de vervaltijd van de antennefosforescentie, wat bewijst dat de antennetriplet het donerende energieniveau is. Vanwege de relatief grote afstand tussen het lanthanide-ion en het Ru^{II} -centrum is de energieoverdrachtssnelheid echter laag ($\sim 10^6 \text{ s}^{-1}$).

Tenslotte is het Nd^{3+} -complex met Lissamine als antenne-chromofoor verwerkt in een polymere golfgeleider. Het fabriceren van de *gedoteerde* golfgeleider en zijn optische eigenschappen zijn beschreven in de appendix. Deze studies hebben gedemonstreerd dat het lanthanidecomplex verwerkt kan worden in polymere materialen met behoud van zijn optische eigenschappen.

Nawoord

In de afgelopen vier jaar heb ik veel plezier gehad in mijn onderzoek, mede dankzij het feit dat ik regelmatig op pad was om te meten. Bovendien heb ik door het multidisciplinaire karakter van mijn onderzoek met veel mensen samengewerkt, en hun inbreng is dan ook bijzonder belangrijk geweest voor de uiteindelijke inhoud van dit proefschrift.

Allereerst wil ik mijn promotor David Reinhoudt bedanken voor de mogelijkheid die hij mij geboden heeft om mijn promotie-onderzoek te doen in zijn internationaal geïntereerde groep. David, jij hebt voor mij een perfecte werkomgeving gecreëerd en ik heb optimaal kunnen profiteren van alle faciliteiten.

Frank van Veggel, jij bent niet alleen in wetenschappelijk maar ook in persoonlijk opzicht een prima begeleider geweest voor mij. Ik denk dat het je gelukt is om het maximale uit mij te halen. Ik ben je dankbaar voor de grote bijdrage die je hebt geleverd aan dit proefschrift.

Natuurlijk wil ik ook Jurriaan Huskens bedanken voor zijn adviezen op het gebied van de lanthanide-complexering, de Nederlandse en Engelse taal en voor het kritisch doornemen van mijn concept-proefschrift.

Hans Hofstraat heeft voor mij de unieke mogelijkheid gecreëerd om gebruik te maken van de meetfaciliteiten bij Akzo Nobel Chemical Research Arnhem (CRA). Hoewel je het vaak erg druk had, wist je altijd wel tijd voor mij vrij te maken. Hans, bedankt voor het tomeloze enthousiasme dat je hebt getoond voor mijn onderzoek.

Akzo Nobel CRA heeft een belangrijke rol gespeeld in mijn onderzoek. Kees Groeneboom wil ik bedanken voor het feit dat ik na het vertrek van Hans Hofstraat gewoon door mocht blijven meten. De mensen op de derde verdieping van CGS wil ik bedanken voor hun steun en belangstelling, met name wil ik Teun de Bruin, Esther van der Linden en Monique Ramsamoedj noemen. Frank Geurts wil ik bedanken voor al zijn hulp met de luminescentie-apparatuur, en voor zijn steun als de metingen weer eens tegenzaten. Verder wil ik ook Benno Hams bedanken voor het spinnen van de golfgeleiders die beschreven staan in de appendix.

Door onze samenwerking met Albert Polman en Lenneke Slooff van het FOM Instituut in Amsterdam heb ik veel geleerd over de fysische eigenschappen van mijn complexen. De vele werkbesprekingen hebben daar zeker ook toe bijgedragen. Lenneke heeft bovendien heel wat belangrijke metingen uitgevoerd, waarvan een deel is opgenomen in dit proefschrift. Lenneke, bedankt en ik wens je veel succes met jouw laatste loodjes.

Ik heb altijd veel lol beleefd aan de metingen die ik met Martijn Werts aan de Universiteit van Amsterdam heb uitgevoerd. In de praktijk is gebleken dat we eigenlijk hetzelfde onderzoek deden en ik heb optimaal van je kennis kunnen profiteren. Martijn, ik ben je bovendien veel dank verschuldigd voor het doornemen van mijn concept-proefschrift. Professor Verhoeven ben ik dankbaar voor zijn interesse in mijn onderzoek en voor zijn adviezen. De overige leden van de groep wil ik bedanken voor de gezelligheid tijdens de lunches.

Joop Peters (TU Delft) dank ik voor de ^{17}O NMR metingen die hij voor mij verricht heeft (hoofdstuk 3). Roel Fokkens (Universiteit van Amsterdam) wil ik bedanken voor het opnemen van de MALDI-TOF spectra (hoofdstuk 7).

Joop Toevank, Irene Wolbers en Mark Brouwer wil ik bedanken omdat zij er altijd voor gezorgd hebben dat chemicaliën en andere materialen vliegensvlug in mijn bezit kwamen. Voor de snelle en kundige analyse van de nieuwe verbindingen wil ik Hanny Visser, Ron Hulst, Annemarie Montanaro-Christenhusz en Tieme Stevens bedanken. Carla van der Ploeg wil ik bedanken voor haar hulp bij de afhandeling van vele administratieve zaken. Jij en Rita de Wilde stonden bovendien altijd open voor een gezellig praatje.

Samen met Jan Scheele en Dirk-Jan van Unen ben ik hier in Twente in november 1995 begonnen. De tijd die ik met jullie doorgebracht heb was mij een waar genoegen en als laatste van de *drie musketiers* ga ik dan SMCT verlaten. Ook de overige vrienden en collegae van SMCT hebben van mijn verblijf in Twente een leuke tijd gemaakt. De vriendschappen, regelmatige etentjes, het uitgaan, het squashen en het voetballen zorgen ervoor dat ik met pijn in het hart Enschede ga verlaten. Hoewel ik alle voormalige en huidige SMCT leden hartelijk wil danken, zijn er enkelen die ik met name wil noemen. Van de ‘oude garde’ zijn dat Wilhelm Huck, Frank Steemers, Esther Kerver en mijn oud-huisgenoot Paul Kenis, en van ‘mijn generatie’ zijn dat Niels van der Veen, Jasper Michels, Menno de Jong, Mercedes Crego Calama, Arianna Friggeri, Simon Flink, Bianca Snellink-Ruël en Henk-Jan van Manen.

Gerald Hebbink en Henk Keizer hebben de moed gehad om bij mij te komen afstuderen. Dit heeft geleid tot de resultaten die beschreven staan in de hoofdstukken 3 en 7. Met de financiële steun van Akzo Nobel heeft Lennart Grave mij een jaar lang synthetisch ondersteund. Lennart, jouw bijdrage is van onschatbare waarde geweest voor het gehele proefschrift. Frank Peters en Patrick Oude Alink hebben in synthetisch opzicht een belangrijke bijdrage geleverd aan hoofdstuk 6, bedankt daarvoor.

Op 19 mei zullen Leonard Prins en Kjeld van Bommel schitteren als mijn paranimfen, waarvoor ik ze bij voorbaat heel dankbaar ben. Kjeld en Leonard, jullie zijn er bijna vanaf het begin bij geweest en met jullie heb ik veel meegemaakt. Bedankt Leo dat je bovendien mijn concept-proefschrift kritisch hebt willen doornemen. Als er eventueel nog fouten inzitten, neem ik die voor mijn rekening.

Bij de AIO's van de groep van professor Nolte uit Nijmegen kon ik altijd mijn wilde verhalen uit Twente kwijt. Ik wil Alexander Kros bedanken voor zijn hulp met de electrochemische metingen. Bovendien kon ik altijd op Rob Jansen en Hans Elemans rekenen als ik iets nodig had.

Mijn ouders wil ik bedanken voor de enorme steun die ze mij hebben gegeven vanaf het moment dat ik ben gaan studeren (en natuurlijk ook daarvoor). Zij hebben mij al vroeg enthousiast gemaakt voor scheikunde. Pa en ma, jullie hebben goed voor mij gezorgd en dankzij jullie ben ik zo ver gekomen. Ook de ouders van Marieke wil ik bedanken voor de goede zorgen.

Lieve Marieke, hoewel je niet precies weet wat ik doe ben je altijd geïnteresseerd geweest in het verloop van mijn onderzoek en ben je een enorme steun voor me geweest.

Steve

Steve Klink

Curriculum Vitae

Stephen (Steve) I. Klink werd geboren op 16 mei 1971 in Alkmaar. In 1989 behaalde hij zijn VWO-diploma aan het Canisius College Mater Dei in Nijmegen. In datzelfde jaar werd begonnen aan de studie scheikunde aan de Katholieke Universiteit Nijmegen. Het propaedeuse-examen werd een jaar later afgelegd. Na het afronden van de predoctorale fase van de lerarenopleiding scheikunde begon hij aan zijn bijvakstage in de Vakgroep Biochemie. Onder leiding van dr. G. W. M. Swart en prof. dr. H. P. J. Bloemers heeft hij onderzoek gedaan naar specifieke eiwitten die tot expressie komen in melanoom-cellijnen. De hoofdvakstage werd verricht in de Vakgroep Organische Chemie onder leiding van dr. R. J. M. Klein Gebbink en prof. dr. R. J. M. Nolte. Tijdens deze periode werd gewerkt aan de synthese en karakterisering van modelsystemen voor ijzer-zwavel-cluster bevattende eiwitten. In 1995 werd het doctoraal examen afgelegd.

In de volgende periode van november 1995 tot januari 2000 is hij met financiële steun van NWO-CW als onderzoeker in opleiding werkzaam geweest binnen de werkeenheid Supramoleculaire Chemie & Technologie van de faculteit Chemische Technologie aan de Universiteit Twente. Tijdens deze periode werd het in dit proefschrift beschreven onderzoek verricht aan de synthese en karakterisering van luminescente lanthanide-complexen onder begeleiding van dr. ir. F. C. J. M. van Veggel en prof. dr. ir. D. N. Reinhoudt. Financiële steun van NWO stelde hem in staat conferenties te bezoeken in Lyon (Frankrijk), Berlijn (Duitsland), Sommerset (New Jersey, VS) en Noordwijkerhout (Nederland).

